JYU DISSERTATIONS 305

Yongjie Zhu

Identifying Task-Related Dynamic Electrophysiological Brain Connectivity

UNIVERSITY OF JYVÄSKYLÄ
FACULTY OF INFORMATION TECHNOLOGY

JYU DISSERTATIONS 305

Yongjie Zhu

Identifying Task-Related Dynamic Electrophysiological Brain Connectivity

Esitetään Jyväskylän yliopiston informaatioteknologian tiedekunnan suostumuksella julkisesti tarkastettavaksi marraskuun 25. päivänä 2020 kello 12.

Academic dissertation to be publicly discussed, by permission of the Faculty of Information Technology of the University of Jyväskylä, on November 25, 2020 at 12 o'clock noon.

JYVÄSKYLÄN YLIOPISTO
UNIVERSITY OF JYVÄSKYLÄ

JYVÄSKYLÄ 2020

Editors
Timo Männikkö
Faculty of Information Technology, University of Jyväskylä
Ville Korkiakangas
Open Science Centre, University of Jyväskylä

Permanent link to this publication: http://urn.fi/URN:ISBN:978-951-39-8348-2

ISBN 978-951-39-8348-2 (PDF)
URN:ISBN:978-951-39-8348-2
ISSN 2489-9003

ABSTRACT

Zhu, Yongjie
Identifying task-related dynamic electrophysiological brain connectivity
Jyväskylä: University of Jyväskylä, 2020, 68 p. (+included articles)
(JYU Dissertations
ISSN 2489-9003; 305)
ISBN 978-951-39-8348-2 (PDF)

How does human cognition emerge from neural dynamics? A proposed hypothesis states that efficient neuronal communication between brain regions through oscillatory synchronization gives the basis for cognitive processing. These synchronized oscillatory networks are transiently forming and dissolving at the timescale of milliseconds to support specific cognitive functions. However, unlike resting-state networks, there is still no appropriate technique for characterizing the complicated organization of such cognitive networks during task performance, especially naturalistic tasks (e.g., music listening).

In this thesis, we exploit the high spatiotemporal resolution of electro- or magnetoencephalography (EEG/MEG) to match the rapid timescales of synchronized neural populations and develop EEG/MEG analysis tools to probe the reconfiguration of electrophysiology brain networks during cognitive task performance.

In the first study, we applied CANDECOMP/PARAFAC (CP) tensor decomposition to single-trial wavelet-transformed representations of source-level EEG data recorded in a simplified and controlled task, to extract the stimuli-induced oscillatory brain activity. In the second study, by combining spatial Fourier independent component analysis with acoustic feature extraction, we probed the spatial-spectral signatures of brain patterns during continuously listening to natural music. In the third study, we examined the connectivity dynamics during natural speech comprehension via performing principal component analysis on envelope-based connectivity measurements concatenated across time or subjects. In the fourth study, we introduced a novel approach based on CP decomposition to investigate the task-related functional networks with a distinct spectrum during self-peace movement and working memory tasks. Then, we extended this tensor-based method of analyzing network dynamics during natural music listening in the fifth study.

In conclusion, these studies introduce novel approaches based on matrix or tensor decomposition to allow for multi-way connectivity analysis considering its non-stationarity, frequency-specificity, and spatial topography.

Keywords: naturalistic stimuli, brain networks, functional connectivity, dynamics, frequency-specificity, tensor decomposition

TIIVISTELMÄ (ABSTRACT IN FINNISH)

Zhu, Yongjie
Tehtäviin liittyvän dynaamisen aivojen toiminnallisen yhteyden tunnistaminen
Jyväskylä: University of Jyväskylä, 2020, 68 s. (+artikkelit)
(JYU Dissertations
ISSN 2489-9003; 305)
ISBN 978-951-39-8348-2 (PDF)

Kuinka kognitio syntyy hermodynamiikasta? Ehdotetun hypoteesin mukaan tehokas hermosolujen välinen viestintä aivoalueiden välillä oskillaatiosynkronoinnin avulla antaa perustan kognitiiviselle prosessoinnille. Nämä synkronoidut värähtelevät verkot ovat ohimeneviä ja dynaamisia millisekuntien ajanjaksossa kognitiivisten toimintojen tukemiseksi. Kuitenkaan ei vieläkään ole sopivaa menetelmää kognitiivisten verkkojen monimutkaisen organisaation karakterisoimiseksi tehtävän suorittamisen aikana, etenkin naturalististen tehtävien yhteydessä.

Tässä opinnäytetyössä hyödynnetään sähkö- tai magnetoenkefalografian (EEG / MEG) korkeaa spatiotemporaalista resoluutiota aivojen nopeiden aikataulujen mukauttamiseksi ja kehitetään EEG / MEG-analyysimenetelmiä koettimistehtävien suorittamisen aikana aivoverkkojen elektrofysiologisten määritysten koettamiseksi.

Ensimmäisessä tutkimuksessa sovelsimme CANDECOMP / PARAFAC (CP) -tensorihajoamista yksinkertaisen tehtävän yhteydessä tallennetuissa EEG-tietojen yhden tutkimuksen aallonmuunnoksilla muunnettuihin esityksiin ärsykkeiden aiheuttaman värähtelevän aivoaktiivisuuden erottamiseksi. Yhdistämällä toisessa tutkimuksessa spatiaalisen Fourier-riippumattoman komponenttianalyysin akustisten ominaisuuksien uuttamiseen, tutkimme aivojen kuvioiden spatiaaliset ja spektriset allekirjoitukset jatkuvan kuunnellen luonnollista musiikkia. Kolmannessa tutkimuksessa tutkimme yhteyksien dynamiikkaa luonnollisen puheen ymmärtämisen aikana suorittamalla pääkomponenttianalyysi kirjekuorepohjaisissa yhteysmittauksissa, jotka on ketjutettu ajan tai aiheiden välillä. Neljännessä tutkimuksessa esittelimme uuden CP-hajoamiseen perustuvan lähestymistavan tutkia tehtävään liittyviä toiminnallisia verkostoja, joilla on selkeä spektri itserauhan liikkeen ja työmuistion aikana. Sitten laajensimme tätä tenoripohjaista menetelmää verkkodynamiikan analysoimiseksi luonnollisen musiikin kuuntelun aikana viidennessä tutkimuksessa.

Nämä tutkimukset esittelevät uusia lähestymistapoja, jotka perustuvat matriisin tai tensorin hajoamiseen monisuuntaisen yhteyden analyysin mahdollistamiseksi ottaen huomioon sen epästatsionaarisuus, taajuusspesifisyys ja alueellinen topografia.

Asiasanat: naturalistiset ärsykkeet, aivoverkot, toiminnallinen yhteys, dynamiikka, taajuusspesifisyys, tensorin hajoaminen

Author

Yongjie Zhu
Faculty of Information Technology
University of Jyväskylä
Finland

Supervisors

Tapani Ristaniemi
Faculty of Information Technology
University of Jyväskylä
Finland

Fengyu Cong
School of Biomedical Engineering
Dalian University of Technology
China

Timo Hämäläinen
Faculty of Information Technology
University of Jyväskylä
Finland

Zheng Chang
Faculty of Information Technology
University of Jyväskylä
Finland

Reviewers

Qibin Zhao
Tensor Learning Unit
RIKEN Center for Advanced Intelligence Project
Japan

Peng Xu
School of Life Science and Technology
University of Electronic Science & Technology of China
China

Opponent

Elvira Brattico
Department of Clinical Medicine
Aarhus University
Denmark

ACKNOWLEDGEMENTS

Looking back on my doctoral experience, it has been not easy but memorable to go all the way. This thesis got its start when I arrived in Finland in October 2016. Without any exaggeration, this thesis would not have been possible completed without my friends to help me. If allowed, I would thank you all.

First of all, I would like to express my sincere gratitude to my supervisor Prof. Tapani Ristaniemi, who accepted me and provided me a chance to come here. During the past few years, he provided me lots of freedom to examine the areas that I discovery and he encouraged every small progress I ever made and supported me to apply for a mobility grant. At our biweekly seminar, he always understood my key points, and gave constructive suggestions and useful comments to improve the quality of the manuscripts. Whenever I faced a problem in study or life, he could always help me in time. His selflessness, humor, goodness to students, and passion for work is the treasure that I will cherish for the rest of my life. This study is to memorize Prof. Tapani Ristaniemi for his great help to me.

I would like to thank my supervisor, Prof. Fengyu Cong, who accepted me as a member of the CSC training program and provided an opportunity to study in Finland. I still remember that my friend suggested me going abroad to pursue Ph.D. Then I met Prof. Cong who recommended me to study in Finland and introduced me to Prof. Ristaniemi. It would have hardly imagined what I would do now (Maybe work in Huawei Ltd) provided that they had not accepted me to this research group four years ago, and it would be too difficult to finish this thesis without his continuously invaluable support and guidance. Since joining the group, I had over many times' discussion with Fengyu online for most of the contents of the thesis and his professional academy attitude, his profound knowledge about brain signal processing and his unbelievable enthusiasm all of these do have really helped me a lot to build my own road map to the interdisciplinary academy life.

I have to thank my supervisors, Prof. Timo Hämäläinen and Dr. Zheng Chang, during the final stage of my doctoral study. In the process of my doctoral thesis examination, Timo always kindly told me how to do in each step, which makes my graduation procedure very smooth. Thank you, Zheng, for the advice on everything in my study and life. You always know everything, both academically and other information and gave me much guidance in my career.

I would like to express my deepest appreciation to Professor Klaus Mathiak from RWTH Aachen University for providing me the warmest environment when I visited his lab from July to September 2019. I would also like to thank all the people who I worked with and helped me during my visit: Dr. Mikhail Zvyagintsev, Patrick Eisner, Jana Zweerings, Erik Röcher, Halim Baqapuri. I want to thank my important co-authors, Jia Liu, Xueqiao Li, Prof. Petri Toiviainen, Dr. Chaoxiong Ye, Dr. Chi Zhang, for thoughtful discussions and manuscript writing.

I have much appreciation to Dr. Piia Astikainen for the kind help and fruitful discussion during my doctoral study. She is the best and most responsible supervisor whom I have ever met and always does her best to help students. She is such a supervisor who I would like to be in the future.

I am very grateful to have Dr. Qibin Zhao from the RIKEN Center for Advanced Intelligence Project in Japan and Prof. Peng Xu from the University of Electronic Science & Technology of China as the reviewers of this dissertation and Prof. Elvira Brattico from the Aarhus University as my opponent.

I have to give special thanks to many researchers, whom I have never met in person, M.W. Woolrich, D. Vidaurre, M.J. Brookes, G.C O'Neill, S.M. Smith, A. Hillebrand, J.F Hipp, F. De Pasquale, A. K. Engel, P. Fries, D. Mantini, EA Allen, U. Hasson, J.L. Gallant, E.S. Finn, DLK Yamins, MAJ van Gerven, R.M. Cichy, N. Kriegeskorte, DS Bassett, O. Sporns, Y. He, RF Betzel, M.W. Cole, M.X Cohen, A. Hyvärinen, Q. Zhao, A. Cichocki, V.D. Calhoun, from all over the world for the inspirations and ideas that their work gives me. Without their pioneering work, this thesis cannot be completed.

I would also like to thank Dr. Yong Zhu, Dr. Xueyan Li, Dr. Deqing Wang, Dr. Ye Ren, Weiyong Xu, Qianru Xu, Xiulin Wang, Wenya Liu, Lili Tian, Rui Yan, and all other group members for happy times we shared during our daily life.

This thesis has been financially supported by the China Scholarship Council, China, and the Mobility Grant from the Faculty of Information Technology, University of Jyväskylä, Finland.

Last, but not least, I am forever grateful to my whole family. Special thanks to my parents: Fucun Zhu, Suzhen Wang. They gently cultured my character and interest in research that makes me be who I am now, while always respecting and supporting my choices. Special thanks to my brothers: Yongwei Zhu, Yonghao Zhu, for the dedication to this family, guaranteeing that I can study outside without any worries until now. Thanks to my little niece, Jiayi Zhu, my little nephew, Ziyan Zhu, and their mom, Licai Li, for the happiness they bring to this family.

To myself, keep calm and carry on.

Jyväskylä, Finland
July 10, 2020
Yongjie Zhu

LIST OF ACRONYMS

fMRI	Functional magnetic resonance imaging
EEG	Electroencephalography
MEG	Magnetoencephalography
FC	Functional connectivity
BOLD	Blood oxygen level dependent
RSN	Resting-state network
ICA	Independent component analysis
PCA	Principal component analysis
FFT	Fast Fourier transform
PLV	Phase locking value
PLI	Phase-lag index
wPLI	Weight phase-lag index
TCA	Tensor component analysis
HMM	Hidden Markov Model
MAR	Multivariate autoregressive models
CP	CANDECOMP/PARAFAC
NCPD	Nonnegative CANDECOMP/PARAFAC decomposition
STFT	Short Time Fourier Transform
STG	Superior temporal gyrus
HCP	Human connectome project
SNR	Signal to noise ratio

LIST OF FIGURES

CONTENTS

LIST OF INCLUDED ARTICLES

I. **Yongjie Zhu**, Xueqiao Li, Tapani Ristaniemi and Fengyu Cong. (2019, May). Measuring the Task Induced Oscillatory Brain Activity Using Tensor Decomposition. *2019 IEEE International Conference on Acoustics, Speech and Signal Processing (ICASSP) (pp. 8593-8597), Brighton, UK.*

II. **Yongjie Zhu**, Chi Zhang, Hanna Poikonen, Petri Toiviainen, Minna Huotilainen, Klaus Mathiak, Tapani Ristaniemi and Fengyu Cong. (2020). Exploring Frequency‐Dependent Brain Networks from Ongoing EEG Using Spatial ICA During Music Listening. *Brain Topography*, 33, 289-302.

III. **Yongjie Zhu**, Jia Liu, Tapani Ristaniemi and Fengyu Cong. (2020). Distinct Patterns of Functional Connectivity During the Comprehension of Natural, Narrative Speech. *International Journal of Neural Systems*, 30(3), 2050007-2050021.

IV. **Yongjie Zhu**, Jia Liu, Chaoxiong Ye, Klaus Mathiak, Piia Astikainen, Tapani Ristaniemi and Fengyu Cong. (2020). Discovering dynamic task-modulated functional networks with specific spectral modes using MEG. *NeuroImage*, 218.doi: https://doi.org/10.1016/j.neuroimage.2020.116924

V. **Yongjie Zhu**, Jia Liu, Klaus Mathiak, Tapani Ristaniemi and Fengyu Cong. (2019). Deriving electrophysiological brain network connectivity via tensor component analysis during freely listening to music. *IEEE Transactions on Neural Systems and Rehabilitation Engineering*, 28(2), 409-418.

AUTHOR'S CONTRIBUTION

Publication I : Yongjie Zhu proposed the methods, conducted the simulation and real data analysis, and wrote the draft of the manuscript. Xueqiao Li provided the real data and mainly explained the results. Tapani Ristaniemi and Fengyu Cong supervised the research and revised the manuscript.

Publication II : Yongjie Zhu proposed the methods, conducted the data analysis, and wrote the draft of the manuscript. Hanna Poikonen provided the data. Tapani Ristaniemi and Fengyu Cong supervised the research and revised the manuscript. All the author revised the manuscript.

Publication III : Yongjie Zhu proposed the methods, conducted the data analysis, and wrote the draft of the manuscript. Jia Liu revised the manuscript. Tapani Ristaniemi and Fengyu Cong supervised the research and revised the manuscript.

Publication IV: Yongjie Zhu proposed the methods, conducted the simulation and real data analysis, and wrote the draft of the manuscript. Jia Liu refined the manuscript. Chaoxiong Ye and Piia Astikainen explained the working memory results. Klaus Mathiak revised the methods. Tapani Ristaniemi and Fengyu Cong supervised the research and revised the manuscript.

Publication V: Yongjie Zhu proposed the methods, conducted the simulation and real data analysis, and wrote the draft of the manuscript. Jia Liu and Klaus Mathiak revised the manuscript. Tapani Ristaniemi and Fengyu Cong supervised the research and revised the manuscript.

1 INTRODUCTION

Although traditional experimental design for neruoscience has been well developed, we still know little about how the human brain works and what happens in our brain during the real-world experience. It becomes recently a central and hot topic of cognitive neuroscience to understand how the human brain perceives the complex inputs in the real-world and how the brain interacts with the dynamic information in our environment. The modern neuroimage techniques provide an opportunity to investigate such questions in non-invasive ways with high spatial and temporal accuracy.

The traditional experimental settings in cognitive neuroscience are typically simple and parametric tasks using abstract stimuli. Such designs rely heavily on the well-controlled variables engaged and isolate targeted cognitive constructs, such as viewing an isolated picture, listening to sounds (e.g. oddball tones). Even though such carefully controlled experimental designs have been important for cognitive neuroscience and allowed us to map cortical function and pinpoint specific brain processes, the ecological validity of such stimuli is debatable and not representative of the real-world experience occurring in everyday life.

To examine the real-world sensory experience over the past decades, an increasing interest in neuroscience has been directed to using naturalistic stimuli such as movies, music, and audio story that integrated the sensory stimuli commonly encountered in our daily life. Although they are still performed on a laboratory environment, these naturalistic paradigms give a reasonable approximation of how we encounter sensory stimuli in our daily lives. Functional magnetic resonance imaging (fMRI) that measures hemodynamic brain activity has been already applied in such naturalistic paradigms. However, fMRI suffers from the poor temporal resolution due to the protracted hemodynamic response. In contrast, electrophysiological techniques, such as electroencephalography (EEG) and magnetoencephalography (MEG), measure directly the activity of neural cell populations with millisecond temporal accuracy, thus allowing to study dynamics of cortical brain activity in high temporal resolution. However, there are few sudies using M/EEG in naturalistic paradigms due to the low singal to noise ratio compared with fMRI. This makes data-analysis challenging.

Therefore, it is necessary to develop novel analysis aproaches to enable investigating the electrophysiological basis under the naturalistic paradigms.

1.1 Introducing functional connectivity

In the 1990s, a new aspect of functional neuroimaging began to be examined for the functional processes, termed as *functional connectivity* (FC). Such measurement was descripted as 'statistical interdependence of signals between distinct brain regions' (Friston, 1994), which was usually calculated by the temporal correlation between neuroimaging signals recorded independently at two spatially separate brain regions. In other words, these spatially separate regions were collaborative working during a certain cognitive process. For an example of such functional connection, if you need to press the button when hearing a tone, the auditory cortex that is processing the sound information and should share this sound message with the motor cortex to execute the button press. Such communication between those spatially separate brain regions is referred to as functional connection. It is important to understand these functional connections, since it is evident that efficient coordination among regions in the human brain facilitates cognition and benefit the task performance. Many studies show that the functional connectivity was disrupted in clinical populations, such as schizophrenia, major depression disorder and Parkinson's disease.

Due to the wide range of functional connectivity, non-invasive neuroimaging methods that enable whole brain coverage have proven to be widely used. Over the past decades, fMRI is the commonly used modality for mapping the functional connectivity across the human brain. It should be acknowledged for the milestone research by Biswal, which initially shown that fMRI was able to enable the researcher to examine the functional connectivity with better spatial resolution and non-invasive way. Biswal et al. found that the temporal correlations existed even without any tasks between blood oxygen level dependent (BOLD) time-courses between the right and left motor areas (Biswal, Zerrin Yetkin, Haughton, & Hyde, 1995). Further work uncovers a several number of robust, brain functional networks connected separate brain areas, known as brain functional networks or *resting-state networks* (RSNs) (Beckmann, DeLuca, Devlin, & Smith, 2005; Corbetta et al., 1998; Fox & Raichle, 2007; Smith et al., 2009). Those functional networks have their own unique spatial properties and are considered to dominate the key mental processes through supporting sensory integration and other ways related to cognition or attention. Most brain networks can be observed even at rest, thus RSN terminology is used.

1.2 Electrophysiological functional networks

There is no doubt that fMRI is important and makes a huge contribution to the study of functional connectivity, but there are limitations to using fMRI to examine human brain. Firstly, the BOLD signal recorded by fMRI reflects the hemodynamic brain activity and is thus an indirect measurement of neural brain activity. The alteration in hemodynamics could cause artificial correlation among separate brain regions. For instance, it is known that the variation of heart rate or respiration could induce changes in BOLD response, which are significantly correlated between separate cortical areas and resemble functional networks (Murphy, Birn, & Bandettini, 2013; Tong, Hocke, Fan, Janes, & Frederick, 2015). Such effect cannot be ignored especially when studying the non-stationary FC (Birn, 2012; Murphy et al., 2013; Tong et al., 2015). Another is that a majority of the dynamical functional processes are obfuscated due to the latent nature of BOLD signals (5-8 seconds of delay after neural activity). These technical limitations could be avoided if we applied electrophysiological recording (e.g. EEG and MEG) to evaluate functional connectivity. These measurement techniques, such as EEG and MEG, can directly record the electrophysiological activity from the synchronized neural current flow with non-invasive way. They have an excellent temporal resolution matching the rapid timescales of the neural activity. In addition, MEG and high-density EEG systems can also achieve relatively good spatial resolution. Thus, those advantages, combined with the source localization technique, make it attractive to examine the electrophysiological mechanism of brain networks with non-invasive nature. Even before the increasing studies of functional connectivity, there were lots of work exploring the relationship between hemodynamic responses and change in neural oscillatory amplitude. The main finding is that there is a good spatial correlation between hemodynamics and neural oscillation activity over a wide frequency range (Logothetis, Pauls, Augath, Trinath, & Oeltermann, 2001; Moradi et al., 2003; Mukamel et al., 2005; Murphy et al., 2013; Singh, Barnes, Hillebrand, Forde, & Williams, 2002; Winterer et al., 2007; Zumer, Brookes, Stevenson, Francis, & Morris, 2010), whereas the spatial patterns between neural oscillation and hemodynamics activity often differ during complicated cognitive tasks (Furey et al., 2006; Liljeström, Hultén, Parkkonen, & Salmelin, 2009; Vartiainen, Liljeström, Koskinen, Renvall, & Salmelin, 2011). Laufs and colleagues observed that the correlation exists between fMRI attentional networks and time-courses of EEG sensor using concurrent EEG/fMRI techniques, first showing the independent electrophysiological evidence of functional connectivity (Laufs et al., 2003). Another further study demonstrated that each of functional networks had specific electrophysiological spectral properties found from EEG measurements by applying independent component analysis (ICA) (Mantini, Perrucci, Del Gratta, Romani, & Corbetta, 2007).

Recently, many studies begun to examine the functional networks using source-level MEG and successfully replicated the topographies of functional

connectivity derived by fMRI. de Pasquale et al. applied seed-based connection methods to MEG at source space to observe the dorsal attention network and the default mode network (De Pasquale et al., 2010). Brookes and his group developed multiple MEG-network analysis approaches, showing many of the fMRI derived networks could be replicated and matched by MEG at rest (Brookes, Hale, et al., 2011; Brookes, Woolrich, et al., 2011). In addition, Hipp et al. demonstrated that functional networks derived by EEG indicated spatial and spectral structures (Hipp, Hawellek, Corbetta, Siegel, & Engel, 2012). Those studies have started to provide evidences that the functional networks derived by fMRI possessed an electrophysiological mechanism. Moreover, electrophysiological functional networks have recently been compared with networks derived by fMRI during naturalistic paradigms (Betti, Corbetta, de Pasquale, Wens, & Della Penna, 2018; Betti et al., 2013; Dmochowski et al., 2014; Lankinen, Saari, Hari, & Koskinen, 2014; Lankinen et al., 2018; Whittingstall, Bartels, Singh, Kwon, & Logothetis, 2010). For example, the spatial topography of FC derived from fMRI and changes induced by natural movie were observed to match well with MEG (Betti et al., 2013).

1.3 Towards the dynamic functional connectivity

Almost all approaches for functional connectivity are adopted to explore the statistic interdependence across cortical regions by calculating the temporal correlation over the duration of the whole experiment process. Such procedure results in functional connectivity from data recorded over minutes or even hours. The underlying assumption of this procedure is that functional connectivity is temporally stationary. However, assessing variance of BOLD signals over time shows that time series are non-stationary and suggests that it is necessary for analysis of functional connectivity to consider the non-stationarity. An increasing number of studies have begun to provide evidences about the non-stationarity. Many studies have applied fMRI to examine the temporal non-stationarity of FC. Chang et al. first examined the non-stationarity using a sliding window method, where FC was estimated across many segmented time windows (Chang & Glover, 2010). They found that the amplitude of functional connections fluctuated relying upon which time window they evaluated. Smith et al. demonstrated that previously derived functional networks were dynamically formed from several components (Smith et al., 2012). A landmark study from Allen et al. demonstrated that the spatial structure of RSNs transiently varies over time (Allen et al., 2014). Those potential results are in line with the non-stationary assumption of dynamic connectivity, and implies that future analysis methods should take temporal non-stationarity onto account to track the dynamic rather than whole time average connectivity (Hutchison et al., 2013). However, as mentioned above, the slow nature of hemodynamic response of fMRI obscures the temporal signature of dynamic connectivity. Thus, MEG and EEG modalities with high time resolution could be used to capture such transient dynamics.

An increasing body of studies are starting to demonstrate that electrophysiological brain networks derived from M/EEG also show the significant non-stationarity in time (Liu, Farahibozorg, Porcaro, Wenderoth, & Mantini, 2017; Tewarie et al., 2019; Zhu, Liu, Ye, et al., 2020). An early study demonstrated the temporal and spectral signatures of dorsal attention and default mode networks by considering the temporal non-stationarity of signals (De Pasquale et al., 2010). Brookes and colleagues developed multiple analysis pipelines for MEG studies and demonstrated that the functional connectivity significantly fluctuated such as in the sensorimotor network (Brookes, Hale, et al., 2011). Vidaurre and his colleagues proposed methods based on Hidden Markov Model to enable to track the patterns of electrophysiological connectivity at a multiple scale of time points (Baker et al., 2014; Vidaurre, Abeysuriya, et al., 2018; Vidaurre, Hunt, et al., 2018; Vidaurre et al., 2016; Vidaurre, Smith, & Woolrich, 2017). Their results uncovered that brain networks (states) with spatial structures similar to RSNs transiently (100-200 ms) reorganized (Baker et al., 2014).

1.4 Naturalistic paradigmas

Traditional experimental settings in cognitive neuroscience relied on relatively simple parametric tasks using an abstract stimulus that are transferred with well-controlled and sparse temporal order (Eickhoff, Milham, & Vanderwal, 2020; Hasson, Malach, & Heeger, 2010; Malcolm, Groen, & Baker, 2016; Sonkusare, Breakspear, & Guo, 2019; Vanderwal, Eilbott, & Castellanos, 2019). Such design tightly controls the variables involved and isolates the targeted behavior or cognitive structure as much as possible. While those approaches have contributed significantly to our understanding of the human brain function over the last decades, its ecological validity remains uncertain. The advantage of using well-controlled and simple stimuli, such as isolated face pictures or beep sounds, is that the signatures of stimuli are well-known and can be varied in a pre-defined manner. These types of experimental designs are very important for investigating specific brain regions or brain processes, especially in the sensory system. However, our daily lives are complex; the events and stimuli around us are continuous, overlapping each other, and spread out on different time scales, ranging from low-level perception of milliseconds to minutes, hours, or years of social interaction (Hari, Parkkonen, & Nangini, 2010). In other words, these abstract stimuli rarely emerge in isolation in our real life but are rather dynamically integrated with multi-modal sensory information. Moreover, our ongoing brain state interplays with the sensory inputs, as we continuously communicate with our environment and other people. Therefore, it is evident that very well-controlled experimental designs could not track the complexity of our brain function, and it is unclear how the findings from well-controlled experimental settings generalize to the real-life situation. For instance, it has been demonstrated that neural responses to complex stimulus, such as naturalistic

pictures, cannot be well forecasted from the response to artificial stimulus such as sinusoidal gratings (Felsen & Dan, 2005), and that rich natural stimulus involve brain regions more widely than simplified stimuli (Bartels & Zeki, 2004). Also, emerging evidence and theoretical consideration imply that the human brain's responses to naturalistic stimuli are more reliably and strongly tuned than to simplistic artificial stimuli (Touryan, Felsen, & Dan, 2005; Yao, Shi, Han, Gao, & Dan, 2007). For example, even in those brain areas that classically respond to static faces (such as the fusiform gyrus), adding natural biological motion to facial stimuli increases the intensity of the cortical response (Schultz & Pilz, 2009). The studies of naturalistic paradigms could therefore uncover phenomena that the very abstract or well-controlled stimuli could not.

It is not surprisingly that the influence of naturalistic studies continues to grow. The landmark fMRI studies by Hasson et al. (Hasson, Nir, Levy, Fuhrmann, & Malach, 2004) and Bartels et al. (Bartels & Zeki, 2004) shown that It is possible to reliably link brain activity to complex natural stimuli (i.e. movies). In their studies, the participants were watching movies and the inter-subject synchronization of brain responses were examined. Later studies have also begun to investigate the brain responses by letting subjects listen natural music (Alluri et al., 2012; Cong, Alluri, et al., 2013), audio narratives (Brennan et al., 2012; Koskinen & Seppä, 2014; Lerner, Honey, Silbert, & Hasson, 2011; Malinen, Hlushchuk, & Hari, 2007; Nummenmaa et al., 2014; Simony et al., 2016; Wilson, Molnar-Szakacs, & Iacoboni, 2008), or play video games (Kätsyri, Hari, Ravaja, & Nummenmaa, 2013).

1.5 Thesis overview

The aim of this thesis is to attempt to probe the electrophysiological underpinnings of functional connectivity during naturalistic stimuli especially natural music, by exploiting the unparalleled spatiotemporal resolution of electrophysiology (i.e. EEG and MEG). It is hoped that the new approaches are developed to enable researchers to analyze the M/EEG data collected during naturalistic stimuli studies, to increase the understanding of dynamic signatures of brain networks in ecologically valid paradigms, and therefore advance the utility of M/EEG in naturalistic experiments in the future. The rest of this thesis is organized as follows.

Chapter 2 reviews the literature on the popular methods used to assess functional connectivity. It then presents some matrix/tensor decomposition techniques and analysis pipelines applied to extract the task-related functional networks in M/EEG studies.

Chapter 3 describes the aim of the studies, the techniques we used and the data we have in this thesis.

Chapter 4 summarizes the contribution and discussion of each publication.

Chapter 5 concludes the whole research work of this thesis, limitations and future directions.

2 MEASUREMENT OF FUNCTIONAL CONNECTIVITY

This chapter focus on the measurement of the functional connectivity (FC) across the separate brain regions. To restate Chapter 1, FC are referred to as a statistical interdependency between recorded signals at spatially separate cortical regions. For fMRI studies, FC usually refers to the correlation of BOLD signals. However, the definition of FC is quite broader for M/EEG. The rich spatio-temporal natures of M/EEG data enables FC to be estimated in many different ways (Brookes et al., 2014; Schölvinck, Leopold, Brookes, & Khader, 2013), and although many types of couplings have been very prominent, two of them are particularly popular. The first one results from the phase synchronisation between band-limited oscillations. The second is based on the correlation between amplitudes of oscillatory signals.

Although the source construction has advantages, it is known that the measurement of inter-region connectivity is hampered by the field spread (for MEG) and volume conduction (for EEG), which is also called signal leakage or cross talk in somewhere (Brookes, Hale, et al., 2011; Brookes et al., 2014; Colclough, Brookes, Smith, & Woolrich, 2015). Such phenomenon arise from the source-constructed errors due to the ill-posed nature of inverse problems, and artificially lead into linear correlations. To ovecome the spurious connections caused by signal leakage, alternative connectivity metrics based on phase and amplitude correlation have been proposed, such as imaginary coherence (Nolte et al., 2004) and orthogonalized amplitude correlation (Brookes, Woolrich, & Barnes, 2012; Hipp et al., 2012). Being insensitive to zero-lag correlations, these techniques have been growingly popular in estimation of correlations that could not be attributed to field spread or volume conduction. In this chapter, we introduced the commonly used approaches to calculatingthe functional connectivity using source constructed M/EEG data in the literature. Although it is not intended to examine each connectivity metric in detail, it covers many technical aspects that need to be addressed for successful studies. Section 2.1 reviews the phase-based and amplitude-based methods for functional

connectivity. Section 2.2 presents the commonly used methods to assessing the dynamic functional connectivity.

2.1 Functional connectivity metrics

How human brain network develops, functions, and supports cognition is a large and increasing topic in many areas of neuroscience (Sporns, 2010). Functional networks work at multiple spatial and temporal scales (Varela, Lachaux, Rodriguez, & Martinerie, 2001). From the most intuitive point of view, the functional connectivity descripts the relationship between pairs of signals. It was commonly used for fMRI study over the past decades. However, for the M/EEG signal, which includes more rich information than fMRI, many different measurements might be considered to explore the underling basis (Schölvinck et al., 2013). Many studies have shown that oscillatory synchronization might be a key mechanism by which neural populations transmit information and form larger networks (Fries, 2005, 2015; Salinas & Sejnowski, 2001; Singer, 1993). Engel and colleagues reviewed the literature of functional connectivity, in which two types of intrinsic coupling modes were suggested (Engel, Gerloff, Hilgetag, & Nolte, 2013). One of them is the envelope-based coupling that measures the relation of power between pairs of signals. Another is the phase-based coupling that assess the synchronization of the signals based on the phase. Figure 1 demonstrates the examples of envelope and phase coupling.

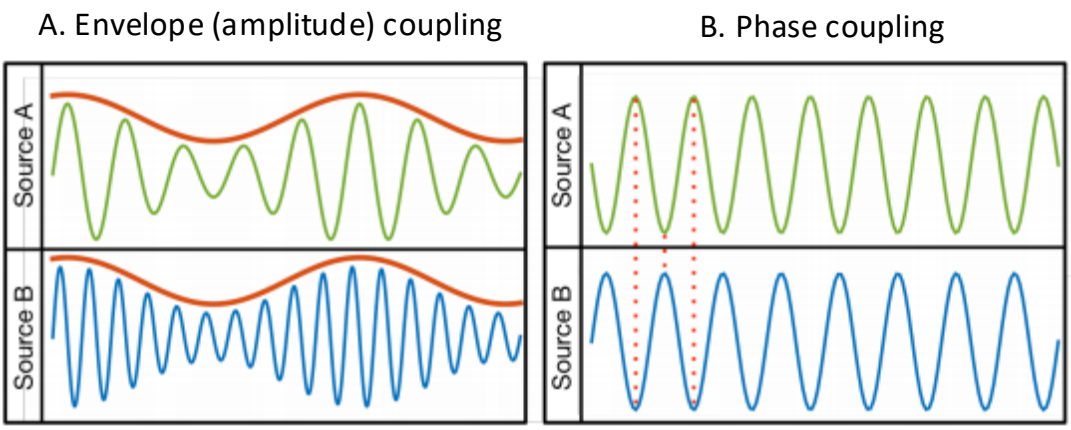

FIGURE 1 Illustration of phase- and envelope-based connectivity analysis (Adapted from (O'Neill, 2016)). A. Envelope connectivity is based on the correlation between envelopes of band-limited signals. B. Phase coupling is based on the relationship of phases of oscillatory signals.

These two types of coupling metrics focus on different aspects of M/EEG signals and tend to reveal different parts of the broader functional connection diagram (Schölvinck et al., 2013). Amplitude-based methods tend to be more similar to the long-range connections measured in fMRI signals and phase-based

connectivity less so (Brookes, Hale, et al., 2011; Tewarie et al., 2016), which is probably indicated in invasive recordings where amplitude correlation appears to be longer range than correlations of the raw time series (Leopold, Murayama, & Logothetis, 2003). However, this does not mean that phase-based methods are useless in the analysis of electrophysiological functional connectivity since they have been successfully applied for variety of electrophysiological studies (Groß et al., 2001; Hillebrand, Barnes, Bosboom, Berendse, & Stam, 2012; Kujala et al., 2007; Marzetti et al., 2013; Nolte et al., 2004). Recent studies have shown the advantages of multi-metric analysis (combining amplitude and phase connectivity measurements), in which the combination of simultaneous phase and amplitude assessment could be better to predict the network patterns measured in fMRI than either amplitude or phase methods could individually (Tewarie et al., 2016). In the current thesis, we used the amplitude-based methods for ongoing M/EEG recordings since it has been successfully to duplicate the functional networks measured by fMRI in the past decades (Colclough et al., 2016). We also used phase-based methods to assess the functional connectivity in task such, working memory and motor experiments.

2.1.1 Phase-based connectivity

Phase-based connectivity methods depend on the distribution of phase differences between two signals. When neuronal populations were functionally coupled, the timing of their oscillatory courses, as estimated via phase, would be synchronized. There are a few advantages using phase-based connectivity methods. They are widely applied in a variety of experiments and have been used to study the organization and dynamics of networks on diverse spatial and temporal scales. This is to some extent owing to the neurophysiological interpretation of phase-based connectivity analyses. Some phase-based methods are also insensitive to time lag (others are sensitive to lag), suggesting that as long as the temporal relationship between activities at two regions is consistent over time and/or trials, the phase lag would not impact the strength of the connectivity. Also, there are several disadvantages. Phase-based measurements usually rely upon accurate time relationships in the same frequency band, so they are susceptible to temporal jitter or uncertainty in the accurate timing of experimental events. Those uncertainties in time may have a greater impact at higher frequencies (Cohen, 2014).

Here, we review some commonly used phase-based methods for functional connectivity. It should be noted that all the phase-based methods introduced can be calculated either over time or trials. Calculation over trials is able to assess task-related phase-based connectivity, which assumes that the connectivity produces a clustering of phase values at each time-frequency point relative to an experiment event across the repeated trials (Cohen, 2014). The metric averaging across time is assuming that connectivity results from phase angle differences being clustered over time. This is a subtle but important distinction. This distinction between calculating connectivity across trials versus time has implications both for analysis and interpretation.

2.1.1.1 Coherence

One of the most popular phase-based metrics is to assess the coherence of two time series. Spectral coherence measiures coupling between two signals at a specific frequency and could be conderded as correlation in the frequency spectral domain. Coherence is seems to be influnced by strong increases or decreases in power due to its combination of power information. For instance, if the connection increases but the power of signals simultaneously decreases, coherence might give a biased result (Lachaux, Rodriguez, Martinerie, & Varela, 1999). Consider two signals *x(t)* and *y(t)*, their coherence is computed as follows:

$$Coh_{xy}(f) = \frac{\left|S_{xy}(f)\right|^2}{S_{xx}(f)S_{yy}(f)}, \tag{1}$$

where S_{xy} is the cross-spectral density of two signals, which are calculated from the Fourier transformed signals: *X(f)* and *Y(f)*.

$$S_{xy}(f) = X(f)Y(f)^T, \tag{2}$$

where *T* indicate the conjugate transpose of a matrix. $S_{xx}(f)$ and $S_{yy}(f)$ are the auto-spectral densities for each signal. Coherence is normalized to a scale from 0 to 1, with 1 being perfect coupling and 0 representing complete independence. Note that the calculation of denominator is simply the product of the average Fourier power of signals and the averaging can be done over trials and time points, depending on whether you are computing coherence over time or trials. For example, in the event-related data we calculated the time-frequency spectral coherence over trials, but in the ongoing data recorded during music-listening we computed the frequency-specific coherence over time in a temporal sliding window, analogous to the way the FFT was computed in sliding time segments in the short-time FFT method, resulting in time-frequency connectivity. Coherence has been widely used to measure connectivity in M/EEG study, which is largely the success of dynamic imaging of coherent sources methods.

2.1.1.2 Phase locking value

It has been argured that the spectral coherence could produce a biased result for the measurment of phase coupling between two singlas (Lachaux et al., 1999). As we mentioned above, this is because calculation of cohenrence is influnced by the power amplitude, or covariance between two signals especially while the signal to noise ratio is low. The phase locking value (PLV) is an alternative metric to precisely measure the phase relation between two signals (Lachaux et al., 1999). Let's consider two signals *x(t)* and *y(t)* from two electrodes or regions. These signals are band filtered to band-limited signals and their instantaneous phase of each signals are defined as $\varphi_x(t)$ and $\varphi_y(t)$, respectively. The phase is typically calculated using Wavelet transform or Hilbert transform. Then, the phase angle differences between two signals are computed as $\theta(t) = \varphi_x(t) - \varphi_y(t)$ at each time point. PLV can be obtained by

$$\text{PLV} = \frac{1}{T}\sum_{t}^{T} e^{i\theta(t)}, \tag{3}$$

where T is the number of time points within a time window or trial. Equation (3) calculates the PLV averaging across time, which is typically used in resting-state or naturalistic task. As we mentioned, we can also examine the consistent phase angle difference over trials by averaging over the repeated trials

$$\mathrm{PLV}(t) = \frac{1}{N}\sum_{n}^{N} e^{i\theta(t,n)}\ , \tag{4}$$

where n indicates the index of trial and N represents the number of trials. PLV over trials is typically used in the repeated well-controlled stimulus. It gives good evidence for task-related modulation in functional connectivity since synchronization must be in the same phase configuration on each trial. In addition, PLV over trials has a high temporal resolution due to the calculation at each time sample individually. The PLV is preferred over trials if you have assumption relating the temporal courses of connectivity over tens to hundreds of milliseconds.

2.1.1.3 Phase Lag-Based Measures

Because affects of field spread are generated instantaneous within measure capabilities of M/EEG acquisition and within the frequency range typically examined in M/EEG research (Stinstra & Peters, 1998), fake connectivity results that are caused by two sensors measuring activities from the identical source would possess phase lags of zero or π. Thus, it is reasonable to reduce spurious connectivity due to field spread or volume conduction by removing zero-phase-lag connectivity. There have already been existing a few phase-based connectivity metrics that are insensitive to zero-phase-connectivity, including imaginary coherence (Nolte et al., 2004), phase-lag index (Stam, Nolte, & Daffertshofer, 2007) and weighted phase-lag index (Vinck, Oostenveld, Van Wingerden, Battaglia, & Pennartz, 2011). These measures are not sensitive to field spread or volume conduction (For the reminder of this chapter, we used signal leakage instead of field speard and volume conduction for convenience), although in a few cases they might still be affected by mixed sources (Peraza, Asghar, Green, & Halliday, 2012).

Imaginary coherence was proposed as a means of using spectral coherence without concern for spurious connectivity due to signal leakage. The calculation of imaginary coherence uses almost the same equation as that for spectral coherence, except that the imaginary part of spectral coherence is performed before the amplitude.

The phase-lag index (PLI) measures the extent to which a distribution of phase differences is distributed across positive or negative sides of imaginary axis on the complex plane. The idear is that if spurious connectivity arises from signal leakage, the phase differences would be distributed around zero radians. In contrast, non-signal-leakage connectivity would generate a phase distribution that is predominantly across the positive or across the negative side of the imaginary axis. Thus, the PLI is obtained by averaging the sign of the imaginary part of the cross-spectral density, instead of averaging the whole vectors. If all

phase differences are on one side of the imaginary axis, the PLI will be high. In contrast, if half of the phase differences are positive and half are negative with respect to the imaginary axis, the PLI will be zero. The PLI can be computed as

$$\mathrm{PLI} = \frac{1}{T}\sum_{t}^{T} sign\left(Im\left(S_{xy}(t)\right)\right), \tag{5}$$

where $Im\left(S_{xy}(t)\right)$ is the imaginary part of the cross-spectral density at time point (or trial) t and *sign* represents the sign of values (+1 for a positive value and -1 for a negative value and 0 for zero value). The PLI is less sensitive to outliers, but it is also less sensitive to the amount of clustering in the distribution. In other words, if the phase values are spread out in polar space but all on one side of the imaginary axis, PLI will still be high.

The weight PLI (wPLI) is an extension of the PLI, where phase differences are weighted in terms of their distance from the real axis (Vinck et al., 2011). It can be calculated as

$$\mathrm{wPLI} = \frac{\frac{1}{T}\sum_{t=1}^{T}\left|Im\left(S_{xy}(t)\right)\right| sign\left(Im\left(S_{xy}(t)\right)\right)}{\frac{1}{T}\sum_{t=1}^{T}\left|Im\left(S_{xy}(t)\right)\right|}, \tag{6}$$

where the numerator is embedded in equation (6), but this equation can also scale the sign of the phase by the amplitude of the imaginary factor (Vinck et al., 2011). Therefore, vectors farther away from zero radians have a greater impact on the connection estimation. As coherence, the weighted term will cause the scaling of wPLI values. Thedenominator will then unscale the final results.

Similar to other phase-based measures, wPLI and PLI can be calculated over the repeated trails at each time or over time points within each segments. Noted that two limitations should be considered when phase-lag-based measures were used. First, if the two signals have slightly different frequency concentrations, PLI could fluatuate rapidly as the phase differences spin around polar space. Another limitation is that condition differences in phase-lag-based metrics can reflect either differences in connectivity or differences in the preferred phase of the connectivity.

2.1.2 Amplitude-based metrics

Amplitude-based (or power-based) functional connectivity analysis provide a series of opportunities to examine connectivity over time and frequency. The phase-based measures introduced above assume that the connections are instantaneous and at the same frequency. Such constraint is not required in amplitude-based measures, which them more flexible for hypothesis-driven and exploratory analysis. Many studies that use amplitude-based measures of band-limited signals in M/EEG have successfully derive the functional networks, which are closely similar to the functional networks observed in fMRI.

2.1.2.1 Envelope correlation

The amplitude-based methods typically depend on bivariate correlation coefficients. Here, we use Pearson Coefficient for assess the correlation between envelops of band-limited signals. The Pearson correlation coefficient is a widely used correlation method and is derived as the covariance of two signals x and y, normalized by the variance of each signal.

$$R = \frac{xy^T}{\sqrt{(xx^T)(yt^T)}} \tag{7}$$

The superscript T indicates the matrix transpose. This equation is similar to the calculation of spectral coherence, which suggests that the covariances normalized by variances provide a general approach to measure bivariate relationships in many cases.

We first need to calculate the amplitude envelop of signals using any time-frequency analysis you prefer. The most widely used is the Hilbert transform, which has been well descripted in the literature (O'Neill, Barratt, Hunt, Tewarie, & Brookes, 2015). In brief, the complex analytic signal is first computed as

$$\mathrm{z}(t) = x(t) + iH\big(x(t)\big), \tag{8}$$

where H indicates the Hilbert transform and is defined as

$$H\big(x(t)\big) = \frac{1}{\pi}\int_{-\infty}^{\infty} \frac{x(t)}{t-u}\,\mathrm{d}u. \tag{9}$$

Then, the signal envelop time series can be obtained by

$$E\big(x(t)\big) = \sqrt{\big(x(t)\big)^2 + \Big(H\big(x(t)\big)\Big)^2}. \tag{10}$$

The envelop time series can then input to the equation to compute the correlation coefficient between spatially separate regions. Like other connectivity methods, the main parameter to choose is the duration of the sliding window applied to estimate the correlation coefficient. The time window should be at least one cycle of the frequency band. For task-related data, you should use time windows of at least two to four cycles, and this number should increase with higher frequencies and with longer task paradigms. For ongoing data, you could divide the data into nonoverlapping segments of a few seconds to calculate a correlation coefficient at each segment.

2.1.2.2 Partial correlation

Partial correlation enables to measure the linear or monotonic relationship between two signals in the same time keeping constant a third signal. In the case of M/EEG amplitude-based measures, partial correlation could beusefull for two considerations. First, we can use them to valid the hypothese about networks consisting of more than two regions or electrodes. Another is that we could use partial correlation to reduce the signal leakage during amplitude-based connectivity. They have been well descripted in the elsewhere (Cohen, 2014) and we here do not introduce them in detail.

2.2 Dynamic functional connectivity techniques

A great number of previous studies have well descripted the spatial signatures of neural connectivity (Bastos & Schoffelen, 2015; Fox & Raichle, 2007; Friston, 2011; O'Neill et al., 2018; Schoffelen & Gross, 2009), however most of them have not considered the temporal structure of the data. For example, when and how the amplitude of connections between spatially separate regions or electrodes fluctuates across the experimental stimuli. A dominant proposed mechanism is that the neuronal communication between regions across the whole brain is the core of human cognition (Fries, 2005, 2015). Such communication was assumed to be coordinated by neural oscillations at certain frequencies (i.e. communication through coherence). Since such modulation of neural oscillations is very rapidly (Bola & Sabel, 2015; Pfurtscheller & Da Silva, 1999), it thus accompanies that connectivity should also vary quickly, especially in response to sensory and cognitive events. It would be crucial for an appropriate characterization of dynamic connectivity to allow us to clarify the essence of how the functional connectivity supports cognitive operations. For instance, the time-locked neural response in classical experiments generally lasts on the scale of hundreds of milliseconds to a few seconds. The formation of these stimuli-related responses is important for recognizing them as top-down or bottom-up, or as the feedforward or feedback process (O'Neill et al., 2018). Static functional connectivity analysis has been commonly used to examine the communication of brain areas during a specific cognitive process (Liddle et al., 2016; Peled et al., 2001). However, compared to dynamic connectivity measures, such static analysis is not time-resolved or frequency-resolved and cannot untangle the route of information processing in the human brain. Thence, a dynamic connectivity technique could provide a deep insight to the integration of information processing in the brain.

Although a large number of studies for functional connectivity have been explored using fMRI, it is not adequately time-resolved to address the issue of network dynamics due to slow nature of the hemodynamic signal (O'Neill, 2016; O'Neill et al., 2018). However, due to its excellent temporal resolution and good spatial coverage, electrophysiological modalities (e.g. M/EEG) provide opportunities for measuring neuronal oscillations and directly assessing rapid changes in neuronal coherence, which is the core of brain dynamic communication. These modalities are in a distinct place to probe the shortest time scale of functional connectivity, especially M/EEG measurements can cover most of the cerebral cortex. However, until only recently we could reliably do such work with non-invasive ways over the whole human brain. Therefore, we could interrogate how the functional networks form and dissolve temporally by examining the dynamic connectivity in the brain on a rapid time scale that is available in electrophysiological data.

In this section, we introduce popular methods for tracking dynamic functional connectivity, especially those techniques applying in non-invasive M/EEG data.

2.2.1 The sliding window approach

The sliding window framework is a simple but fundamental way to examine dynamic connectivity by using connectivity metrics mentioned last section within a time segment. As shown in Figure 2, the brain signals are divided into temporal windows with length d, so that a window centering on time point t has boundaries with $\pm 0.5d$. Then, the window is shifted forward in time a certain step s, connectivity is measured in this new window, and the procedure is repeated, resulting in a time course of connectivity. The advantage of the sliding window method is that most static connectivity metrics could be compatible with it with little modification due to its resemblance to the static analysis, which makes it a flexible method. However, the main parameter to select is the length of window, which is not trivial. In other words, different connectivity metrics require different lengths to evaluate functional connectivity.

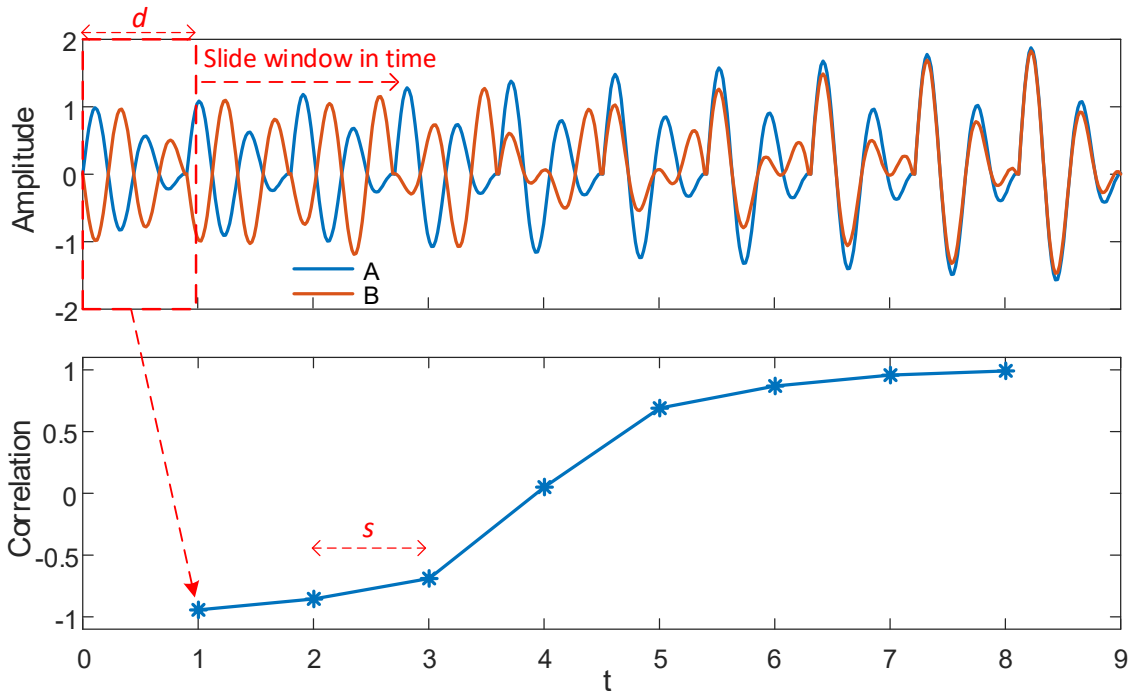

FIGURE 2 Schematic diagram of sliding window approach to estimate connectivity dynamic. Connectivity is estimated over a width of $\boldsymbol{d}$ =1s. The window is enabled to move in steps (here, $\boldsymbol{s}$ = 1) repeatedly, resulting in a time courses of connectivity. This example demonstrates a period of high anticorrelation between signals A and B, followed by high positive correlation.

2.2.1.1 Identification of repeating patterns of connectivity

When examine dynamic connectivity, it is common to assess connectivity between all pairs of brain regions within lots of time windows. This requires for an automatic approach to assist analysis of large data due to the estimates of massive connectivity matrices. In the last decade, lots of approaches have been developed to extract features from massive connectivity matrices to find interpretable and functionally meaningful network patterns. Many of those approaches rely on the assumption that functional connectivity is expressed in repeating or recurrent temporal or spatial patterns (O'Neill et al., 2018).

2.2.1.1.1 K-means clustering

K-means clustering aims to partition observations (here typically adjacent matrices) into groups or clusters in which each matrix belongs to the cluster with the nearest mean. Here, a cluster will include connectivity maps with proximal topologies across time (or recurrent spatial patterns of connectivity). K-means categorize each snapshot of connectivity into one of a predifined number of 'states', in which each state corresponds to a set of connection patterns. This method allows us to study the connectivity dynamics by collapsing down whole adjacent matrices into several networks. For repeated stimili task, each state of each trial is followed with a binary time course from k-means clustering, represting whether a state was active or inactive. These results sometimes are not interpretable, but if we average each time course across trials, so that we can obtain a probabilistic time course, revealing the likelihood of any network emerging at a specific time point. This technique has widely used to fMRI data since it was proposed by (Allen et al., 2014). It is subsequently applied to MEG data(de Pasquale, Della Penna, Sporns, Romani, & Corbetta, 2016; O'Neill, Barratt, et al., 2015; O'Neill, Bauer, et al., 2015) and EEG data (Hassan et al., 2015; Mheich, Hassan, Khalil, Berrou, & Wendling, 2015). It should be noted that there exist several limitations in K-mean clustering. One is that the number of clusters requires to be pre-deifined. Another is that K-means caregorises all the connectivity matrices derived from all the windows into multiple states, in which only one is active at a given time point. In some cases, this mignt not an appropriate assumption that all states are mutually exclusive (O'Neill et al., 2018).

2.2.1.1.2 Matrix decomposition

Matrix decomposition (e.g., ICA), an unsupervised machine learning technique, is another popular method to extract network patterns via finding common activated time courses in M/EEG (Brookes, Liddle, et al., 2012; Brookes, Woolrich, et al., 2011; Hall, Woolrich, Thomaz, Morris, & Brookes, 2013; Knyazev, Savostyanov, Bocharov, Tamozhnikov, & Saprigyn, 2016; Koelewijn et al., 2017; Koelewijn et al., 2015; Luckhoo et al., 2012; Nugent et al., 2017; Nugent, Robinson, Coppola, Furey, & Zarate Jr, 2015; Ramkumar, Parkkonen, Hari, & Hyvärinen, 2012; Ramkumar, Parkkonen, & Hyvärinen, 2014). ICA has been applied to temporal-spatial data to find spatial patterns (functional networks) based on the

fact that voxels or electrodes of each pattern share the similar timecourses. Differently from using ICA to activation timecourses, alternative strategy is to apply ICA to a collection of connectivity timecourses (e.g. obtained from sliding windows) to find functional networks based on shared modulation in connectivity (O'Neill et al., 2017). The number of extrated connnctivity timecourses representing a dynamic process (time evolution) for each independent network would be lower than the number of original connectivity estimated. ICA can do this because it extracts common connectivity timecourses over a set of connections between resiongs, which enables to identifying spatially overlapped networks if each connectivity topography had a distinct temporal nature (see figure 3).

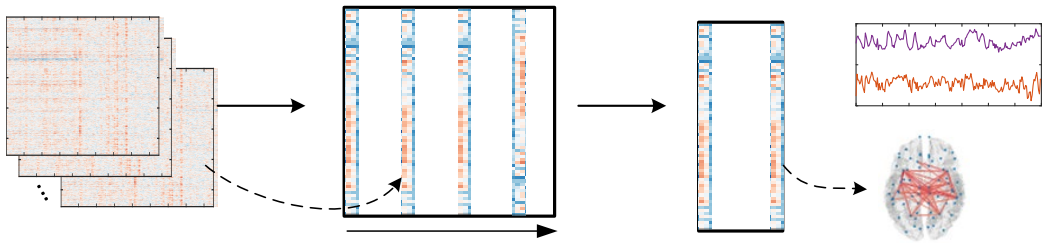

FIGURE 3 The schematic diagram of ICA performing dynamic FC analysis. Dynamic FC matrix can be obtained based on sliding window procedure and then concatenated across time (or subject). Temporal ICA was here applied to extract connectivity patterns. Each row of the estimated source matrix represents the temporally independent process of FC, collapsed over all connections. Each column of the mixing matrix expresses the contribution of each individual connections to the temporally independent component, which can be thought of as a pattern of FC.

Other approaches based on matrix decomposition contain principal component analysis (Leonardi et al., 2013; Tang, Lu, & Yang, 2019), dictionary learning (Grandjean et al., 2017), and dynamic community detection (Al-sharoa, Al-khassaweneh, & Aviyente, 2018; Li et al., 2019; Martinet et al., 2020; Vaiana, Goldberg, & Muldoon, 2019). Dynamic community detection expands common used community detection in static networks, which has been proved to uncover similar functional networks derived from ICA (Crossley et al., 2013). The key idea that an optimization is implemented on a graph-theory function, referred as modularity, which measures the ratio of within community connections to between community connections (Mucha, Richardson, Macon, Porter, & Onnela, 2010). Every node of the network is thus clustered into a specific community.

2.2.1.1.3 Tensor decomposition

Tensor decomposition, a high order extension of matrix decomposition, can be used to reduce dimensions of multi-way data (e.g. from spectral, spatial and temporal modes of data) and extract low-dimensional, interacted descriptors. For example, in a traditional EEG study, three tensor modes could be time, frequency,

and electrodes (Mørup, Hansen, Herrmann, Parnas, & Arnfred, 2006). In neurophysiological measures, the different modes could correspond to neuron, time, and trial (Williams et al., 2018). Here for studying connectivity, tensor component analysis (TCA) has been increasingly used to a variety of connectivity data structures (Escudero, Acar, Fernández, & Bro, 2015; Mahyari & Aviyente, 2014; Ozdemir, Bernat, & Aviyente, 2017; Pester, Ligges, Leistritz, Witte, & Schiecke, 2015; Spyrou, Parra, & Escudero, 2018). Such technique has recently been used to M/EEG data and to derive the frequency-specific network dynamics during repeated task (Zhu, Liu, Ye, et al., 2020) and naturalistic stimuli (Zhu, Liu, Mathiak, Ristaniemi, & Cong, 2019). In these cases, TCA was applied to atlas-based M/EEG data over connections, time and frequency to derive separate components with low-dimensional features, corresponding to a pattern of FC with rapidly temporal dynamics and specific spectal mode. Figure 4 demonstrates the schematic diagram of TCA examining such multi-way dynamic FC.

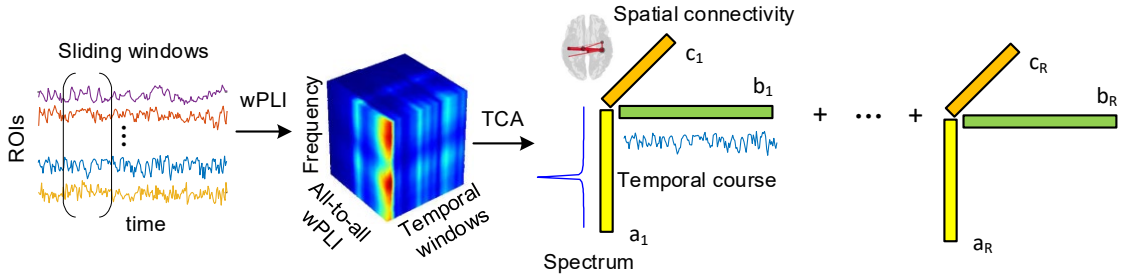

FIGURE 4 The schematic diagram of tensor component analysis (TCA) for multi-way dynamic FC. Temporally and spectrally resolved connectivity was calculated using time-frequency estimate (e.g. wPLI) based on sliding window procedure, resulting in connection data in tensor format. Tensor decomposition (e.g. with CP model) was performed to extract low-dimensional, interacted descriptions of connection data: connectivity factor, reflecting spatial patterns of FC; temporal factor, reflecting rapidly time-evolving of the FC; spectral factor, reflecting spectral signatures of FC.

However, the unresolved issue remains whether all these different methods of extracting repeating functional modes that capture similar or complementary spatio-temporal information. Are all methods sensitive to FC changes that occur in the same time scale, or is it necessary to apply pattern recognition techniques to identify FC modulations that occur in different time scales? These issues should be addressed in future study.

2.2.1.2 Statistical inference

After the acquisition of connectivity patterns, it might be most difficult to determine quantitatively whether or not its temporal change arises from a genuine nonstationary process, or is only due to stochastic noise. Indeed, many shreds of evidence demonstrated that a connection induced by a stationary process could be artificially deemed dynamic due to changes in the signal to noise ratio (SNR) of experiment data (Betzel, Fukushima, He, Zuo, & Sporns, 2016;

Hindriks et al., 2016; Lindquist, Xu, Nebel, & Caffo, 2014). Thus, effective statistical testing should be used to evaluate which changes in connectivity patterns are really meaningful. Due to a large number of time points, we need to test, a statistical test of dynamic connectivity data is much more complicated than static connectivity.

In a task-related setting where time locking can be implemented, a solution of the non-parametric statistic (Maris & Oostenveld, 2007), widely used to test for significant modulation in the power of M/EEG, could be applied to assess connectivity dynamics. The key idea is that the trial-averaged time courses of connectivity are significantly tested, generating a time-evolving non-parametric null distribution though adapting pseudo-trials. For instance, the randomized trial onset time courses are used to generate average time courses of pseudo-trials, which enable us to examine whether the beginning of a trial or onset of a stimulus significantly modulates the levels of connectivity. This strategery could also be used to other null-hypotheses, such as assessing the differences in functional connectivity between groups, in which shuffled assigning each subject to one of two groups is used to generate the null distributions. If time courses of connectivity are derived using matrix/tensor decomposition, a similar non-parametric technique based on phase-randomization or sign flupping can be performed (Brookes et al., 2014; Hunt et al., 2012; O'Neill et al., 2017; Winkler, Ridgway, Webster, Smith, & Nichols, 2014; Zhu, Liu, Ye, et al., 2020). The core idea is to produce a surrogate time course by phase randomization of time courses or randomly choosing parts of components with multiplying by -1 and then examine the trial averaged components. A null distribution could be generated by repeating this process. If a temporal change in functional connectivity was not preserved over all participants, then the surrogate temporal courses would possess the same amplitude as the ture trial-average time course. In turn, if the changes were ture, the magnitude of temporal courses of surrogate would be significantly diminished and thus the real time courses would be exceeding the threshold of null distribution.

2.2.2 Hidden Markov Models

Distinct from categorizing many connectivity matrices into several states, the Hidden Markov Model (HMM) directly exploits data to infer discrete multiple states (Rabiner, 1989). Instead of measuring connectivity in a sliding window way, the idea of HMM is that all the observations belonging to same state are put together effectively to descript networks by performing estimation at the state space (Baker et al., 2014; Vidaurre, Hunt, et al., 2018; Vidaurre et al., 2017). This therefore has an advantage of avoiding the requirement of pre-defining the length of sliding window. The inferred state is descripted by its spatial signature (e.g. the mean and covariance) and temporal signature (e.g. the activation time courses) at source level. HMM inference performing on observed data estimates the probability that each state is active at each time point of the multivariate time series and describes the probability distribution of each state.

Before HMM inference, the number of states should be determined. Many techniques have been introduced to estimate the optimal number of states (Beal, Ghahramani, & Rasmussen, 2002). We here do not present it but the review can be found elsewhere (O'Neill et al., 2018). Compared to these data-driven determination approaches, manual confirmation of results is suggested to make sure that the inferred states are at least interpretable. HMM has many variations to use based on the observation model. For example, Gaussian observation model was used to characterize the envelop of MEG data at resting state over the entire cerebral cortex (Baker et al., 2014). This type of HMM characterizes the state with a mean representing the average amplitude activation and a covariance matrix representing the functional connectivity based on envelop correlations. The result demonstrates that the resting-state networks are fast transiently forming and dissolving. To utilize the phase information, another version based on multivariate autoregressive models was proposed, call HMM-MAR (Vidaurre et al., 2016). This model performs on raw data rather than amplitude envelops, enabling to exploit the phase information. The inferred states are therefore characterized not only by amplitude but also by phase-coupling. Another benefit of this model is that the underlying descriptors of the data could be spatially, temporally, and spectrally resolved. The HMM-MAR has been proved to descript rapid spectrally resolved changes in somatosensory regions during a motor task (Vidaurre, Abeysuriya, et al., 2018). Another alternative is proposed to reduce the model complexity of HMM-MAR based on a time-embedded transformation of the data in conjunction with a simple Gaussian observation model, called TDE-HMM (Vidaurre, Hunt, et al., 2018). TDE-HMM could identify states with particular auto-correlation and non-zero lag cross-correlations that approximate the state-specific power spectra and phase-locking information accessible with the HMM-MAR. This novel model has been successfully proved to descript the frequency-specific network dynamics at rest (Vidaurre, Hunt, et al., 2018).

3 AIMS OF THE THESIS

The aim of this thesis is to develop methodology to allow us to analyze network dynamics using M/EEG data recorded during a task performance, especially during naturalistic music listening, with the focus on spatially, temporally and spectrally resolved functional connectivity. Therefore, our goal here is extending the analysis frameworks of M/EEG studies from simplified well-controlled paradigms to naturalistic stimuli approximating real-life situations. The main techniques used in this thesis are tensor component analysis, connectivity measures and statistic inference. In addition, the work is to shed light on the oscillatory mechanisms of functional networks observed in fMRI by examining the spectral signatures of connectivity. The specific aims of the individual studies are as follows

1. To examine whether tensor decomposition could be used to extract induced brain dynamics at source level data during a conventional well-controlled experiment. (*Publication I*)

2. To develop an approach combining spatial Fourier ICA and musical feature extraction to reveal spatial and spectral brain activity during music listening. (*Publication II*)

3. To develop an approach to find the differences of functional connectivity during naturalistic speech comprehension. (*Publication III*)

4. To examine whether tensor decomposition could be used to extract spectra-specific connectivity patterns during a conventional well-controlled experiment. (*Publication IV*)

5. To develop an approach based on tensor decomposition to derive the frequency-specific functional connectivity during naturalistic music listening. (*Publication V*)

4 SUMMARIES OF STUDIES

4.1 Measuring the task Induced oscillatory brain activity using tensor decomposition (*Publication I*)

Yongjie Zhu, Xueqiao Li, Tapani Ristaniemi and Fengyu Cong. (2019, May). Measuring the Task Induced Oscillatory Brain Activity Using Tensor Decomposition. *2019 IEEE International Conference on Acoustics, Speech and Signal Processing (ICASSP)* (pp. 8593-8597), Brighton, UK.

4.1.1 Motivation

The electrophysiological basis of brain functional networks is not yet understood via analyzing fMRI data, but M/EEG could offer an opportunity to examine such neural underpinnings of functional networks in the human brain. The EEG is composed of activities of a set of generators producing rhythmic activities in multiple frequency bands. During a sensory stimulus, these generators are synchronized and work together in a coherent style. These coupling activities give rise to 'evoked' or 'induced' oscillations (Başar, Başar-Eroğlu, Karakaş, & Schürmann, 1999; Başar, Schürmann, Demiralp, Başar-Eroglu, & Ademoglu, 2001). The evoked oscillations are phase-locked to specific event and the induced are not. To produce the data representation of evoked oscillations, single trial EEG data are first averaged across trials and then converted into time-frequency representation through wavelet analysis, resulting in a multi-way data representation. The analysis for such evoked oscillation based on tensor decomposition has been studied (Cong et al., 2015; Cong, Phan, et al., 2013). However, tensor decomposition has not yet been used to analyze the induced neural oscillations. Here, we attempt to examine the induced brain activity during a task execution using tensor decomposition.

4.1.2 Methods

We used one group of EEG data recorded during a task of irony comprehension (Zhu, Li, Ristaniemi, & Cong, 2019). In brief, we applied one-sentence spoken lines and colored pictures as stimuli. If the keyword in commenting sentence was semantically congruent with the content of the contextual pictures, the trail provided a neutral meaning. We analyzed the source-level EEG data to find the induced neural oscillations. The time-frequency representation of single-trail source-reconstructed EEG data constructed a third-order tensor with three factors of time*trails, frequency, and source space. non-negative Nonnegative CP decomposition (NCPD) was performed to identify the temporal, spectral, and spatial changes in electrophysiological brain activity. Statistical testing based on phase-randomization was implemented to examine the task-modulated brain components. Figure 5 demonstrates the steps of analysis pipeline.

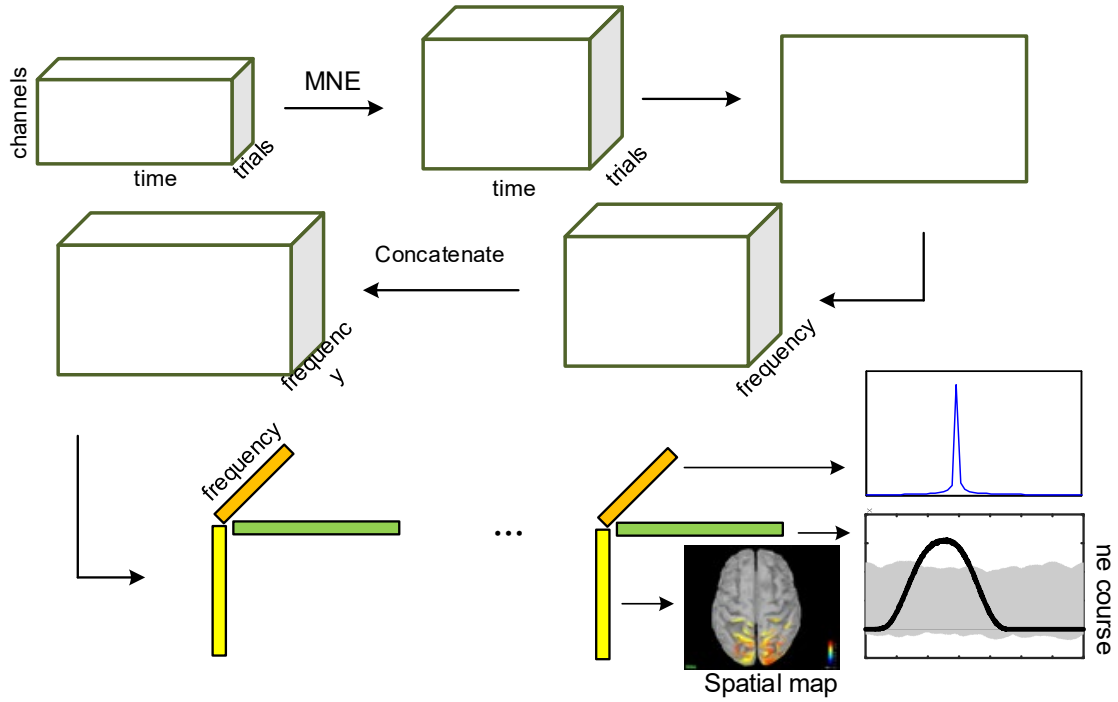

FIGURE 5 The schematic illustration of the pipeline.

4.1.3 Results

The components extracted by NCPD contains three interacted factors, i.e. spectral, temporal, and spatial factors. Two components showing significant task modulation are regarded as induced neural oscillations. The first row of Figure 6 shows that the Delta brain oscillation emerged in the right temporal-occipital junction during 800 ms after the onset. The second row of Figure 6 demonstrates that the Theta rhythm emerged in the left frontal area corresponding to Broca's area, which is significantly related to language cognition, during 400 ms after the onset.

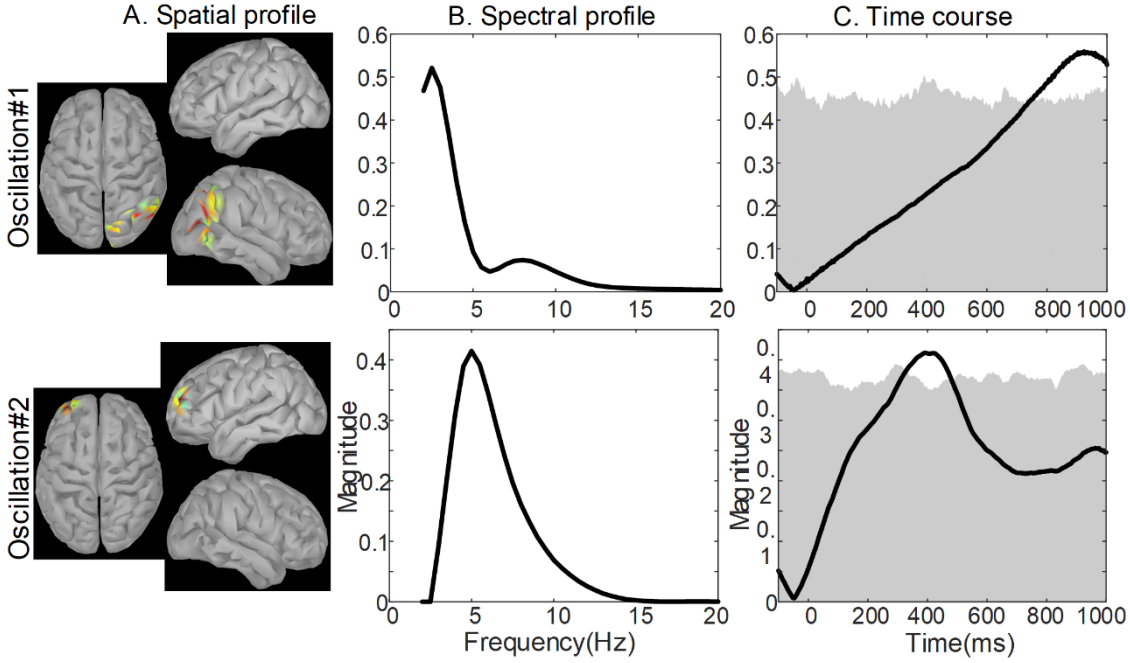

FIGURE 6 Results of experiment data. A: spatial maps of extracted components. B: Spectral factors of the components. C: Time courses of components, averaged across trials in all subjects (black line). The grey shaded region represents the null distribution ($p_{corrected} < .05$) based on a hypothesis that the response is not time locked to the tasks.

4.1.4 Discussion and conclusion

This work presented an approach based on NCPD to identify task-induced neural oscillations. It enables to characterize the brain oscillatory patterns that transiently form and dissolve to support a cognitive process during a simple task. The presented method was applied to EEG data recorded during a task of irony comprehension, showing two components related to the task. One shows that the Delta oscillations are elicited in Broca's region after 400 ms of stimuli onset. Another demonstrates that Theta rhythm is related to comprehension of irony in right temporal-occipital junction after 800 ms of the onset. These neural oscillations emerging in those brain areas could be expected since previous studies have also reported that the similar brain regions are related to humor comprehension (Mobbs, Greicius, Abdel-Azim, Menon, & Reiss, 2003; Shibata et al., 2017).

During a cognitive process, different neural oscillations would be emerging at different brain areas at different time, resulting in a complex data to analyze. For such data, the introduced method combining wavelet transform with tensor decomposition offer a way of extracting spectral, spatial, and temporal information linking to stimuli.

4.2 Spatial ICA reals freuency-dependent brain networks during musicl listening (*Publication II*)

Yongjie Zhu, Chi Zhang, Hanna Poikonen, Petri Toiviainen, Minna Huotilainen, Klaus Mathiak, Tapani Ristaniemi and Fengyu Cong. (2020). Exploring Frequency-Dependent Brain Networks from Ongoing EEG Using Spatial ICA During Music Listening. *Brain Topography*, 33, 289-302.

4.2.1 Motivation

Alluri et al. examined the functional networks of musical features during a naturalistic paradigm, where subjects continuously listened to an entire music clip while their fMRI data were recorded (Alluri et al., 2012). They observed larger-scale brain responses in cognitive, motor, and limbic brain networks during continuous processing of low-level (timbral) and high-level (tonal and rhythmical) acoustic features. However, the oscillatory mechanism of these functional responses is not fully understood since the fMRI measuring BOLD signals cannot directly access to the electrical processes. Thus, EEG data were recorded in the same music listening environment, and we attempted to exploit the direct electrical activity measurements of EEG modality to address this issue. In addition, applying spatial ICA in Fourier domain, called spatial Fourier-ICA (Ramkumar et al., 2014), allows us to examine the frequency-specific brain networks emerging from dynamic processing of musical features.

4.2.2 Methods

We collected EEG data of 14 right-handed and healthy adults with BioSemi electrode caps (64 channels) during a 512 s long musical clip of modern tango previously used in the study (Alluri et al., 2012). After preprocessing of EEG data, Short Time Fourier Transform (STFT) were performed with 3 s length and 2s overlap of the adjacent windows. The source-lever data were then obtained using source reconstruction. Spatial ICA were applied to time by frequency/voxel data to extract independent spatial–spectral patterns and its temporal courses. Simultaneously, five long-term musical feature time series were calculated based on the 3-s-length and 2-s-overlaping of windows used in the computational analyses, resulting in the same sampling rate to temporal courses of EEG. This allows us for correlation analysis between their temporal courses to determine which independent spatial–spectral component was significantly modulated by musical features. The spatial maps of retained components (significantly correlated with music) from all subjects were then clustered into several groups to examine the consistency between subjects. We visualized the centroid maps of clusters, and the spectra of their included components (see figure 7).

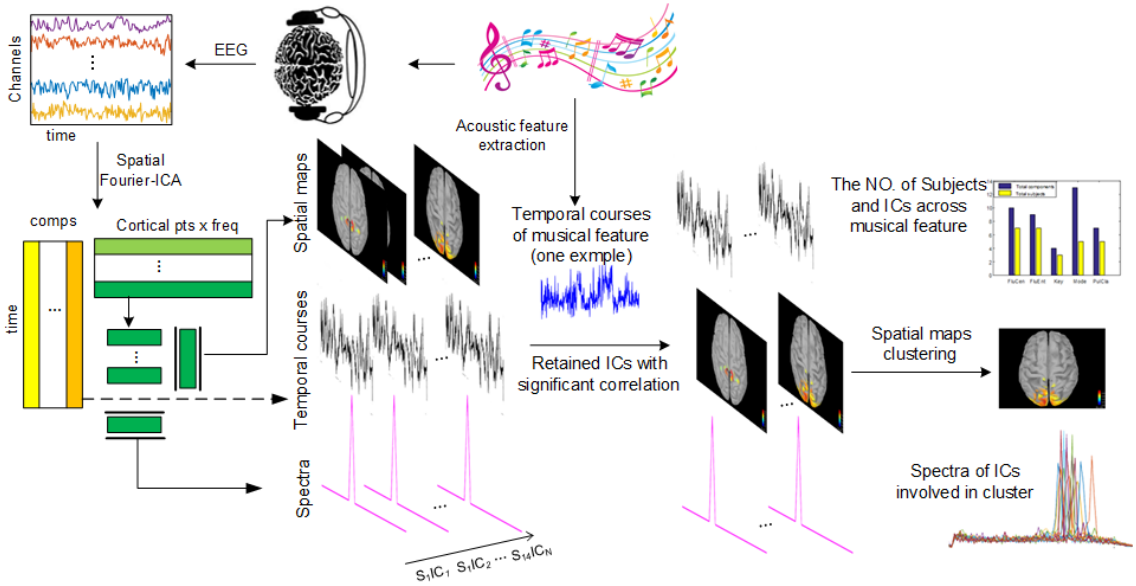

FIGURE 7 The schematic illustration of the pipeline combining spatial Fourier-ICA with musical feature extraction.

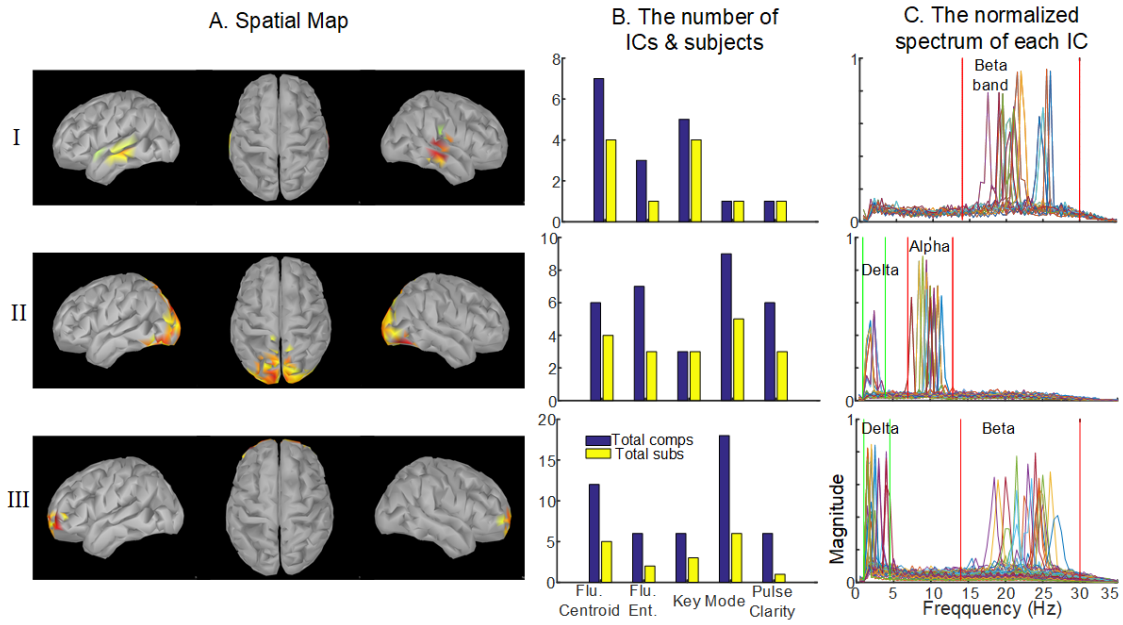

FIGURE 8 The clustering results. A. the centroid of spectral profiles in cluster. B. the number of ICs and subjects involved in the cluster. C. the spectra of each components belonging to this cluster.

4.2.3 Results

We obtained three spectral-spatial patterns significantly correlated with music features. First, there exist brain responses with involved Beta oscillations in bilateral superior temporal gyrus (STG). This Beta-dependent brain pattern seems to be linked to dynamic processing of musical features such as Fluctuation Centroid and Key (Figure 8 I). Second, row II of Figure 8 shows relatively large-

scale brain activity in bilateral visual regions. The spectrum of this pattern is dominated by Alpha oscillations focusing on 10 Hz with several independent components of Delta. The last one is the increased activity associated with musical features in bilateral prefrontal gyrus (Figure 8 III). There regions are recruited with spectrum involved in both Beta and Delta rhythm.

4.2.4 Discussion and conclusion

We observed Beta-specific brain networks in the bilateral STG emerged for processing musical features. This bilateral STG were mostly recruited during freely music listening, which was engaged in musical feature processing. Interestingly, Beta oscillations were increased in these brain regions that were observed in previous fMRI study. Here, Beta rhythm related to motor and rhythmic processes were involved, because listeners might voluntarily engage in mental activities related to motor. Alpha oscillatory visual networks were also found. Alpha oscillations play an important role in basic cognitive process, which is linked to suppression and selection of attention. Thus, this could be the reason that the alpha-specific power over visual cortices was larger when attention was focused on the auditory stimuli. In addition, prefrontal cortex offers the structural basis for multiple higher cognitive functions and oscillatory dynamics of prefrontal cortex provides a functional basis for flexible cognitive control of goal-directed behavior. Delta and Beta oscillations are crucial to predicting the occurrence of auditory targets. That may be why we observed delta-beta rhythms in prefrontal cortex. These results imply that brain networks for musical feature processing might be frequency-specific.

4.3 Distinct Patterns of Functional Connectivity During the Comprehension of Natural, Narrative Speech (*Publication III*)

Yongjie Zhu, Jia Liu, Tapani Ristaniemi and Fengyu Cong. (2020). Distinct Patterns of Functional Connectivity During the Comprehension of Natural, Narrative Speech. *International Journal of Neural Systems*, 30(3), 2050007-2050021.

4.3.1 Motivation

Recent studies show that when people successfully comprehend a narrative speech, a stable EEG component emerges in the centro-parietal region of the brain, but it does not appear when listening to meaningless speech (Broderick, Anderson, Di Liberto, Crosse, & Lalor, 2018; Di Liberto, O'Sullivan, & Lalor, 2015). However, it is not clear whether specific patterns of functional connectivity would emerge in the brain when successfully comprehending a story. Additionally, Shine et al. applied principal component analysis (PCA) to examine the integration of brain functional networks during multitasking, and found that low-dimensional representations were associated with dissociable cognitive

functions and specific patterns of network-level topology (Shine, Breakspear, et al., 2019; Shine, Hearne, et al., 2019). Based on these studies, we would like to adopted PCA techniques to examine the functional network configuration during the comprehension of narrative speech.

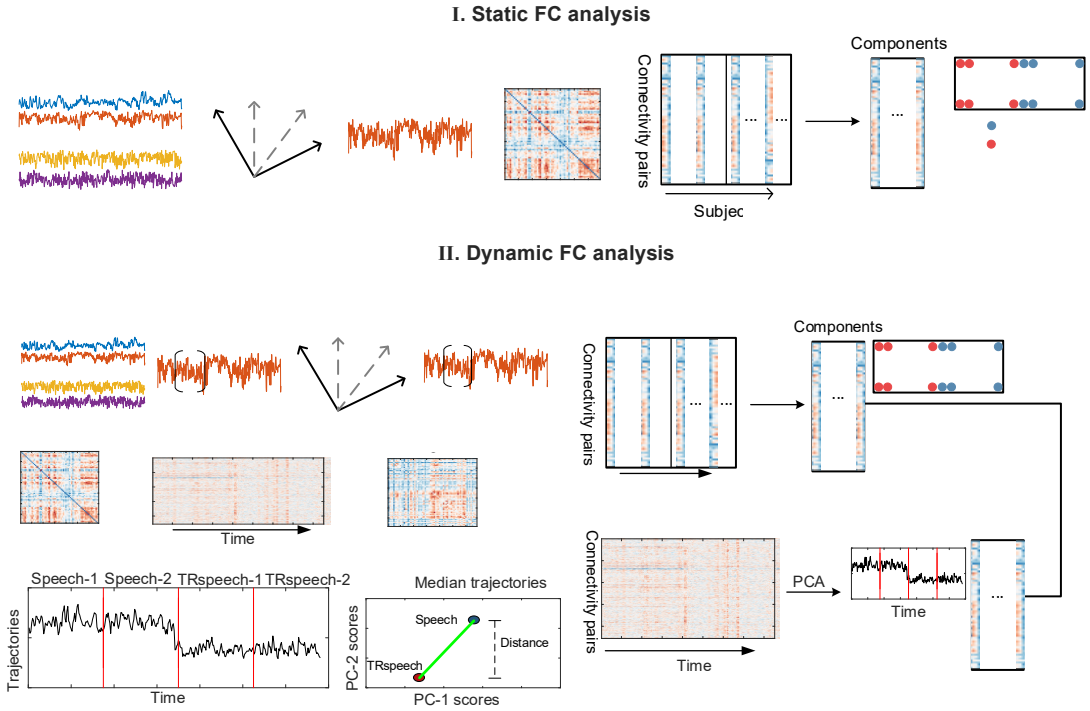

FIGURE 9 The pipeline of analysis. Before the calculation of FC, leakage reduction was performed via orthogonal correction. For static FC analysis, PCA was used to subject-concatenated adjacent matrices (I). For dynamic FC, PCA was used to temporally concatenated adjacent matrices. The condition-specific spatial patterns were determined by similarity analysis with static FC (II.B). The median trajectories were tested between conditions (II.C).

4.3.2 Methods

We analyzed the 128-channel EEG data collected under two conditions: listening to natural, narrative audiobook and the same audiobook in a time-reversed fashion (Broderick et al., 2018). We used the Hilbert-envelop-based correlations between pairs of brain region signals derived from source-level EEG as metric of connectivity. We first examined the static functional connectivity (FC) that was computed across whole time and PCA was performed on the adjacent matrices that are concatenated across subjects (Figure 9I). We then analyzed the dynamic FC based on a sliding window technique. PCA was also applied to temporally concatenated dynamic FC across subjects/runs (Figure 9II). We examined the differences in trajectory of temporal evolutions of extracted FC (characterized by principle components) between two conditions (speech vs reversed speech). Finally, we examined the role of time-locked events on FC dynamics by measuring the similarity between temporal dynamic FCs over conditions and runs. Please see (Zhu, Liu, Ristaniemi, & Cong, 2020) for more details.

4.3.3 Results

We observed a specific FC patterns characterized by the first principal component, which explained 39.8% of the variance (Figure 10). It can differentiate the normal speech listening condition from the time-reversed speech condition. Its projection coefficients were significantly different between two conditions. This condition-dependent pattern explained the specific changes in FC under the speech comprehension. We found that the dynamic FC analysis also shown condition specificity over time, especially when subjects successfully comprehended both the same and different speech.

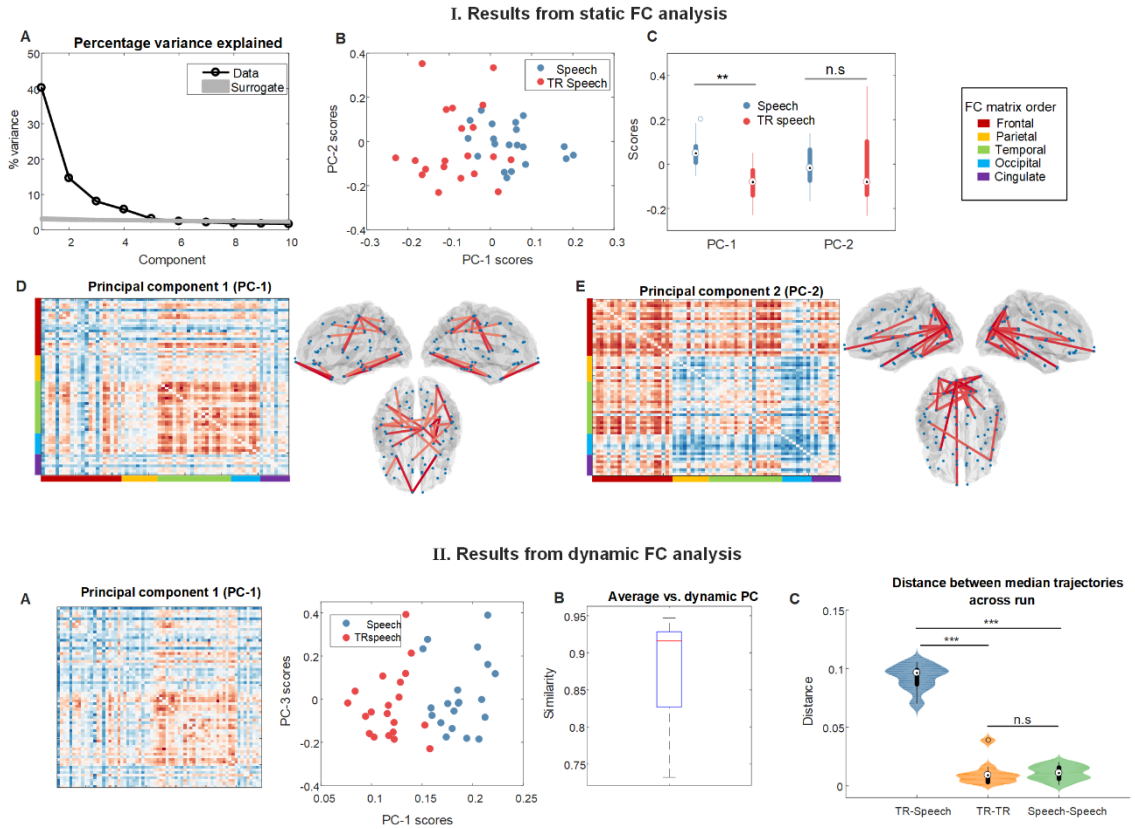

FIGURE 10 The results of FC analysis. I.A. Explained variance by each component (black line) and surrogates (gray line). I.B. The projections of first two components and their boxplot (I.C), and FC profiles (I.D&E). II.A. Condition-specific FC and similarity with static FC (II.B). II.C. The differences in median orbit.

4.3.4 Discussion and conclusion

The brain networks are highly dynamic and can tune spatial topology at a very fine time-scale under a chaning environment. We here presented an analysis framework and examined the reorganization of FC during comprehending speech. The results shown that the pattern of dynamic FC during speech-comprehension might be explained by a single mode of variation. Such FC pattern, during successfully comprehending a natural speech, can track the fluctuations over subjects, which appears as a continuous brain functional state across time.

4.4 Discovering dynamic task-modulated functional networks with specific spectral modes (*Publication IV*)

Yongjie Zhu, Jia Liu, Chaoxiong Ye, Klaus Mathiak, Piia Astikainen, Tapani Ristaniemi and Fengyu Cong. (2020). Discovering dynamic task-modulated functional networks with specific spectral modes using MEG. *NeuroImage*, 218.

4.4.1 Motivation

Human brain consists of billions of interconnected neurons that form a very complicated dynamic system, where populations of neurons are clustered into functional units with unique information-processing capabilities (Babiloni et al., 2005; Hillebrand et al., 2012). Effective neural communication between theses separate units is crucial for cognition (Salinas & Sejnowski, 2001; Siegel, Donner, & Engel, 2012). The interactions between separate regions via neuronal synchronization might offer a possible basis of such communication (i.e., communication through coherence), which means neuronal populations route information by mediating their oscillatory patterns with the oscillations of the receptor population at certain frequencies (Fries, 2005, 2015). Additionally, phase-coupling between separate neuronal populations in specific frequency has been generally accepted as a mechanism for coordinating the integration and flow of cognitive contents (Buzsáki & Draguhn, 2004; Vidaurre, Hunt, et al., 2018). An accumulating evidence demonstrated that such frequency-dependent phase-coupling is crucial for task performance, in which task-related information is delivered via phase-locking across the entire brain (Bola & Sabel, 2015; Fries, 2015). For example, MEG studies have shown that large scale functional networks engaged in cognitive tasks involve different frequency ranges in their coordination. In other words, functional networks demonstrate the specificity in spectral domain. Moreover, increasing studies show that functional networks display extremely temporally variable neuronal dynamics on rapid timescales (Kopell, Gritton, Whittington, & Kramer, 2014), which suggest functional connectivity is temporally non-stationary. However, few studies investigating dynamic brain networks have simultaneously considering temporal non-stationarity, spectral structure, and spatial signatures. We thus attempt to apply tensor decomposition to characterize the large-scale coupling network dynamics during traditional well-controlled task paradigms.

4.4.2 Methods

We analyzed MEG data from the human connectome project (HCP), including a motor task and a 2-back working memory task (Larson-Prior et al., 2013). We first calculate the time-frequency domain connectivity among spatially separate brain regions pre-defined by cortical parcellation. *Weighted phase lag index* (wPLI) is applied as a metric of measuring the connectivity due to its insensitivity to signal leakage (Vinck et al., 2011). After measurement of wPLI at each time point and

frequency point, we form a three-way tensor containing frequency, time, and connection. We then perform tensor decomposition with CP model (Kolda & Bader, 2009) to extract separate components with low-dimensional factors, corresponding to a functional connectivity pattern with fast transient dynamics and specific spectral mode. After CP decomposition, we attempt to determine the task-modulated component by permutation test on its temporal courses (see figure 11).

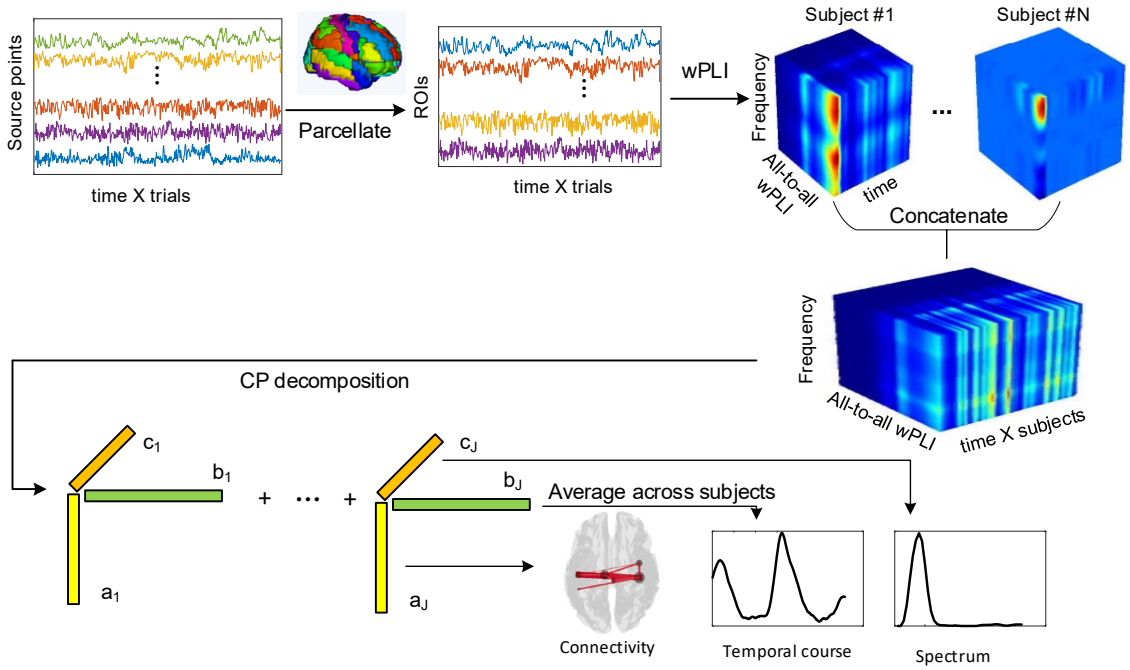

FIGURE 11 The schematic illustration of the pipeline based on CP decomposition for analyzing multi-way FC. CP decomposition can extract low-dimensional, interacted descriptions of connection data: connectivity factor, reflecting spatial patterns of FC; temporal factor, reflecting rapidly time-evolving of the FC; spectral factor, reflecting spectral signatures of FC.

4.4.3 Results

For the motor task, we observed two significantly task-modulated brain networks with distinct spectra (Figure 12). One demonstrates the connections within the primary somatosensory and motor regions with Beta dominate spectrum, which is modulated by the hand movement task. Another one exhibiting connections across visual regions with low frequency spectrum is significantly modulated by visual cues. For the working memory task, multiple brain networks with specific spectral modes demonstrate the task modulation (Figure 13). For example, face presentation modulates right lateralized connections between visual and temporal areas with a spectral mode spanning alpha band, Beta-specific motor network is related to button press execution and other high-order cognition networks including language-related network also emerge during working memory.

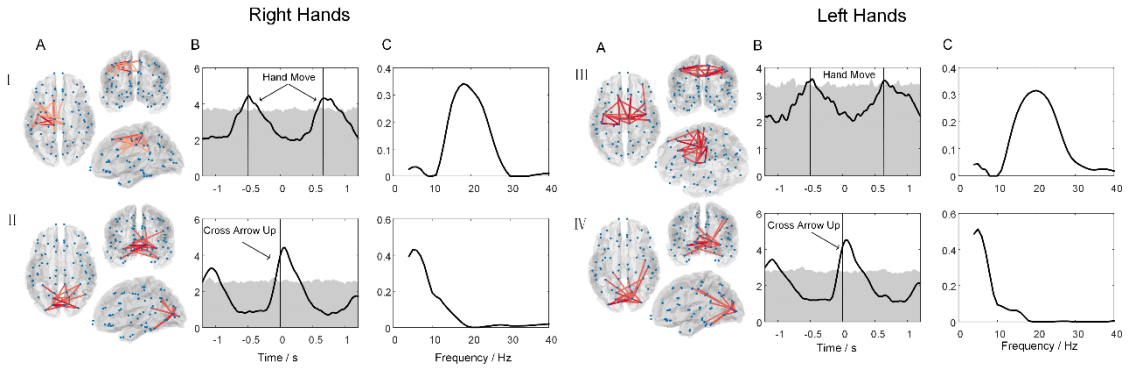

FIGURE 12 Results of the hand movement experiments. The left side shows the results of the right hands' movement, and the right side shows the results of the left hands' movement.

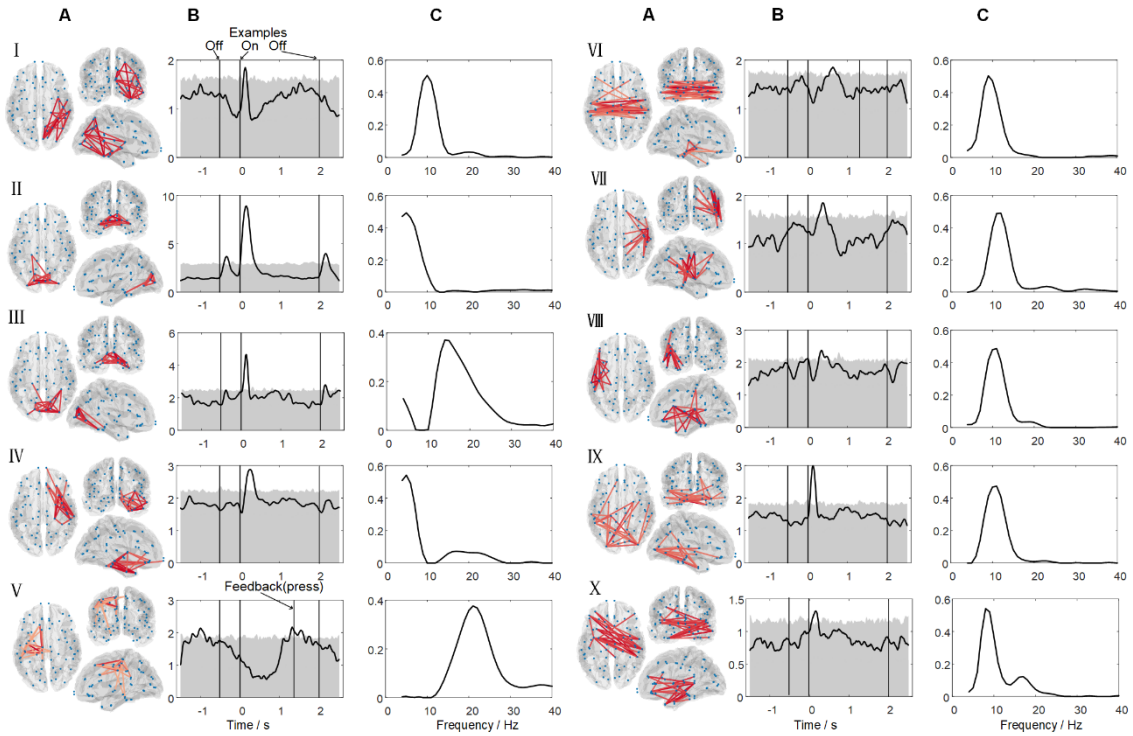

FIGURE 13 Results of 2-back working memory task. A) 3D network visualization. B) Average temporal course (black line) and null distribution based on randomized onset times (shaded areas). C) Spectral mode of the network patterns. Row I: right-lateralized connections between visual and temporal areas with a spectral mode spanning alpha band. Rows II and III: primary visual networks with theta and high-alpha dominant spectrum. IV: connections between right frontal areas and temporal areas related to theta band. V: Beta-specific motor network. VI: a bilateral temporal connectivity network with dominated alpha rhythm. VII: alpha-dependent right-lateralized temporoparietal network. VIII: language-related network. IX: visual to parietal with alpha-dominant spectrum. X: connections between left frontal regions and right temporal regions.

4.4.4 Discussion and conclusion

This study presents a tensor-based framework for extracting phase-coupling dynamic networks with specific spectra. Such analysis framework enables us to characterize transient reconfiguration of electrophysiological functional networks at a timescale of sub-seconds when applied to MEG data of traditional paradigms. Previous approaches of MEG-networks typically pre-select the frequency band or the temporal window around the task onset before computing connectivity. The current method based on CP decomposition is completely data-driven. We validate the framework in a simplified motor task, where we successfully identified a sensorimotor network with Beta-dominate spectrum during finger movement and a visual network with Theta-dominate spectrum modulated by visual cues. However, several key points should be noted. Note that there is significant variability in the time courses of functional connectivity across subjects due to the high temporal resolution of MEG connectivity. Such variance is demonstrated in the averaged temporal courses across subjects. Another limitation is that the task-modulated components were identified by averaging their temporal courses. Such less-relaxed assumption may reject some components probably engaged in task as a result of the inter-subject differences.

4.5 Deriving the frequency-specific functional connectivity during naturalistic music listening with tensor decomposition (*Publication V*)

Yongjie Zhu, Jia Liu, Klaus Mathiak, Tapani Ristaniemi and Fengyu Cong. (2019). Deriving electrophysiological brain network connectivity via tensor component analysis during freely listening to music. *IEEE Transactions on Neural Systems and Rehabilitation Engineering*, 28(2), 409-418.

4.5.1 Motivation

We have applied the tensor-based framework to the traditional simplified task experiments and successfully identified task-modulated electrophysiological brain networks. Here, we would like to applied such framework to ongoing EEG data collected during natural music listening to track the transient network dynamics in a naturalistic fashion.

4.5.2 Methods

We used EEG data of 14 right-handed and healthy adults with BioSemi electrode caps (64 channels). Source-level data were obtained from the preprocessed EEG though source reconstruction. Whole brain was divided into 68 anatomical regions based on an Atlas. We obtained a representative time series for each region by defining a seed voxel. We estimate the time-frequency connectivity

between all pairs of regions based on a sliding window method (3s duration, 2s overlap). In each time window, we measured the wPLI. All the temporal windows result in time-frequency connectivity, as a function of time and frequency, and construct a three-way tensor. Then, we applied the CP decomposition on temporally concatenated tensor to extract the spatial, temporal, and spectral factors. Five acoustic features including tonal and rhythmic features were extracted by frame-by-frame analysis technique (3s duration, 2s overlap) from musical audio. We performed a surrogate permutation procedure to examine how music modulates electrophysiological brain networks (Figure 14).

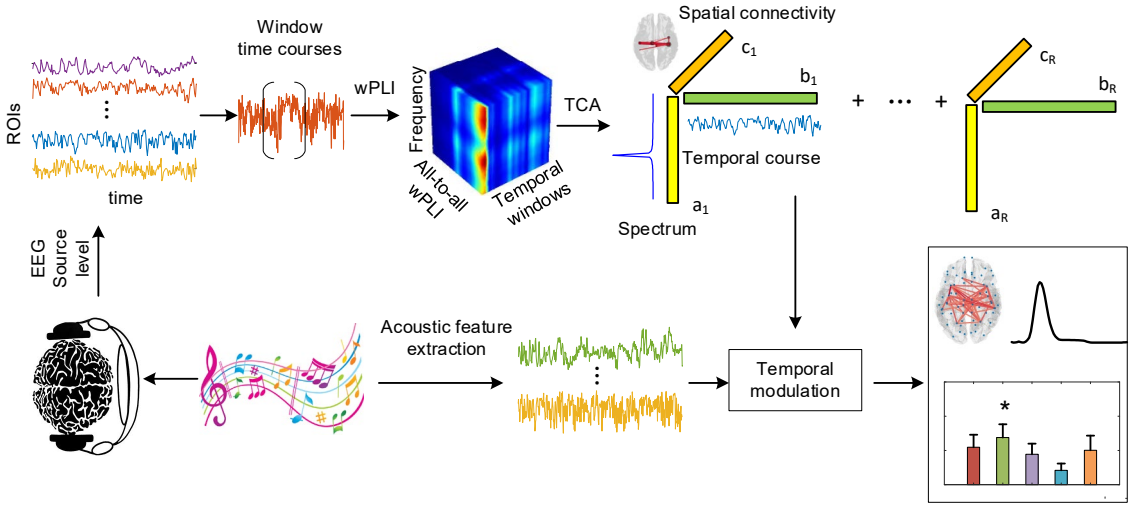

FIGURE 14 The schematic illustration of the pipeline combining CP decomposition with musical feature extraction. Correlation analysis is then conducted between temporal courses of musical features and TCA components to examine the modulation of brain patterns.

4.5.3 Results

We obtained multiple brain networks with specific spectra modulated significantly by musical features, which includes higher-order cognitive, sensorimotor and auditory networks (Figure 15). The higher-order cognitive brain networks such as bilateral frontal functional networks have distinct spectral patterns. One of them is involved in low-frequency rhythms (3-8 Hz); anther one is dominated by Beta oscillations (20-30 Hz). We also observed a 10 Hz unilateral functional networks, relating to Broca's and temporal regions, which are associated with semantic integration. A sensorimotor network with Beta-dominate spectrum is modulated by Fluctuation Entropy. Several networks mainly related to auditory regions were observed during music listening.

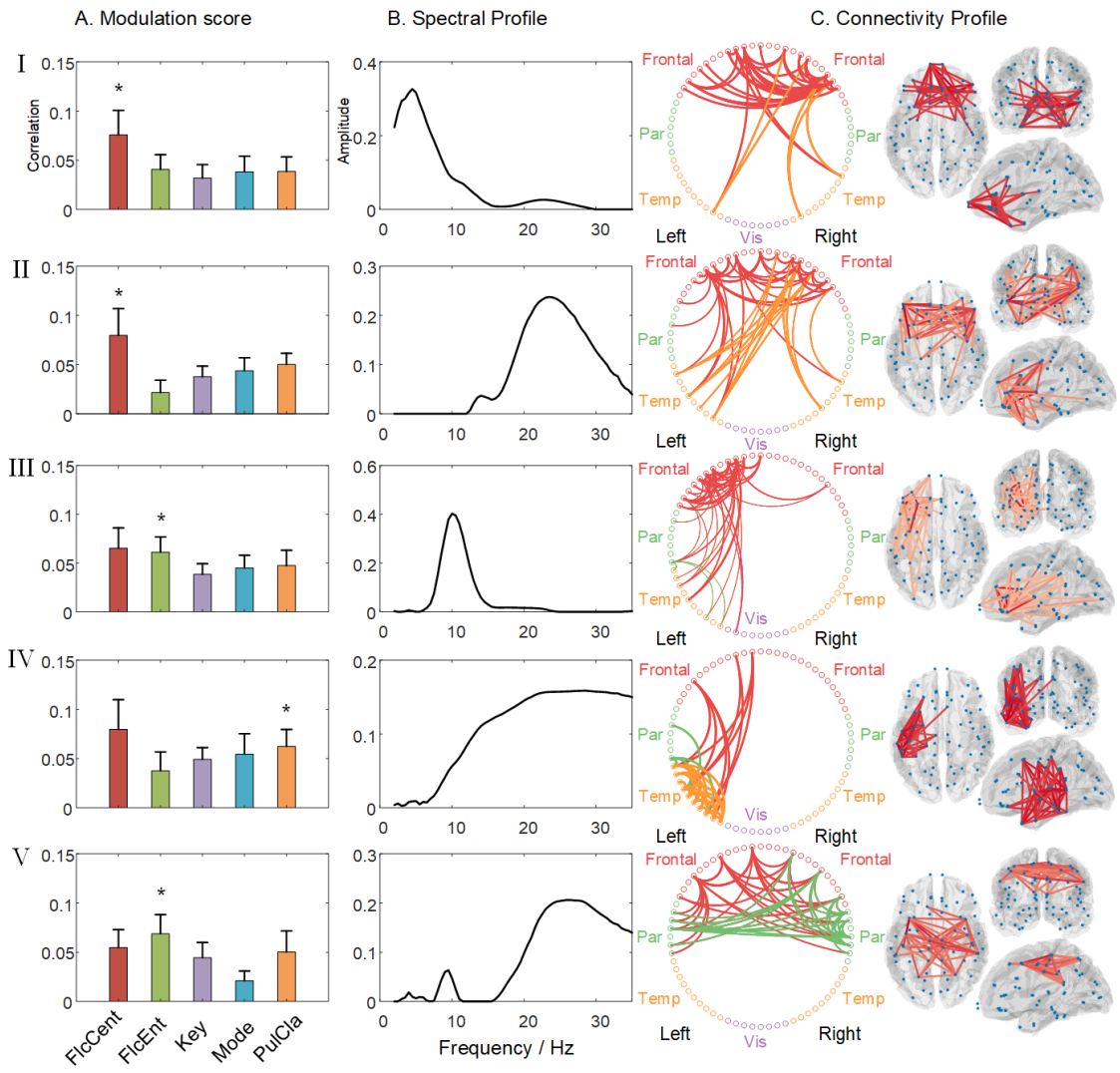

FIGURE 15 The results for music-listening data. A. The modulation scores for each musical feature are computed from the temporal course and averaged across subjects. Error bars represent standard errors of mean. An asterisk indicates that the component is modulated significantly differently from surrogate data. B. The spectral profiles are obtained from the spectral factor matrix. C. The circular phase-coupling plots and the 3D visualization of the connectivity profiles. Each node/dot represents one brain region. I. Anterior higher-order cognitive network with dominant delta/theta frequencies. II. Beta-specific higher-order cognitive network. III &IV. Language-related network with distinct spectral modes. V. Beta-specific motor network.

4.5.4 Discussion and conclusion

This work presents the tensor-based framework successfully applied to natural music listening, in which it tracks the temporal evolutions of electrophysiological brain networks. It enables to better understand the reconfiguration of functional networks and might provide a new insight into the characterization of temporal and spectral dynamics of phase-coupling networks under naturalistic conditions.

5 DISCUSSION AND CONCLUSIONS

These studies in this thesis introduce novel approaches to examine the non-stationarity and frequency-specificity of electrophysiological network connectivity. Increasing pieces of evidence have shown that functional connectivity exhibits dynamic behavior at the time scales of milliseconds (for neural activity) or seconds (for cerebral blood flow), with a rich spatiotemporal structure (de Pasquale, Corbetta, Betti, & Della Penna, 2018; Gonzalez-Castillo et al., 2015; Khambhati, Sizemore, Betzel, & Bassett, 2018; Sadaghiani, Poline, Kleinschmidt, & D'Esposito, 2015). Moreover, functional connectivity computed by M/EEG has also been proven to differ across frequency bands (Bola & Sabel, 2015; Brookes et al., 2014). For such multi-way and multi-scale connectivity analysis, we have shown that it is possible to examine the time scale on which connectivity could be measured from minutes and seconds to sub-seconds through exploiting the high time resolution of M/EEG. Specifically, we presented several analysis frameworks mainly based on matrix/tensor decomposition to assess the dynamic electrophysiological connectome during task performance, especially naturalistic tasks. In the first study, we applied CP decomposition to single-trial wavelet-transformed representations of EEG data recorded in simplified paradigms, to extract the stimuli-induced oscillatory brain activity. In the second study, by combining spatial Fourier-ICA with acoustic feature extraction, we probed the spatial-spectral signatures of brain patterns during continuously listening to natural music. In the third study, we examined the connectivity dynamics during natural speech comprehension via performing PCA on envelope-based connectivity measurements concatenated across time or subjects. In the fourth study, we introduced a novel approach based on CP decomposition to investigate the task-related functional networks with a distinct spectrum during self-peace movement and working memory tasks. Then, we extended this tensor-based method of analyzing network dynamics during natural music listening in the fifth study.

5.1 Methodological considerations

5.1.1 Measures of connectivity

As we mentioned, there are typically two categories of coupling methods measuring connectivity, which concentrates on different aspects of the electrophysiological signal. They tend to uncover different components of broad functional connectivity profile due to for example the rich spatial and temporal information of MEG. Envelope-based connectivity tends to better characterize the long-range connectivity that resemble these functional networks observed in fMRI and it has been shown to successfully duplicate results obtained in fMRI during both task and resting states (Colclough et al., 2016). Before the increasing interest in connectivity analysis, there was a lot of studies to explore the relationship between the hemodynamic responses and fluctuation in amplitude of neuronal oscillations. Subsequently, it is natural to apply amplitude-based connectivity in M/EEG data to resemble functional networks observed in fMRI and there have been many developed approaches based on amplitude correlation to examine the relations. Thus, envelope-based connectivity would be a good choice if you aimed to compare electrophysiological functional networks with those seen in fMRI.

However, phase-based measures also play a crucial role in electrophysiological network connectivity analysis since they have been successfully applied in many studies. They typically rely partly on whether the analysis is hypothesis- or data-driven. For example, if a small number of specific connectivity patterns was hypothesized, coherence combined with correction of signal leakage would be an appropriate option due to its maximal sensitivity to detecting connections. On the other hand, measures of connectivity that is insensitive to signal leakage would be a good option under the situations, where there are no or few hypotheses. Another consideration is that averaging over trials or time when calculating connectivity. It depends on the experiment paradigms. For example, we used the calculation averaging over trials in the repeated stimuli paradigms since its higher temporal resolution allows to better track fast transient changes in connectivity, but we applied averaging over time in naturalistic tasks because it is more sensitive to detect high-frequency connectivity.

5.1.2 Limitations of the sliding window method

In naturalistic paradigms, the sliding window is commonly used to measure the dynamic connectivity. We need to determine the length of the window during sliding window and thus the crucial issue is how to select the window length. There is a trade-off between the temporal precision and the SNR when choosing the window length. In other words, if the length was too small, results would be contaminated by noise; contrarily, if the length was too long, it might fail to track fast transient fluctuations in connectivity. The optimal length would match the

timescale of underlying variations of connectivity, but such timescale is unknowable and might fluctuate over the time course of a task. Similar to time-frequency analysis for nonstationary signals, a window length should depend on the frequency band. In other words, it should rely on the number of degrees of freedom in a time window of the signal. Some studies have already investigated the effect of window length on dynamic analysis and introduced the instruction based on Fourier theory (O'Neill et al., 2018; O'Neill et al., 2017). It should be carefully considered in the future study.

5.1.3 Matrix decomposition

Matrix decomposition such as ICA and PCA enables data-driven exploration of dynamic connectivity. There are two strategies of applying ICA for functional network analysis. One is to directly perform ICA on data of activation time series without calculating connectivity between regions or electrodes and another apply it on data of connectivity time courses. For the direct application on activation time courses, ICA based on the independence assumption of underlying sources has been widely used in both fMRI and M/EEG studies. In fMRI studies, spatial ICA could be performed on spatiotemporal data to extract statistically independent spatial map that was considered as coherent functional network (Damoiseaux et al., 2006; De Luca, Beckmann, De Stefano, Matthews, & Smith, 2006). The idea is that the source points comprising spatial map share the same temporal courses (rows of mixing matrix) and thus these independent spatial maps together with associated time courses were thought of as functional networks (high temporal correlations among these voxels). In M/EEG studies for connectivity, temporal ICA could be used to band-limited Hilbert envelope signals from all source points and then the extracted temporally independent components were correlated with time courses of each voxels to determine the spatial maps that represent the functional networks (Brookes, Woolrich, et al., 2011). This procedure needs to pre-select the frequency band or is implemented independently for each frequency band of interest. Subsequently, ICA of Fourier envelope of electrophysiology data were proposed to allow data-driven exploration of frequency-dependent functional networks (Ramkumar et al., 2012; Ramkumar et al., 2014). Thus, in our *publication II*, we adopted this spatial Fourier-ICA to ongoing EEG data recorded during naturalistic music-listening based on the consideration of its advantage that automatically extracts specific oscillatory activity from wideband data without pre-selecting the frequency band of interest (Zhu, Zhang, et al., 2020).

Distinct from directly implementing decomposition on activation time courses, ICA or PCA could be implemented on connectivity time courses to look at connectivity patterns with temporally covarying. For example, applying ICA to connectivity time courses could allow to extract common temporal courses across connections between pairs of nodes (O'Neill et al., 2017). In this procedure, each temporally independent component indicates the time evolution of connectivity and each column of the mixing matrix represents a pattern of connections with similarly modulated way, representing a network in which all

connections share a similar behavior (O'Neill et al., 2017). Similarly, PCA could also be applied to connectivity data. In this case, PCA allows to uncover hidden patterns of coherent connectivity dynamics across time or multiple subjects (Leonardi et al., 2013). It has been shown the success in the extraction of meaningful patterns in functional connectivity fluctuations in our *publication III*.

However, in some cases, there might be several inconveniences when using matrix decomposition despite its success in dynamic connectivity analysis. For example, multi-way data were reorganized into a two-way data to facilitate ICA estimation, which might inevitably lose some potentially existing interactions between different modes. Alternatively, one could perform independently multiple decomposition such as for each frequency band of interest.

5.1.4 Tensor decomposition

Tensor decomposition, as a high order extension of matrix decomposition, can be used for multi-way analysis. Similar to the application of matrix decomposition in neuroimaging data, there are also two strategies comprised of implementing decomposition on representations of activation data and connectivity data. In our *publication I*, we performed tensor decomposition on data representations of single-trial time courses to examine the stimuli-induced oscillatory brain activity. Following this, we implemented decomposition on the multi-way connectivity representations in our *publications IV, V*. Although tensor decomposition allows multi-way analysis for connectivity dynamics, it should be careful with the interpretation of results. Additionally, tensor decomposition, such as CP model, implicitly leverages the principle of parallel proportional profiles. This, for an example of the neuroimaging data with time, electrode and subject, implied that the underlying brain process has the exact same time courses and spatial topography across subjects, which is a rather strict assumption in this case. Future work should note this implicit assumption.

5.2 Brain activity during naturalistic paradigms

In these studies of this thesis, electrophysiology brain networks were examined not only during repetitive tasks but also in naturalistic paradigms. It is more beneficial for a deeper understanding of adaptive brain function to investigate the oscillatory mechanism and network interactions during naturalistic conditions, compared with the experiment design with simplified repeated tasks (Sonkusare et al., 2019). In addition, they have the potential to reduce boredom and repetitive cognitive demands especially for children during naturalistic conditions (Vanderwal et al., 2019). However, there still are issues to be addressed in future work. Unlike simplified tasks, and more similar to resting state, these natural conditions lack apparent or intrinsic measurements of the task performance and attention. To possibly address this issue, there are an increasing number of solutions, including non-disruptive solutions such as in-scanner eye-

tracking, and semi-disruptive measures such as feedback of button press during music listening.

Another challenge it to disentangle the stimuli-related signal changes or fluctuations in connectivity under the complex, dynamic conditions. Many approaches were introduced in the past decades to address this gap. For example, inter-subject functional connectivity based on stimuli-locked dynamics was developed to reveal shared, stimulus-locked patterns of functional connectivity (Simony et al., 2016). Other studies have been starting to address this challenge to achieve the rich level of stimuli annotation required to benefit the model-based approach (Bartels & Zeki, 2004; Häusler & Hanke, 2016; Lahnakoski et al., 2012; Salmi et al., 2014). Similar to the annotation of stimulus, we automatically extracted cognition-related musical features from the music stimulus as the time series of annotation to determine the music-related fluctuations of brain functional connectivity.

Another open question is that whether complex cognitive dynamics that occur during naturalistic stimuli be separated into discrete and independent neural processes associated with specific events/tasks (e.g. the presence or absence of faces, or certain auditory features during movie watching), and to what degree is a naturalistic stimulus simply just a sum of its task-parts? (Eickhoff et al., 2020) Our approach based on matrix/tensor decomposition might provide a new insight into such question. The idea is to identify separate brain network dynamics extracted from signal decomposition and to perform correlation analysis with specific mysical feature extracted from music stimulus.

5.3 Future directions

This thesis investigated the network dynamics in a group of healthy subjects during experimental tasks especially during music listening. We will study differences in neural processing between normal and abnormal subjects in future work. Some studies already shown that natural task such as movie watching might more easily evoke attentional performance in attention-deficit hyperactivity disorder, or other psychotic illness (Rikandi et al., 2017; Salmi et al., 2019). We will extend our frameworks to allow us to examine the neural difference between groups.

Another direction is to examine the individual differences in brain responses during naturalistic conditions. At present, there are two ongoing movements in cognitive neuroscience. One is shifting focus from group-level inference to individual characterization (Bartolomeo, Malkinson, & De Vito, 2017; Dubois & Adolphs, 2016; Seghier & Price, 2018). Another one is exploiting the complexity of naturalistic paradigms to complement tightly well-controlled experimental tasks (Sonkusare et al., 2019). However, relatively few studies combine these two aspects, probably since traditional analysis methods for naturalistic imaging data are designed to detect shared responses rather than between-subject variability (Finn et al., 2020).

YHTEENVETO (SUMMARY IN FINNISH)

Tämän tutkielman tutkimukset esittävät uusia lähestymistapoja sähköfysiologisen verkkoyhteyden ei-stationaarisuuden ja taajuusspesifisyyden tutkimiseen. Esitimme erityisesti useita analyysikehyksiä, jotka perustuvat pääasiassa matriisin / tensorin hajoamiseen, jotta voidaan arvioida dynaamista elektrofysiologista konnekomia tehtävän suorittamisen aikana, erityisesti naturalististen tehtävien aikana. Ensimmäisessä tutkimuksessa käytimme CP-hajotusta yksinkertaistettuihin paradigmoihin tallennettujen EEG-tietojen yksitutkimuksisilla, aaltomuodolla muunnetuilla esityksillä ärsykkeiden aiheuttaman värähtelevän aivotoiminnan purkamiseksi. Toisessa tutkimuksessa yhdistämällä spatiaalinen Fourier-ICA akustisten ominaisuuksien poimimiseen tutkimme aivokuvioiden avaruus-spektriset allekirjoitukset kuunnellessamme jatkuvasti luonnollista musiikkia. Tulokset osoittivat, että musiikillisten ominaisuuksien käsittelyn aivoverkot olivat taajuusriippuvaisia. Kolmannessa tutkimuksessa tutkimme yhteyden dynamiikkaa luonnollisen puheen ymmärtämisen aikana suorittamalla PCA:ta kirjekuoripohjaisilla liitettävyysmittauksilla, jotka on ketjutettu ajallisesti tai aiheista, ja osoitimme, että erilliset aivoverkot syntyvät onnistuneen puheen ymmärtämisen aikana. Neljännessä tutkimuksessa esiteltiin uusi CP-hajoamiseen perustuva lähestymistapa tehtävään liittyvien toiminnallisten verkkojen tutkimiseksi, joilla on erillinen spektri itse rauhan liikkumisen ja työmuistin tehtävien aikana. Sitten laajensimme tätä tensoripohjaista menetelmää verkkodynamiikan analysoimiseksi luonnollisen musiikin kuuntelun aikana viidennessä tutkimuksessa. Nämä tulokset osoittivat, että toiminnallisella liitännällä on dynaaminen käyttäytyminen millisekuntien (hermostollisen toiminnan) tai sekuntien (aivoverenkierron) asteikkoalueilla, joilla on rikas spatiotemporaalinen rakenne ja joiden on myös osoitettu eroavan taajuuskaistojen välillä.

REFERENCES

Al-sharoa, E., Al-khassaweneh, M., & Aviyente, S. (2018). Tensor based temporal and multilayer community detection for studying brain dynamics during resting state fMRI. *IEEE Transactions on Biomedical Engineering, 66*(3), 695-709.

Allen, E. A., Damaraju, E., Plis, S. M., Erhardt, E. B., Eichele, T., & Calhoun, V. D. (2014). Tracking whole-brain connectivity dynamics in the resting state. *Cerebral cortex, 24*(3), 663-676.

Alluri, V., Toiviainen, P., Jääskeläinen, I. P., Glerean, E., Sams, M., & Brattico, E. (2012). Large-scale brain networks emerge from dynamic processing of musical timbre, key and rhythm. *Neuroimage, 59*(4), 3677-3689.

Babiloni, F., Cincotti, F., Babiloni, C., Carducci, F., Mattia, D., Astolfi, L., . . . Ni, Y. (2005). Estimation of the cortical functional connectivity with the multimodal integration of high-resolution EEG and fMRI data by directed transfer function. *Neuroimage, 24*(1), 118-131.

Baker, A. P., Brookes, M. J., Rezek, I. A., Smith, S. M., Behrens, T., Probert Smith, P. J., & Woolrich, M. W. (2014). Fast transient networks in spontaneous human brain activity. *eLife, 3*.

Bartels, A., & Zeki, S. (2004). The chronoarchitecture of the human brain—natural viewing conditions reveal a time-based anatomy of the brain. *Neuroimage, 22*(1), 419-433.

Bartolomeo, P., Malkinson, T. S., & De Vito, S. (2017). Botallo's error, or the quandaries of the universality assumption. *Cortex, 86*, 176-185.

Başar, E., Başar-Eroğlu, C., Karakaş, S., & Schürmann, M. (1999). Are cognitive processes manifested in event-related gamma, alpha, theta and delta oscillations in the EEG? *Neuroscience letters, 259*(3), 165-168.

Başar, E., Schürmann, M., Demiralp, T., Başar-Eroglu, C., & Ademoglu, A. (2001). Event-related oscillations are 'real brain responses'—wavelet analysis and new strategies. *International Journal of Psychophysiology, 39*(2-3), 91-127.

Bastos, A., & Schoffelen, J. (2015). A Tutorial Review of Functional Connectivity Analysis Methods and Their Interpretational Pitfalls. *Frontiers in systems neuroscience, 9*, 1–23.

Beal, M. J., Ghahramani, Z., & Rasmussen, C. E. (2002). *The infinite hidden Markov model.* Paper presented at the Advances in neural information processing systems.

Beckmann, C. F., DeLuca, M., Devlin, J. T., & Smith, S. M. (2005). Investigations into resting-state connectivity using independent component analysis. *Philosophical Transactions of the Royal Society B: Biological Sciences, 360*(1457), 1001-1013.

Betti, V., Corbetta, M., de Pasquale, F., Wens, V., & Della Penna, S. (2018). Topology of functional connectivity and hub dynamics in the beta band as temporal prior for natural vision in the human brain. *Journal of Neuroscience, 38*(15), 3858-3871.

Betti, V., Della Penna, S., de Pasquale, F., Mantini, D., Marzetti, L., Romani, G. L., & Corbetta, M. (2013). Natural scenes viewing alters the dynamics of functional connectivity in the human brain. *Neuron, 79*(4), 782-797.

Betzel, R. F., Fukushima, M., He, Y., Zuo, X.-N., & Sporns, O. (2016). Dynamic fluctuations coincide with periods of high and low modularity in resting-state functional brain networks. *Neuroimage, 127*, 287-297.

Birn, R. M. (2012). The role of physiological noise in resting-state functional connectivity. *Neuroimage, 62*(2), 864-870.

Biswal, B., Zerrin Yetkin, F., Haughton, V. M., & Hyde, J. S. (1995). Functional connectivity in the motor cortex of resting human brain using echo - planar MRI. *Magnetic resonance in medicine, 34*(4), 537-541.

Bola, M., & Sabel, B. A. (2015). Dynamic reorganization of brain functional networks during cognition. *Neuroimage, 114*, 398-413.

Brennan, J., Nir, Y., Hasson, U., Malach, R., Heeger, D. J., & Pylkkänen, L. (2012). Syntactic structure building in the anterior temporal lobe during natural story listening. *Brain and language, 120*(2), 163-173.

Broderick, M. P., Anderson, A. J., Di Liberto, G. M., Crosse, M. J., & Lalor, E. C. (2018). Electrophysiological correlates of semantic dissimilarity reflect the comprehension of natural, narrative speech. *Current Biology, 28*(5), 803-809.

Brookes, M. J., Hale, J. R., Zumer, J. M., Stevenson, C. M., Francis, S. T., Barnes, G. R., . . . Nagarajan, S. S. (2011). Measuring functional connectivity using MEG: methodology and comparison with fcMRI. *Neuroimage, 56*(3), 1082-1104.

Brookes, M. J., Liddle, E. B., Hale, J. R., Woolrich, M. W., Luckhoo, H., Liddle, P. F., & Morris, P. G. (2012). Task induced modulation of neural oscillations in electrophysiological brain networks. *Neuroimage, 63*(4), 1918-1930.

Brookes, M. J., O'Neill, G. C., Hall, E. L., Woolrich, M. W., Baker, A., Corner, S. P., . . . Barnes, G. R. (2014). Measuring temporal, spectral and spatial changes in electrophysiological brain network connectivity. *Neuroimage, 91*, 282-299.

Brookes, M. J., Woolrich, M., Luckhoo, H., Price, D., Hale, J. R., Stephenson, M. C., . . . Morris, P. G. (2011). Investigating the electrophysiological basis of resting state networks using magnetoencephalography. *Proceedings of the National Academy of Sciences, 108*(40), 16783-16788.

Brookes, M. J., Woolrich, M. W., & Barnes, G. R. (2012). Measuring functional connectivity in MEG: a multivariate approach insensitive to linear source leakage. *Neuroimage, 63*(2), 910-920.

Buzsáki, G., & Draguhn, A. (2004). Neuronal oscillations in cortical networks. *Science, 304*(5679), 1926-1929.

Chang, C., & Glover, G. H. (2010). Time–frequency dynamics of resting-state brain connectivity measured with fMRI. *Neuroimage, 50*(1), 81-98.

Cohen, M. X. (2014). *Analyzing neural time series data: theory and practice*. Cambridge, MA: MIT press.

Colclough, G. L., Brookes, M. J., Smith, S. M., & Woolrich, M. W. (2015). A symmetric multivariate leakage correction for MEG connectomes. *Neuroimage, 117*, 439-448.

Colclough, G. L., Woolrich, M. W., Tewarie, P., Brookes, M. J., Quinn, A. J., & Smith, S. M. (2016). How reliable are MEG resting-state connectivity metrics? *Neuroimage, 138*, 284-293.

Cong, F., Alluri, V., Nandi, A. K., Toiviainen, P., Fa, R., Abu-Jamous, B., . . . Huotilainen, M. (2013). Linking brain responses to naturalistic music through analysis of ongoing EEG and stimulus features. *IEEE Transactions on Multimedia, 15*(5), 1060-1069.

Cong, F., Lin, Q.-H., Kuang, L.-D., Gong, X.-F., Astikainen, P., & Ristaniemi, T. (2015). Tensor decomposition of EEG signals: a brief review. *Journal of neuroscience methods, 248*, 59-69.

Cong, F., Phan, A.-H., Astikainen, P., Zhao, Q., Wu, Q., Hietanen, J. K., . . . Cichocki, A. (2013). Multi-domain feature extraction for small event-related potentials through nonnegative multi-way array decomposition from low dense array EEG. *International Journal of Neural Systems, 23*(02), 1-18.

Corbetta, M., Akbudak, E., Conturo, T. E., Snyder, A. Z., Ollinger, J. M., Drury, H. A., . . . Van Essen, D. C. (1998). A common network of functional areas for attention and eye movements. *Neuron, 21*(4), 761-773.

Crossley, N. A., Mechelli, A., Vértes, P. E., Winton-Brown, T. T., Patel, A. X., Ginestet, C. E., . . . Bullmore, E. T. (2013). Cognitive relevance of the community structure of the human brain functional coactivation network. *Proceedings of the National Academy of Sciences, 110*(28), 11583-11588.

Damoiseaux, J. S., Rombouts, S., Barkhof, F., Scheltens, P., Stam, C. J., Smith, S. M., & Beckmann, C. F. (2006). Consistent resting-state networks across healthy subjects. *Proceedings of the National Academy of Sciences, 103*(37), 13848-13853.

De Luca, M., Beckmann, C. F., De Stefano, N., Matthews, P. M., & Smith, S. M. (2006). fMRI resting state networks define distinct modes of long-distance interactions in the human brain. *Neuroimage, 29*(4), 1359-1367.

de Pasquale, F., Corbetta, M., Betti, V., & Della Penna, S. (2018). Cortical cores in network dynamics. *Neuroimage, 180*, 370-382.

De Pasquale, F., Della Penna, S., Snyder, A. Z., Lewis, C., Mantini, D., Marzetti, L., . . . Romani, G. L. (2010). Temporal dynamics of spontaneous MEG activity in brain networks. *Proceedings of the National Academy of Sciences, 107*(13), 6040-6045.

de Pasquale, F., Della Penna, S., Sporns, O., Romani, G., & Corbetta, M. (2016). A dynamic core network and global efficiency in the resting human brain. *Cerebral cortex, 26*(10), 4015-4033.

Di Liberto, G. M., O'Sullivan, J. A., & Lalor, E. C. (2015). Low-frequency cortical entrainment to speech reflects phoneme-level processing. *Current Biology, 25*(19), 2457-2465.

Dmochowski, J. P., Bezdek, M. A., Abelson, B. P., Johnson, J. S., Schumacher, E. H., & Parra, L. C. (2014). Audience preferences are predicted by temporal reliability of neural processing. *Nature communications, 5*(1), 1-9.

Dubois, J., & Adolphs, R. (2016). Building a science of individual differences from fMRI. *Trends in Cognitive Sciences, 20*(6), 425-443.

Eickhoff, S. B., Milham, M., & Vanderwal, T. (2020). Towards clinical applications of movie fMRI. *Neuroimage, 217*, 116860.

Engel, A. K., Gerloff, C., Hilgetag, C. C., & Nolte, G. (2013). Intrinsic coupling modes: multiscale interactions in ongoing brain activity. *Neuron, 80*(4), 867-886.

Escudero, J., Acar, E., Fernández, A., & Bro, R. (2015). Multiscale entropy analysis of resting-state magnetoencephalogram with tensor factorisations in Alzheimer's disease. *Brain research bulletin, 119*, 136-144.

Felsen, G., & Dan, Y. (2005). A natural approach to studying vision. *Nature neuroscience, 8*(12), 1643-1646.

Finn, E. S., Glerean, E., Khojandi, A. Y., Nielson, D., Molfese, P. J., Handwerker, D. A., & Bandettini, P. A. (2020). Idiosynchrony: From shared responses to individual differences during naturalistic neuroimaging. *Neuroimage, 215*, 116828.

Fox, M. D., & Raichle, M. E. (2007). Spontaneous fluctuations in brain activity observed with functional magnetic resonance imaging. *Nature reviews neuroscience, 8*(9), 700-711.

Fries, P. (2005). A mechanism for cognitive dynamics: neuronal communication through neuronal coherence. *Trends in Cognitive Sciences, 9*(10), 474-480.

Fries, P. (2015). Rhythms for cognition: communication through coherence. *Neuron, 88*(1), 220-235.

Friston, K. J. (1994). Functional and effective connectivity in neuroimaging: a synthesis. *Human brain mapping, 2*(1 - 2), 56-78.

Friston, K. J. (2011). Functional and effective connectivity: a review. *Brain connectivity, 1*(1), 13-36.

Furey, M. L., Tanskanen, T., Beauchamp, M. S., Avikainen, S., Uutela, K., Hari, R., & Haxby, J. V. (2006). Dissociation of face-selective cortical responses by attention. *Proceedings of the National Academy of Sciences, 103*(4), 1065-1070.

Gonzalez-Castillo, J., Hoy, C. W., Handwerker, D. A., Robinson, M. E., Buchanan, L. C., Saad, Z. S., & Bandettini, P. A. (2015). Tracking ongoing cognition in individuals using brief, whole-brain functional connectivity patterns. *Proceedings of the National Academy of Sciences, 112*(28), 8762-8767.

Grandjean, J., Preti, M. G., Bolton, T. A., Buerge, M., Seifritz, E., Pryce, C. R., . . . Rudin, M. (2017). Dynamic reorganization of intrinsic functional networks in the mouse brain. *Neuroimage, 152*, 497-508.

Groß, J., Kujala, J., Hämäläinen, M., Timmermann, L., Schnitzler, A., & Salmelin, R. (2001). Dynamic imaging of coherent sources: studying neural interactions in the human brain. *Proceedings of the National Academy of Sciences, 98*(2), 694-699.

Hall, E. L., Woolrich, M. W., Thomaz, C. E., Morris, P. G., & Brookes, M. J. (2013). Using variance information in magnetoencephalography measures of functional connectivity. *Neuroimage, 67*, 203-212.

Hari, R., Parkkonen, L., & Nangini, C. (2010). The brain in time: insights from neuromagnetic recordings. *Annals of the New York Academy of Sciences, 1191*, 89-109.

Hassan, M., Benquet, P., Biraben, A., Berrou, C., Dufor, O., & Wendling, F. (2015). Dynamic reorganization of functional brain networks during picture naming. *Cortex, 73*, 276-288.

Hasson, U., Malach, R., & Heeger, D. J. (2010). Reliability of cortical activity during natural stimulation. *Trends in Cognitive Sciences, 14*(1), 40-48.

Hasson, U., Nir, Y., Levy, I., Fuhrmann, G., & Malach, R. (2004). Intersubject synchronization of cortical activity during natural vision. *Science, 303*(5664), 1634-1640.

Häusler, C., & Hanke, M. (2016). An annotation of cuts, depicted locations, and temporal progression in the motion picture" Forrest Gump". *F1000Research, 5*, 2273-2273.

Hillebrand, A., Barnes, G. R., Bosboom, J. L., Berendse, H. W., & Stam, C. J. (2012). Frequency-dependent functional connectivity within resting-state networks: an atlas-based MEG beamformer solution. *Neuroimage, 59*(4), 3909-3921.

Hindriks, R., Adhikari, M. H., Murayama, Y., Ganzetti, M., Mantini, D., Logothetis, N. K., & Deco, G. (2016). Can sliding-window correlations reveal dynamic functional connectivity in resting-state fMRI? *Neuroimage, 127*, 242-256.

Hipp, J. F., Hawellek, D. J., Corbetta, M., Siegel, M., & Engel, A. K. (2012). Large-scale cortical correlation structure of spontaneous oscillatory activity. *Nature neuroscience, 15*(6), 884-890.

Hunt, L. T., Kolling, N., Soltani, A., Woolrich, M. W., Rushworth, M. F., & Behrens, T. E. (2012). Mechanisms underlying cortical activity during value-guided choice. *Nature neuroscience, 15*(3), 470-476.

Hutchison, R. M., Womelsdorf, T., Allen, E. A., Bandettini, P. A., Calhoun, V. D., Corbetta, M., . . . Gonzalez-Castillo, J. (2013). Dynamic functional connectivity: promise, issues, and interpretations. *Neuroimage, 80*, 360-378.

Kätsyri, J., Hari, R., Ravaja, N., & Nummenmaa, L. (2013). The opponent matters: elevated fMRI reward responses to winning against a human versus a computer opponent during interactive video game playing. *Cerebral cortex, 23*(12), 2829-2839.

Khambhati, A. N., Sizemore, A. E., Betzel, R. F., & Bassett, D. S. (2018). Modeling and interpreting mesoscale network dynamics. *Neuroimage, 180*, 337-349.

Knyazev, G. G., Savostyanov, A. N., Bocharov, A. V., Tamozhnikov, S. S., & Saprigyn, A. E. (2016). Task-positive and task-negative networks and their relation to depression: EEG beamformer analysis. *Behavioural brain research, 306*, 160-169.

Koelewijn, L., Bompas, A., Tales, A., Brookes, M. J., Muthukumaraswamy, S. D., Bayer, A., & Singh, K. D. (2017). Alzheimer's disease disrupts alpha and beta-band resting-state oscillatory network connectivity. *Clinical neurophysiology, 128*(11), 2347-2357.

Koelewijn, L., Hamandi, K., Brindley, L. M., Brookes, M. J., Routley, B. C., Muthukumaraswamy, S. D., . . . te Water Naudé, J. (2015). Resting - state oscillatory dynamics in sensorimotor cortex in benign epilepsy with centro - temporal spikes and typical brain development. *Human brain mapping, 36*(10), 3935-3949.

Kolda, T. G., & Bader, B. W. (2009). Tensor decompositions and applications. *SIAM review, 51*(3), 455-500.

Kopell, N. J., Gritton, H. J., Whittington, M. A., & Kramer, M. A. (2014). Beyond the connectome: the dynome. *Neuron, 83*(6), 1319-1328.

Koskinen, M., & Seppä, M. (2014). Uncovering cortical MEG responses to listened audiobook stories. *Neuroimage, 100*, 263-270.

Kujala, J., Pammer, K., Cornelissen, P., Roebroeck, A., Formisano, E., & Salmelin, R. (2007). Phase coupling in a cerebro-cerebellar network at 8–13 Hz during reading. *Cerebral cortex, 17*(6), 1476-1485.

Lachaux, J. P., Rodriguez, E., Martinerie, J., & Varela, F. J. (1999). Measuring phase synchrony in brain signals. *Human brain mapping, 8*(4), 194-208.

Lahnakoski, J. M., Salmi, J., Jääskeläinen, I. P., Lampinen, J., Glerean, E., Tikka, P., & Sams, M. (2012). Stimulus-related independent component and voxel-wise analysis of human brain activity during free viewing of a feature film. *PloS one, 7*(4).

Lankinen, K., Saari, J., Hari, R., & Koskinen, M. (2014). Intersubject consistency of cortical MEG signals during movie viewing. *Neuroimage, 92*, 217-224.

Lankinen, K., Saari, J., Hlushchuk, Y., Tikka, P., Parkkonen, L., Hari, R., & Koskinen, M. (2018). Consistency and similarity of MEG-and fMRI-signal time courses during movie viewing. *Neuroimage, 173*, 361-369.

Larson-Prior, L. J., Oostenveld, R., Della Penna, S., Michalareas, G., Prior, F., Babajani-Feremi, A., . . . Di Pompeo, F. (2013). Adding dynamics to the Human Connectome Project with MEG. *Neuroimage, 80*, 190-201.

Laufs, H., Krakow, K., Sterzer, P., Eger, E., Beyerle, A., Salek-Haddadi, A., & Kleinschmidt, A. (2003). Electroencephalographic signatures of attentional and cognitive default modes in spontaneous brain activity fluctuations at rest. *Proceedings of the National Academy of Sciences, 100*(19), 11053-11058.

Leonardi, N., Richiardi, J., Gschwind, M., Simioni, S., Annoni, J.-M., Schluep, M., . . . Van De Ville, D. (2013). Principal components of functional connectivity: a new approach to study dynamic brain connectivity during rest. *Neuroimage, 83*, 937-950.

Leopold, D. A., Murayama, Y., & Logothetis, N. K. (2003). Very slow activity fluctuations in monkey visual cortex: implications for functional brain imaging. *Cerebral cortex, 13*(4), 422-433.

Lerner, Y., Honey, C. J., Silbert, L. J., & Hasson, U. (2011). Topographic mapping of a hierarchy of temporal receptive windows using a narrated story. *Journal of Neuroscience, 31*(8), 2906-2915.

Li, Q., Wang, X., Wang, S., Xie, Y., Li, X., Xie, Y., & Li, S. (2019). Dynamic reconfiguration of the functional brain network after musical training in young adults. *Brain Structure and Function, 224*(5), 1781-1795.

Liddle, E. B., Price, D., Palaniyappan, L., Brookes, M. J., Robson, S. E., Hall, E. L., . . . Liddle, P. F. (2016). Abnormal salience signaling in schizophrenia: the role of integrative beta oscillations. *Human brain mapping, 37*(4), 1361-1374.

Liljeström, M., Hultén, A., Parkkonen, L., & Salmelin, R. (2009). Comparing MEG and fMRI views to naming actions and objects. *Human brain mapping, 30*(6), 1845-1856.

Lindquist, M. A., Xu, Y., Nebel, M. B., & Caffo, B. S. (2014). Evaluating dynamic bivariate correlations in resting-state fMRI: a comparison study and a new approach. *Neuroimage, 101*, 531-546.

Liu, Q., Farahibozorg, S., Porcaro, C., Wenderoth, N., & Mantini, D. (2017). Detecting large - scale networks in the human brain using high - density electroencephalography. *Human brain mapping, 38*(9), 4631-4643.

Logothetis, N. K., Pauls, J., Augath, M., Trinath, T., & Oeltermann, A. (2001). Neurophysiological investigation of the basis of the fMRI signal. *Nature, 412*(6843), 150-157.

Luckhoo, H., Hale, J. R., Stokes, M. G., Nobre, A. C., Morris, P. G., Brookes, M. J., & Woolrich, M. W. (2012). Inferring task-related networks using independent component analysis in magnetoencephalography. *Neuroimage, 62*(1), 530-541.

Mahyari, A. G., & Aviyente, S. (2014). *Identification of dynamic functional brain network states through tensor decomposition.* Paper presented at the 2014 IEEE International Conference on Acoustics, Speech and Signal Processing (ICASSP).

Malcolm, G. L., Groen, I. I., & Baker, C. I. (2016). Making sense of real-world scenes. *Trends in Cognitive Sciences, 20*(11), 843-856.

Malinen, S., Hlushchuk, Y., & Hari, R. (2007). Towards natural stimulation in fMRI—issues of data analysis. *Neuroimage, 35*(1), 131-139.

Mantini, D., Perrucci, M. G., Del Gratta, C., Romani, G. L., & Corbetta, M. (2007). Electrophysiological signatures of resting state networks in the human brain. *Proceedings of the National Academy of Sciences, 104*(32), 13170-13175.

Maris, E., & Oostenveld, R. (2007). Nonparametric statistical testing of EEG-and MEG-data. *Journal of neuroscience methods, 164*(1), 177-190.

Martinet, L.-E., Kramer, M., Viles, W., Perkins, L., Spencer, E., Chu, C., . . . Kolaczyk, E. (2020). Robust dynamic community detection with applications to human brain functional networks. *Nature communications, 11*(1), 1-13.

Marzetti, L., Della Penna, S., Snyder, A. Z., Pizzella, V., Nolte, G., de Pasquale, F., . . . Corbetta, M. (2013). Frequency specific interactions of MEG resting

state activity within and across brain networks as revealed by the multivariate interaction measure. *Neuroimage, 79*, 172-183.

Mheich, A., Hassan, M., Khalil, M., Berrou, C., & Wendling, F. (2015). A new algorithm for spatiotemporal analysis of brain functional connectivity. *Journal of neuroscience methods, 242*, 77-81.

Mobbs, D., Greicius, M. D., Abdel-Azim, E., Menon, V., & Reiss, A. L. (2003). Humor modulates the mesolimbic reward centers. *Neuron, 40*(5), 1041-1048.

Moradi, F., Liu, L., Cheng, K., Waggoner, R., Tanaka, K., & Ioannides, A. (2003). Consistent and precise localization of brain activity in human primary visual cortex by MEG and fMRI. *Neuroimage, 18*(3), 595-609.

Mørup, M., Hansen, L. K., Herrmann, C. S., Parnas, J., & Arnfred, S. M. (2006). Parallel factor analysis as an exploratory tool for wavelet transformed event-related EEG. *Neuroimage, 29*(3), 938-947.

Mucha, P. J., Richardson, T., Macon, K., Porter, M. A., & Onnela, J.-P. (2010). Community structure in time-dependent, multiscale, and multiplex networks. *Science, 328*(5980), 876-878.

Mukamel, R., Gelbard, H., Arieli, A., Hasson, U., Fried, I., & Malach, R. (2005). Coupling between neuronal firing, field potentials, and FMRI in human auditory cortex. *Science, 309*(5736), 951-954.

Murphy, K., Birn, R. M., & Bandettini, P. A. (2013). Resting-state fMRI confounds and cleanup. *Neuroimage, 80*, 349-359.

Nolte, G., Bai, O., Wheaton, L., Mari, Z., Vorbach, S., & Hallett, M. (2004). Identifying true brain interaction from EEG data using the imaginary part of coherency. *Clinical neurophysiology, 115*(10), 2292-2307.

Nugent, A. C., Luber, B., Carver, F. W., Robinson, S. E., Coppola, R., & Zarate Jr, C. A. (2017). Deriving frequency - dependent spatial patterns in MEG - derived resting state sensorimotor network: A novel multiband ICA technique. *Human brain mapping, 38*(2), 779-791.

Nugent, A. C., Robinson, S. E., Coppola, R., Furey, M. L., & Zarate Jr, C. A. (2015). Group differences in MEG-ICA derived resting state networks: application to major depressive disorder. *Neuroimage, 118*, 1-12.

Nummenmaa, L., Saarimäki, H., Glerean, E., Gotsopoulos, A., Jääskeläinen, I. P., Hari, R., & Sams, M. (2014). Emotional speech synchronizes brains across listeners and engages large-scale dynamic brain networks. *Neuroimage, 102*, 498-509.

O'Neill, G. C. (2016). *Dynamic electrophysiological connectomics.* (PhD), University of Nottingham, (33502)

O'Neill, G. C., Barratt, E. L., Hunt, B. A., Tewarie, P. K., & Brookes, M. J. (2015). Measuring electrophysiological connectivity by power envelope correlation: a technical review on MEG methods. *Physics in Medicine and Biology, 60*(21), 271-295.

O'Neill, G. C., Bauer, M., Woolrich, M. W., Morris, P. G., Barnes, G. R., & Brookes, M. J. (2015). Dynamic recruitment of resting state sub-networks. *Neuroimage, 115*, 85-95.

O'Neill, G. C., Tewarie, P., Vidaurre, D., Liuzzi, L., Woolrich, M. W., & Brookes, M. J. (2018). Dynamics of large-scale electrophysiological networks: A technical review. *Neuroimage, 180*, 559-576.

O'Neill, G. C., Tewarie, P. K., Colclough, G. L., Gascoyne, L. E., Hunt, B. A., Morris, P. G., . . . Brookes, M. J. (2017). Measurement of dynamic task related functional networks using MEG. *Neuroimage, 146*, 667-678.

Ozdemir, A., Bernat, E. M., & Aviyente, S. (2017). Recursive tensor subspace tracking for dynamic brain network analysis. *IEEE Transactions on Signal and Information Processing over Networks, 3*(4), 669-682.

Peled, A., Geva, A. B., Kremen, W. S., Blankfeld, H. M., Esfandiarfard, R., & Nordahl, T. E. (2001). Functional connectivity and working memory in schizophrenia: an EEG study. *International Journal of Neuroscience, 106*(1-2), 47-61.

Peraza, L. R., Asghar, A. U., Green, G., & Halliday, D. M. (2012). Volume conduction effects in brain network inference from electroencephalographic recordings using phase lag index. *Journal of neuroscience methods, 207*(2), 189-199.

Pester, B., Ligges, C., Leistritz, L., Witte, H., & Schiecke, K. (2015). Advanced Insights into Functional Brain Connectivity by Combining Tensor Decomposition and Partial Directed Coherence. *PloS one, 10*(6), 1-18.

Pfurtscheller, G., & Da Silva, F. L. (1999). Event-related EEG/MEG synchronization and desynchronization: basic principles. *Clinical neurophysiology, 110*(11), 1842-1857.

Rabiner, L. R. (1989). A tutorial on hidden Markov models and selected applications in speech recognition. *Proceedings of the IEEE, 77*(2), 257-286.

Ramkumar, P., Parkkonen, L., Hari, R., & Hyvärinen, A. (2012). Characterization of neuromagnetic brain rhythms over time scales of minutes using spatial independent component analysis. *Human brain mapping, 33*(7), 1648-1662.

Ramkumar, P., Parkkonen, L., & Hyvärinen, A. (2014). Group-level spatial independent component analysis of Fourier envelopes of resting-state MEG data. *Neuroimage, 86*, 480-491.

Rikandi, E., Pamilo, S., Mäntylä, T., Suvisaari, J., Kieseppä, T., Hari, R., . . . Raij, T. (2017). Precuneus functioning differentiates first-episode psychosis patients during the fantasy movie Alice in Wonderland. *Psychological medicine, 47*(3), 495-506.

Sadaghiani, S., Poline, J.-B., Kleinschmidt, A., & D'Esposito, M. (2015). Ongoing dynamics in large-scale functional connectivity predict perception. *Proceedings of the National Academy of Sciences, 112*(27), 8463-8468.

Salinas, E., & Sejnowski, T. J. (2001). Correlated neuronal activity and the flow of neural information. *Nature reviews neuroscience, 2*(8), 539-550.

Salmi, J., Glerean, E., Jääskeläinen, I. P., Lahnakoski, J. M., Kettunen, J., Lampinen, J., . . . Sams, M. (2014). Posterior parietal cortex activity reflects the significance of others' actions during natural viewing. *Human brain mapping, 35*(9), 4767-4776.

Salmi, J., Metwaly, M., Tohka, J., Alho, K., Leppämäki, S., Tani, P., . . . Laine, M. (2019). ADHD desynchronizes brain activity during watching a distracted multi-talker conversation. *Neuroimage, 216*, 116352.

Schoffelen, J. M., & Gross, J. (2009). Source connectivity analysis with MEG and EEG. *Human brain mapping, 30*(6), 1857-1865.

Schölvinck, M. L., Leopold, D. A., Brookes, M. J., & Khader, P. H. (2013). The contribution of electrophysiology to functional connectivity mapping. *Neuroimage, 80*, 297-306.

Schultz, J., & Pilz, K. S. (2009). Natural facial motion enhances cortical responses to faces. *Experimental Brain Research, 194*(3), 465-475.

Seghier, M. L., & Price, C. J. (2018). Interpreting and utilising intersubject variability in brain function. *Trends in Cognitive Sciences, 22*(6), 517-530.

Shibata, M., Terasawa, Y., Osumi, T., Masui, K., Ito, Y., Sato, A., & Umeda, S. (2017). Time course and localization of brain activity in humor comprehension: An ERP/sLORETA study. *Brain research, 1657*, 215-222.

Shine, J. M., Breakspear, M., Bell, P. T., Martens, K. A. E., Shine, R., Koyejo, O., . . . Poldrack, R. A. (2019). Human cognition involves the dynamic integration of neural activity and neuromodulatory systems. *Nature neuroscience, 22*(2), 289-296.

Shine, J. M., Hearne, L. J., Breakspear, M., Hwang, K., Müller, E. J., Sporns, O., . . . Cocchi, L. (2019). The low-dimensional neural architecture of cognitive complexity is related to activity in medial thalamic nuclei. *Neuron, 104*(5), 849-855.

Siegel, M., Donner, T. H., & Engel, A. K. (2012). Spectral fingerprints of large-scale neuronal interactions. *Nature reviews neuroscience, 13*(2), 121-134.

Simony, E., Honey, C. J., Chen, J., Lositsky, O., Yeshurun, Y., Wiesel, A., & Hasson, U. (2016). Dynamic reconfiguration of the default mode network during narrative comprehension. *Nature communications, 7*, 12141.

Singer, W. (1993). Synchronization of cortical activity and its putative role in information processing and learning. *Annual review of physiology, 55*(1), 349-374.

Singh, K. D., Barnes, G. R., Hillebrand, A., Forde, E. M., & Williams, A. L. (2002). Task-related changes in cortical synchronization are spatially coincident with the hemodynamic response. *Neuroimage, 16*(1), 103-114.

Smith, S. M., Fox, P. T., Miller, K. L., Glahn, D. C., Fox, P. M., Mackay, C. E., . . . Laird, A. R. (2009). Correspondence of the brain's functional architecture during activation and rest. *Proceedings of the National Academy of Sciences, 106*(31), 13040-13045.

Smith, S. M., Miller, K. L., Moeller, S., Xu, J., Auerbach, E. J., Woolrich, M. W., . . . Glasser, M. F. (2012). Temporally-independent functional modes of spontaneous brain activity. *Proceedings of the National Academy of Sciences, 109*(8), 3131-3136.

Sonkusare, S., Breakspear, M., & Guo, C. (2019). Naturalistic Stimuli in Neuroscience: Critically Acclaimed. *Trends in Cognitive Sciences, 23*(8), 699-714.

Sporns, O. (2010). *Networks of the Brain*. Cambridge, MA: MIT press.

Spyrou, L., Parra, M., & Escudero, J. (2018). Complex tensor factorization with PARAFAC2 for the estimation of brain connectivity from the EEG. *IEEE Transactions on Neural Systems and Rehabilitation Engineering, 27*(1), 1-12.

Stam, C. J., Nolte, G., & Daffertshofer, A. (2007). Phase lag index: assessment of functional connectivity from multi channel EEG and MEG with diminished bias from common sources. *Human brain mapping, 28*(11), 1178-1193.

Stinstra, J., & Peters, M. (1998). The volume conductor may act as a temporal filter on the ECG and EEG. *Medical and Biological Engineering and Computing, 36*(6), 711-716.

Tang, M., Lu, Y., & Yang, L. (2019). Temporal–Spatial Patterns in Dynamic Functional Brain Network for Self-Paced Hand Movement. *IEEE Transactions on Neural Systems and Rehabilitation Engineering, 27*(4), 643-651.

Tewarie, P., Bright, M. G., Hillebrand, A., Robson, S. E., Gascoyne, L. E., Morris, P. G., . . . Brookes, M. J. (2016). Predicting haemodynamic networks using electrophysiology: The role of non-linear and cross-frequency interactions. *Neuroimage, 130*, 273-292.

Tewarie, P., Liuzzi, L., O'Neill, G. C., Quinn, A. J., Griffa, A., Woolrich, M. W., . . . Brookes, M. J. (2019). Tracking dynamic brain networks using high temporal resolution MEG measures of functional connectivity. *Neuroimage, 200*, 38-50.

Tong, Y., Hocke, L. M., Fan, X., Janes, A. C., & Frederick, B. d. (2015). Can apparent resting state connectivity arise from systemic fluctuations? *Frontiers in human neuroscience, 9*, 285.

Touryan, J., Felsen, G., & Dan, Y. (2005). Spatial structure of complex cell receptive fields measured with natural images. *Neuron, 45*(5), 781-791.

Vaiana, M., Goldberg, E. M., & Muldoon, S. F. (2019). Optimizing state change detection in functional temporal networks through dynamic community detection. *Journal of Complex Networks, 7*(4), 529-553.

Vanderwal, T., Eilbott, J., & Castellanos, F. X. (2019). Movies in the magnet: Naturalistic paradigms in developmental functional neuroimaging. *Developmental cognitive neuroscience, 36*, 100600.

Varela, F., Lachaux, J.-P., Rodriguez, E., & Martinerie, J. (2001). The brainweb: phase synchronization and large-scale integration. *Nature reviews neuroscience, 2*(4), 229-239.

Vartiainen, J., Liljeström, M., Koskinen, M., Renvall, H., & Salmelin, R. (2011). Functional magnetic resonance imaging blood oxygenation level-dependent signal and magnetoencephalography evoked responses yield different neural functionality in reading. *Journal of Neuroscience, 31*(3), 1048-1058.

Vidaurre, D., Abeysuriya, R., Becker, R., Quinn, A. J., Alfaro-Almagro, F., Smith, S. M., & Woolrich, M. W. (2018). Discovering dynamic brain networks from big data in rest and task. *Neuroimage, 180*, 646-656.

Vidaurre, D., Hunt, L. T., Quinn, A. J., Hunt, B. A., Brookes, M. J., Nobre, A. C., & Woolrich, M. W. (2018). Spontaneous cortical activity transiently organises into frequency specific phase-coupling networks. *Nature communications, 9*(1), 1-13.

Vidaurre, D., Quinn, A. J., Baker, A. P., Dupret, D., Tejero-Cantero, A., & Woolrich, M. W. (2016). Spectrally resolved fast transient brain states in electrophysiological data. *Neuroimage, 126*, 81-95.

Vidaurre, D., Smith, S. M., & Woolrich, M. W. (2017). Brain network dynamics are hierarchically organized in time. *Proceedings of the National Academy of Sciences, 114*(48), 12827-12832.

Vinck, M., Oostenveld, R., Van Wingerden, M., Battaglia, F., & Pennartz, C. M. (2011). An improved index of phase-synchronization for electrophysiological data in the presence of volume-conduction, noise and sample-size bias. *Neuroimage, 55*(4), 1548-1565.

Whittingstall, K., Bartels, A., Singh, V., Kwon, S., & Logothetis, N. K. (2010). Integration of EEG source imaging and fMRI during continuous viewing of natural movies. *Magnetic resonance imaging, 28*(8), 1135-1142.

Williams, A. H., Kim, T. H., Wang, F., Vyas, S., Ryu, S. I., Shenoy, K. V., . . . Ganguli, S. (2018). Unsupervised discovery of demixed, low-dimensional neural dynamics across multiple timescales through tensor component analysis. *Neuron, 98*(6), 1099-1115.

Wilson, S. M., Molnar-Szakacs, I., & Iacoboni, M. (2008). Beyond superior temporal cortex: intersubject correlations in narrative speech comprehension. *Cerebral cortex, 18*(1), 230-242.

Winkler, A. M., Ridgway, G. R., Webster, M. A., Smith, S. M., & Nichols, T. E. (2014). Permutation inference for the general linear model. *Neuroimage, 92*, 381-397.

Winterer, G., Carver, F. W., Musso, F., Mattay, V., Weinberger, D. R., & Coppola, R. (2007). Complex relationship between BOLD signal and synchronization/desynchronization of human brain MEG oscillations. *Human brain mapping, 28*(9), 805-816.

Yao, H., Shi, L., Han, F., Gao, H., & Dan, Y. (2007). Rapid learning in cortical coding of visual scenes. *Nature neuroscience, 10*(6), 772-778.

Zhu, Y., Li, X., Ristaniemi, T., & Cong, F. (2019). *Measuring the Task Induced Oscillatory Brain Activity Using Tensor Decomposition.* Paper presented at the ICASSP 2019-2019 IEEE International Conference on Acoustics, Speech and Signal Processing (ICASSP).

Zhu, Y., Liu, J., Mathiak, K., Ristaniemi, T., & Cong, F. (2019). Deriving electrophysiological brain network connectivity via tensor component analysis during freely listening to music. *IEEE Transactions on Neural Systems and Rehabilitation Engineering, 28*(2), 409-418.

Zhu, Y., Liu, J., Ristaniemi, T., & Cong, F. (2020). Distinct Patterns of Functional Connectivity During the Comprehension of Natural, Narrative Speech. *International Journal of Neural Systems, 30*(3), 2050007-2050007.

Zhu, Y., Liu, J., Ye, C., Mathiak, K., Astikainen, P., Ristaniemi, T., & Cong, F. (2020). Discovering dynamic task-modulated functional networks with specific spectral modes using MEG. *Neuroimage, 218*. doi:https://doi.org/10.1016/j.neuroimage.2020.116924

Zhu, Y., Zhang, C., Poikonen, H., Toiviainen, P., Huotilainen, M., Mathiak, K., . . . Cong, F. (2020). Exploring Frequency‐Dependent Brain Networks from Ongoing EEG Using Spatial ICA During Music Listening. *Brain Topography, 33*, 289-302.

Zumer, J. M., Brookes, M. J., Stevenson, C. M., Francis, S. T., & Morris, P. G. (2010). Relating BOLD fMRI and neural oscillations through convolution and optimal linear weighting. *Neuroimage, 49*(2), 1479-1489.

ORIGINAL PAPERS

I

MEASURING THE TASK INDUCED OSCILLATORY BRAIN ACTIVITY USING TENSOR DECOMPOSITION

by

Yongjie Zhu, Xueqiao Li, Tapani Ristaniemi & Fengyu Cong 2019

2019 IEEE International Conference on Acoustics, Speech, and Signal Processing (ICASSP), Brighton, UK

DOI: 10.1109/ICASSP.2019.8682355

MEASURING THE TASK INDUCED OSCILLATORY BRAIN ACTIVITY USING TENSOR DECOMPOSITION

Yongjie Zhu [1,2], Xueqiao Li [3], Tapani Ristaniemi [2], Fengyu Cong [1,2]

[1] School of Biomedical Engineering, Faculty of Electronic and Electrical Engineering, Dalian University of Technology, 116024, Dalian, China
[2] Faculty of Information Technology, University of Jyvaskyla, Jyväskylä,40014, Finland
[3] Department of Psychology, University of Jyvaskyla, Jyväskylä, 40014, Finland

ABSTRACT

The characterization of dynamic electrophysiological brain activity, which form and dissolve in order to support ongoing cognitive function, is one of the most important goals in neuroscience. Here, we introduce a method with tensor decomposition for measuring the task-induced oscillations in the human brain using electroencephalography (EEG). The time frequency representation of source-reconstructed single-trail EEG data constructed a third-order tensor with three factors of time $*$ trails, frequency and source points. We then used a non-negative Canonical Polyadic decomposition (NCPD) to identify the temporal, spectral and spatial changes in electrophysiological brain activity. We validate this method using both simulation EEG data and real EEG data recorded during a task of irony comprehension. The results demonstrated that proposed method can track dynamics of the temporal-spectral modes of the rhythm in the brain on a timescale commensurate to the task they are undertaking.

***Index Terms*—** EEG, source localization, neural oscillations, tensor decomposition.

1. INTRODUCTION

During the past decade, the characterization of brain functional networks and their dynamics has become an important field of study [1]. Most efforts focusing on the functional networks have been made through functional magnetic resonance imaging (fMRI) technique due to high spatial resolution [2]. Unfortunately, fMRI temporal resolution is limited since it indirectly measures the consequences of neural activity. The electrophysiological underpinnings of the human brain are not yet fully understood through fMRI. The direct non-invasive measures of neural activity such as electro- or magnetoencephalography (EEG/MEG) provide a means to study the neural oscillations.

The EEG consists of the activity of an ensemble of generators producing rhythmic activity in several frequency ranges [3]. By application of sensory stimulation these generators are coupled and act together in a coherent way. This synchronization and enhancement of EEG activity gives rise to 'evoked' or 'induced' oscillations (the former being phase-locked to the event, the latter not) [3, 4]. To obtain the data representation of the evoked oscillations, the single trial EEG data were first averaged and then transformed to the time-frequency domain by means of wavelet analysis. The obtained data representations were with multi modes since EEG had many channels in sensor space. The analysis for multi-way data (channel $\times$ time $\times$ frequency) of the evoked oscillation based on tensor decomposition has been studied [5-7] (for review see [8]). In contrast, the data of induced oscillation can be generated by transforming the single trial EEG to time-frequency domain, which resulted in another data formation with channel $\times$ time$*$trial $\times$ frequency. In addition, to examine functional brain structure, source reconstruction techniques are applied to sensor-level EEG data, which can somehow overcome the limited spatial resolution of the EEG [9, 10]. Thus, a new data representation can be generated with source $\times$ time $*$ trial $\times$ frequency. CANDECOMP/PARAFAC (CP), as a basic tensor decomposition method, can be applied to source-reconstructed data to extract task-induced neural oscillations.

In this study, we proposed a method based on NCPD for measuring the task-induced oscillations in the human brain. The time frequency representation of single-trail source-reconstructed EEG data constructed a third-order tensor with three factors of time$*$trails, frequency and source space. NCPD was performed to identify the temporal, spectral and spatial changes in electrophysiological brain activity. The proposed method was validated using both simulated EEG data and real EEG data recorded during a task of irony comprehension. The results demonstrated that proposed method can tracks dynamics of the temporal-spectral modes of the rhythm in the brain.

2. MATERIALS AND METHODS

2.1. Data description

2.1.1. Simulated data

We simulated EEG data using Brainstorm toolbox [11]. Three oscillating current dipoles perpendicular to the cortical surface were placed pre-selected brain regions (Fig.1). The duration of each trail of the simulated measurement was 1400

ms from -200 to 1200 ms. Each oscillatory source, generated using different frequent sine wave (8Hz, 15Hz, 25Hz, see Fig.1), was amplitude modulated by a different smoothed Hanning widow (Fig. 2) with a SNR of 20 dB. Next, we applied a forward solution with a boundary-element conductor model from template anatomy to simulate the 128-channel EEG data. Finally, to make the simulations more realistic, the magnitudes of different trails were different and were normal distribution.

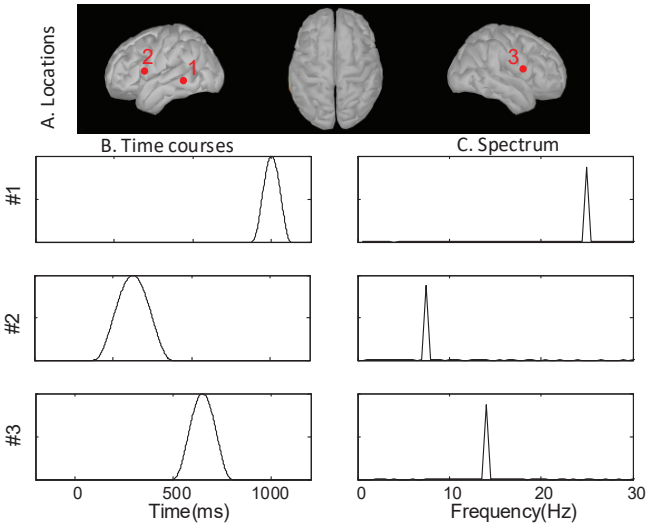

Fig. 1. Locations (A) of the simulated oscillatory current sources on an inflated and flattened brain surface and the time courses (B) and spectrum (C) of the three sources.

2.1.2. Experimental data

The data was collected at the University of Jyvaskyla, Finland. Thirty-eight participants were included in the final sample, in which there were 17 dysphoric participants and 21 control participants. The study was approved by the Ethics Committee of the University of Jyvaskyla. Stimuli with one-sentence spoken lines and colored pictures were applied. Each stimulus trial consisted of an introductory sentence, a contextual picture, and a commenting sentence. There were two different types of stimuli (two conditions). If the keyword in commenting sentence was semantically congruent with the content of the contextual pictures, the trail provided a neutral meaning; otherwise, the keyword was semantically incongruent with the picture composed an ironic meaning. The commenting sentences were presented twice to the participants combined with the congruent and incongruent contextual pictures. There were 90 trials in each condition.

EEG data were collected by NeurOne system (Bittium Biosignals Ltd, Kuopio, Finland) with a 128-Channel Net (HydroCel Geodesic Sensor Net, Electric Geodesic Inc, USA), and preprocessed using EEGlab [12]. They were down-sampled to 250 Hz to reduce the size of datasets without losing important data information. The 0.5 Hz high-pass and 20 Hz low-pass filters were applied on EEG data. Next, EEG data were visually checked and the bad channels were interpolated using a spherical spline model. After this, EEG data was extracted into 1100 ms long segments relative to the onset of keywords, starting from 100 ms before the presentation of keywords. Segments whose maximum exceeds 150 μV for all channels were rejected. Hereinafter, when EEG is mentioned, it means the preprocessed one.

In order to extract task-induced neural oscillations, the data used in this study were from the control group with incongruent (ironic) stimuli. It should be noted that we do not intend to examine the difference between groups or stimulus.

2.2. Third-order tensor of source-level EEG data

The forward model and the inverse model were computed with a MATLAB toolbox Brainstorm [11]. The forward model was calculated using the symmetric boundary element method and default MNI MRI template (Colin 27). Preprocessed single-trial data were used to compute the inverse model, which was estimated using the weighted Minimum Norm Estimate. Finally, activation time-courses at 4003 vertices were estimated.

Spectral decomposition of source-reconstructed EEG from single trials was conducted with Morlet wavelet. 275 linearly spaced time points form -100 ms to 1000 ms and 37 frequency points linearly spaced between 2 Hz and 20 Hz were estimated for each trial. Therefore, for every subject, we obtained a 3D tensor of 37 (frequency points) × 275∗'number of trials' (time points) × 4003 (source points). Absolute values of the decomposed data were analyzed to investigate task-induced changes in oscillatory power.

2.3. Nonnegative Canonical polyadic decomposition (CPD)

In this paper, we denote a scalar variable by lowercase letter, such as x; a vector by boldface lowercase letter, such as $\boldsymbol{x}$; a matrix by boldface uppercase letter, such as $\boldsymbol{X}$; and a high order tensor by boldface script letter, such as $\boldsymbol{\mathcal{X}}$. Operator $\circ$ represents outer product of vectors, $\circledast$ denotes the Hadarmard product, $[\![\ \ ]\!]$ represents Kruskal operator, and $\|\ \|_F$ means Frobenius norm. Nonnegative CANDECOMP/PARAFAC decomposition is abbreviated as NCP for convenience in following contents.

The NCP model [13] can be formulated as follows. For a given Nth-order tensor $\boldsymbol{\mathcal{X}} \in \mathbb{R}_+^{I_1 \times I_2 \times \cdots \times I_N}$ performing a factorization into a set of N unknown non-negative matrices whose elements are non-negative: $\boldsymbol{U}^{(n)} = [\boldsymbol{u}_1^{(n)}, \boldsymbol{u}_2^{(n)}, \cdots, \boldsymbol{u}_J^{(n)}] \in \mathbb{R}_+^{I_n \times J} (n = 1,2,\cdots,N)$ can be described as:

$$\boldsymbol{\mathcal{X}} \approx [\![\boldsymbol{U}^{(1)}, \cdots, \boldsymbol{U}^{(N)}]\!], \quad (1)$$

where J is the number of extracted components, I_n is the size in mode-n, The Kruskal operator for estimated non-negative matrices in (1) can be represented by the sum of J rank-1 tensors in outer productor form:

$$[\![\boldsymbol{U}^{(1)}, \cdots, \boldsymbol{U}^{(N)}]\!] = \sum_{j=1}^{J} \boldsymbol{\mathcal{U}}_j = \sum_{j=1}^{J} \boldsymbol{u}_j^{(1)} \circ \boldsymbol{u}_j^{(2)} \circ \cdots \circ \boldsymbol{u}_j^{(N)}, \quad (2)$$

where $\mathcal{U}_j (j = 1,2,\cdots,J)$ are the rank-1 tensors. The target of NCP is to obtain the suitable $\boldsymbol{U}^{(n)}$ and one J here is defined to correspond to one NCP model. Each factor $\boldsymbol{U}^{(n)}$ explains the data tensor along a corresponding mode. Hence, one factor can be considered as features of the data onto the subspace spanned by the others. Most algorithms for NCP are to minimize a squared Euclidean distance as the following optimization problem:

$$\min_{\boldsymbol{U}^{(1)},\cdots,\boldsymbol{U}^{(N)}} \frac{1}{2} \left\| \mathcal{X} - [\![\boldsymbol{U}^{(1)},\cdots,\boldsymbol{U}^{(N)}]\!] \right\|_F^2. \quad (3)$$

In this paper, we applied the hierarchical alternating least squares (HALS) algorithm whose simplified version for NMF has been proved to be superior to the multiplicative algorithms [14]. The HALS is related to the column-wise version of the ALS algorithm for 3-D data [5]. The HALS algorithm used in this study sequentially updates components u by a simple update rule

$$\boldsymbol{u}_j^{(n)} \leftarrow \mathcal{X} \bar{\times}_{-n} \{\boldsymbol{u}_j\} - \boldsymbol{U}_{-j}^{(n)} \{\boldsymbol{U}_{-j}^T \boldsymbol{u}_j\}^{\circledast -n}, \quad (4)$$

where $\mathcal{X} \bar{\times}_{-n} \{\boldsymbol{u}_j\}$ is sequentially computed as the $(N-1)$ tensor-vector multiplications among all modes, but mode-n. It should be noted that this study does not intend to propose an NCP algorithm. Therefore, any NCP algorithm can work for the data. In this paper, the CPD was performed to the third-order data (N=3). After decomposition, the jth component containing spectral, temporal, spatial factor can be represented by $\mathcal{U}_j = \boldsymbol{u}_j^{(1)} \circ \boldsymbol{u}_j^{(2)} \circ \boldsymbol{u}_j^{(3)}$ according to Eqn (2).

2.4. Component number estimation

In the application of tensor decomposition to EEG data, it is necessary to determine a proper component number, which is the rank-1 tensor number J in (2). Determining this number is very important to NCP because different numbers in different quantitative levels may probably correspond to very different decomposition results. In this study, DIFFIT (difference of fit) method was applied to determine the number of components [15]. DIFFIT measures the change of the fit (explained variance of the raw data by the proposed model) and the core tensor of the decomposition among a number of models [5]. We run ten times for each J and average the fits to obtain a more precise estimation. After DIFFIT estimation, J = 5 was selected for simulated dataset and J = 10 for real EEG dataset.

2.5. Testing for task-related brain activity

After tensor decomposition, a set of J brain activity, showing interactions among spectral temporal and spatial modes, were yielded. In all tensor-based methods, it is a general question that which components extracted need to be retained and which just reflect noise. In this study, the statistical significance of each obtained component was accessed by a permutation procedure based on surrogate data [16]. Phase-randomized surrogate time courses of equal mean and autocorrelation to the extracted temporal factor of the component were obtained. The phase-randomization was computed by rotating the phase $\phi(f)$ by an independent random variable $\varphi(f)$ which was uniformly chosen in the range of [0, 2π) [16].

We first averaged the time courses matrix $\boldsymbol{U}^{(2)}$ over all trials in all subjects yielding a new matrix, $\bar{\boldsymbol{U}}^{(2)}$, containing J trial averaged time courses of component. The size of $\bar{\boldsymbol{U}}^{(2)}$was $N_{trial} \times J$, (where N_{trial} denotes the number time points per trial; 350 for simulated data and 275 for real data). Then, the phase randomization permutation process was performed [17]. Following this, an empirical null distribution was constructed. A matrix $\hat{\boldsymbol{U}}_{NULL}^{(2)}$ was generated in the same way as $\bar{\boldsymbol{U}}^{(2)}$, but prior to averaging over trials, the phases of time courses for each trial were randomized. We reasoned that if the components extracted were not related to the cognitive tasks, this phase randomization would no effect on the magnitude of the trial averaged time courses, and therefore the magnitudes of fluctuations in $\hat{\boldsymbol{U}}_{NULL}^{(2)}$ and $\bar{\boldsymbol{U}}^{(2)}$ would match. However, if the components contained trial-onset-locked increases or decreases in brain activity, then these would be maintained in $\bar{\boldsymbol{U}}^{(2)}$ but diminished in $\hat{\boldsymbol{U}}_{NULL}^{(2)}$. This procedure was repeated 5000 times. A component was deemed significant if, at any one time point in the trial average, the associated column of $\bar{\boldsymbol{U}}^{(2)}$ fluctuated such that it fell outside a threshold defined by the null distribution. The threshold for significance was defined at 0.05 and it should be noted this was corrected by Bonferroni correction for multiple comparisons across J components [17].

3. RESULTS

3.1. Simulation results

Fig. 2 shows the envelope time courses and the power spectra for all three correctly reconstructed brain networks and one noise artifact (we just present one artifact for demonstration). As can be seen that the location, spectra and the averaged time courses of the pre-set brain sources were reconstructed successfully. Fig. 2C shows the time course of the brain activity, represented as the corresponding trial averaged time courses of components in $\bar{\boldsymbol{U}}^{(2)}$. The grey area represents the null distribution generated by randomizing the phase of the trial time courses ($\hat{\boldsymbol{U}}_{NULL}^{(2)}$). Again, the black line represents the average response across all trials in all subjects, and the grey distribution is the 95th percentile threshold for the null distribution.

3.2. Results from experimental EEG data

Fig. 3 shows the results of our method applied to the real EEG data. Although 10 components were extracted, we just present two components that demonstrated significant task modulation. Clearly, the 1st row of Fig. 3 indicates that the Delta brain oscillation appeared in the right temporal-

occipital junction during 800 ms after onset. The 2nd row of Fig. 3 shows that the Theta rhythm emerges in the left frontal area corresponding to Broca's area, which is significantly related with language cognition, during 400 ms after onset.

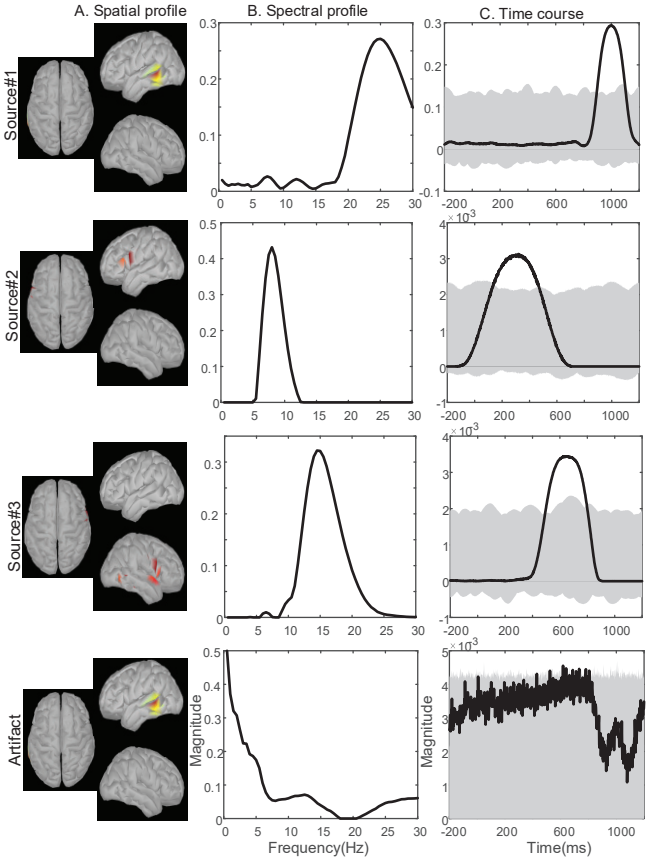

Fig. 2. Results of simulation. A: spatial maps of extracted components. B: Spectral factor of the components. C: Time courses of components, averaged across trials (black line). The grey shaded region represents the null distribution based on a hypothesis that the response is not time locked to the tasks. Significance ($p_{corrected} < .05$) is attributed if the black line appears outside the null distribution. Rows 1 to 3 show the three induced oscillatory sources. Row 4 demonstrates an artifact.

4. DISCUSSION

This paper has introduced a method mainly based on tensor decomposition to extract task-induced brain oscillations, which allows characterization of transiently forming and dissolving electrophysiological brain activity. The proposed method was validated by both simulated data and real EEG data. When application to real EEG data collected from task of irony comprehension, we found brain activity of interest, which was associated with irony comprehension. The results demonstrated that the Delta rhythm was elicited in Broca's area after 400ms of the ironic stimulus and the theta oscillation involved in comprehension of irony in right temporal-occipital junction after 800ms of the stimulus. Actually, such elicited brain activity in those brain regions can be expected since the previous studies has also reported that the same brain areas were associated with humor comprehension [18, 19].

The proposed approach is different from the previous reports where the tensor decomposition was applied to extract multi-domain feature of ERP (event-related potential) [5-7]. Here, we performed tensor decomposition to trials concatenated source-level data to extract the task-induced brain oscillation, which allows examination of temporal spectral dynamics in brain cortex during task performance or cognitive process.

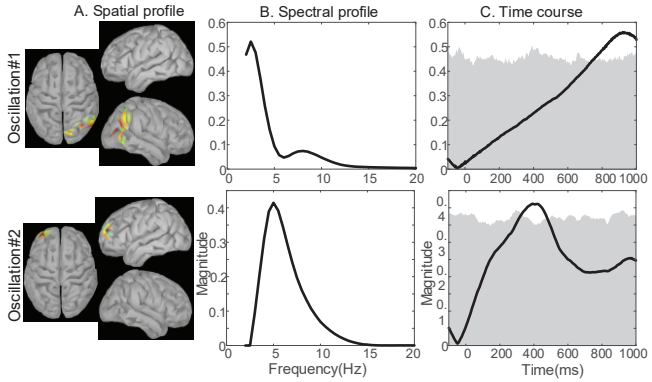

Fig. 3. Results of experiment data. A: spatial maps of extracted components. B: Spectral factors of the components. C: Time courses of components, averaged across trials in all subjects (black line). The grey shaded region represents the null distribution ($p_{corrected} < .05$) based on a hypothesis that the response is not time locked to the tasks. Row 1 shows the Delta oscillation involved in comprehension of irony in right temporal-occipital junction after 800 ms of the stimulus onset. Row 2 demonstrates the Theta rhythm was elicited in Broca's area after 400 ms of the ironic stimulus onset.

As we all known, it is very complex to decode brain response to external stimulus. During a cognitive process, different brain rhythm would be emerging in different regions at different time, which causes the complexity of analysis for the EEG data. Therefore, the analysis for the data must account for temporal non-stationarity, spatial inhomogeneities, and spectral structure [20]. The time frequency representation of source level data based on wavelet transformation can well describe the property of the brain data. Tensor decomposition technique provides a means to extract information from such big and complex data.

5. ACKNOWLEDGEMENT

This work was partially supported by the Fundamental Research Funds for the Central Universities [DUT16JJ(G)03] in Dalian University of Technology in China, and National Natural Science Foundation of China (Grant No. 81471742) and the scholarships from China Scholarship Council (No. 201600090042).

6. REFERENCES

[1] J. Damoiseaux et al., "Consistent resting-state networks across healthy subjects," Proceedings of the national academy of sciences, vol. 103, no. 37, pp. 13848-13853, 2006.

[2] S. M. Smith et al., "Correspondence of the brain's functional architecture during activation and rest," Proceedings of the National Academy of Sciences, vol. 106, no. 31, pp. 13040-13045, 2009.

[3] E. rol Başar, M. artin Schürmann, T. amer Demiralp, C. anan Başar-Eroglu, and A. hmet Ademoglu, "Event-related oscillations are 'real brain responses'—wavelet analysis and new strategies," International Journal of Psychophysiology, vol. 39, no. 2-3, pp. 91-127, 2001.

[4] E. Başar, C. Başar-Eroğlu, S. Karakaş, and M. Schürmann, "Are cognitive processes manifested in event-related gamma, alpha, theta and delta oscillations in the EEG?," Neuroscience letters, vol. 259, no. 3, pp. 165-168, 1999.

[5] F. Cong et al., "Benefits of multi-domain feature of mismatch negativity extracted by non-negative tensor factorization from EEG collected by low-density array," International journal of neural systems, vol. 22, no. 06, p. 1250025, 2012.

[6] F. Cong et al., "Multi-domain feature extraction for small event-related potentials through nonnegative multi-way array decomposition from low dense array EEG," International journal of neural systems, vol. 23, no. 02, p. 1350006, 2013.

[7] D. Wang, Y. Zhu, T. Ristaniemi, and F. Cong, "Extracting multi-mode ERP features using fifth-order nonnegative tensor decomposition," Journal of neuroscience methods, vol. 308, pp. 240-247, 2018.

[8] F. Cong, Q.-H. Lin, L.-D. Kuang, X.-F. Gong, P. Astikainen, and T. Ristaniemi, "Tensor decomposition of EEG signals: a brief review," Journal of neuroscience methods, vol. 248, pp. 59-69, 2015.

[9] Y. Jonmohamadi, G. Poudel, C. Innes, and R. Jones, "Source-space ICA for EEG source separation, localization, and time-course reconstruction," NeuroImage, vol. 101, pp. 720-737, 2014.

[10] S. Sockeel, D. Schwartz, M. Pélégrini-Issac, and H. Benali, "Large-scale functional networks identified from resting-state EEG using spatial ICA," PloS one, vol. 11, no. 1, p. e0146845, 2016.

[11] F. Tadel, S. Baillet, J. C. Mosher, D. Pantazis, and R. M. Leahy, "Brainstorm: a user-friendly application for MEG/EEG analysis," Computational intelligence and neuroscience, vol. 2011, p. 8, 2011.

[12] A. Delorme and S. Makeig, "EEGLAB: an open source toolbox for analysis of single-trial EEG dynamics including independent component analysis," Journal of neuroscience methods, vol. 134, no. 1, pp. 9-21, 2004.

[13] N. D. Sidiropoulos, L. De Lathauwer, X. Fu, K. Huang, E. E. Papalexakis, and C. Faloutsos, "Tensor decomposition for signal processing and machine learning," IEEE Transactions on Signal Processing, vol. 65, no. 13, pp. 3551-3582, 2017.

[14] A. Cichocki and A.-H. Phan, "Fast local algorithms for large scale nonnegative matrix and tensor factorizations," IEICE transactions on fundamentals of electronics, communications and computer sciences, vol. 92, no. 3, pp. 708-721, 2009.

[15] R. Bro and H. A. Kiers, "A new efficient method for determining the number of components in PARAFAC models," Journal of Chemometrics: A Journal of the Chemometrics Society, vol. 17, no. 5, pp. 274-286, 2003.

[16] D. Kim, K. Kay, G. L. Shulman, and M. Corbetta, "A new modular brain organization of the BOLD signal during natural vision," Cerebral Cortex, pp. 1-17, 2017.

[17] G. C. O'neill et al., "Measurement of dynamic task related functional networks using MEG," NeuroImage, vol. 146, pp. 667-678, 2017.

[18] D. Mobbs, M. D. Greicius, E. Abdel-Azim, V. Menon, and A. L. Reiss, "Humor modulates the mesolimbic reward centers," Neuron, vol. 40, no. 5, pp. 1041-1048, 2003.

[19] M. Shibata et al., "Time course and localization of brain activity in humor comprehension: An ERP/sLORETA study," Brain research, vol. 1657, pp. 215-222, 2017.

[20] M. J. Brookes et al., "Measuring temporal, spectral and spatial changes in electrophysiological brain network connectivity," Neuroimage, vol. 91, pp. 282-299, 2014.

II

EXPLORING FREQUENCY-DEPENDENT BRAIN NETWORKS FROM ONGOING EEG USING SPATIAL ICA DURING MUSIC LISTENING

by

Yongjie Zhu, Chi Zhang, Hanna Poikonen, Petri Toiviainen, Minna Huotilainen, Klaus Mathiak, Tapani Ristaniemi & Fengyu Cong 2020

Brain Topography, 33, 289-302

DOI: https://doi.org/10.1007/s10548-020-00758-5

Brain Topography
https://doi.org/10.1007/s10548-020-00758-5

ORIGINAL PAPER

Exploring Frequency-Dependent Brain Networks from Ongoing EEG Using Spatial ICA During Music Listening

Yongjie Zhu[1,2] · Chi Zhang[1] · Hanna Poikonen[6] · Petri Toiviainen[3] · Minna Huotilainen[4] · Klaus Mathiak[5] · Tapani Ristaniemi[2] · Fengyu Cong[1,2]

Received: 14 August 2019 / Accepted: 20 February 2020

Abstract

Recently, exploring brain activity based on functional networks during naturalistic stimuli especially music and video represents an attractive challenge because of the low signal-to-noise ratio in collected brain data. Although most efforts focusing on exploring the listening brain have been made through functional magnetic resonance imaging (fMRI), sensor-level electro- or magnetoencephalography (EEG/MEG) technique, little is known about how neural rhythms are involved in the brain network activity under naturalistic stimuli. This study exploited cortical oscillations through analysis of ongoing EEG and musical feature during freely listening to music. We used a data-driven method that combined music information retrieval with spatial Fourier Independent Components Analysis (spatial Fourier–ICA) to probe the interplay between the spatial profiles and the spectral patterns of the brain network emerging from music listening. Correlation analysis was performed between time courses of brain networks extracted from EEG data and musical feature time series extracted from music stimuli to derive the musical feature related oscillatory patterns in the listening brain. We found brain networks of musical feature processing were frequency-dependent. Musical feature time series, especially fluctuation centroid and key feature, were associated with an increased beta activation in the bilateral superior temporal gyrus. An increased alpha oscillation in the bilateral occipital cortex emerged during music listening, which was consistent with alpha functional suppression hypothesis in task-irrelevant regions. We also observed an increased delta–beta oscillatory activity in the prefrontal cortex associated with musical feature processing. In addition to these findings, the proposed method seems valuable for characterizing the large-scale frequency-dependent brain activity engaged in musical feature processing.

Keywords Frequency-specific networks · Music information retrieval · EEG · Independent components analysis

Introduction

Understanding how our brain perceives complex and continuous inputs from the real-world has been an attractive problem in cognitive neuroscience in the past few decades. Brain imaging technology provides an opportunity to address this issue. However, revealing brain states is generally more

Handling editor: Christoph M. Michel.

Yongjie Zhu and Chi Zhang have contributed equally to this work.

✉ Fengyu Cong
cong@dlut.edu.cn

1 School of Biomedical Engineering, Faculty of Electronic and Electrical Engineering, Dalian University of Technology, Dalian 116024, China

2 Faculty of Information Technology, University of Jyväskylä, Jyväskylä 40014, Finland

3 Department of Music, Art and Culture Studies, University of Jyväskylä, Jyväskylä 40014, Finland

4 CICERO Learning Network and Cognitive Brain Research Unit, Faculty of Educational Sciences, University of Helsinki, Helsinki 00014, Finland

5 Department of Psychiatry, Psychotherapy and Psychosomatics, Medical Faculty, RWTH Aachen, Pauwelsstraße 30, Aachen 52074, Germany

6 Institute of Learning Sciences and Higher Education, ETH Zürich, Zürich, Switzerland

Published online: 02 March 2020

difficult during real-word experiences than those recorded brain activities during resting-state or simplified abstract stimuli like controlled and rapidly repeated stimuli (Hasson et al. 2010; Malcolm et al. 2016; Spiers and Maguire 2007). The question of how to disentangle stimuli-induced brain activity from spontaneous activity still remains open for scientific research due to the complexity of natural situations. In the present study, we attempt to formulate an approach with several analysis techniques including spatial ICA, source localization, acoustic feature extraction, and temporal correlation to examine the elicited oscillatory brain networks using ongoing electroencephalography (EEG) recorded during music listening.

Recently, the brain state under the naturalistic stimuli including music and movie has been investigated through functional magnetic resonance imaging (fMRI) (Alluri et al. 2012a, b; Alluri et al. 2013; Burunat et al. 2014, 2016a, b; Liu et al. 2017; Toiviainen et al. 2014), MEG (Koskinen et al. 2013; Lankinen et al. 2014) and EEG (Cong et al. 2013a, b; Daly et al. 2014, 2015; Schaefer et al. 2013; Sturm et al. 2015; Zhu et al. 2019, 2020). Alluri et al. explored the neural correlates of music feature processing as it occurs in a realistic or naturalistic environment, where eleven participants attentively listened to the whole piece of music (Alluri et al. 2012a, b; Burunat et al. 2016b, a). They successfully identified brain regions involved in processing of musical features in a naturalistic paradigm and found large-scale brain responses in cognitive, motor and limbic brain networks during continuous processing of low-level (timbral) and high-level (tonal and rhythmical) acoustic features using fMRI. Burunat et al. studied the replicability of Alluri's findings using a similar methodological approach with a similar group of participants and found the processing mechanisms for low-level musical features were more reliable than high-level features (Burunat et al. 2016b, a). Unfortunately, all BOLD measurements by fMRI are to some degree confounded since they are indirect assessments of brain activity; they relate to blood flow and not to electrical processes and are therefore limited by poor temporal resolution due to the protracted hemodynamic response (Brookes et al. 2014; Li et al. 2019). After that, Cong et al. used an analogous to correlation analysis technique to investigate neural rhythms based on ongoing EEG data collected during listening to same music stimuli (Cong et al. 2013a, b; Wang et al. 2016). They found the theta and alpha oscillations along central and occipital area of scalp topology seems significantly associated with high-level (tonal and rhythmical) acoustic features processing. Also, many other studies tried to examine the neural underpinnings of music listening based on sensor-level EEG data (Jäncke et al. 2015, 2018; Markovic et al. 2017), in which different frequency bands were extracted using time–frequency analysis methods and further analyzed separately (e.g., event-related synchronizations and oscillatory power changes). Those studies showed the influence of different music listening styles on neurophysiological and psychological state interpreted by brain activation. Some sensor-level EEG studies examined the physiological correlates of continuous changes in subjective emotional states while listening to a complete music piece (Mikutta et al. 2012, 2014). Compared with sensor-level EEG analysis, recent studies adopted a mathematical approach (called sLORETA–ICA) combing source localization techniques with ICA to detect the independent functional networks during music listening (Jäncke and Alahmadi 2016; Rogenmoser et al. 2016). Although the aforementioned studies investigated the oscillatory activation or functional networks during music listening, the specific networks emerging from dynamic processing of musical features are not yet fully understood (Meyer et al. 2006). For example, there is evidence indicating that timbral feature processing was associated with increased activations in cognitive areas of the cerebellum, and sensory and default mode network cerebrocortical areas, but musical pulse, and tonality processing recruited cortical and subcortical cognitive, motor and emotion-related circuits (Alluri et al. 2012a, b; Meyer et al. 2006). Thus, we aimed to examine the electrophysiological underpinnings of these networks emerging from dynamic processing of musical features.

Independent component analysis (ICA) is a well-established data-driven approach increasingly used to factor resting-state fMRI data into temporally covarying, spatially independent sources or networks. By contrast, in the analysis of EEG/MEG data, ICA has mainly been applied for artifact rejection. However, spatial Fourier–ICA was proposed for data-driven characterization of oscillatory brain activity using EEG/MEG data. Compared with other ICA method applied to the context of music listening, spatial Fourier–ICA used in the current study can automatically extract narrowband oscillations from broadband data without having to manually specify a frequency band of interest. So far, spatial Fourier–ICA has already been proved to be fruitful in gaining insights into electrophysiological underpinnings of networks (Kauppi et al. 2013; Li et al. 2018; Ramkumar et al. 2014).

By applying spatial Fourier–ICA in combination with acoustical feature extraction, this study aims at probing the spatial–spectral patterns under music listening. Particularly, the current study attempts to provide an analysis framework for identifying the spatial, temporal, and spectral signatures of brain activation recruited during dynamic processing of music features. Similar to our previous music listening studies (Alluri et al. 2012a, b; Cong et al. 2013a, b), we extracted five musical features from the musical stimulus, and spatial, temporal, and spectral factors using spatial Fourier–ICA to EEG data. We then analyzed the correlation between temporal courses and the musical feature time series to identify

frequency-specific brain networks emerging from dynamic processing of musical features. We expected spatial Fourier-ICA to reveal functionally oscillatory EEG source contributing to the musical feature processing.

Material and Methods

Data Acquisition

Participants

Fourteen right-handed and healthy adults aged 20 to 46 years old were recruited to take part in the current experiment after signing written informed consent. None of them was reported about hearing loss or history of neurological illnesses and none of them had professional musical education. However, many participants reported background in different music-related interests such as learning to play an instrument, producing music with a computer, singing. Table 1 demonstrates the age and the non-professional musical background of each participant. This study was approved by the local ethics committee.

EEG Data Acquisition

During the experiment, participants were informed to listen to the music with eyes open. A 512 s long musical piece of modern tango by Astor Piazzolla was used as the stimulus. Music was presented through audio headphones with about 30 dB of gradient noise attenuation. This music clip had appropriate duration for the experimental setting, because of its high range of variation in several musical features such as dynamics, timbre, tonality and rhythm (Alluri et al. 2012a, b). The EEG data were recorded according to the international 10–20 system with BioSemi electrode caps (64 electrodes in the cap and 5 external electrodes at the tip of the nose, left and right mastoids and around the right eye both vertically and horizontally). EEG were sampled at a rate of 2048 Hz and stored for further processing in offline. The external electrode at the tip of the nose was used as the reference. EEG channels were re-referenced using a common average. The data preprocessing was carried out using EEGLAB (Delorme and Makeig 2004). The EEG data were visually inspected for artefacts and bad channels were interpolated using a spherical spline model. A notch filter at 50 Hz was applied to remove noise. High-pass and low-pass filter with 1 Hz and 30 Hz cutoff frequencies were then applied as our previous investigation of the frequency domain revealed that no useful information was found in higher frequencies (Cong et al. 2013a, b). Finally, the data were down-sampled to 256 Hz. In order to remove EOG (i.e., eye blinks), ICA was performed on EEG data of each participant. To additionally remove any DC-jumps occasionally present in the data, we differentiated each time series, applied a median filter to reject large discontinuities and reintegrated the signals back (Ramkumar et al. 2012).

Musical Features

Based on the length of the window used in the computational analyses, the musical features can be generally classified into two categories: long-term features and short-term features (Alluri et al. 2012a, b; Cong et al. 2013a, b). Five long-term musical features including Mode, Key Clarity, Fluctuation Centroid, Fluctuation Entropy and Pulse Clarity

Table 1 Age and musical background of each participant

No. of participant	Age	Years of musical activity	Instrument	Years of activity in dance	Type of dance
Sub01	20	15	Piano/singing	None	
Sub02	23	13	Piano/flute	None	
Sub03	23	16	Cello	None	
Sub04	23	None		6	Ballet
Sub05	20	2	Piano	None	
Sub06	42	15	Alto saxophone	None	
Sub07	46	None		None	
Sub08	22	7	Piano	None	
Sub09	21	None		None	
Sub10	34	6	Piano/keyboards	None	
Sub11	31	5	Piano	None	
Sub12	25	7	Piano/violin	7	Folk dance
Sub13	25	None		None	
Sub14	24	3	Piano	None	

were examined here. They were extracted using a frame-by-frame analysis approach commonly used in the field of Music Information Retrieval (MIR). The duration of the frames was 3 s and the overlap between two adjacent frames 67% of the frame length. The chosen length of the frame was approximately consistent with the length of the auditory sensory memory (Alluri et al. 2012a, b). This analysis process yielded the time series of musical feature at a sampling frequency of 1 Hz, in accordance with the short-time Fourier transform (STFT) analysis of EEG data. Thus, both the musical features and temporal courses of EEG had 512 time points. All the features were extracted using the MIRtoolbox (Lartillot et al. 2008) in MATLAB environment.

For the completeness of the content, we briefly introduce the five features below. We extracted two tonal and three rhythmic features. For the tonal features, Mode represents the strength of major or minor mode. Key Clarity is defined as the measure of the tonal clarity. The rhythmic features included Fluctuation Centroid, Fluctuation Entropy, and Pulse Clarity. Fluctuation Centroid is the geometric mean of the fluctuation spectrum, representing the global repartition of rhythm periodicities within the range of 0–10 Hz (Alluri et al. 2012a, b). This feature indicates the average frequency of these periodicities. Fluctuation entropy is the Shannon entropy of the fluctuation spectrum, representing the global repartition of rhythm periodicities. Fluctuation entropy is a measure of the noisiness of the fluctuation spectrum (Alluri et al. 2012a, b; Cong et al. 2013a, b). Pulse Clarity, naturally, is an estimate of clarity of the pulse (Alluri et al. 2012a, b; Cong et al. 2013a, b).

Source Localization

For each subject, the brain's cortical surface was reconstructed from an anatomical MRI template in Brainstorm (Tadel et al. 2011). Dipolar current sources were estimated at cortical-constrained discrete locations (source points) separated by 15 mm. Each hemisphere was modelled by a surface of approximately 2000 vertices, thus a mesh of approximately 4000 vertices modelled the cortical surface for each subject.

The measured EEG signals are generated by postsynaptic activity of ensembles of cortical pyramidal neurons of the cerebral cortex (Lei and Yao 2011). These cortical pyramidal neurons can be modelled as current dipoles located at cortical surface (Lin et al. 2006). The scalp potentials generated by each dipole depend on the characteristics of the various tissues of the head and are measured by the EEG scalp electrodes (Tian et al. 2011). With the geometry of the anatomy and the conductivity of the subject's head, the time course of the dipole's activity can be assessed by solving two consecutive problems: the forward problem and the inverse problem.

The forward problem is to model the contribution of each dipole to the signals of the EEG electrodes by solving Maxwell's equations, which takes the geometry and conductivity of head tissues into account. In this study, a forward solution was calculated using the symmetric boundary element method (BEM) for each source point while a relative conductivity coefficient was assigned to each tissue (with default MNI MRI template).

To solve the inverse problem, minimum-norm estimate (Lin et al. 2006) was adapted with a loose orientation constraint favoring source currents perpendicular to the local cortical surface (no noise modelling). When computing the inverse operator (1) the source orientations were constrained to be normal to the cortical surface; (2) a depth weighting algorithm was used to compensate for any bias affecting the superficial sources calculation; and (3) a regularization parameter, $\lambda^2 = 0.1$ was used to minimize numerical instability, and to effectively obtain a spatially smoothed solution. Finally, an inverse operator G of dimensions $N_s \times N_c$ (where N_s is the number of source points and N_c is the number of channels: $N_s \gg N_c$) was obtained to map the data from sensor-space to source-space. Here, we had $N_s = 4000$ and $N_c = 64$.

Spatial Fourier Independent Component Analysis

Spatial Fourier-ICA was recently proposed to characterize oscillatory EEG/MEG activity in cortical source space (Ramkumar et al. 2012, 2014). The main idea was to apply complex-valued ICA to short-time Fourier transforms of source-level EEG/MEG signals to reveal physiologically meaningful components. We briefly introduced the main steps of spatial Fourier-ICA for the completeness of the content. Figure 1 demonstrates the analysis pipeline based on spatial Fourier-ICA and acoustical feature extraction.

Time–Frequency Data in Cortical Source Space

Preprocessed EEG data $\boldsymbol{Y}_0$ (N_c channels $\times$ N_p sampling points) were transformed by STFT to obtain complex-valued time–frequency representation (TFR) data $\boldsymbol{Y}_1$ (N_c, N_f, N_t). To obtain TFR data in source space, three-way sensor-space TFR data $\boldsymbol{Y}_1$ was reorganized as two-way matrix $\hat{\boldsymbol{Y}}_1$ (N_c, $N_t \times N_f$). The source-space TFR data $\hat{\boldsymbol{Y}}_2$ was then obtained by left-multiplying the linear inverse operator $\boldsymbol{G}$ (N_s, N_c) which was computed using the minimum-norm estimate inverse solution sensor-space data $\hat{\boldsymbol{Y}}_1$,

$$\hat{\boldsymbol{Y}}_2 = \boldsymbol{G}\hat{\boldsymbol{Y}}_1 \tag{1}$$

Two-way data $\hat{\boldsymbol{Y}}_2$ (N_s, $N_t \times N_f$) can be rearranged as a three-way tensor format $\boldsymbol{Y}_2$ (N_s, N_t, N_f). For application of spatial Fourier ICA, we then rearranged the three-way tensor

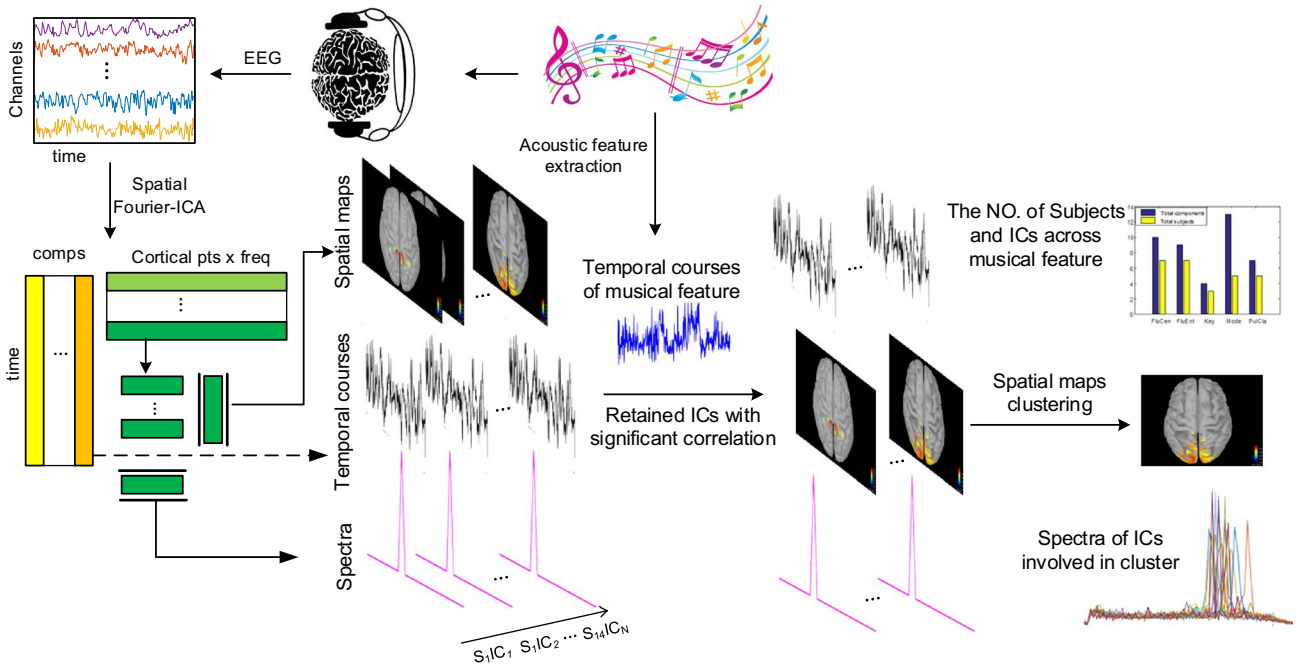

Fig. 1 Analysis pipeline based on spatial Fourier–ICA and acoustical feature extraction. Temporal, spectral and spatial profiles of brain pattern were extracted using spatial Fourier–ICA. Musical feature time series were extracted using acoustical feature extraction. Then, correlation analysis between temporal course of components and musical time series were performed to retain music elicited components. The spatial maps of retained components were clustered into several patterns

$\boldsymbol{Y}_2$ as a two-way matrix X_0 (N_t,$N_f \times N_s$). Thus, each row of $\boldsymbol{X}_0$ was comprised of the complex-valued short-time Fourier coefficients from each source point for specific time points and each column represented a time point corresponding to a short-time window. In this study, the Hamming-widow with 3-s-length and 2-s-overlap of the adjacent windows was selected, resulting in a sampling rate of 1 Hz in time dimension. This sampling rate was in consistent with musical feature time series (see Musical features). The duration of EEG was 512 s, so we had $N_t = 512$ time points. We adopted a 512-point FFT to calculate the STFT resulting in 256 frequency bins (Range of frequency: 1–128 Hz) for each window. We selected the range of frequency bins covering 1–30 Hz ($N_f = 60$) for further analysis.

Application of Complex-Valued ICA on Reshaped Data

For data $\boldsymbol{X}_0$, we applied complex-valued ICA (A. Hyvarinen et al. 2010) and treated each row as an observed signal assumed to be a linear mixture of unknown spatial spectral pattern. Since the original data ($\boldsymbol{X}_0$) dimension was relatively high for the complex ICA calculation, data dimension reduction was required in the preprocessing step of ICA. A common approach of data dimension reduction is principal component analysis (PCA) which is linear. Here we extended PCA to the complex domain by considering complex-valued eigenvalue decomposition (Li et al. 2011). The choice of model order was based on previous studies (Abou-Elseoud et al. 2010; Smith et al. 2009), which suggested the number of a dimension slightly larger than the expected number of underlying sources. In this study, we tried different model orders and found that 20 was a reasonable order, which preserved much of the information in the data and reduced the dimensionality of the results. Then we extracted 20 independent components using complex-valued FastICA algorithm which applied ICA to STFT of EEG data in order to find more interesting sources than with time-domain ICA (A. Hyvarinen et al., 2010). This method is especially useful for finding sources of rhythmic activity. After complex-valued ICA, a mixing matrix $\widehat{\boldsymbol{A}}$ (N_t, $N_{ic} = 20$ is number of components) and estimated source matrix $\widehat{S}$ were obtained. Each column of $\widehat{A}$ represented the temporal course for each independent component (IC). The ICs in the rows of $\widehat{S}$ (N_{ic}, $N_f \times N_s$) represented spatial-spectral patterns, which can be decomposed into the spatial power map and power spectra.

Spatial Map, Spectrum, and Temporal Course of ICs

By reshaping each row of $\widehat{\boldsymbol{S}}$ for each IC, we obtained a matrix (N_f, N_s), which meant there was a Fourier coefficient spectrum for each cortical source point. To obtain and visualize the spatial map of the IC, we computed the average of the squared magnitude of the complex Fourier coefficients

across those frequency bins. Since the distribution of mean squared Fourier amplitude over the whole brain is highly non-Gaussian, we did not apply conventional z-score-based thresholding; instead, we applied a threshold to display for each component map only source points with the top 5% squared Fourier amplitude (Ramkumar et al. 2012). Then we analyzed the correlation coefficient of the spatial maps in those frequency bins and those spatial maps were similar. To visualize and obtain the spectrum of each IC, we calculated the mean of the Fourier power spectrum across those source points exceeding the 95th percentile (Ramkumar et al. 2012). Finally, we extracted the absolute values of the column of mixing matrix $\widehat{\boldsymbol{A}}$ corresponding to the row of the estimated IC as the time course, which reflected fluctuations of the Fourier amplitude envelope for the specific frequency and spatial profile.

Stability of ICA Decomposition

To examine the stability of ICA, we applied 100 times ICA decomposition for each subject with different initial conditions. For the real-valued case, ICASSO toolbox (Himberg et al. 2004) has been used to evaluate stability among multiple estimates of the fastICA algorithm (Hyvarinen 1999). All the components estimated from all runs were collected and clustered based on the absolute value of the correlation coefficients among the squared source estimates of ICASSO. Finally, the stability index Iq was computed for each component. Iq reflects the isolation and compactness of a cluster (Himberg et al. 2004). Iq is calculated as follows:

$$\mathrm{Iq} = \overline{S}(i)_{int} - \overline{S}(i)_{ext}, \mathrm{i} = 1, \ldots, \mathrm{J} \tag{2}$$

where $\overline{S}(i)_{int}$ denotes the average intra-cluster similarity; $\overline{S}(i)_{ext}$ indicates average inter-cluster similarity and J is the number of clusters. The Iq ranges from '0′ to '1′. When Iq approaches '1′, it means that the corresponding component is extracted in almost every ICA decomposition application. This indicates a high stability of the ICA decomposition for that component. Otherwise, it means the ICA decomposition is not stable. Correspondingly, if all the clusters are isolated with each other, ICA decomposition should be stable. In general, there is no established criterion upon which to base a threshold for cluster quality. Given the preliminary nature of this investigation, we consider the decomposition is stable if the Iq is greater than 0.7.

In this study, the ICASSO toolbox was modified to be available for the complex-valued case as well. The correlation matrix was used as the similarity measure for clustering in real-valued ICASSO. For the complex case, since the ICs were complex-valued, we just considered the correlation matrix among the magnitude ICs to perform the clustering (Li et al. 2011). Then, we took the Iq as the criterion to examine stability of the ICA estimate.

Testing for Stimulus-Related Networks

After ICA decomposition, we obtained $20 \times 14 = 280$ ICs (14 subjects, 20 components for each subject). Now the challenge is to determine which one of these represents the genuine brain responses. In all ICA based methods, it is a general question that which independent components need to be retained or which component just reflects noise. Here, we examine which components were modulated significantly by the musical features. We computed the correlation (Pearson's correlation coefficient) between the time courses of musical features and the time courses of those ICs (the dimensionality of both them is 512 points) in order to select stimulus-related activations. We used the Monte Carlo method and permutation tests presented in our previous research (Alluri et al. 2012a, b; Cong et al. 2013a, b) to calculate the threshold of significant correlation coefficient. In this method, a Monte Carlo simulation of the approach was performed to determine the threshold for multiple comparisons. We kept those ICs whose time courses were significantly correlated ($p < 0.05$) with the time courses of musical features for further analysis.

Cluster Analysis

The selected ICs had been represented by spatial map, spectrum, and temporal course. Since spatial ICA was carried out on individual level EEG data, we needed to examine the inter-subject consistency among participants. In this study, we focused on the spatial pattern emerging in the process of freely listening to music, so a group level data analysis was performed by clustering spatial maps of the selected ICs to evaluate the consistency among the participants. For reliable clustering, we applied a conventional z-score-based normalization to each spatial map. All spatial maps of the screened components significantly correlated with musical features were clustered into M clusters to find common spatial patterns among most of participants. Here for simplicity, a conventional k-means cluster algorithm was used with the Kaufman Approach (KA) for initializing the algorithm. We used the minimum description length (MDL) to determine the number of clusters M. Afterwards we countered the number of subjects involved in ICs in each cluster. If the number of subjects in one cluster is less than half of the all subjects, this cluster would be discarded for the reason that such a cluster does not reveal information shared among enough participants. For the retained clusters, the spatial-spectral-temporal information was obtained, which was represented by the centroid of the cluster, the spectra

of ICs and the numbers of subjects whose temporal courses were involved in this cluster.

Results

Musical Features

Five musical features were extracted by MIRtoolbox (Lartillot and Toiviainen 2007) with 3 s time-widow and 2 s overlap, resulting in 1 Hz sampling rate of temporal course. They are Fluctuation Centroid, Fluctuation Entropy, Key Clarity, Mode and Pulse Clarity. The time series of these features had a length of 512 samples, which matched the length of the time course of the EEG components. Figure 2 shows their temporal courses.

Stability of ICA Decomposition

We extracted 20 ICs using modified ICASSO with 100 runs for each subjects' data, then we obtained the stability index Iq. Figure 3 shows the magnitude of Iqs for each participant, greater than 0.7 for most ICs. The 20 ICs were separated with each other for every participant from the view of clustering. Thus, the ICA estimate was stable and the results of ICA decomposition in this study were satisfactory for each participant data to further analysis.

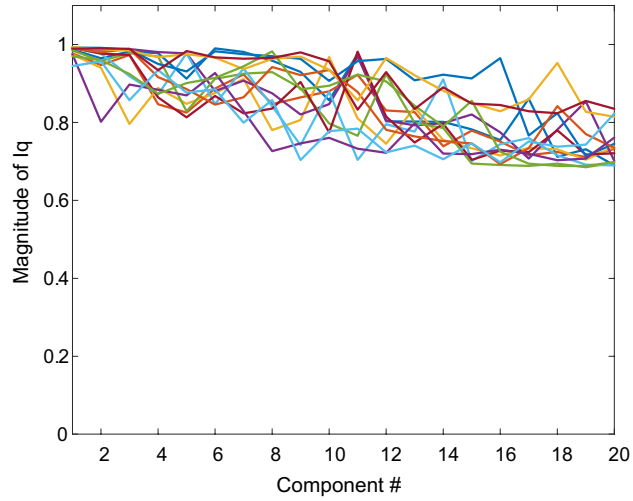

Fig. 3 Iq of each component extracted. Different curves represent different participants

Interesting Clusters: Frequency-Specific Networks

After 85 ICs whose spatial maps were significantly correlated with musical features were selected, we set the number of clusters as five by performing MDL to estimate the optimal model order. Then the spatial maps of ICs were clustered into five clusters. Three clusters representing

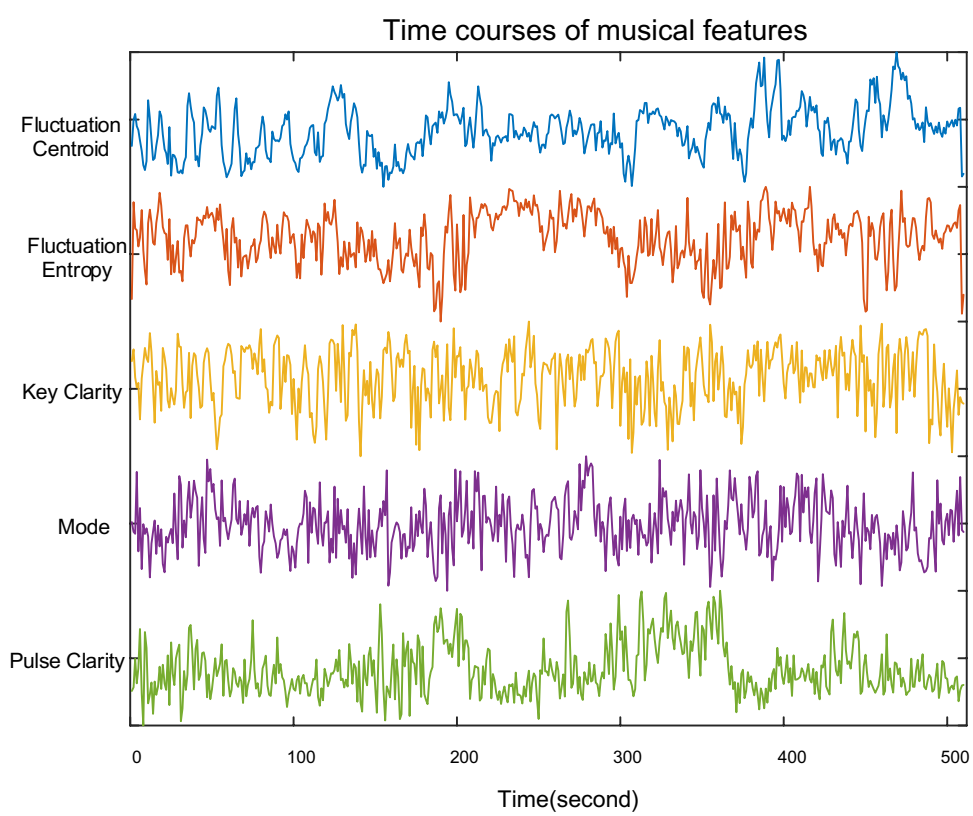

Fig. 2 Time course of five musical features

frequency-specific networks were chosen since the number of subjects in the cluster is more than half of the all subjects. Figure 4 demonstrates one of these clusters including the centroid of all spatial maps (Fig. 4a), the distribution of number of subjects across musical features (Fig. 4b) and the spectrum of the ICs in this cluster (Fig. 4c). Then we computed the correlation coefficients among spatial maps in each cluster to evaluate the performance of clustering. Figure 5 shows the inter-cluster similarity. We computed the mean of the correlation coefficients in each cluster and the corresponding standard deviation (SD). For cluster#1, the mean is 0.642 and the corresponding standard deviation (SD) is 0.1238. For cluster#2, the mean is 0.7125 and SD is 0.0572. For cluster#3, the mean is 0.8084 and SD is 0.0747. This indicates that the spatial patterns are similar across the participants. In the Table 2, we listed the participants whose EEG data were correlated with every musical feature in each cluster.

Beta-Specific Network

Figure 4 shows results of the Beta-specific brain networks engaged in processing music features. The spatial map displays that musical features were associated with increased activation in the bilateral superior temporal gyrus (STG). The spectrum of ICs in this cluster illustrates the beta rhythm (focusing on 20 Hz) was involved in generating this network. Thus, relatively large-scale brain region generated by beta rhythm was activated in the bilateral STG and the magnitude of activation in right hemisphere was a little stronger than left hemisphere. This Beta-specific network was found in seven subjects during music free-listening (see the first row of Table 2). Fluctuation Centroid were associated with this brain networks among subjects 2, 4, 5, and 12. The brain networks of subjects 1, 2, 3 and 13 were correlated with key feature. For fluctuation entropy, pulse clarity and mode,

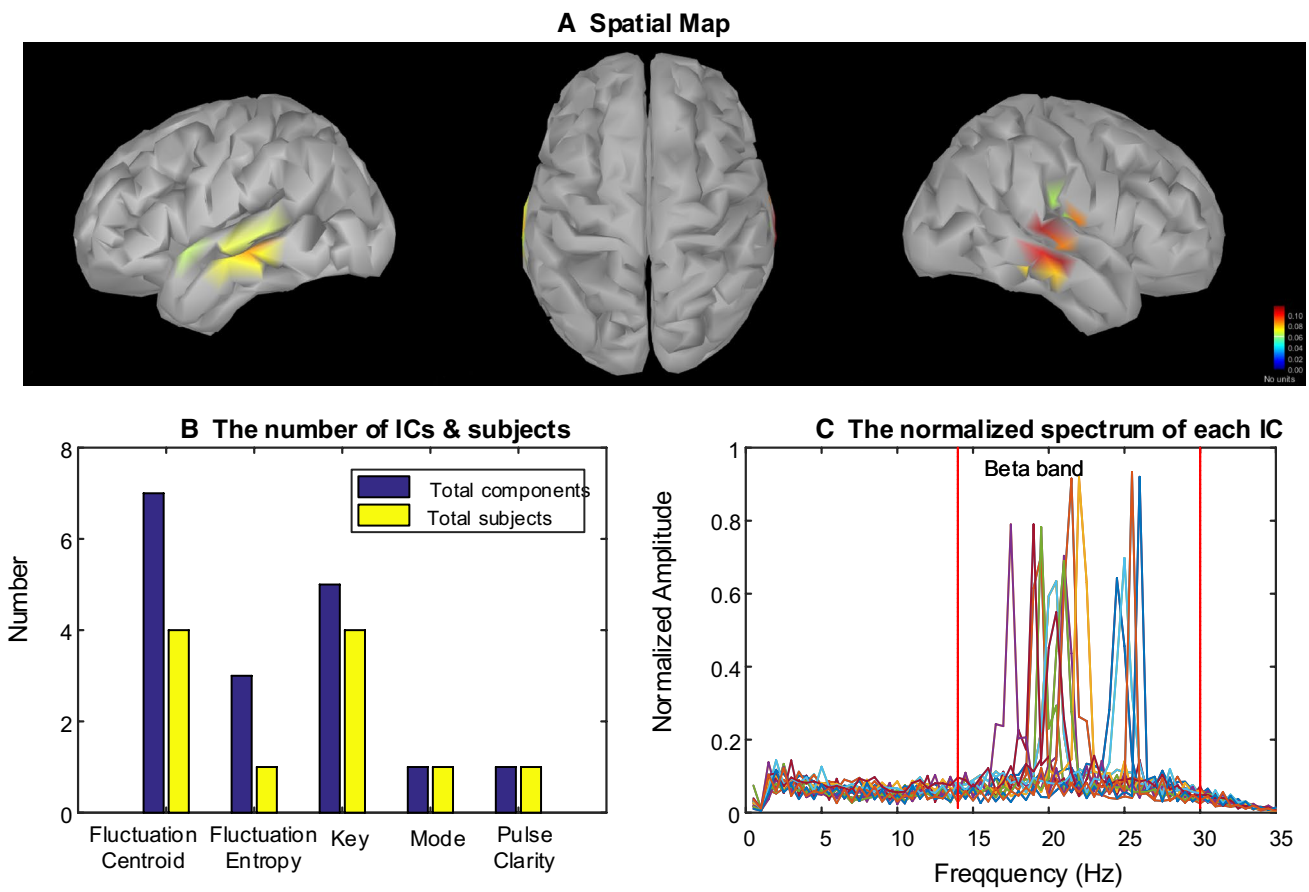

Fig. 4 Cluster#1: Beta-specific networks. **a** The centroid of the spatial maps in the cluster, which reflected a spatial pattern across most of participants. The bilateral superior temporal gyrus (STG) was activated (from left to right: left hemisphere, top view, right hemisphere). **b** The number of ICs and subjects involved in the cluster were distributed across musical features. **c** The spectra of each components were located in delta or beta band. Different curves represent different ICs

there was one subject involved in this cluster respectively. In addition, the number of ICs correlated with the musical features was more than the number of participants since there were 20 ICs for each subject.

Alpha-Specific Network

Figure 6 displays relatively large brain activity in the bilateral occipital lobe according to the spatial map. As can be seen, the oscillations of this pattern were dominated by alpha rhythm (focusing on 10 Hz) with few ICs located in Delta band. There were eight participants appearing alpha-specific occipital networks under free-listening to music. The second row of the Table 2 shows the subjects involved in the networks linked with each musical feature.

Delta-Beta-Specific Network

Figure 7a illustrates increased activity linked with musical features in bilateral prefrontal gyrus (PFG). The spectrum (Fig. 7c) shows both beta and delta oscillations recruited these areas across participants. The delta-beta-specific networks were found in eight subjects. Mode was associated with this brain networks among subjects 2, 3, 4, 6, 7 and 9. The networks of subjects 4, 5, 7, 9 and 11 were correlated with Fluctuation Centroid (see the third row of Table 2).

Discussion

In this study, we investigated spatial spectral profiles of brain networks during music free-listening. To this end, we proposed a novel method combing spatial ICA, source localization and music information retrieval. EEG data were recorded when participants listened to a piece of music freely. Firstly, we applied STFT to preprocessed EEG data. After this, an inverse operator was obtained using source localization and the sensor-space data was mapped to source-space data. Then complex-valued ICA was performed to extract spatial-spectral patterns. The stability of ICA estimate was evaluated using a complex-value ICASSO. Meanwhile, the temporal evolutions of five long-term musical features were extracted by the commonly used MIRtoolbox. Following this, the spatial-spectral ICs related to music stimuli were chosen by correlating their temporal course with the temporal course of musical features. To examine the inter-subject consistency, a cluster analysis was applied to spatial patterns of the retained ICs. Overall, our results highlighted the frequency-dependent brain networks during freely listening to music. The results are consistent with previous findings published in other studies (Alluri et al. 2012a, b; Cong et al. 2013a, b; Janata et al. 2002).

It was found that beta-specific brain networks in the bilateral STG emerged from dynamic processing of musical features (see Fig. 4). The bilateral STG were mostly activated

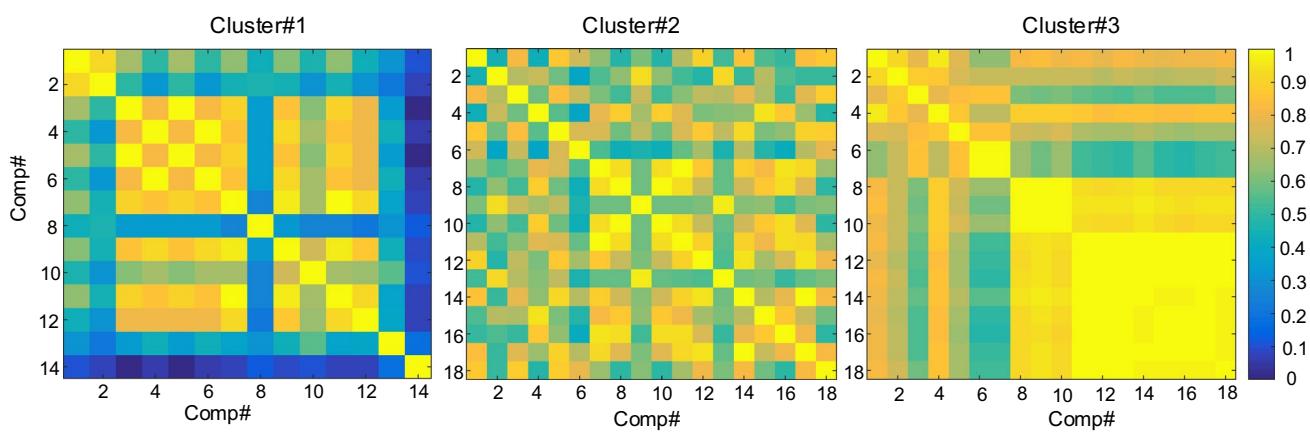

Fig. 5 Correlation coefficients matrix among spatial maps of the ICs in each cluster. The mean correlation coefficient in cluster#1 is 0.642 and the corresponding standard deviation (SD) is 0.1238. For cluster#2 the mean is 0.7125 and SD is 0.0572. For cluster#3, the mean is 0.8084 and SD is 0.0747

Table 2 Participants involved in each cluster across musical features among 14 subjects (from 1 to 14)

Cluster	Musical features					Total subjects
	Fluctuation centroid	Fluctuation entropy	Key clarity	Mode	Pulse clarity	
#1	2 4 5 12	2	1 2 3 13	4	5	7
#2	1 8 10 14	8 11 13	7 8 14	2 8 11 14	1 10 13	8
#3	4 5 7 9 11	3 6	5 6 9	2 3 4 6 7 9	7	8

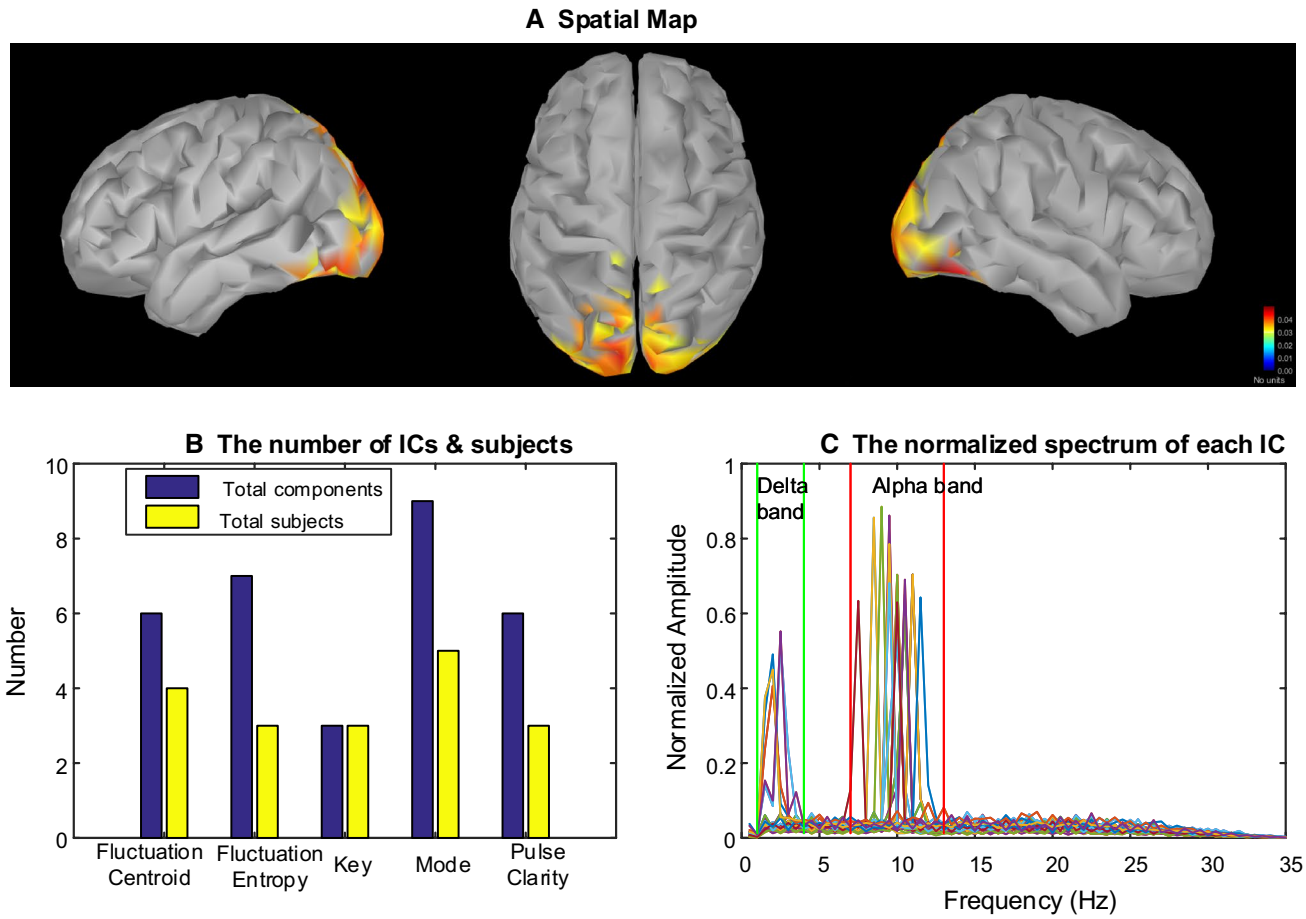

Fig. 6 Cluster#2: Alpha–Delta-specific networks. **a** The centroid of the spatial maps in the cluster, which reflected a spatial pattern across most of participants. As can be seen that the bilateral occipital cortex was activated (from left to right: left hemisphere, top view, right hemisphere). **b** The number of ICs and subjects involved in the cluster were distributed across musical features. **c** The spectra of each components were located in delta or beta band. Different curves represent different ICs

during music listening, which was involved in long-term musical features processing. It was interesting to note that the beta oscillations were enhanced in this bilateral spatial profile (see Fig. 4c). This spatial-spectral pattern appeared more related with Fluctuation Centroid and Key processing than Fluctuation Entropy, Mode and Pulse Clarity (see Fig. 4b). The same areas were found in previous studies where timbre-related features were correlated with activations in large areas of the temporal lobe using fMRI (Alluri et al. 2012a, b). Besides, early MEG studies demonstrated that cortical rhythm activity in beta band activity (15–30 Hz) was tightly coupled to behavioral performance in musical listening and associated with predicting the upcoming note events (Doelling and Poeppel 2015). Since beta bands have been associated with motor and rhythmic processes, listeners may voluntarily engage in mental activities related to motor during listening to segments engaged in dancing (Meyer et al. 2006; Poikonen et al. 2018b). For the participants who like dancing, music is comprehensive and collaborative. Music forms a setting in which dancers produce movements that are coherent with (or intentionally in contrast to) the prevailing sound in terms of rhythm, sentiment, and movement style (Poikonen et al. 2018a). When freely listening, a participant might be more focused on the gist of the music than to the sequence of an individual instrument, melody contour, or rhythmic pattern. Importantly, in the current study, no participant was familiar with the presented music stimuli. Thus, the beta-specific brain networks emerging in the bilateral STG could reflect the activation of higher-level brain processes (Pearce et al. 2010; Poikonen et al. 2018b).

We also observed alpha oscillatory visual networks (see Fig. 6), which is in line with our previous study (Cong et al. 2013a, b). Alpha oscillations play an important role in basic cognitive process, which is linked to suppression and selection of attention (Klimesch 2012). Event-related brain activation in alpha band has been found in studies with sensory

or motor tasks and with attention and working memory tasks. For example, alpha event-related synchronization was showed over the leg area of the motor cortex while event-related desynchronization in alpha was observed over the hand area when participants performed hand-movement tasks. This compensatory distribution of alpha activity demonstrates that alpha oscillation in task-irrelevant regions is associated with cortical disengagement (Pfurtscheller 2003). That could be the reason that the alpha-specific power over visual cortices was larger when attention was focused on the auditory stimuli.

A delta-beta oscillatory network in prefrontal cortex were also observed during listening to music (see Fig. 7). Helfrich et al. argued that the prefrontal cortex provides the structural basis for numerous higher cognitive functions and oscillatory dynamics of prefrontal cortex provide a functional basis for flexible cognitive control of goal-directed behavior (Helfrich and Knight 2016). Besides, prefrontal cortex has the function of entrainment as a mechanism of top-down control (Helfrich and Knight 2016). Our findings provided the evidence that the higher cognitive function with specific rhythms were involved in continuous and naturalistic music. Janata et al. identified an area in the rostromedial prefrontal cortex as a possible brain units for tonal processing (Janata et al. 2002). In addition, some studies demonstrated that oscillations in the delta and beta bands were instrumental in predicting the occurrence of auditory targets (Arnal et al. 2015; Doelling and Poeppel 2015). Music is shown to be a powerful stimulus modulating emotional arousal, an increase of posterior alpha, central delta, and beta rhythm was observed during high arousal (Mikutta et al. 2012; Poikonen et al. 2016a, b; Poikonen et al. 2016a, b). That may explain why the delta–beta oscillations in this study appears in prefrontal cortex (Fig. 7).

From the methodology consideration, most of these studies investigated one pattern of the spatial spectral profile

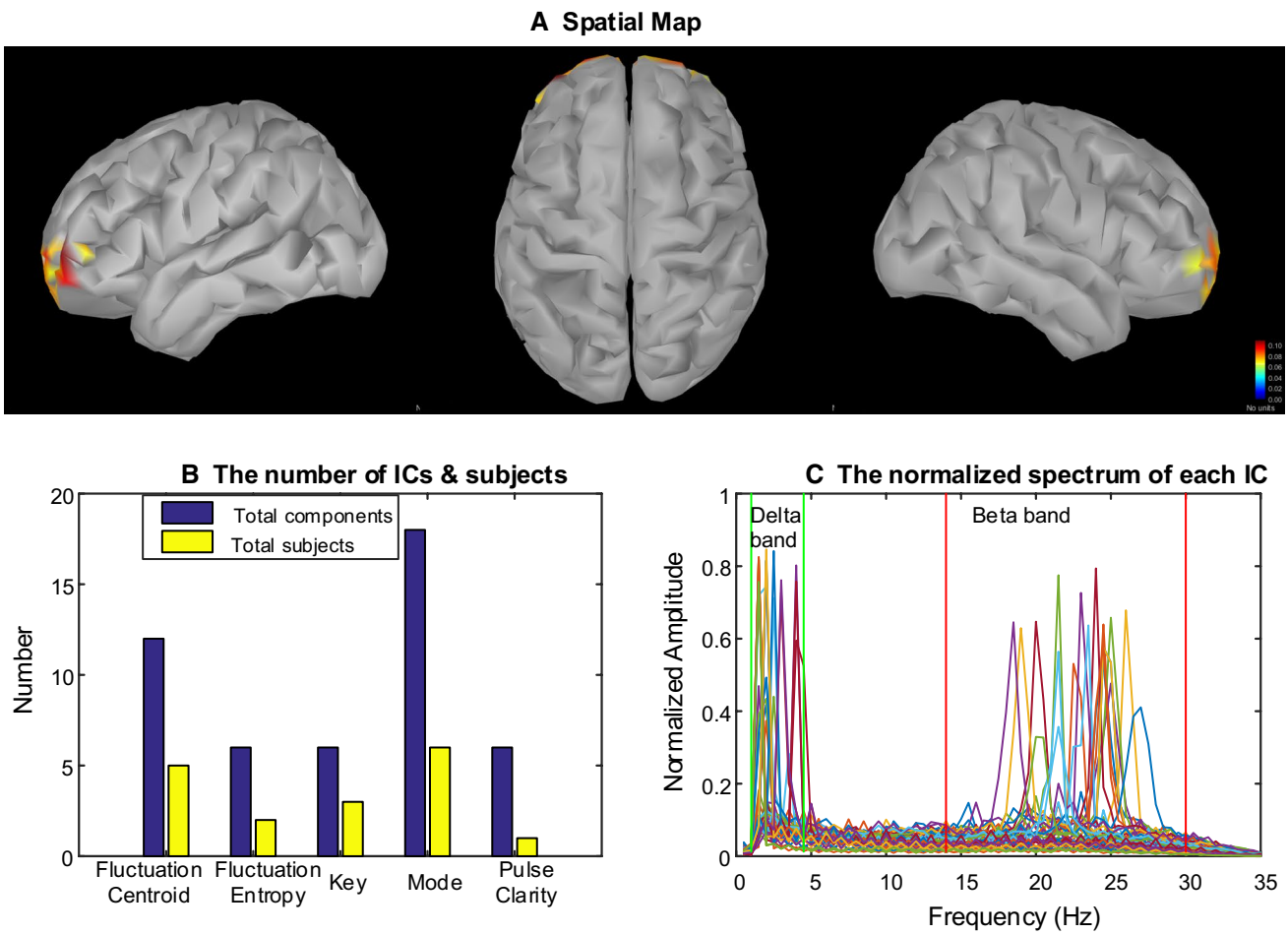

Fig. 7 Cluster#3: Alpha–Beta-specific networks. **a** The centroid of the spatial maps in the cluster, which reflected a spatial pattern across most of participants. As can be seen that the bilateral prefrontal cortex was activated (from left to right: left hemisphere, top view, right hemisphere). **b** The number of ICs and subjects involved in the cluster was distributed across musical features. **c** The spectra of each components were located in delta or beta band. Different curves represent different ICs

and did not examined the interplay between brain networks and spectral mode. In contrast, we studied the interactions between brain region and cortical oscillations and found the brain networks during music listening were frequency-dependent. In terms of our proposed approach for analysis of frequency-specific networks during naturalistic music listening, we can credibly find the spatial-spectral patterns elicited by musical stimulus. There are some related approaches using spatial ICA in a variety of specific techniques to investigate the RSNs under MEG data. Nugent et al. proposed a method named as MultibandICA to derive frequency-specific spatial profile in RSNs. However, six frequency bands (delta, theta, alpha, beta, gamma, high gamma) firstly need to be extracted from the MEG data and were concatenated in certain dimensionality; ICA was then performed to concatenated data (Nugent et al. 2017). Similar methods were proposed in (Sockeel et al. 2016). Here distinctly, the proposed approach is completely data-driven and does not require pre-define the frequency band. Another important asset of our study is that the clustering was applied to the spatial maps to examine the inter-subject consistency in proposed method. The correlation coefficients were then computed in each cluster. We observed that the individual spatial-spectral profiles in every retained cluster were similar but the corresponding time courses were different. This is different from analysis of event-related potential (ERP) where temporal ICA components sharing identical spatial profiles might be similar. The differences might be resulted from different responses of participants under real-word experiences. In the future, we will attempt to develop group spatial ICA to analyze group-level data where the individual data are concatenated in time dimension.

Conclusion

In this study, we introduced a novel framework with several techniques including Fourier ICA, source estimation, acoustic feature extraction, and clustering for exploiting the spectral–spatial structure of brain during naturalistic stimulus. A complex-value ICA applied to source-space time–frequency representation of EEG data. Following this, a modified ICASSO was performed to evaluate the stability of ICA estimate and a cluster analysis was applied to examine the inter-subject consistency. The identified networks involved in music perception were in line with those previous studies. Further, we found that brain networks under music listening were frequency-specific and three frequency-dependent networks associated with processing musical features were observed.

Acknowledgement Open access funding provided by University of Jyväskylä (JYU). This work was supported by the National Natural Science Foundation of China (Grant No. 91748105), the Fundamental Research Funds for the Central Universities [DUT2019] in Dalian University of Technology in China, and the scholarship from China Scholarship Council (No. 201600090042).

Appendix

The features were extracted from the stimulus on a frame-by-frame basis (see (Alluri and Toiviainen 2010) for more details). A brief description of each of the acoustic features is presented below. A detailed explanation can be found in the user manual of the MIRToolbox (Lartillot and Toiviainen 2007).

Mode strength of major of minor mode.

Key Clarity the strength of the estimated key, computed as the maximum of cross-correlations between the chromagram extracted from the music and tonality profiles representing all the possible key candidates.

Fluctuation Centroid geometric mean of the fluctuation spectrum representing the global repartition of rhythm periodicities within the range of 0–10 Hz, indicating the average frequency of these periodicities.

Fluctuation Entropy Shannon entropy of the fluctuation spectrum (Pampalk et al. 2002) representing the global repartition of rhythm periodicities. Fluctuation entropy is a measure of the noisiness of the fluctuation spectrum. For example, a noisy fluctuation spectrum can be indicative of several co-existing rhythms of different periodicities, thereby indicating a high level of rhythmic complexity.

Pulse Clarity the strength of rhythmic periodicities sound, representing how easily the underlying pulsation in music can be perceived.

References

Abou-Elseoud A, Starck T, Remes J, Nikkinen J, Tervonen O, Kiviniemi V (2010) The effect of model order selection in group PICA. Hum Brain Mapp 31(8):1207–1216

Alluri V, Toiviainen P (2010) Exploring perceptual and acoustical correlates of polyphonic timbre. Music Perception: An Interdisciplinary Journal 27(3):223–242

Alluri V, Toiviainen P, Jaaskelainen IP, Glerean E, Sams M, Brattico E (2012a) Large-scale brain networks emerge from dynamic processing of musical timbre, key and rhythm. Neuroimage 59(4):3677–3689. https://doi.org/10.1016/j.neuroimage.2011.11.019

Alluri V, Toiviainen P, Jääskeläinen IP, Glerean E, Sams M, Brattico E (2012b) Large-scale brain networks emerge from dynamic processing of musical timbre, key and rhythm. Neuroimage 59(4):3677–3689

Alluri V, Toiviainen P, Lund TE, Wallentin M, Vuust P, Nandi AK, … Brattico E (2013) From Vivaldi to Beatles and back: predicting lateralized brain responses to music. Neuroimage 83:627–636. https://doi.org/10.1016/j.neuroimage.2013.06.064

Arnal LH, Doelling KB, Poeppel D (2015) Delta-Beta Coupled Oscillations Underlie Temporal Prediction Accuracy. Cereb Cortex 25(9):3077–3085. https://doi.org/10.1093/cercor/bhu103

Brookes MJ, O'neill, GC, Hall, EL, Woolrich MW., Baker A, Corne, SP, … Barnes GR (2014) Measuring temporal, spectral and spatial changes in electrophysiological brain network connectivity. Neuroimage 91:282–299

Burunat I, Alluri V, Toiviainen P, Numminen J, Brattico E (2014) Dynamics of brain activity underlying working memory for music in a naturalistic condition. Cortex 57:254–269. https://doi.org/10.1016/j.cortex.2014.04.012

Burunat I, Toiviainen P, Alluri V, Bogert B, Ristaniemi T, Sams M, Brattico E (2016a) The reliability of continuous brain responses during naturalistic listening to music. Neuroimage 124(Pt A):224–231. https://doi.org/10.1016/j.neuroimage.2015.09.005

Burunat I, Toiviainen P, Alluri V, Bogert B, Ristaniemi T, Sams M, Brattico E (2016b) The reliability of continuous brain responses during naturalistic listening to music. NeuroImage 124:224–231

Cong F, Alluri V, Nandi AK, Toiviainen P, Fa R, Abu-Jamous B, … Huotilainen M (2013) Linking brain responses to naturalistic music through analysis of ongoing EEG and stimulus features. IEEE Trans Multimed 15(5):1060–1069

Daly I, Malik A, Hwang F, Roesch E, Weaver J, Kirke A, … Nasuto SJ (2014) Neural correlates of emotional responses to music: an EEG study. Neurosci Lett 573:52–57. https://doi.org/10.1016/j.neulet.2014.05.003

Daly I, Williams D, Hallowell J, Hwang F, Kirke A, Malik A, … Nasuto SJ (2015) Music-induced emotions can be predicted from a combination of brain activity and acoustic features. Brain Cogn 101:1–11. https://doi.org/10.1016/j.bandc.2015.08.003

Delorme A, Makeig S (2004) EEGLAB: an open source toolbox for analysis of single-trial EEG dynamics including independent component analysis. J Neurosci Methods 134(1):9–21. https://doi.org/10.1016/j.jneumeth.2003.10.009

Doelling KB, Poeppel D (2015) Cortical entrainment to music and its modulation by expertise. Proc Natl Acad Sci USA 112(45):E6233–6242. https://doi.org/10.1073/pnas.1508431112

Hasson U, Malach R, Heeger DJ (2010) Reliability of cortical activity during natural stimulation. Trends Cogn Sci 14(1):40–48. https://doi.org/10.1016/j.tics.2009.10.011

Helfrich RF, Knight RT (2016) Oscillatory dynamics of prefrontal cognitive control. Trends Cogn Sci 20(12):916–930. https://doi.org/10.1016/j.tics.2016.09.007

Himberg J, Hyvarinen A, Esposito F (2004) Validating the independent components of neuroimaging time series via clustering and visualization. Neuroimage 22(3):1214–1222. https://doi.org/10.1016/j.neuroimage.2004.03.027

Hyvarinen A (1999) Fast and robust fixed-point algorithms for independent component analysis. IEEE Trans Neural Netw 10(3):626–634. https://doi.org/10.1109/72.761722

Hyvarinen A, Ramkumar P, Parkkonen L, Hari R (2010) Independent component analysis of short-time Fourier transforms for spontaneous EEG/MEG analysis. Neuroimage 49(1):257–271. https://doi.org/10.1016/j.neuroimage.2009.08.028

Janata, P., Birk, J. L., Van Horn, J. D., Leman, M., Tillmann, B., & Bharucha, J. J. (2002). The cortical topography of tonal structures underlying Western music. Science, 298 (5601), 2167–2170.

Jäncke L, Alahmadi N (2016) Detection of independent functional networks during music listening using electroencephalogram and sLORETA-ICA. Neuroreport 27(6):455–461

Jäncke L, Kühnis J, Rogenmoser L, Elmer S (2015) Time course of EEG oscillations during repeated listening of a well-known aria. Front Hum Neurosci 9:401

Jäncke L, Leipold S, Burkhard A (2018) The neural underpinnings of music listening under different attention conditions. Neuroreport 29(7):594–604

Kauppi J-P, Parkkonen L, Hari R, Hyvärinen A (2013) Decoding magnetoencephalographic rhythmic activity using spectrospatial information. Neuroimage 83:921–936

Klimesch W (2012) alpha-band oscillations, attention, and controlled access to stored information. Trends Cogn Sci 16(12):606–617. https://doi.org/10.1016/j.tics.2012.10.007

Koskinen M, Viinikanoja J, Kurimo M, Klami A, Kaski S, Hari R (2013) Identifying fragments of natural speech from the listener's MEG signals. Hum Brain Mapp 34(6):1477–1489. https://doi.org/10.1002/hbm.22004

Lankinen K, Saari J, Hari R, Koskinen M (2014) Intersubject consistency of cortical MEG signals during movie viewing. Neuroimage 92:217–224. https://doi.org/10.1016/j.neuroimage.2014.02.004

Lartillot O, Toiviainen P (2007) A Matlab toolbox for musical feature extraction from audio. Paper presented at the International conference on digital audio effects.

Lartillot O, Toiviainen P, Eerola T (2008) A matlab toolbox for music information retrieval. In Data analysis, machine learning and applications (pp. 261–268): Springer.

Lei X, Yao D (2011) EEG source localization based on multiple fMRI spatial patterns. In Advances in Cognitive Neurodynamics (II) (pp. 381–385): Springer.

Li C, Yuan H, Shou G, Cha Y-H, Sunderam S, Besio W, Ding L (2018) Cortical statistical correlation tomography of EEG resting state networks. Front Neurosci 12.

Li F, Yi C, Song L, Jiang Y, Peng W, Si Y, … Zhang Y (2019) Brain network reconfiguration during motor imagery revealed by a large-scale network analysis of scalp EEG. Brain Topogr 32(2):304–314

Li H, Correa NM, Rodriguez PA, Calhoun VD, Adali T (2011) Application of independent component analysis with adaptive density model to complex-valued fMRI data. IEEE Trans Biomed Eng 58(10):2794–2803. https://doi.org/10.1109/TBME.2011.2159841

Lin FH, Belliveau JW, Dale AM, Hamalainen MS (2006) Distributed current estimates using cortical orientation constraints. Hum Brain Mapp 27(1):1–13. https://doi.org/10.1002/hbm.20155

Liu C, Abu-Jamous B, Brattico E, Nandi AK (2017) Towards tunable consensus clustering for studying functional brain connectivity during affective processing. Int J Neural Sys 27(02):1650042

Malcolm GL, Groen II, Baker CI (2016) Making sense of real-world scenes. Trends Cogn Sci 20(11):843–856. https://doi.org/10.1016/j.tics.2016.09.003

Markovic A, Kühnis J, Jäncke L (2017) Task context influences brain activation during music listening.Front Hum Neurosci 11:342

Meyer M, Baumann S, Jancke L (2006) Electrical brain imaging reveals spatio-temporal dynamics of timbre perception in humans. Neuroimage 32(4):1510–1523

Mikutta C, Altorfer A, Strik W, Koenig T (2012) Emotions, arousal, and frontal alpha rhythm asymmetry during Beethoven's 5th symphony. Brain Topogr 25(4):423–430

Mikutta C, Maissen G, Altorfer A, Strik W, König T (2014) Professional musicians listen differently to music. Neuroscience 268:102–111

Nugent AC, Luber B, Carver FW, Robinson SE, Coppola R, Zarate CA Jr (2017) Deriving frequency-dependent spatial patterns in MEG-derived resting state sensorimotor network: A novel multiband ICA technique. Hum Brain Mapp 38(2):779–791. https://doi.org/10.1002/hbm.23417

Pampalk E, Rauber A, Merkl D (2002) Content-based organization and visualization of music archives. In: Proceedings of the tenth ACM international conference on Multimedia. pp 570–579

Pearce MT, Ruiz MH, Kapasi S, Wiggins GA, Bhattacharya J (2010) Unsupervised statistical learning underpins computational, behavioural, and neural manifestations of musical expectation. Neuroimage 50(1):302–313

Pfurtscheller G (2003) Induced oscillations in the alpha band: functional meaning. Epilepsia 44:2–8

Poikonen H, Alluri V, Brattico E, Lartillot O, Tervaniemi M, Huotilainen M (2016a) Event-related brain responses while listening to entire pieces of music. Neuroscience 312:58–73

Poikonen H, Toiviainen P, Tervaniemi M (2016b) Early auditory processing in musicians and dancers during a contemporary dance piece. Sci Rep 6:33056

Poikonen H, Toiviainen P, Tervaniemi M (2018a) Dance on cortex: Enhanced theta synchrony in experts when watching a dance piece. Eur J Neurosci 47(5):433–445

Poikonen H, Toiviainen P, Tervaniemi M (2018b) Naturalistic music and dance: cortical phase synchrony in musicians and dancers. PloS One 13(4):e0196065

Ramkumar P, Parkkonen L, Hari R, Hyvärinen A (2012) Characterization of neuromagnetic brain rhythms over time scales of minutes using spatial independent component analysis. Hum Brain Mapp 33(7):1648–1662

Ramkumar P, Parkkonen L, Hyvärinen A (2014) Group-level spatial independent component analysis of Fourier envelopes of resting-state MEG data. Neuroimage 86:480–491

Rogenmoser L, Zollinger N, Elmer S, Jäncke L (2016) Independent component processes underlying emotions during natural music listening. Soc Cogn Affect Neurosci 11(9):1428–1439

Schaefer RS, Desain P, Farquhar J (2013) Shared processing of perception and imagery of music in decomposed EEG. Neuroimage 70:317–326. https://doi.org/10.1016/j.neuroimage.2012.12.064

Smith SM, Fox PT, Miller KL, Glahn DC, Fox PM, Mackay CE, … Laird AR (2009) Correspondence of the brain's functional architecture during activation and rest. Proc Nat Acad Sci 106(31):13040–13045

Sockeel S, Schwartz D, Pelegrini-Issac M, Benali H (2016)Large-scale functional networks identified from resting-state EEG using spatial ICA. PLoS One 11(1):e0146845. https://doi.org/10.1371/journal.pone.0146845

Spiers HJ, Maguire EA (2007) Decoding human brain activity during real-world experiences. Trends Cogn Sci 11(8):356–365. https://doi.org/10.1016/j.tics.2007.06.002

Sturm I, Dahne S, Blankertz B, Curio G (2015) Multi-variate EEG analysis as a novel tool to examine brain responses to naturalistic music stimuli PLoS One 10(10):e0141281. https://doi.org/10.1371/journal.pone.0141281

Tadel F, Baillet S, Mosher JC, Pantazis D, Leahy RM (2011) Brainstorm: a user-friendly application for MEG/EEG analysis. Comput Intell Neurosci 2011:879716. https://doi.org/10.1155/2011/879716

Tian Y, Klein RM, Satel J, Xu P, Yao D (2011) Electrophysiological explorations of the cause and effect of inhibition of return in a cue–target paradigm. Brain Topogr 24(2):164–182

Toiviainen P, Alluri V, Brattico E, Wallentin M, Vuust P (2014) Capturing the musical brain with Lasso: dynamic decoding of musical features from fMRI data. Neuroimage 88:170–180. https://doi.org/10.1016/j.neuroimage.2013.11.017

Wang D, Cong F, Zhao Q, Toiviainen P, Nandi AK, Huotilainen M, Ristaniemi T, Cichocki A (2016) Exploiting ongoing EEG with multilinear partial least squares during free-listening to music. In: Paper presented at the Machine Learning for Signal Processing (MLSP), 2016 IEEE 26th International Workshop on

Zhu Y, Liu J, Mathiak K, Ristaniemi T, Cong F (2020) Deriving electrophysiological brain network connectivity via tensor component analysis during freely listening to music. IEEE Trans Neural Syst Rehabil Eng 28(2):409–418

Zhu Y, Liu J, Ristaniemi T, Cong F (2019) Distinct patterns of functional connectivity during the comprehension of natural, narrative speech. Int J Neural Syst. https://doi.org/10.1142/S0129065720500070

III

DISTINCT PATTERNS OF FUNCTIONAL CONNECTIVITY DURING THE COMPREHENSION OF NATURAL, NARRATIVE SPEECH

by

Yongjie Zhu, Jia Liu, Tapani Ristaniemi & Fengyu Cong 2020

International Journal of Neural Systems, 33(3), 2050007-2050021

DOI: https://doi.org/10.1142/S0129065720500070

International Journal of Neural Systems

DISTINCT PATTERNS OF FUNCTIONAL CONNECTIVITY DURING THE COMPREHENSION OF NATURAL, NARRATIVE SPEECH

YONGJIE ZHU
School of Biomedical Engineering, Faculty of Electronic and Electrical Engineering
Dalian University of Technology, 116024, Dalian,China
Faculty of Information Technology
University of Jyväskylä, 40014, Jyväskylä, Finland
E-mail: yongjie.zhu@foxmail.com

JIA LIU
Faculty of Information Technology
University of Jyväskylä, 40014, Jyväskylä, Finland
E-mail: jialiu15@foxmail.com

TAPANI RISTANIEMI
Faculty of Information Technology
University of Jyväskylä, 40014, Jyväskylä, Finland
E-mail: tapani.ristaniemi@jyu.fi

FENGYU CONG*
School of Biomedical Engineering, Faculty of Electronic and Electrical Engineering
Dalian University of Technology, 116024, Dalian,China
Faculty of Information Technology
University of Jyväskylä, 40014, Jyväskylä, Finland
E-mail: cong@dlut.edu.cn

Recent continuous task studies, such as narrative speech comprehension, show that fluctuations in brain functional connectivity (FC) are altered and enhanced compared to the resting-state. Here, we characterized the fluctuations in FC during comprehension of speech and time-reversed speech conditions. The correlations of Hilbert envelope of source-level EEG were used to quantify FC between spatially separate brain regions. A symmetric multivariate leakage correction was applied to address the signal leakage issue before calculating FC. The dynamic FC was estimated based on a sliding time window. Then, principal component analysis (PCA) was performed on individually concatenated and temporally concatenated FC matrices to identify FC patterns. We observed that the mode of FC induced by speech comprehension can be characterized with a single principal component. The condition-specific FC demonstrated decreased correlations between frontal and parietal brain regions and increased correlations between frontal and temporal brain regions. The fluctuations of the condition-specific FC characterized by a shorter time demonstrated that dynamic FC also exhibited condition-specificity over time. The FC is dynamically reorganized and FC dynamic pattern varies along a single mode of variation during speech comprehension. The proposed analysis framework seems valuable for studying the reorganization of brain networks during continuous task experiments.

Keywords: Reorganization; functional connectivity; naturalistic speech; speech comprehension; natural paradigms.

1. Introduction

During real-life experiences (e.g., watching a movie or listening to a speech), it is necessary to continuously integrate and parse information.[1, 2] Previous studies have identified a group of high-order brain regions, including the temporal parietal junction, posterior cingulate cortex, temporal pole, and medial prefrontal cortex, which can

*Corresponding author.

accumulate and integrate information during comprehension of a narrative story.[3, 4] Although the neural correlation of local information processing has been well investigated in previous studies, integrating information at the whole-brain level may also be critical to understanding brain functions.[5, 6] Advances in methodology and brain imaging technology have enabled us to examine how the brain mediates information flow in large-scale functional networks during continuous task execution.[5, 7-10]

Function connectivity (FC), based on statistical interdependencies between signals recorded using neuroimaging technology,[11-14] is a widely-used approach to describe the large-scale configuration of brain functional activity.[15-18] FC modes provide fingerprints for the organization of functional brain networks during resting state[19-21] and continuous task performance.[22-25] Recent studies have demonstrated that there is a robust relationship between the functional networks during the resting-state and continuous task execution.[26-28] Particularly, naturalistic task paradigms, such as movie-watching[29, 30] and comprehension of a narrative story,[3, 4, 31] are interesting because of their ecological validity. Some studies have shown that FC is much reliable to demonstrate distinct individual differences when subjects involved in the naturalistic paradigm. For example, Londei et al. found that dynamics of the connectivity patterns within and toward somatosensory and motor areas are modulated by the degree of reproducibility of auditory speech material.[32] A systematic reconfiguration of the cortical interactions, with changes in functional network assignments, has been demonstrated during challenging listening situations.[33] In addition, Broderick and colleagues applied an approach based on a computational model to low-frequency noninvasively electroencephalographic (EEG) data recorded from subjects when they listened to narrative speech; and a prominent component was produced, which was very sensitive to whether or not subjects understood the speech they heard. Their results showed that the human brain responds to the contextual semantic content when successfully comprehending naturalistic speech.[34] However, electrophysiological network connectivity between different brain regions for such low-frequency oscillations has been lacking for continuous speech. Furthermore, the condition-specific changes and increased reliability of functional brain connectivity may be induced by the task-dependent involvement of specific brain areas[29, 35] and reconfiguration of brain network may emerge during successful comprehension of narrative speech.[33] Based on these studies, we describe an approach for examining the brain network connectivity at low-frequency oscillations during speech comprehension. We hypothesized that distinct modes of brain networks would emerge and the reconfiguration of FC during comprehension of speech could be quantified in terms of systematic fluctuations in FC patterns.

In the present study, we used correlation of Hilbert envelope as a means to quantify FC between spatially separate brain areas. This metric has been used widely in recent years[36-38] and has been characterized as an 'intrinsic mode' of functional coupling in the human brain. The high-density EEG were recorded and able to measure high spatiotemporal resolution networks.[39, 40] We calculated the whole-brain connectivity between separate brain regions, which are predefined based on Desikan-Killiany atlas.[41] To examine the reconfiguration of FC, we analyzed the fluctuations in grand averaged (over time) and dynamic (time-resolved) FC during listening to narrative speech and time-reversed speech (TR-speech). Here, the TR-speech can be used as a control to exclude brain processes induced by the low-level features of speech since it has the same long-term amplitude spectrum as normal speech but is not perceived as intelligible speech.[42] Principal component analysis (PCA) was used to characterize the variations in FC patterns over subjects. PCA and related techniques have been applied to describe FC fluctuations during the resting-state,[43] movie-watching[29] and whole-brain connectivity dynamics.[44, 45] Based on the projections of scores on the principal components (PCs) for the individual subject, we identified FC modes dependent on the successful comprehension of speech condition. Furthermore, to examine whether fluctuations in grand averaged FC reflected a constant (temporally stationary) functional state or the occurrence of functional patterns altering over time, we extended our analysis beyond grand-average FC states and investigated the temporal fluctuations in FC states using dynamic FC based on a sliding-window technique. To examine the role of time-locked events on dynamic FC during speech-comprehension condition (similar to inter-subject synchronization), we estimated the similarity between instantaneous dynamic FC (each windowed FC) across conditions and runs.

2. Material and methods

2.1. *Study design*

The open access EEG data used in this paper have been described in details elsewhere.[34, 42] There were 10 subjects and they took part in two experiments. During the experiments, subjects were introduced to listen to a narrative speech and time-reversed speech, separately. The EEG data were recorded during listening task. In the first experiment (condition), subjects underwent 20 runs (trials), each of which was of the same length (less than 180 seconds), in which they listened to a professional audio-book edition of a classic American work of fiction (in this study we just used 2 runs to examine the dynamic organization during natural speech-comprehension). The audio was read by a single American English speaker. The runs retained the storylines, with neither duplicates nor discontinuities. During the audio-playing, the mean speech rate was 210 words/min. In a similar way, during the second experiment subjects were presented with the same runs in the same order, but with each of the speech stimuli played in reverse (time-reversed speech). All speech stimuli were played monophonically at a sampling rate of 44.1 kHz using Sennheiser headphones in a sound-attenuated room when participants maintained fixation on a cross centered on a screen and minimized eye blinking and other movement activities.

2.2. *Data description and preprocessing*

During all experiments, dense array 128-channel EEG data (plus two mastoid channels) were recorded at a sampling rate of 512 Hz using a BioSemi ActiveTwo system. Offline, the data were filtered with a band-pass filter between 1 and 30 Hz since initial investigation of the frequency range uncovered that no useful information was observed in higher frequencies, and down-sampled to 128 Hz. We then re-referenced EEG data to the common average channels[46] in MATLAB2016b. To identify bad channels with artifacts noise, the EEG signals were visually inspected and the standard deviation of each channel time series was compared with that of the spherical surrounding channels. Bad channels with excessive noise were interpolated using a spherical spline model in EEGLAB.[47] Independent component analysis (ICA) was performed to remove ocular EEG artifacts.[48, 49]

2.3. *Source reconstruction*

Following preprocessing, source localization was performed using an open access software Brainstorm.[50] The forward model, describing the signal mode produced by the unit dipole at each predefined position on the brain model surface, was computed using the symmetric BEM method[51] based on default Colin27 MRI template provided by the Montreal Neurological Institute (MNI). Preprocessed data were adopted to compute the inverse model, which was estimated by the weighted Minimum-norm Estimation (wMNE).[52] It has been proved that wMNE is well-established to estimate large-scale FC networks since it solves the volume conduction problems and thus reduces the correlation of spurious signal.[53, 54] When calculating the inverse operator, we adopted the configuration of parameters described in the previous study[53]: (1) the current source orientations were constrained to perpendicular to the cortical surface; (2) the depth weighting algorithm was adopted to compensate for any deviations affecting the computation of superficial sources[53, 55]; and (3) a regularization parameter, $\lambda^2 = 0.1$ was adopted to minimize numerical instability, reduce the wMNE sensitivity to noise, and effectively achieve a spatially smoothing estimation.[53] In this procedure, source-level time series at 15,002 voxels were obtained. The cortical surface was then parcellated into 68 anatomical regions of interest (ROIs) based on the Desikan-Killiany atlas[56] and the center of mass of each area was defined as a representative time series to be used to calculate FC.

2.4. *Functional connectivity estimation*

We aimed to perform an all-to-all whole-brain FC analysis by estimating connectivity between all possible pairs of Desikan-Killiany regions. In M/EEG, a significant confound of source level connectivity is that the ill-posed inverse problem plus inaccuracies in the forward solution, leads to a degree of spatial blurring and mislocalization of sources.[57, 58] This confound means that two source-reconstructed time series (e.g. from two brain regions) may be significantly correlated, purely due to 'signal leakage' (for review see Ref.[38]). The estimated connectivity between separate brain regions may not be accurate without careful control.[58] Signal leakage issue has been well investigated and there are now a lot of techniques for leakage reduction.[37, 57, 59] Most approaches are based on the fact that leakage manifests as a zero-time lag linear superposition of underlying signals so that

although the true zero-lag connection is sacrificed, orthogonalization of source-reconstructed signals can effectively remove leakage.[58] Colclough et al. recently proposed an effective method of simultaneously orthogonalizing over a set of multiple brain regions.[60] Based on their study, here, signals (time-courses) from all N=68 brain areas are symmetrically orthogonalized in a single calculation. The complete mathematical details of the procedure can be found in previous study.[60] In brief, two steps need to be conducted in the method: First, find a set of orthogonal time-courses that are closest to the data matrix and have a simple analytical solution. Second, the solution is finessed by iteratively adjusting the lengths and orientations of the corrected vectors until the solution is as close as possible to the uncorrected time-courses.[61] This results in a set of matrices, whose rows consist of the orthogonalized time-courses for all 68 Desikan-Killiany brain areas. Following signal leakage correction, the Hilbert transformation was applied to extract the amplitude envelopes of the time-courses. The FC matrices were constructed based on Pearson correlation coefficient between all pairs of the amplitude envelopes of ROIs in terms of grand average FC. To extract dynamic FC (time-resolved FC), we applied a sliding window approach.[44, 62] The window length was set as 5 s and the overlap was 4 s between two adjacent windows. Within each window, we calculated connectivity between all pairs of Desikan–Killiany regions. It should be noted that the signal leakage reduction step was performed on each time window separately (separate orthogonalization for each window), rather than on the whole time series during grand average FC analysis. This conduction can be explained in previous study,[63] where it has proved that leakage relies heavily on signal to noise ratio (SNR) and the SNR is different in different time windows.

2.5. *Principal component analysis*

During grand averaged FC analysis, the FC matrices were calculated based on Pearson correlation between all pairs of the amplitude envelopes of 68 ROIs (over whole time) for all subjects and runs (see Section **Functional connectivity estimation**).

To perform PCA, the lower triangular parts of FC (i.e. $68 \times (68-1)/2$ connections) matrices were concatenated across subjects/runs (10×4 subjects/runs) resulting in the group-level connectivity matrix with dimensions 2278×40 (number of connections $\times$ number of subjects/runs). PCA was then performed to the resulting group-level connectivity matrix. To determine the components which reflect only noise, the PCA analyses were repeated for 1000 surrogate time-courses for each subject/run. The surrogate time-courses of each individual subject were phase-randomized and the properties of the surrogate time-courses were preserved in spectral domain.[29, 64] The dimensionality of the data was represented by the proportion of explained variance of the principal components (PCs) that are greater than those of the surrogates. Since the data were decomposed by PCA into orthogonal axes with related projections (scores) of each individual observation (subject or run in this study), we used these projections scores to characterize the principal components. The PC associated with speech-comprehension condition was considered as the one demonstrating clear separation between different conditions and significant difference levels based on the PC projection scores (i.e., the scores higher than 0 represented the speech-comprehension runs, whereas the scores less than 0 presented the time-reversed speech runs).

To examine the consistency of PCs, the analysis was repeated using 2 separate runs. For both runs, the group-level connectivity matrices contained the concatenated lower triangular FC matrices of 1 time-reversed speech run and 1 speech-comprehension run (i.e., 2278×20 matrices). The consistency was characterized as Pearson Correlation of the components and their projection scores across runs (See Figure 1**G-H).**

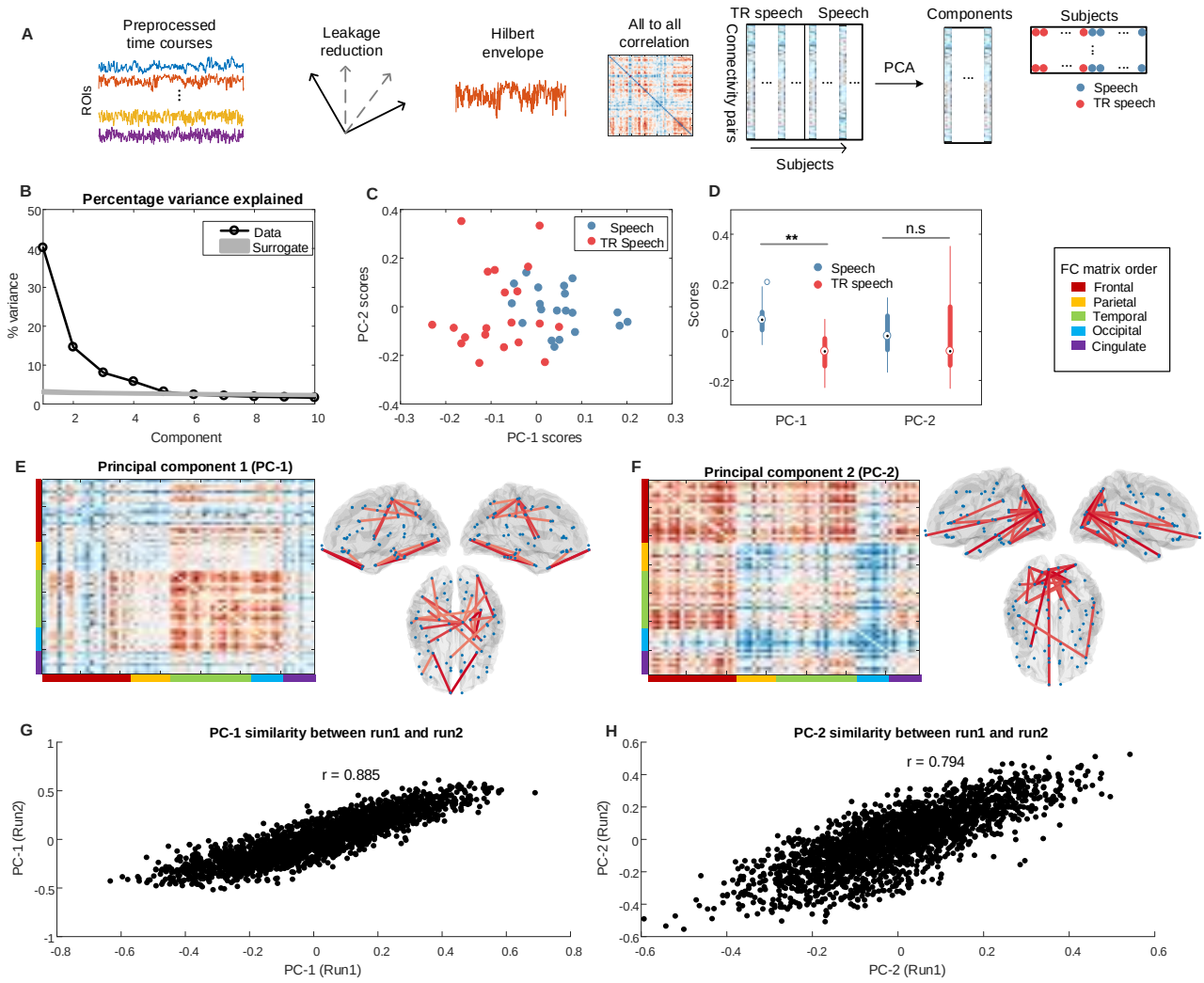

Fig. 1. **A** The analysis pipeline using principal component analysis (PCA). The time-courses of ROIs were firstly corrected to remove signal leakage; then, the FC matrix was constructed using Hilbert envelope correlation; finally, the PCA was performed over FCs of 2 time-reversed speech and 2 speech-comprehension condition concatenated across 10 subjects. **B** Explained variance by each PC (black line) and phase-random surrogates (gray line). The first 4 PCs were above the noise level (Surrogate data); the first PC (**E**) explained 39.8% of the variation, while the second (**F**) explained 14.6%. **C** The projections of first two PCs and D Boxplot of first 2 PCs projections, showing that the first component is dependent to speech-comprehension condition. **E-F** The first 2 components and their 3-D representations with threshold (top 5%) for visualization. **G-H** The similarity of the first 2 PC between two separated run analysis.

2.6. *PCA trajectories of dynamic FC*

The PCA was repeated for average dynamic FC to establish the link between grand averaged FC (whole time correlation) and dynamic FC. After determining the grand average condition-specific dynamic FC component, we applied PCA to concatenated dynamic FC matrices over time for each subject (i.e., 2 time-reversed speech and 2 speech-comprehension runs). The condition-specific temporal components (connectivity) were determined as the PC exhibiting the highest similarity to the grand average condition-specific dynamic FC components. Then, we measured the trajectories (i.e., fluctuations of PC scores over time) of the condition-specific temporal components of individuals. In this study, the term "trajectory" was better than "scores" to highlight the fact that the PCA was applied to time-concatenated connectivity matrices. We examined whether the PC exhibiting highest similarity to

the condition-specific connectivity differentiated between time-reversed speech and speech-comprehension trajectories. We characterized the condition-specific differences by computing the average Euclidean distance between the median trajectories of the time-reversed speech and speech-comprehension conditions. The Euclidean distances between median trajectories were defined as the squared difference between median PC projection scores of time-reversed speech and speech-comprehension trajectories. For each subject, to evaluate the significance of the distinction, we compared the condition-specific Euclidean distance with those of the surrogates. We randomly shuffled the trajectories of each individual subject and then reassigned them into two groups. The p-values were assessed by comparing the distance between condition-specific trajectories with the distance of the surrogates. Since the trajectories of each individual PC are time-dependent, we evaluated the distinction between different conditions across subjects by computing the median distances across runs and conditions. For each individual subject, the median distance of trajectory between time-reversed speech and speech-comprehension conditions was computed. Next, the distances between two separate runs of time-reversed speech and speech-comprehension conditions were computed. Finally, we adopted permutation tests to compare the average distance across runs and conditions.

2.7. *Dynamic FC similarity across conditions and runs*

During continuous perception, human brain automatically divides experiences into discrete events.[65] To examine the role of time-locked events on dynamic FC in speech-comprehension condition (similar to inter-subject synchronization), we estimated the Pearson similarity between instantaneous dynamic FC (each windowed FC) across conditions and runs. For each time window, we computed the Pearson similarity between the FC matrix of a single subject (k) and the average FC across the remaining of the subjects ($n \neq k$). The average dynamic FC was computed to test the FC similarity in 3 different circumstances: across conditions (i.e., if subject k is at time-reversed speech run 1, the average dynamic FC was computed for speech-comprehension run 1), across runs (i.e., if subject k is at time-reversed speech run 1, the average dynamic FC was computed for time-reversed speech run 2) and within runs (i.e., if subject k is at time-reversed speech run 1, the average dynamic FC was computed for time-reversed speech run 1) (Fig 3**A**).

2.8. *Statistical analysis*

The comparisons between conditions (time-reversed speech vs. speech-comprehension) were performed using permutation tests since the size of samples remines relatively small. During the permutation tests, the randomization was also carefully controlled to keep the dependence across two conditions.

To evaluate the association between measures, Spearman's correlations were used due to limited number of samples. Pearson correlation was applied as a measure of similarity between connectivity matrices. (i.e., PC scores, FCs, and dynamic FCs).

3. Results

To characterize the fluctuations in FC across subjects during time-reversed speech and speech-comprehension conditions, PCA was applied over subjects (Figure 1**A**). PCA decomposed high-dimensional group-level connectivity matrices into orthogonal principal components that explained the most variance of the data. The projections provided a score for each individual observation (i.e., subject/run) along the PCs. We performed PCA on concatenated vectorized connectivity matrices for all subjects during two separate runs of time-reversed speech and speech-comprehension conditions. We then examined the scores (i.e., projections of PCs by individual subjects) during two conditions.

3.1. *Distinct modes of variation in FC during speech comprehension*

The first principal component (PC-1), explaining 39.8% of the variance (Fig. 1**B**), was able to distinguish the speech-comprehension condition from time-reversed speech condition. The projection scores of PC-1 were significantly different between two conditions ($p < 0.001$) (Fig. 1**C-D**). We considered this principal component as a condition-specific PC. This result demonstrated that the condition-specific changes in FC can be explained with a single pattern of variation (PC-1). The second principal component (PC-2) (Fig .1**B**), explaining 14.6% of the variance, reflected a FC mode that was preserved across runs. There was no significant difference in the scores of PC-1 between two conditions (Fig. 1**C-D**). This result showed that the principal

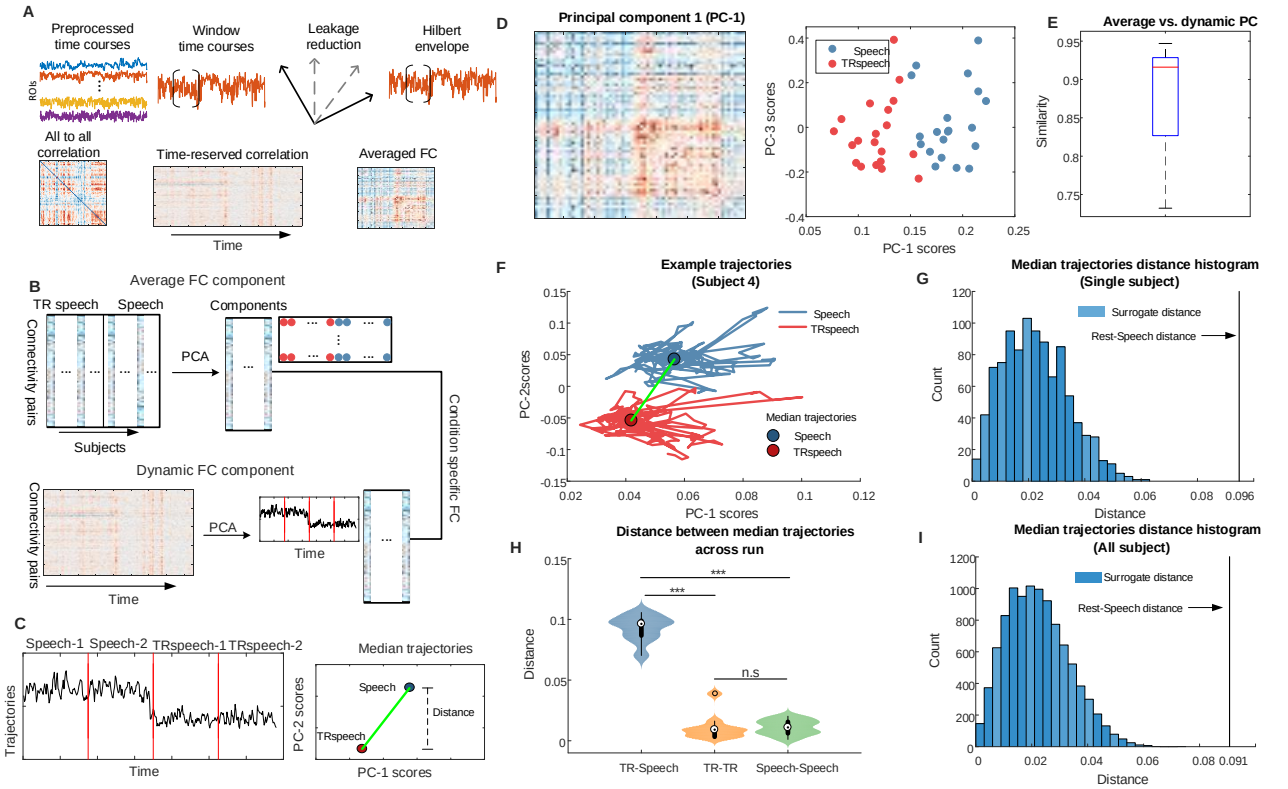

Fig. 2. FC based on a sliding-window approach. **A** The pipeline of dynamic FC analysis. The source-reconstructed time-courses were leakage-corrected within each window (window length 5 s, overlap 4 s). Dynamic FCs were estimated based on windowed Hilbert envelop correlation. **B** The pipeline describing the PCA applied to average dynamic FCs across subjects (top), where the static adjacent matrixes were concatenated across subjects, and dynamics FCs across time for each subject (bottom). A condition-specific component was determined based on the maximum similarity between dynamic FC components and average condition-specific FC component (**D**). The grand average component and dynamic condition-specific component were very similar across subjects (**E**). **C** Based on the trajectories of condition-specific dynamic FC components, the distance between the median trajectories of time-reversed speech (TR speech) and speech-comprehension (Speech) conditions were computed. **F** Example trajectory for single individual (Subject 4). **G** The distance between the median trajectories of TR speech and Speech conditions compared to the histogram of the distances for 1000 randomly split trajectories (Subject4) and **I** for all subjects. **H** The median trajectory distances between TR speech and Speech conditions, between 2 TR speech runs and between 2 Speech runs. The distance between conditions was significantly higher than the distance between runs (permutation tests, 10000 permutations). *** represents $p < 0.0001$, **n.s**. represents $p > 0.05$.

component of variation in FC reflected the common connectivity pattern over two conditions.

PCA analysis was repeated for 1000 surrogate FC matrices across all subjects to determine the components explaining a significant fraction of variance (see section **Principal component analysis**). The explained variance of the first 4 components was larger than the explained variance of surrogate FC matrices. Considering a large amount of variance explained by the first 2 PCs, we chose the 2 PCs for further analysis. The rest of the components did not exhibit any specificity regarding the speech-comprehension condition and were not presented.

To examine the consistency of the condition-specific PCs over runs, PCA analysis was repeated for each run separately and the Pearson similarities between PCs across runs were quantified. For each run, the condition-specific PCs showing high consistency across runs were identified. The similarities between PCs were significantly correlated across runs for condition-specific FC and common FC (r=0.885 for PC-1 component, r=0.794 for PC-2 component) (Fig. 1**G-H**). These results showed that the condition-specific PC and the related projection scores were consistent across runs.

3.2. *Condition-specific FC trajectories in dynamic FC*

The grand average FC metric is not able to distinguish between a temporally stationary pattern of FC and fluctuations in FC. Thus, we analyzed dynamic fluctuations in FC (also known as time-resolved FC). In the current study, we examined the hypothesis that brain FC continuously reconfigured during speech-comprehension. The dynamic FC was estimated based on a sliding window technique. We used envelope correlation as a means to quantify connectivity between spatially separate brain regions (see section **Functional connectivity estimation**). This metric has been used extensively in recent years and has been described as an 'intrinsic mode' of functional coupling in the human brain. Here, we set window length as 5 s and overlapped with 4 s between adjacent frames (see section **Discussion** about the window length). First, the source-localized time series of separate brain regions were segmented into overlapping time windows. Second, leakage reduction step was applied to each window, separately. Hilbert envelope was extracted from the corrected time series. Finally, we computed 'all-to-all' connectivity between separate brain regions (Fig. 2A).

To establish the link between the dynamic FC analyses and grand average FC (whole time correlation). The average dynamic FC across time was calculated and PCA was performed over subjects. The analysis results suggested that the PC based on averaged dynamic FC also showed condition specificity (Fig. 2). In addition, condition-specific PC of average dynamic FC was similar to those grand average FCs (r=0.92) (Fig. 2**E**). Thus, the condition specific FC patterns from average dynamic connectivity were in line with those based on grand average FC.

For each participant, PCA was applied to the dynamic FCs over time (Fig. 2**B**). We considered the condition-specific component for each individual subject as the one that was the highest correlated with the grand average condition-specific component (Fig. 2**D**). For most subjects, the trajectories (PC projection scores) of the condition-specific components reflected a significant difference between conditions (Fig. 2**H**). For each subject, we characterized the condition-specificity by comparing the median of trajectories (median PC projection scores) during the time-reversed speech and the speech-comprehension conditions (Fig. 2**C**). Then, we measured the Euclidean distance between the median trajectories of TR-speech and speech conditions (Fig. 2**C**). We compared the distance between TR-speech and speech median trajectories with the distance between 1000 trajectories of randomly shuffled groups (Fig. 2**G-I**). The results of all subjects demonstrated a significantly larger distance between TR-speech and speech trajectories than any other trajectories of randomly shuffled groups ($p<0.0001$) (Fig. 2**I**). Due to the time-dependence of the condition-specific PC trajectories, we evaluated the significance of the median distances of trajectory between conditions/runs across subjects. We observed that the median distance across conditions (i.e., TR-speech/speech conditions) was significantly greater than the median distance across runs (i.e. TR-speech-run1/TR-speech-run2 and speech-run1/speech-run2) ($p<0.0001$, permutation tests, 10000 permutation runs) (Fig. 2**H**). We observed no significant difference between the median distance across runs for time-reversed speech and speech-comprehension conditions (Fig. 2**H**). These results suggested the emergence of a preserved FC mode during speech-comprehension condition at a short time scale.

3.3. *Condition-specific FC patterns within and across runs*

The first principal component (PC-1), explaining 39.8% of the variance (Fig. 1**B**), was able to distinguish the speech-comprehension condition from time-reversed speech condition. The projection scores of PC-1 were significantly different between two conditions ($p < 0.001$) (Fig. 1**C-D**). To investigate the role of time-locked events on FC dynamics during speech-comprehension (similar to inter-subject synchronization analysis), we computed the Pearson similarity between dynamic FCs over conditions and runs. Briefly, for each time window, we calculated the similarity between the FC matrix of an individual subject (k) and the average FCs across the remaining subjects ($n \neq k$). The average FCs were computed to examine the FC matrix similarity in 3 different cases: across conditions (e.g. if subject k is at time-reversed speech run 1, the average FC matrix was computed for speech-comprehension run 1), across runs (e.g., if subject k is at time-reversed speech run 1, the average FC matrix was computed for time-reversed speech run 2) and within runs (e.g., if subject k is at time-reversed speech run 1, the average FC matrix was computed for time-reversed speech run 1) (Fig. 3**A**).

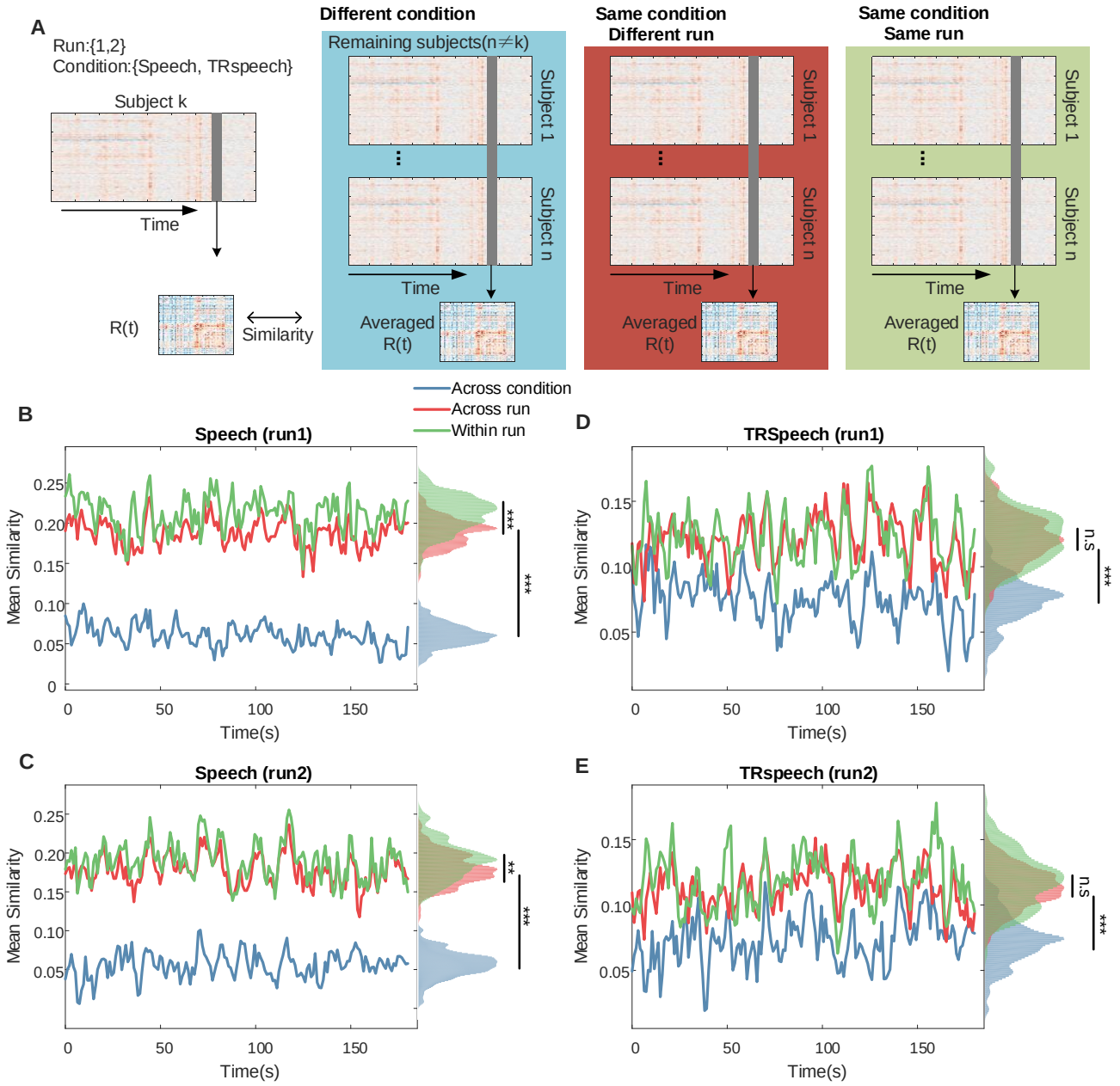

Fig. 3. Time-resolved similarity between dynamic FCs across conditions and runs. **A** The analysis pipeline. For each individual subject the dynamic FC at each window was compared to the average dynamic FC across the rest of subjects at the same window. Blue lines/shades represent that the average dynamic FCs were computed for different condition (i.e. if subject k is TR speech, average dynamic FC were computed across subjects for Speech condition (excluding subject k)). Red lines/shades represent that the average dynamic FCs were computed for the same condition but different runs (i.e. if subject k is at TR Speech in run 1, average dynamic FC were computed for the TR speech run 2). Green lines/shades represent that the average dynamic FCs were computed for the same condition and the same run (i.e. if subject k is at TR speech in run 1, average PLVs were computed for the TR speech run 1). **B-C** During speech-comprehension, the similarity between dynamic FCs was significantly lower across conditions, but the similarity between FCs was significantly higher within runs compared to across runs. **D-E** During TR speech the similarity between dynamic FCs were significantly lower across conditions, but there was no significant difference between the similarities across runs. The histograms indicate the distributions of similarity measures over time, whereas *** represents the $p < 0.0001$, ** represents the $p < 0.001$ assessed by permutation tests across subjects. **n.s.** represents $p > 0.05$.

The similarity across runs both for TR-speech and speech-comprehension conditions was significantly larger than the similarity across conditions ($p<0.001$ for both runs: permutation tests, 10000 permutation runs) (Fig. 3). This result confirmed the continuous functional reconfiguration during speech-comprehension condition. Additionally, this result also demonstrated that during speech-comprehension, the similarity between dynamic FC was higher, even when the subjects were listening to different semantic content. The average similarity between dynamic FCs demonstrated no significant difference across runs for resting-state runs ($p=0.54$ for run 1, $p=0.28$ for run 2, permutation tests, 10000 permutations) (Fig. 3**D-E**). In contrast, the average similarity between dynamic FCs was significantly higher for the same speech run than across runs ($p<0.0001$ for run 1, $p<0.001$ for run 2, permutation tests, 10000 permutations) (Fig. **3B-C**). These results showed that the dynamics of FC during speech-comprehension reflected both the effects of time-locked events and a continuous reorganization of brain networks.

4. Discussion

This paper has investigated the reconfiguration of functional connectivity (FC) during speech-comprehension condition. The results demonstrated that FC dynamic pattern under speech-comprehension varies along with a single mode of variation. During the comprehension of natural speech, the connectivity pattern captures the variations over subjects, which emerges as a continuous brain functional state across time.

We adopted PCA to characterize the variations in FC across subjects and conditions. We found that one of the PCs (PC-2) reflected the common pattern of variations in both conditions, whereas another PC (PC-1) reflected the difference between time-reversed speech and speech-comprehension conditions. The patterns of the components characterized the intra- and inter-hemispheric connectivity within occipital and temporal regions as well as their connections with frontal and parietal regions, which are line with increased brain connectivity in language/auditory networks.[66, 67] These results demonstrated that the increased communication between separate brain regions associated with auditory processing and attention are primarily driven by the time-locked events during comprehension of natural speech. This characterization is consistent with the large-scale auditory and sensory-motor networks emerging during comprehension of natural, narrative speech.[32] The condition-specific component (PC-1) demonstrated increased connectivity within sensory-motor areas and reduced connectivity between frontal-parietal brain regions and cingulate. The enhanced sensory-motor areas connectivity reflects the ability to transform auditory speech into appropriate sensory and motor representations. These results are in line with previous studies showing brain functional reorganization during comprehension of speech.[32, 33] Furthermore, the enhanced frontal-temporal connectivity may indicate a strong functional cross-talk between ventral attention and auditory regions. Previous studies also observed the reconfiguration of a frontal-temporal network in adaptation to cued speech comprehension, where related frontal-temporal cortical regions were referred to as the auditory-control network.[33]

The result about emerging of a condition-specific pattern in grand averaged FC may be not sufficient to draw a conclusion about the reorganization of FC during speech comprehension. Therefore, we examined how the condition-specific component relates to the dynamic FC. We applied a sliding window approach combining with Hilbert envelop correlation between brain regions to characterize dynamic FC over time. The findings also showed condition-specific PC on grand average dynamic FC across subjects and individual dynamic FC over time. The trajectories of the condition-specific PCs demonstrated that this PC might emerge as a stationary pattern during comprehension of speech. This conclusion was resulted from analyzing the similarity between instantaneous dynamic FC and the average dynamic FC across individuals under different runs/conditions. The similarity was significantly higher when the individuals were involved in the same conditions (i.e., TR-speech/TR-speech and speech/speech) than they were in different conditions (i.e. TR-speech/speech). In addition, only during speech comprehension, the similarity of the dynamic FC was higher for individuals in the same run (i.e. run 1/run 2) than in the different runs (i.e. run 1/run 2). Overall, these results demonstrated that whole-brain connectivity is reorganized over time. Previous studies also observed that dynamics of FC states are highly stable relying on the narrative of a story although the connectivity patterns were similar over time.[4] Our results showed that the dynamics of the distinct connectivity

states might display time-locked events. Previous studies also demonstrated that humans automatically segment experiences into discrete events during realistic, continuous perception.[65] We speculated that the reconfiguration of the brain networks in higher-order regions might reflect the adaptation of the brain's intrinsic networks to coordinate the large-scale flow of information during speech comprehension. The dynamics of the condition-specific component may suggest that these changes of the FC patterns are related to higher-level processing of the narrative.

The PCA analysis in our study revealed two different modes of fluctuations that were related to the FC condition-specific variations. Although the PC-2 was consistent with the variations in empirical and model data, the PC-1 demonstrated a substantial condition-dependence. Furthermore, the PC-1 exhibited a similar pattern with typical of default mode network (DMN), which involves the medial frontal, temporal, and cingulate cortices. These local regions continuously change their module property in adaptation to the comprehension of speech.[33] We speculated a group of temporal and cingulate cortices merge with other temporal regions from the default mode network and form a new common mode during comprehension of speech. This result is consistent with the robust and reproducible reconfiguration of default mode network during narrative comprehension.[4]

From the methodological considerations, although a lot of methods have been proposed to EEG analysis for various applications, such as detection of epilepsy, Alzheimer's disease and so on,[68-71] the approach proposed in the current paper provided an analysis framework that used M/EEG imaging technique to investigate the reorganization of brain connectivity during naturalistic paradigm (e.g. music-listening, movie-watching, story-listening and speech comprehension). During analysis for the dynamic FC, the window length (here 5 s), one core parameter, requires setting. This parameter setting warrants further discussion. An appropriate selection of window length is important and stands for a trade-off between temporal resolution and the accuracy of the derived connectivity matrices.[38, 58] In this study, elements of the connectivity matrices are derived from the temporal correlation of envelope time-courses within the window. It is well known that the accuracy of the correlation between two signals (r) is associated with the number of degrees of freedom (η). Specifically, if assuming no underlying correlation between two time series then the standard deviation of correlation, $\sigma(r) = 1/\sqrt{\eta}$. In other words, the noise in adjacency matrices is increased as η is decreased. Furthermore, the number of degrees of freedom in a fixed-window time series is independent of the numbers of sample points. In the view of Fourier theory, an upper limit on degree of freedom for envelope data is given by $\eta = B_w\delta$, in which δ is the window length and B_w denotes bandwidth of the carrier signal. Typically, bandwidth is set by the scientific question to be asked. For example, previous studies were interested in beta band networks for self-paced motor study.[58, 72] Here, $\sigma(r) = 0.08$, which was deemed acceptable. Future studies should keep this computation in mind.

Finally, it should be noted that there are several limitations when interpreting the results in the current study. The most important limitation of the current study is the small number of the sample even though our results are validated using both surrogate data and permutation tests. Therefore, the results need replication in a separate independent dataset. Furthermore, the design of this study from previous studies did not allow us to compare the obtained results with other conditions (i.e. different narrative speech). Also, the current study did not allow us to compare the results with resting-state since the open access data did not include the resting-state condition. Future studies may study the variants of speech-comprehension condition, different task performance or other naturalistic paradigms (e.g., free music-listening, movie-watching, etc.). When analyzing large-scale neurophysiological networks using MEG/EEG, the common problem is non-physiological spread of electrical activity through volume conduction causing spurious correlations between signals.[73] Here, we used signal leakage reduction technique to address this problem. This technique has been well studied and believed to be an optimal approach for large-scale functional connectivity analysis.[38, 58, 60] Yet, it should be noted that the technique can only reduce the volume conduction problem, not address it completely. Another limitation of this study is the use of coarse (34 regions per hemisphere), anatomically defined parcellation based on default MNI MRI template. The simultaneous individual MRI scanning may facilitate the co-registration for EEG electrode. Additionally, we only examined the functional connectivity at the band of 1-30 Hz as it has been shown low-frequency oscillations

contribute to the naturalistic speech comprehension.[34, 42] Recently it has been suggested that functional connectivity is dependent on frequency band during the task execution such as working-memory and self-paced motor task.[61, 74] In a future study, we will examine whether functional connectivity during speech comprehension is frequency-dependent or not.

5. Conclusion

The brain FC is highly dynamic and able to adjust topology on a very fine time-scale during changing environment. Here, we proposed an analytical approach and investigated the reconfiguration of the brain functional networks during comprehension of natural, narrative speech. Our findings demonstrated that FC dynamic patterns under speech-comprehension vary along with a single mode of variation. Furthermore, our analysis method seems valuable for studying the reorganization of dynamic brain networks based on M/EEG data during natural task experiments.

Acknowledgements

This work was supported by the National Natural Science Foundation of China (Grant No. 91748105&81471742), the Fundamental Research Funds for the Central Universities [[DUT2019] in Dalian University of Technology in China, and the scholarship from China Scholarship Council (No. 201600090042; No. 201600090044).

References

1. Simony E., Honey C. J., Chen J., Lositsky O., Yeshurun Y., Wiesel A. and Hasson U. 2016, "Dynamic reconfiguration of the default mode network during narrative comprehension," *Nature communications* **7**, 12141.
2. Liu C., Abu-Jamous B., Brattico E. and Nandi A. K. 2017, "Towards tunable consensus clustering for studying functional brain connectivity during affective processing," *International journal of neural systems* **27**, 1650042.
3. Lerner Y., Honey C. J., Silbert L. J. and Hasson U. 2011, "Topographic mapping of a hierarchy of temporal receptive windows using a narrated story," *J Neurosci* **31**, 2906-15.
4. Simony E., Honey C. J., Chen J., Lositsky O., Yeshurun Y., Wiesel A. and Hasson U. 2016, "Dynamic reconfiguration of the default mode network during narrative comprehension," *Nat Commun* **7**, 12141.
5. Deco G., Tononi G., Boly M. and Kringelbach M. L. 2015, "Rethinking segregation and integration: contributions of whole-brain modelling," *Nature Reviews Neuroscience* **16**, 430.
6. Tononi G. 2004, "An information integration theory of consciousness," *BMC neuroscience* **5**, 42.
7. Bassett D. S., Wymbs N. F., Porter M. A., Mucha P. J., Carlson J. M. and Grafton S. T. 2011, "Dynamic reconfiguration of human brain networks during learning," *Proc Natl Acad Sci U S A* **108**, 7641-6.
8. Schmidt C., Piper D., Pester B., Mierau A. and Witte H. 2018, "Tracking the reorganization of module structure in time-varying weighted brain functional connectivity networks," *International journal of neural systems* **28**, 1750051.
9. Alarcón G., Jiménez-Jiménez D., Valentín A. and Martín-López D. 2018, "Characterizing EEG Cortical Dynamics and Connectivity with Responses to Single Pulse Electrical Stimulation (SPES)," *International journal of neural systems* **28**, 1750057.
10. Ahmadlou M., Adeli A., Bajo R. and Adeli H. 2014, "Complexity of functional connectivity networks in mild cognitive impairment subjects during a working memory task," *Clinical Neurophysiology* **125**, 694-702.
11. Yuvaraj R., Murugappan M., Acharya U. R., Adeli H., Ibrahim N. M. and Mesquita E. 2016, "Brain functional connectivity patterns for emotional state classification in Parkinson's disease patients without dementia," *Behavioural brain research* **298**, 248-260.
12. Ahmadlou M. and Adeli H. 2011, "Functional community analysis of brain: A new approach for EEG-based investigation of the brain pathology," *Neuroimage* **58**, 401-408.
13. delEtoile J. and Adeli H. 2017, "Graph theory and brain connectivity in Alzheimer's disease," *The Neuroscientist* **23**, 616-626.
14. Biswal B., Zerrin Yetkin F., Haughton V. M. and Hyde J. S. 1995, "Functional connectivity in the motor cortex of resting human brain using echo‐planar MRI," *Magnetic resonance in medicine* **34**, 537-541.
15. Brookes M. J., Wood J. R., Stevenson C. M., Zumer J. M., White T. P., Liddle P. F. and Morris P. G. 2011, "Changes in brain network activity during working memory tasks: a magnetoencephalography study," *Neuroimage* **55**, 1804-15.
16. Li F., Peng W., Jiang Y., Song L., Liao Y., Yi C., Zhang L., Si Y., Zhang T. and Wang F. 2019, "The dynamic brain networks of motor imagery: time-varying causality analysis of scalp EEG," *International journal of neural systems* **29**, 1850016.
17. Correas A., Rodríguez Holguín S., Cuesta P., López-Caneda E., García-Moreno L. M., Cadaveira F. and Maestú F. 2015, "Exploratory analysis of power spectrum and functional connectivity during resting state in young binge drinkers: A MEG study," *International journal of neural systems* **25**, 1550008.
18. Ahmadlou M., Adeli H. and Adeli A. 2012, "Graph theoretical analysis of organization of functional brain networks in ADHD," *Clinical EEG and neuroscience* **43**, 5-13.
19. Smith S. 2016, "Linking cognition to brain connectivity," *Nat Neurosci* **19**, 7-9.
20. Smith S. M., Nichols T. E., Vidaurre D., Winkler A. M., Behrens T. E., Glasser M. F., Ugurbil K., Barch D. M., Van Essen D. C. and Miller K. L. 2015, "A positive-negative

mode of population covariation links brain connectivity, demographics and behavior," *Nat Neurosci* **18**, 1565-7.
21. Ahmadlou M. and Adeli H. 2017, "Complexity of weighted graph: A new technique to investigate structural complexity of brain activities with applications to aging and autism," *Neuroscience letters* **650**, 103-108.
22. Telesford Q. K., Lynall M. E., Vettel J., Miller M. B., Grafton S. T. and Bassett D. S. 2016, "Detection of functional brain network reconfiguration during task-driven cognitive states," *Neuroimage* **142**, 188-200.
23. Xie H., Calhoun V. D., Gonzalez-Castillo J., Damaraju E., Miller R., Bandettini P. A. and Mitra S. 2018, "Whole-brain connectivity dynamics reflect both task-specific and individual-specific modulation: A multitask study," *Neuroimage* **180**, 495-504.
24. Dima D. C., Perry G., Messaritaki E., Zhang J. and Singh K. D. 2018, "Spatiotemporal dynamics in human visual cortex rapidly encode the emotional content of faces," *Hum Brain Mapp* **39**, 3993-4006.
25. Heinrichs-Graham E. and Wilson T. W. 2015, "Spatiotemporal oscillatory dynamics during the encoding and maintenance phases of a visual working memory task," *Cortex* **69**, 121-30.
26. Cole M. W., Bassett D. S., Power J. D., Braver T. S. and Petersen S. E. 2014, "Intrinsic and task-evoked network architectures of the human brain," *Neuron* **83**, 238-51.
27. Cole M. W., Ito T., Bassett D. S. and Schultz D. H. 2016, "Activity flow over resting-state networks shapes cognitive task activations," *Nat Neurosci* **19**, 1718-1726.
28. Cheng L., Zhu Y., Sun J., Deng L., He N., Yang Y., Ling H., Ayaz H., Fu Y. and Tong S. 2018, "Principal states of dynamic functional connectivity reveal the link between resting-state and task-state brain: An fmri study," *International journal of neural systems* **28**, 1850002.
29. Demirtaş M., Ponce-Alvarez A., Gilson M., Hagmann P., Mantini D., Betti V., Romani G. L., Friston K., Corbetta M. and Deco G. 2019, "Distinct modes of functional connectivity induced by movie-watching," *NeuroImage* **184**, 335-348.
30. Kauppi J. P., Jaaskelainen I. P., Sams M. and Tohka J. 2010, "Inter-subject correlation of brain hemodynamic responses during watching a movie: localization in space and frequency," *Front Neuroinform* **4**, 5.
31. Regev M., Simony E., Lee K., Tan K. M., Chen J. and Hasson U. 2018, "Propagation of information along the cortical hierarchy as a function of attention while reading and listening to stories," *bioRxiv*, 291526.
32. Londei A., D'Ausilio A., Basso D., Sestieri C., Gratta C. D., Romani G. L. and Belardinelli M. O. 2010, "Sensory-motor brain network connectivity for speech comprehension," *Hum Brain Mapp* **31**, 567-80.
33. Alavash M., Tune S. and Obleser J. 2019, "Modular reconfiguration of an auditory control brain network supports adaptive listening behavior," *Proc Natl Acad Sci U S A* **116**, 660-669.
34. Broderick M. P., Anderson A. J., Di Liberto G. M., Crosse M. J. and Lalor E. C. 2018, "Electrophysiological correlates of semantic dissimilarity reflect the comprehension of natural, narrative speech," *Current Biology* **28**, 803-809. e3.
35. Hua C., Wang H., Wang H., Lu S., Liu C. and Khalid S. M. 2019, "A Novel Method of Building Functional Brain Network Using Deep Learning Algorithm with Application in Proficiency Detection," *International journal of neural systems* **29**, 1850015.
36. Engel A. K., Gerloff C., Hilgetag C. C. and Nolte G. 2013, "Intrinsic coupling modes: multiscale interactions in ongoing brain activity," *Neuron* **80**, 867-86.
37. O'Neill G. C., Barratt E. L., Hunt B. A., Tewarie P. K. and Brookes M. J. 2015, "Measuring electrophysiological connectivity by power envelope correlation: a technical review on MEG methods," *Phys Med Biol* **60**, R271-95.
38. O'Neill G. C., Tewarie P., Vidaurre D., Liuzzi L., Woolrich M. W. and Brookes M. J. 2018, "Dynamics of large-scale electrophysiological networks: A technical review," *Neuroimage* **180**, 559-576.
39. Mammone N., De Salvo S., Bonanno L., Ieracitano C., Marino S., Marra A., Bramanti A. and Morabito F. C. 2018, "Brain Network Analysis of Compressive Sensed High-Density EEG Signals in AD and MCI Subjects," *IEEE Transactions on Industrial Informatics* **15**, 527-536.
40. Lai M., Demuru M., Hillebrand A. and Fraschini M. 2018, "A comparison between scalp-and source-reconstructed EEG networks," *Scientific reports* **8**, 12269.
41. Desikan R. S., Ségonne F., Fischl B., Quinn B. T., Dickerson B. C., Blacker D., Buckner R. L., Dale A. M., Maguire R. P. and Hyman B. T. 2006, "An automated labeling system for subdividing the human cerebral cortex on MRI scans into gyral based regions of interest," *Neuroimage* **31**, 968-980.
42. Di Liberto G. M., O'Sullivan J. A. and Lalor E. C. 2015, "Low-frequency cortical entrainment to speech reflects phoneme-level processing," *Current Biology* **25**, 2457-2465.
43. Leonardi N., Richiardi J., Gschwind M., Simioni S., Annoni J. M., Schluep M., Vuilleumier P. and Van De Ville D. 2013, "Principal components of functional connectivity: a new approach to study dynamic brain connectivity during rest," *Neuroimage* **83**, 937-50.
44. Allen E. A., Damaraju E., Plis S. M., Erhardt E. B., Eichele T. and Calhoun V. D. 2014, "Tracking whole-brain connectivity dynamics in the resting state," *Cereb Cortex* **24**, 663-76.
45. Ghosh-Dastidar S., Adeli H. and Dadmehr N. 2008, "Principal component analysis-enhanced cosine radial basis function neural network for robust epilepsy and seizure detection," *IEEE Transactions on Biomedical Engineering* **55**, 512-518.
46. Nunez P. L. and Srinivasan R. 2006, Electric fields of the brain: the neurophysics of EEG. (Oxford University Press, USA).
47. Delorme A. and Makeig S. 2004, "EEGLAB: an open source toolbox for analysis of single-trial EEG dynamics including independent component analysis," *Journal of neuroscience methods* **134**, 9-21.
48. Cong F., Kalyakin I., Huttunen-Scott T., Li H., Lyytinen H. and Ristaniemi T. 2010, "Single-trial based independent component analysis on mismatch negativity in children," *International journal of neural systems* **20**, 279-292.
49. Rembado I., Castagnola E., Turella L., Ius T., Budai R., Ansaldo A., Angotzi G. N., Debertoldi F., Ricci D. and Skrap M. 2017, "Independent component decomposition of human somatosensory evoked potentials recorded by

micro-electrocorticography," *International journal of neural systems* **27**, 1650052.
50. Tadel F., Baillet S., Mosher J. C., Pantazis D. and Leahy R. M. 2011, "Brainstorm: a user-friendly application for MEG/EEG analysis," *Computational intelligence and neuroscience* **2011**, 8.
51. Gramfort A., Papadopoulo T., Olivi E. and Clerc M. 2010, "OpenMEEG: opensource software for quasistatic bioelectromagnetics," *Biomedical engineering online* **9**, 45.
52. Hämäläinen M. S. and Ilmoniemi R. J. 1994, "Interpreting magnetic fields of the brain: minimum norm estimates," *Medical & biological engineering & computing* **32**, 35-42.
53. Bola M. and Sabel B. A. 2015, "Dynamic reorganization of brain functional networks during cognition," *Neuroimage* **114**, 398-413.
54. Palva S. and Palva J. M. 2012, "Discovering oscillatory interaction networks with M/EEG: challenges and breakthroughs," *Trends Cogn Sci* **16**, 219-30.
55. Lin F. H., Belliveau J. W., Dale A. M. and Hämäläinen M. S. 2006, "Distributed current estimates using cortical orientation constraints," *Human brain mapping* **27**, 1-13.
56. Desikan R. S., Segonne F., Fischl B., Quinn B. T., Dickerson B. C., Blacker D., Buckner R. L., Dale A. M., Maguire R. P., Hyman B. T., Albert M. S. and Killiany R. J. 2006, "An automated labeling system for subdividing the human cerebral cortex on MRI scans into gyral based regions of interest," *Neuroimage* **31**, 968-80.
57. Hipp J. F., Hawellek D. J., Corbetta M., Siegel M. and Engel A. K. 2012, "Large-scale cortical correlation structure of spontaneous oscillatory activity," *Nat Neurosci* **15**, 884-90.
58. O'Neill G. C., Tewarie P. K., Colclough G. L., Gascoyne L. E., Hunt B. A. E., Morris P. G., Woolrich M. W. and Brookes M. J. 2017, "Measurement of dynamic task related functional networks using MEG," *Neuroimage* **146**, 667-678.
59. Brookes M. J., Woolrich M. W. and Barnes G. R. 2012, "Measuring functional connectivity in MEG: a multivariate approach insensitive to linear source leakage," *Neuroimage* **63**, 910-20.
60. Colclough G. L., Brookes M. J., Smith S. M. and Woolrich M. W. 2015, "A symmetric multivariate leakage correction for MEG connectomes," *Neuroimage* **117**, 439-48.
61. O'neill G. C., Tewarie P. K., Colclough G. L., Gascoyne L. E., Hunt B. A., Morris P. G., Woolrich M. W. and Brookes M. J. 2017, "Measurement of dynamic task related functional networks using MEG," *NeuroImage* **146**, 667-678.
62. Mammone N., De Salvo S., Ieracitano C., Marino S., Marra A., Corallo F. and Morabito F. 2017, "A permutation disalignment index-based complex network approach to evaluate longitudinal changes in brain-electrical connectivity," *Entropy* **19**, 548.
63. O'Neill G. C., Bauer M., Woolrich M. W., Morris P. G., Barnes G. R. and Brookes M. J. 2015, "Dynamic recruitment of resting state sub-networks," *Neuroimage* **115**, 85-95.
64. Kim D., Kay K., Shulman G. L. and Corbetta M. 2017, "A new modular brain organization of the BOLD signal during natural vision," *Cerebral Cortex*, 1-17.
65. Baldassano C., Chen J., Zadbood A., Pillow J. W., Hasson U. and Norman K. A. 2017, "Discovering Event Structure in Continuous Narrative Perception and Memory," *Neuron* **95**, 709-721 e5.
66. Alday P. M. 2018, "M/EEG analysis of naturalistic stories: a review from speech to language processing," *Language, Cognition and Neuroscience*, 1-17.
67. Alexandrou A. M., Saarinen T., Kujala J. and Salmelin R. 2018, "Cortical entrainment: what we can learn from studying naturalistic speech perception," *Language, Cognition and Neuroscience*, 1-13.
68. Sankari Z. and Adeli H. 2011, "Probabilistic neural networks for diagnosis of Alzheimer's disease using conventional and wavelet coherence," *Journal of neuroscience methods* **197**, 165-170.
69. Ahmadlou M., Adeli H. and Adeli A. 2013, "Spatiotemporal analysis of relative convergence of EEGs reveals differences between brain dynamics of depressive women and men," *Clinical EEG and neuroscience* **44**, 175-181.
70. Adeli H., Ghosh-Dastidar S. and Dadmehr N. 2007, "A wavelet-chaos methodology for analysis of EEGs and EEG subbands to detect seizure and epilepsy," *IEEE Transactions on Biomedical Engineering* **54**, 205-211.
71. Sharma P., Khan Y. U., Farooq O., Tripathi M. and Adeli H. 2014, "A wavelet-statistical features approach for nonconvulsive seizure detection," *Clinical EEG and neuroscience* **45**, 274-284.
72. Vidaurre D., Quinn A. J., Baker A. P., Dupret D., Tejero-Cantero A. and Woolrich M. W. 2016, "Spectrally resolved fast transient brain states in electrophysiological data," *Neuroimage* **126**, 81-95.
73. Palva J. M., Wang S. H., Palva S., Zhigalov A., Monto S., Brookes M. J., Schoffelen J.-M. and Jerbi K. 2018, "Ghost interactions in MEG/EEG source space: A note of caution on inter-areal coupling measures," *Neuroimage* **173**, 632-643.
74. Mammone N., Ieracitano C., Adeli H., Bramanti A. and Morabito F. C. 2018, "Permutation Jaccard distance-based hierarchical clustering to estimate EEG network density modifications in MCI subjects," *IEEE transactions on neural networks and learning systems* **29**, 5122-5135.

IV

DISCOVERING DYNAMIC TASK-MODULATED FUNCTIONAL NETWORKS WITH SPECIFIC SPECTRAL MODES USING MEG

by

Yongjie Zhu, Jia Liu, Chaoxiong Ye, Klaus Mathiak, Piia Astikainen, Tapani Ristaniemi & Fengyu Cong 2020

NeuroImage, 218, 116924

DOI: https://doi.org/10.1016/j.neuroimage.2020.116924

NeuroImage 218 (2020) 116924

Contents lists available at ScienceDirect

NeuroImage

journal homepage: www.elsevier.com/locate/neuroimage

Discovering dynamic task-modulated functional networks with specific spectral modes using MEG

Yongjie Zhu [a,b,c], Jia Liu [a,b], Chaoxiong Ye [f,g], Klaus Mathiak [c], Piia Astikainen [g], Tapani Ristaniemi [b], Fengyu Cong [a,b,d,e,*]

[a] School of Biomedical Engineering, Faculty of Electronic and Electrical Engineering, Dalian University of Technology, 116024, Dalian, China
[b] Faculty of Information Technology, University of Jyväskylä, 40014, Jyväskylä, Finland
[c] Department of Psychiatry, Psychotherapy and Psychosomatics, Medical Faculty, RWTH Aachen University, Pauwelsstraße 30, D-52074, Aachen, Germany
[d] School of Artificial Intelligence, Faculty of Electronic Information and Electrical Engineering, Dalian University of Technology, Dalian, China
[e] Key Laboratory of Integrated Circuit and Biomedical Electronic System, Liaoning Province. Dalian University of Technology, Dalian, China
[f] Institute of Brain and Psychological Sciences, Sichuan Normal University, Chengdu, 610000, China
[g] Department of Psychology, University of Jyväskylä, 40014, Jyväskylä, Finland

ARTICLE INFO

Keywords:
Tensor decomposition
MEG
Functional connectivity
Frequency-specific oscillations
Dynamic brain networks
Canonical polyadic decomposition

ABSTRACT

Efficient neuronal communication between brain regions through oscillatory synchronization at certain frequencies is necessary for cognition. Such synchronized networks are transient and dynamic, established on the timescale of milliseconds in order to support ongoing cognitive operations. However, few studies characterizing dynamic electrophysiological brain networks have simultaneously accounted for temporal non-stationarity, spectral structure, and spatial properties. Here, we propose an analysis framework for characterizing the large-scale phase-coupling network dynamics during task performance using *magnetoencephalography* (MEG). We exploit the high spatiotemporal resolution of MEG to measure time-frequency dynamics of connectivity between parcellated brain regions, yielding data in tensor format. We then use a *tensor component analysis* (TCA)-based procedure to identify the spatio-temporal-spectral modes of covariation among separate regions in the human brain. We validate our pipeline using MEG data recorded during a hand movement task, extracting a transient motor network with beta-dominant spectral mode, which is significantly modulated by the movement task. Next, we apply the proposed pipeline to explore brain networks that support cognitive operations during a working memory task. The derived results demonstrate the temporal formation and dissolution of multiple phase-coupled networks with specific spectral modes, which are associated with face recognition, vision, and movement. The proposed pipeline can characterize the spectro-temporal dynamics of functional connectivity in the brain on the subsecond timescale, commensurate with that of cognitive performance.

1. Introduction

The brain is composed of billions of interconnected neurons, forming an extremely complex dynamic system in which populations of neurons are organized into functional units with specific information-processing capabilities (Babiloni et al., 2005; Hillebrand et al., 2012). Yet, efficient neuronal coordination between these spatially separated units is necessary for cognitive functions (Salinas and Sejnowski, 2001; Siegel et al., 2012; Varela et al., 2001). The interactions among distributed regions through oscillatory synchronization may provide a possible mechanism of such coordination (Fries, 2005, 2015). In other words, neuronal populations transmit information by coordinating their oscillatory activity with the oscillations of the receptor population at certain frequencies (Vidaurre et al., 2018). Moreover, different oscillatory patterns (i.e., different frequencies) provide the basis for different functions (Buzsáki and Draguhn, 2004; Vidaurre et al., 2018). Meanwhile, phase-coupling between separate populations of neurons in specific frequency rhythms has been well-established as a mechanism for regulating the integration and flow of cognitive contents (Engel et al., 2013; Salinas and Sejnowski, 2001; Vidaurre et al., 2018). It has also been shown that such frequency-specific phase-coupling plays an important role in task performance, in which task-related information is transmitted through

* Corresponding author. School of Biomedical Engineering, Faculty of Electronic and Electrical Engineering, Dalian University of Technology, 116024, Dalian, China.
E-mail addresses: yongjie.zhu@foxmail.com (Y. Zhu), cong@dlut.edu.cn (F. Cong).

https://doi.org/10.1016/j.neuroimage.2020.116924
Received 28 October 2019; Received in revised form 31 March 2020; Accepted 4 May 2020
Available online 20 May 2020

phase-locking across spatially distributed cortical regions (Bola and Sabel, 2015; Fries, 2015).

Magnetoencephalography (MEG) recordings have demonstrated that large-scale networks activated in cognitive tasks involve different frequency bands in their communications. For instance, the connectivity between the left and the right motor regions, quantified by the correlation of band-limited power, is maximized in the beta band (13–30 Hz), but not significant at low frequencies (1–8 Hz) or high frequency (i.e. >40 Hz) (Brookes et al., 2012a,b; Brookes et al., 2014; Brookes et al., 2012a,b; Hipp et al., 2012). Moreover, certain frequency bands are related to distinct cognitions. For example, electrophysiological studies of working memory have shown that power and coherence in the beta band decrease with increased memory load in the frontoparietal network. However, the power in theta the band only increases in the frontal regions, while the power in the alpha band exhibits a reduction with increased task load in the parietal nodes (Brookes et al., 2012a,b; Brookes et al., 2014). These findings imply that connectivity patterns at distinct frequency bands may subserve different cognitive functions.

In addition to specificity in spectral features, functional networks exhibit highly temporally variable neuronal dynamics on rapid timescales (Bola and Sabel, 2015; Kopell et al., 2014). In order to effectively track such network dynamics, many studies have explored the organization of brain functional networks using MEG, since the temporal richness of MEG can match the rapid timescales of the brain's functional connectivity (O'Neill et al., 2017; Schölvinck et al., 2013; Tewarie et al., 2019b). For example, Vidaurre and colleagues have published multiple papers using a set of methods based on the *Hidden Markov Model*, showing that functional brain networks reorganize and coordinate transiently on the timescale of milliseconds (Baker et al., 2014; Quinn et al., 2018; Vidaurre et al., 2018; Vidaurre et al., 2017). O'Neill et al. proposed an *independent component analysis* (ICA)-based method for time-varying functional connectivity, demonstrating the temporal evolution of dynamic networks at a specific frequency band on the timescale of seconds during a task (O'Neill et al., 2017). Lachaux and colleagues presented a practical method based on phase-locking for the direct quantification of frequency-specific synchronization with time resolution at the millisecond scale (J. P. Lachaux, Rodriguez, Martinerie and Varela, 1999; Varela et al., 2001). Also, the brain networks are recently understood as a multi-scale network and can be characterized over temporal scales with precision ranging from sub-millisecond to that of the entire lifespan (Betzel and Bassett, 2017; Betzel et al., 2016; Khambhati et al., 2019).

Considering the temporal non-stationarity and frequency specificity of the functional connectivity, previously applied methods typically required pre-specification of a frequency band and/or a time window before connectivity calculation. Those methods need to filter the neuroimaging data into specific frequency bands and examine the temporal dynamics of interactions for one specific frequency band by one (de Pasquale et al., 2012; de Pasquale et al., 2016). For examples, Betti et al. linked the dynamics of formation and dissolution of networks and of hub networks during movie observation to the one occurring during resting stage using a fixed frequency band (Betti et al., 2018; Betti et al., 2013). O'Neill et al. provided an overview of the studies on the dynamics of connectivity carried out with fixed frequency intervals but without pre-specification of the time window (O'Neill et al., 2018; O'Neill et al., 2015). However, the above-mentioned methods were reliant on a priori selection of frequency bands, and few studies have attempted to explore the formation and dissolution of the frequency-dependent dynamic brain networks during task performance within a completely data-driven approach.

In the current study, we undertake an analysis of the spectral features and temporal evolution of dynamic connectivity during a task. Our proposed framework is based on the measurement of the time-frequency domain connectivity between pairs of separate brain regions predefined through cortical parcellation. *Weighted phase lag index* (wPLI) is used as a means of quantifying the connectivity since it is insensitive to signal leakage and similar bias effects (Hillebrand et al., 2012; Palva et al., 2018; Vinck et al., 2011). After calculation of the wPLI for each time point and frequency point, we construct a *third-order tensor* (a three-dimensional data array) including frequency, time, and connectivity (vectorized upper triangular parts of the connectivity matrix). The three-dimensional data is then analyzed using *tensor component analysis* (TCA), which is a multi-dimensional decomposition technique and is an extension of matrix factorization (e.g., principal component analysis (PCA) or ICA). TCA can extract separate components with low-dimensional features (factors), each of which corresponds to a functional connectivity pattern with rapidly temporal dynamics and distinct spectral dynamics. It should be noted that unlike PCA or ICA, the factors extracted by tensor decomposition do not require orthogonality or independence. According to this property, tensor decomposition can achieve a demixing of high-dimensional data and examine the interaction across different modalities (Zhou and Cichocki, 2012; Zhou et al., 2016). For example, in an EEG study, three tensor modes could correspond to time, frequency, and channel (Mørup et al., 2006). In fMRI studies, the different modes could be voxel, time, and patient (Hunyadi et al., 2017). In neurophysiological measurements, they could span neuron, time, and trial (Williams et al., 2018). Previous TCA-based studies of brain connectivity mainly applied TCA to channel-level EEG data to detect the change points of the dynamic network states (Liu et al., 2014; Mahyari and Aviyente, 2014; Mahyari et al., 2016; Samdin et al., 2016) and examine the spatial-temporal properties of the network community (Al-sharoa, Al-khassaweneh, & Aviyente, 2018; Ozdemir et al., 2017; Tang et al., 2019). Also, TCA was applied to EEG channel level connectivity over time, frequency and subjects to explore the connectivity patterns within the considered electrodes (Pester et al., 2015), and to ongoing EEG data over temporal sliding windows, frequency, and subjects to link musical features to brain networks (Zhu et al., 2019a,b). Here distinct from this, we applied TCA to atlas-based MEG data over network connectivity, time and frequency to provide a pipeline to track the temporal evolution of frequency-dependent functional networks at the millisecond scale during task performance. We performed tensor decomposition to extract three interacted, low-dimensional descriptions of time-frequency phase-coupling networks, which includes connectivity factors reflecting functional network patterns, temporal factors reflecting rapidly temporal evolution of the functional networks, and the spectral factors reflecting spectral features of networks. The proposed pipeline is completely data-driven and enables the characterization of the temporal, spectral, and spatial features of the electrophysiological network connectivity all at once. In other words, this allows us to identify which involved frequency bands, where and when significant modulations in connectivity occur.

2. Material and methods

2.1. Data description

We analyzed MEG data from the human connectome project (HCP; www.humanconnectome.org), including a motor task and an N-back working memory task (Larson-Prior et al., 2013). Sixty-two subjects participated in the motor task and 82 subjects in the working memory task. Most were right-handed as measured with the Edinburgh Handedness Inventory, with a mean lateralization quotient of 65% and $SD = 44\%$ (Oldfield, 1971). Data were recorded using a whole-head 248-channel magnetometer system (MAGNES 3600 WH, 4D Neuroimaging, San Diego, CA) with the participants in supine position. Data were continuously recorded with a sampling rate of 2034.5 Hz and a bandwidth of DC-400 Hz. Digitization of the participants' head shape and of the locations of the fiducial coils was accomplished with a Polhemus 3Space Fasttrak system. Participants performed a sequence of tasks, described in detail in the reference manual provided by HCP. Just prior to the N-back working memory task the participant underwent three runs of approximately 6 min of resting-state MEG recording.

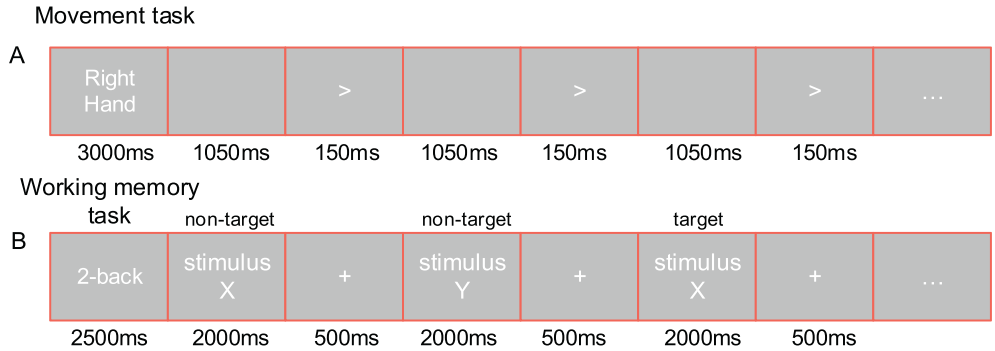

Fig. 1. Experiment task. A) Right hand movements in motor task paradigm. Block begins with a 3 s cue instructing the participant which limb to move in that trial. B) Two-back condition in the working memory task. Two-back blocks were signaled by a presentation of "2-back" for 2500 ms. Participants indicated whether the presented stimulus matched the stimulus two trials earlier.

During the motor task, participants were presented with visual cues instructing the movement of either the right hand, left hand, right foot, or left foot. Movements were paced with a visual cue, which was presented in a blocked design. Each block started with an instruction screen, indicating the limb (arm or leg) and the side to be involved in the current block. A set of pacing stimuli were presented in sequence, each one instructing the subject to make a brisk movement. The pacing stimulus was composed of a small arrow in the center of the screen (see Fig. 1). The interval between consecutive stimuli was fixed to 1200 ms. The arrow stayed on the screen for 150 ms and the screen was black for the remaining 1050 ms. There were 8 blocks of movement per motor effector. 10 pacing stimuli were presented in sequence. This yielded in total of 80 movements per motor effector. Here, for simplicity, we only used data with right- and left-hand movements.

During the N-back working memory task, subjects were presented with pictures of tools or faces. There were two memory load conditions: 0-back and 2-back tasks. 0-back task is a match-to-sample condition during which a cue target image was presented at the beginning of a block. A set of images were presented in a sequence, and each of them was displayed for 2000 ms. At the end of this interval, a button press had to be executed by participants with the index or middle finger of the right hand as to whether this current image matched the target or not. For the 2-back condition block, participants were presented with a sequence of images and had to respond whether each image matched the image two positions earlier or not. The response had to take place within a 500-ms period after stimulus presentation, during which a fixation cross was presented on the center of the screen. Participants were presented with 8 blocks in the 2-back condition. A sequence of 10 images is presented in each block. This yielded in total number of 80 trials.

2.2. Preprocessing and source reconstruction

We used the same criteria set in the HCP pipelines to remove bad channels, segments and bad independent components.[1] Briefly, epochs had been extracted from the continuous recording. Epochs containing superconducting quantum interference device (SQUID) jumps, bad sensors, or bad segments, defined as excessive signal amplitude changes $>\sim 10^{-12}T$, were excluded from further processing. Eye movement-related signals and cardiac signals had been identified with ICA and projected out of the data. For the motor task, trial duration was set from −1.2 to 1.2 s relative to the onset of the arrow that instructs subjects to execute the movement. For the working memory task, trial duration was set from −1.5 to 2.5 s relative to the onset of the image that subjects had to match or not with the target image. After bandpass filtering (1–48 Hz), the data were down-sampled to 256 Hz. Following this preprocessing, the cortical surface of the brain was reconstructed from an anatomical individual MRI offered by HCP. The reconstructed cortical surface was decimated to 4098 evenly distributed vertices per hemisphere. The preprocessed data epochs were used to compute the inverse model, which was estimated using cortically constrained and depth-weighted (p = 0.8) L2 minimum-norm estimate (wMNE) (Lin et al., 2006). The noise covariance matrix was calculated from the empty-room recordings, separately for each subject's data provided by HCP. The cortical surface was then parcellated into 68 anatomical regions based on the Desikan-Killiany Atlas (Desikan et al., 2006). This atlas discretized the neocortex into 34 parcels (areas) per hemisphere. For each parcel, we performed a principal component analysis to extract spatially orthogonal components that describe the activity, ordered by amount of variance explained. We selected the first principal component as a representation of the parcel's time course of activity. Thus, for each trial, a source-level data matrix M was created with dimension $n_n \times n_s$, where $n_n = 68$ represented the number of anatomical regions and n_s represented the number of samples ($n_s = 615$ for the motor task, $n_s = 1024$ for the working memory task). The main steps of the subsequent data processing pipeline are outlined in Fig. 2.

2.3. Spectral decomposition

To estimate the spectral densities of the parcellated time-series data, continuous wavelet transform with Complex Morlet wavelets was performed on source space data matrix M for a single trial. A total of 42 linearly spaced frequencies and full time points were estimated. The wavelet contained three cycles at the lowest frequency (4 Hz); the number of cycles increased up to 15 cycles at the highest frequency (45 Hz), and 42 frequency points from 4 Hz to 45 Hz were obtained. Thus, for each trial, a third-order tensor was obtained with dimension $n_n \times n_s \times n_f$, where $n_f = 42$ represented the number of frequency points.

2.4. Functional connectivity estimation

To estimate phase-coupling between all pairs of regions for each frequency and time point, wPLI (Vinck et al., 2011) was computed; i.e., the sign of the phase difference between two signals is weighted by the magnitude of the imaginary component of the cross-spectrum:

$$wPLI_{(f,t)} = \frac{\left|\sum_{n=1}^{N}\left(\left|im\left(S_1^n(f,t)S_2^{n*}(f,t)\right)\right| sign\left(im\left(S_1^n(f,t)S_2^{n*}(f,t)\right)\right)\right)\right|}{\sum_{n=1}^{N}\left|im\left(S_1^n(f,t)S_2^{n*}(f,t)\right)\right|}, \quad (1)$$

where $S_1^n(f,t)$ and $S_2^n(f,t)$ are wavelet-decomposed time-frequency representations from regions 1 and region 2 respectively, from trial n and for frequency point f and time point t. N is the number of trials. * represents the complex conjugate, $im()$ is the imaginary part of a complex value, and || represents an absolute value operation. For each subject, a third-order tensor of connections $\mathcal{P}$ was created with dimension $n_c \times n_s \times n_f$, where

[1] https://www.humanconnectome.org/documentation/MEG/MEG1_Release_Reference_Manual.pdf.

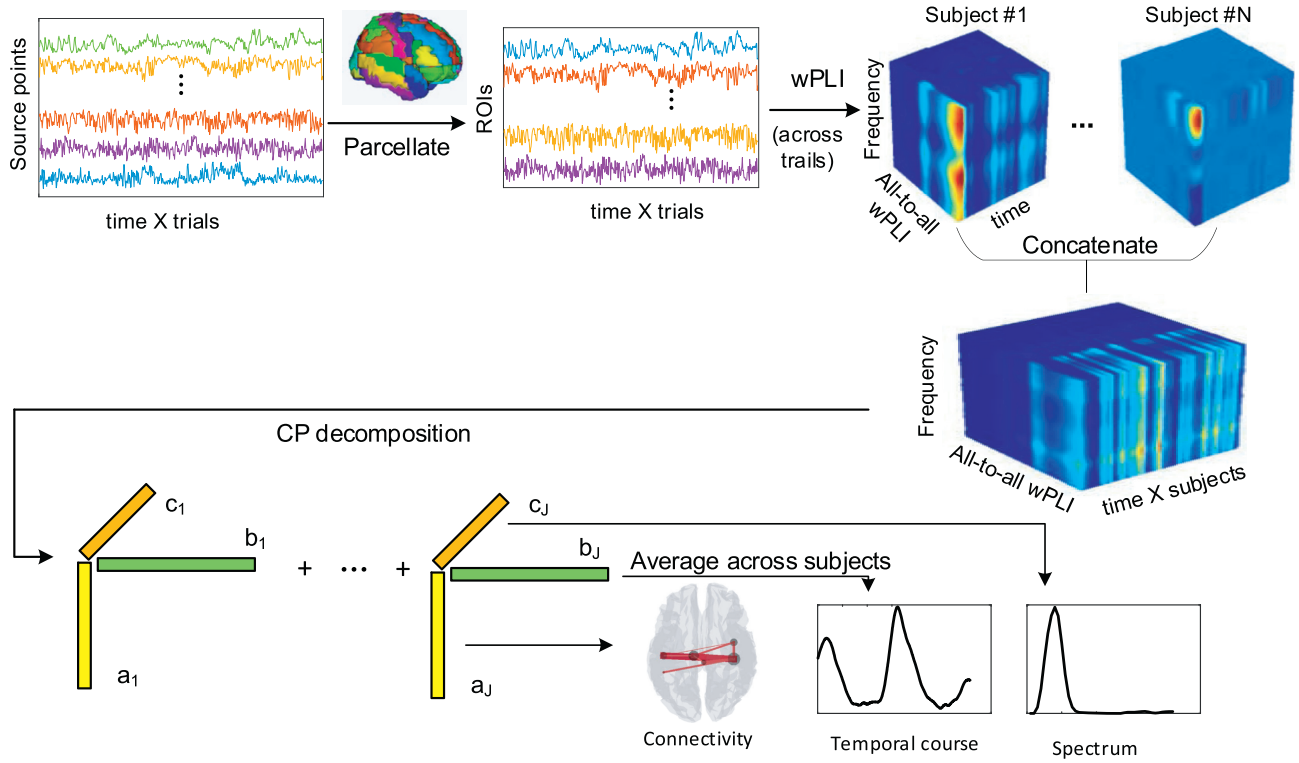

Fig. 2. Analysis pipeline. Data were preprocessed, divided into stimulus-locked epochs, and projected into the source-space using the weighted MNE algorithm. Signals of 68 ROIs based on anatomical brain regions were transformed with a Complex Morlet wavelet. For each time-point and frequency-point, an adjacency matrix containing wPLI estimates was then generated (vectorized using upper triangular parts). For each subject, a three-way tensor (with time by frequency by connection) was obtained. These individual wPLI (average across trails) tensors were concatenated across subjects in temporal dimension. Nonnegative CANDECOMP/PARAFAC (CP) decomposition was performed on the temporally concatenated tensor to extracted low-dimensional components including temporal factors, spectral factors, and connectivity factors.

$n_c = 2278$ denotes the number of pairs of regions ($68^*(68-1)/2$). These three-way arrays were then concatenated over time to generate a new tensor $\mathcal{X}$ with dimension $n_c \times n_t \times n_f$, where $n_t = n_s{}^* n_p$ and n_p denotes the number of the participants ($n_p = 61$ for the motor task and $n_p = 83$ for the working memory task).

2.5. Tensor decomposition

The most common method for dimensionality reduction and component analysis of electrophysiological data has been based on decomposition techniques such as PCA and ICA. However, these two-way analysis techniques commonly applied on matrices may fail to find the underlying structures in multi-dimensional data sets (Cong et al., 2012; Williams et al., 2018). Here, we use the CANDECOMP/PARAFAC (CP) model (Sidiropoulos et al., 2017), a direct extension of bilinear factor models to multilinear data, to identify a set of low-dimensional components characterizing variability along each of the modalities. A brief description of the CP model follows.

Each element in the obtained tensor $\mathcal{X} \in \mathbb{R}_+^{n_c \times n_t \times n_f}$, $x_{c,f,t}$ denotes the connection (wPLI) between two regions at time point t within frequency bin f. Here, the indices c, t, and f each range from 1 to n_c, n_s, and n_f, respectively. It should be noted that all the elements are non-negative, since wPLI takes values between 0 and 1. CP decomposition approximates the data as a sum of outer products of three vectors producing an additional set of low-dimensional factors, which can be described as:

$$\mathcal{X} \approx \sum_{j=1}^{J} \boldsymbol{a}_j \circ \boldsymbol{b}_j \circ \boldsymbol{c}_j, \tag{2}$$

where operator $\circ$ represents the outer product of vectors, and J is the number of extracted components. $\boldsymbol{a}_j, \boldsymbol{b}_j$, and $\boldsymbol{c}_j$ ($n = 1, 2, \cdots, J$) are the factor vectors. We can think of $\boldsymbol{a}_j$ as the functional network pattern across the whole-brain connections, and we can consider $\boldsymbol{b}_j$ as spectral factors across frequency. These connectivity factors and spectral factors constitute a structure that is common across time. The third set of factors, $\boldsymbol{c}_j$, can be considered as temporal factors, which characterizes the temporal evolution of the frequency-specific functional connectivity patterns identified by connection and spectral factors. Thus, TCA for wPLI data can capture temporal dynamics of the functional connectivity on a timescale of milliseconds with a specific spectral feature. Such frequency-specific connectivity patterns may be modulated by a task across time during task performance. In addition, another benefit of TCA is a dimension reduction of the original high-dimensional data, reducing $n_c \times n_s \times n_f$ data points to $J(n_c + n_s + n_f)$ elements.

The non-negative CP model optimization is to solve the following minimization problem:

$$\min_{\boldsymbol{A},\boldsymbol{B},\boldsymbol{C}} \frac{1}{2} \left| \mathcal{X} - \sum_{j=1}^{J} \boldsymbol{a}_j \circ \boldsymbol{b}_j \circ \boldsymbol{c}_j \right|_F^2, \tag{3}$$

where $_F$ represents the Frobenius norm. Matrix $\boldsymbol{A} = [\boldsymbol{a}_1, \ \boldsymbol{a}_2, \cdots, \boldsymbol{a}_j]$ is the connectivity factor matrix, $\boldsymbol{B} = [\boldsymbol{b}_1, \boldsymbol{b}_2, \cdots, \boldsymbol{b}_j]$ is spectral factor matrix, and $\boldsymbol{C} = [\boldsymbol{c}_1, \boldsymbol{c}_2, \cdots, \boldsymbol{c}_j]$ is temporal factor matrix. Like many matrix factorization methods, the CP model can only be fit by iterative optimization algorithms. Such procedures may converge in suboptimal local minima, but in other applications, all estimations for many runs have converged to similar reconstruction errors (Cong et al., 2012; Mackevicius et al., 2019; Williams et al., 2018). For example, Williams et al. applied the TCA to neural data to extract low-dimensional neural dynamics across multiple timescales, where the majority of runs for optimization successfully converged with high data fit value (Williams et al.,

2018). In the current study, we apply the classic method of *alternating least-squares* (ALS) to estimate the factor matrices (Cichocki et al., 2015; Kolda and Bader, 2009). To solve the minimization problem in Equation (3), the ALS algorithm fixes two of the factor matrices and optimizes over the third one. This is a least-squares subproblem that is convex and has a closed-form solution. For illustration, consider estimating the connectivity factor matrices $\boldsymbol{A}$, while fixing the spectral factor matrices $\boldsymbol{B}$ and temporal factor matrices $\boldsymbol{C}$. This yields in the following updating rule:

$$\boldsymbol{A} \leftarrow \operatorname{argmin}_{\tilde{A}} \frac{1}{2}\left|\mathcal{X} - \sum_{j=1}^{J} \boldsymbol{a}_j \circ \boldsymbol{b}_j \circ \boldsymbol{c}_j\right|_F^2, \tag{4}$$

which can be estimated as a linear least-squares problem. We terminated the CP decomposition process when the absolute difference value of data fitting of the adjacent two iterations was less than very small positive value such as $1e-8$, or the maximum number of iterations was more than 1000. Here, TCA was performed on temporally concatenated data across subjects. This means that the connectivity factor and the spectral factor of the brain networks (components) are common to all subjects but the temporal factor is subject-dependent. Each subject has their own temporal courses, representing the time evolution of the frequency-specific networks at each time points. The ALS algorithm is available in several open-source toolboxes (Bader and Kolda, 2012; Vervliet et al., 2016).

2.6. Selection of component number

In the application of tensor decomposition, a crucial issue is the determination of the number of components to be extracted. Actually, the choice of the number of components to extract is an inherent problem of model order selection, which is usually for the linear transform model or other dimensionality reduction methods (Cong et al., 2012, 2013; Mørup and Hansen, 2009). Although many different methods have been developed in the past few years, there does not exist a perfect solution for all conditions. Here, we used the DIFFIT method as a reference to inform this choice. DIFFIT refers to the difference in data fitting, and is calculated based on model reconstruction error and the explained variance (Timmerman and Kiers, 2000; Wang et al., 2018). The reconstruction error of the CP model is defined as

$$ReErr(J) = \frac{\left|\mathcal{X} - \sum_{j=1}^{J} \boldsymbol{a}_j \circ \boldsymbol{b}_j \circ \boldsymbol{c}_j\right|_F}{|\mathcal{X}|_F}. \tag{5}$$

Reconstruction error provides a metric analogous to the fraction of unexplained variance often used in PCA, since it is normalized to range between 0 and 1. Let the number of components $J \in [1, \mathscr{J}]$, where $\mathscr{J}$ is the empirically maximal number of underlying components. A fit is the variance of raw data explained by a proposed model and can be obtained as

$$Fit(J) = 1 - ReErr(J) = 1 - \frac{\left|\mathcal{X} - \sum_{j=1}^{J} \boldsymbol{a}_j \circ \boldsymbol{b}_j \circ \boldsymbol{c}_j\right|_F}{|\mathcal{X}|_F}. \tag{6}$$

Unlike PCA, the optimization procedure of tensor decomposition may have suboptimal solutions (local minima), and there is no guarantee that optimization routines will find the best set of parameters for decomposition. Thus, we run the optimization algorithm underlying the CP model at each value of J 20 times from random initial conditions, and the average data fitting $\overline{Fit(J)}$ is calculated across many runs. Then, the difference fit of the two adjacent fits is

$$DIF(J) = \overline{Fit(J)} - \overline{Fit(J-1)}. \tag{7}$$

Next, the ratio of the adjacent difference fits reads as

$$DIFFIT(J) = \frac{DIF(J)}{DIF(J+1)}. \tag{8}$$

The model $\tilde{J}$ with the largest DIFFIT value is considered as the appropriate tensor factorization model for the raw data tensor.

2.7. Testing the task-modulation connectivity

The above analyses yielded a set of $\tilde{J}$ brain networks (TCA components) with distinct spectral features, temporal courses, and connectivity patterns. Here, we sought to determine which extracted components were significantly modulated by the tasks. It should be noted that our procedure was based on previously theory, which has been well described elsewhere (O'Neill et al., 2017; Winkler et al., 2014; Zhu et al., 2019a,b). We first averaged the temporal factor matrix $\boldsymbol{C}$ (with a dimension of $n_s n_p \times \tilde{J}$) across subjects, yielding a new temporal matrix $\overline{\boldsymbol{C}}$ (with a dimension of $n_s \times \tilde{J}$) containing $\tilde{J}$ subject-averaged temporal courses. After this, an empirical null distribution was constructed based on phase randomization (Brookes et al., 2014).

We defined a "sham" matrix, $\tilde{\boldsymbol{C}}_{\text{onset}}$, which was constructed in exactly the same way as $\overline{\boldsymbol{C}}$, but prior to averaging over subjects, the onset of individual temporal courses was randomly shuffled based on phase-randomization. The phase-randomization was computed by taking the Fourier transform, randomizing the phase angle, and then transforming back. The properties of the derived time series of each individual subject were exactly preserved in the spectral domain. We reasoned that if no task induced response was expected, the randomly shuffled onset times would be meaningless, and therefore the magnitudes of fluctuations in $\tilde{\boldsymbol{C}}_{\text{onset}}$ and $\overline{\boldsymbol{C}}$ would match. However, if the individual temporal courses contained time-locked responses in brain connectivity, which were robust over subjects, then these would be preserved in $\overline{\boldsymbol{C}}$ but diminished in $\tilde{\boldsymbol{C}}_{\text{onset}}$. This procedure was repeated 5000 times to generate an empirical null distribution for each extracted component.

A component was considered significant if, at any one time point in the subject average, the corresponding column of $\overline{\boldsymbol{C}}$ fluctuated such that it fell outside a threshold defined by the null distribution (randomized onset). The threshold for significance was defined at level $P < 0.05$. This significant level was corrected based on Bonferroni correction for multiple comparisons across the multiple ($\tilde{J}$) components. In addition, a two-tailed distribution was allowed since the magnitude of the average temporal courses could be either greater than, or less than the null distribution. Thus, the threshold for significance was set at $P_{corrct} < 0.05/(2 \times \tilde{J}) = 0.025/\tilde{J}$.

3. Results

In the following section, we show the flexibility of our framework in the real MEG dataset. However, our proposed framework was also validated in simulation and compared with permutation test procedure without TCA (see Supplementary material). These simulation results can be found in the Appendix.

We firstly ran CP at each value of J—linearly increasing from 1 to 40 ($\mathscr{J} = 40$)—20 times with random initial conditions, which enabled us to examine whether some runs converged to local minima with low data fitting value (or high reconstruction error). Fig. 3 demonstrates the averaged fit values (Fig. 3A), the difference of fit values (DIF) and the DIFFIT (Fig. 3B). As can be seen that the variance (shaded areas of Fig. 3A) of the fit values from the 20 times is very low, and reveals that all runs at fixed component number J yield the same data fitting. For the motor task, it can be seen that the DIF values become very close to 0 when the component number $J > 20$ and a local maximum on DIFFIT at $J = 20$ emerges. This suggests the data fitting value starts to converge, which can be also found from the data fitting curve. The data fitting curve also reveals that all runs at fixed J yield similar results, indicating that all local minima in the optimization process are similar to each other and thus are

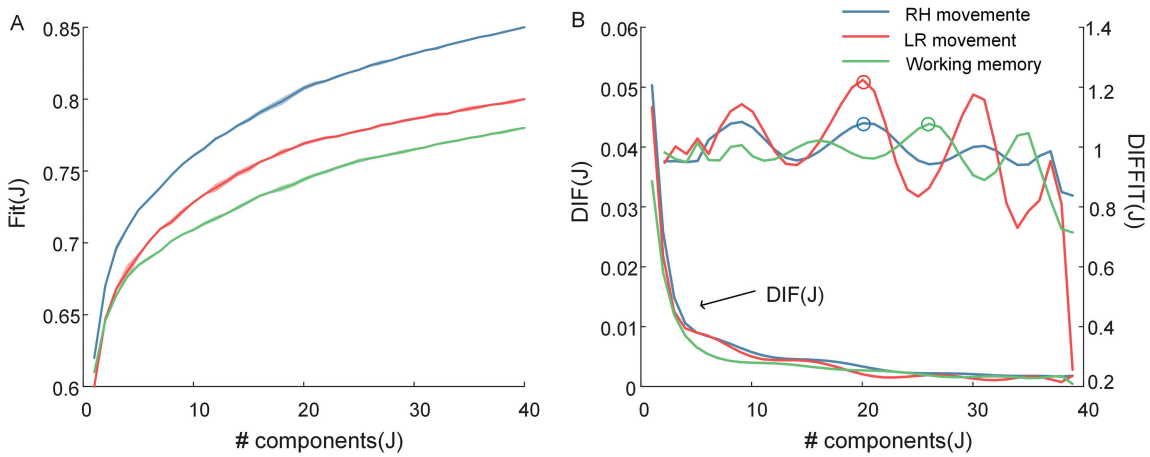

Fig. 3. A) Fit value plotted against number of components. B) difference of fit values and the DIFFIT plotted against number of components. For the movement experiments, we chose 20 components decomposed by the CP model. For the working memory task, 25 components were extracted since the delta fit was relatively small. It should be noted that the results were robust when the number of components was set from 15 to 25.

presumably similar to the global minimum. Fig. 3B demonstrates that $J = 25$ may be the appropriate model for CP decomposition in the working memory task since the DIF values are close to 0 after $J = 25$. Hereinafter, we set $\tilde{J} = 20$ for the motor task and $\tilde{J} = 25$ for the working memory task. Note that the DIFFIT method just gives a reference to select the number of underlying components, and we discuss this further below.

Fig. 4 demonstrates the results of the proposed approach performed on the movement data. While $\tilde{J} = 20$ rank-1 components were extracted, here we presented only two brain network patterns that exhibited significant task modulation. The other brain networks are shown in the Supplementary material. In Fig. 4, the right side shows the results of the left-hand movement data and the left side shows the results of the right-hand movement data. Each row of Fig. 4 represents a component with three factors. Fig. 4A demonstrates the connectivity factor representing the brain network pattern, which is demonstrated in 3D visualization and thresholded (top 5%) for clarity. Fig. 4B shows the temporal factor reflecting the time evolution of this network, which is represented as the associated averaged temporal factor of the individual in $\overline{\boldsymbol{C}}$ (with a dimension of $n_s \times \tilde{J}$) and plotted by black line. The time line of the event is marked by the vertical line. The gray shaded area indicates the null distribution constructed by randomly shuffling the time onset ($\tilde{\boldsymbol{C}}_{\text{onset}}$), which is the 95th percentile threshold. Fig. 4C shows the spectral factor reflecting the oscillatory feature of this network. A network shown in Row I, representing primary somatosensory and motor regions, is modulated significantly by the left-hand movement task (Fig. 4B). It is also found in right-hand movement data depicted in Row III. It should be noted that the results are slightly different for different sides of the hand movements. The 3D visualization demonstrates that network connectivity is mainly located in the left primary somatosensory cortex for right-hand movement (Row I of Fig. 4A), and on the right primary somatosensory cortex for the left-hand movement (Row III of Fig. 4A). Fig. 4C in Rows I and III show the spectral features of the sensorimotor network modulated by the movement task. It can be clearly seen that the sensorimotor network is associated with frequency modes ranging from 15 to 30 Hz, corresponding to the classical beta band. Rows II and IV show another visual network, modulated significantly by visual cues. The spectral feature suggests that this visual network is related to the theta and alpha bands. This spectra-specific visual network is derived from both left- and right-hand movement tasks.

Fig. 5 demonstrates the results of our analysis pipeline applied to the 2-back working memory data. Obviously, the increased cognitive load induced by 2-back working memory tasks elicits alterations in a large

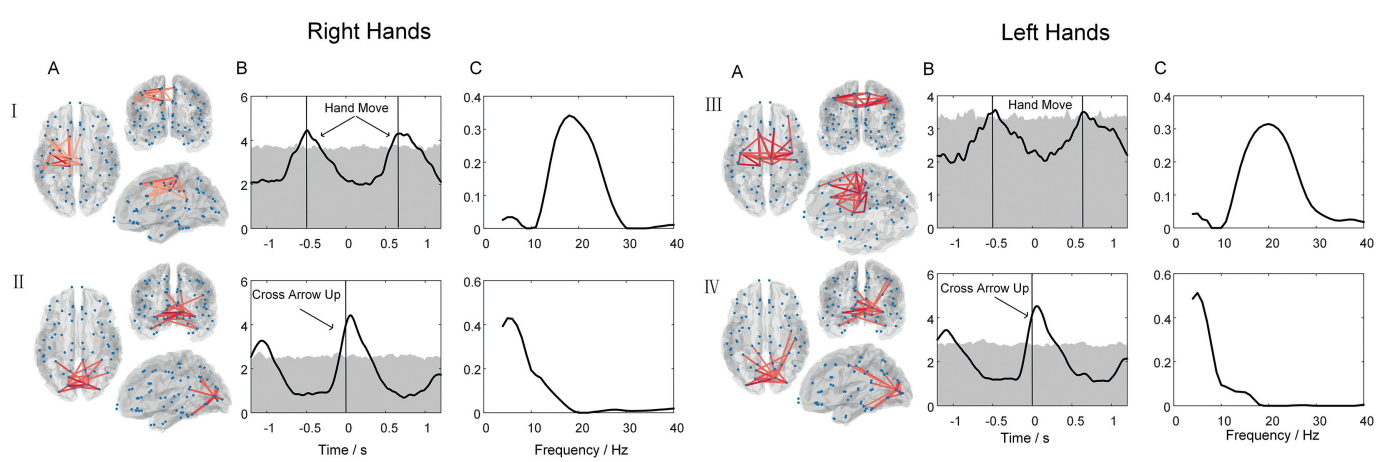

Fig. 4. Results of the hand movement experiments. The left side shows the results of the right hands' movement, and the right side shows the results of the left hands' movement. The separate columns show A) 3D representation of connectivity factors, thresholded (top 5%) for visualization. Each node indicates one brain region and darker color of lines shows stronger connections. B) The temporal courses of the network patterns during finger movement task, averaged across subject (black line). The gray shaded region represents the null distribution based on the hypothesis that the response is not time-locked to the stimulus. C). The spectral mode of the network. Rows I and III show the beta oscillatory motor networks modulated significantly by movement task. Rows II and IV show the theta oscillatory visual networks modulated significantly by the presentation of cross arrows.

number of functional networks. We present 10 of the 25 brain networks extracted that exhibited significant modulation by the 2-back working memory task. Each row in the column indicates one component with three factors, including connectivity networks represented as 3D visualization (Fig. 5A), temporal evolution represented as averaged time courses across subjects alongside a null distribution based on randomly shuffled time onset (Fig. 5B), and spectral features (Fig. 5C).

Two primary visual networks shown in Rows II and III of Fig. 5 are significantly modulated by the figure stimuli, which is unsurprising in light of the visual nature of the task. Their connectivity magnitudes increase by around 200 ms after both presentation and disappearance of the figure stimuli, but the connectivity during presentation increases more than during disappearance of the stimuli. Although these two networks both involve the visual regions, their spectral features are different. The spectral mode of network II peaks around 5 Hz, spanning theta and low alpha bands, but the spectral mode of network III peaks around 13 Hz across high alpha and low beta bands. Row IX, with spectrum peaking at 10 Hz, demonstrates connections between the primary visual and parietal regions, showing an increase in connectivity around 150 ms after the presentation of the figure stimuli. Row I shows a right-lateralized connection between visual and temporal areas with a spectral mode spanning the alpha band, which exhibits a significant enhancement immediately during the appearance of the stimuli. Rows IV to X show that transient functional networks with distinct spectral features form in later task phases. Row IV shows an increase in connectivity between right frontal areas and temporal areas related to the theta band, around, 300 ms after presentation of the stimuli. Row X indicates that a connection between left frontal regions and right temporal regions emerges by 300 ms after the stimuli, with a spectral feature across theta and alpha bands. A high-alpha right-lateralized tempo-parietal network appearing around 400 ms after the stimuli is shown in Row VII. Row VI shows a bilateral temporal connectivity network with dominated alpha rhythm, emerging at 600 ms after the stimuli. The network also captures areas associated with semantic processing and is thus termed the *semantic network*. Row VIII highlights a left-lateralized network that incorporates regions of temporal, parietal, and frontal cortex. The regions implicated are strongly associated with the production of language as well as shape and pattern recognition. A beta sensorimotor network is also derived during feedback. Row V demonstrates that a sensorimotor network involved in beta rhythm emerges during the execution of the button press. The connection exhibits strong enhancement in left motor areas, since participants executed the button press with their right-hand. In addition, the significant increases span a large range, from 1200 ms to 2000 ms, since the timing of the button press was different for different subjects. This result is in line with the results of the motor task (Fig. 3). It is worth noting that the brain areas involved in these networks incorporate the primary sensory cortices, association areas, and cognitive networks that would be associated with semantic processing, face recognition, and verbalization, and so these networks are plausible given the task. These are further addressed in our discussion.

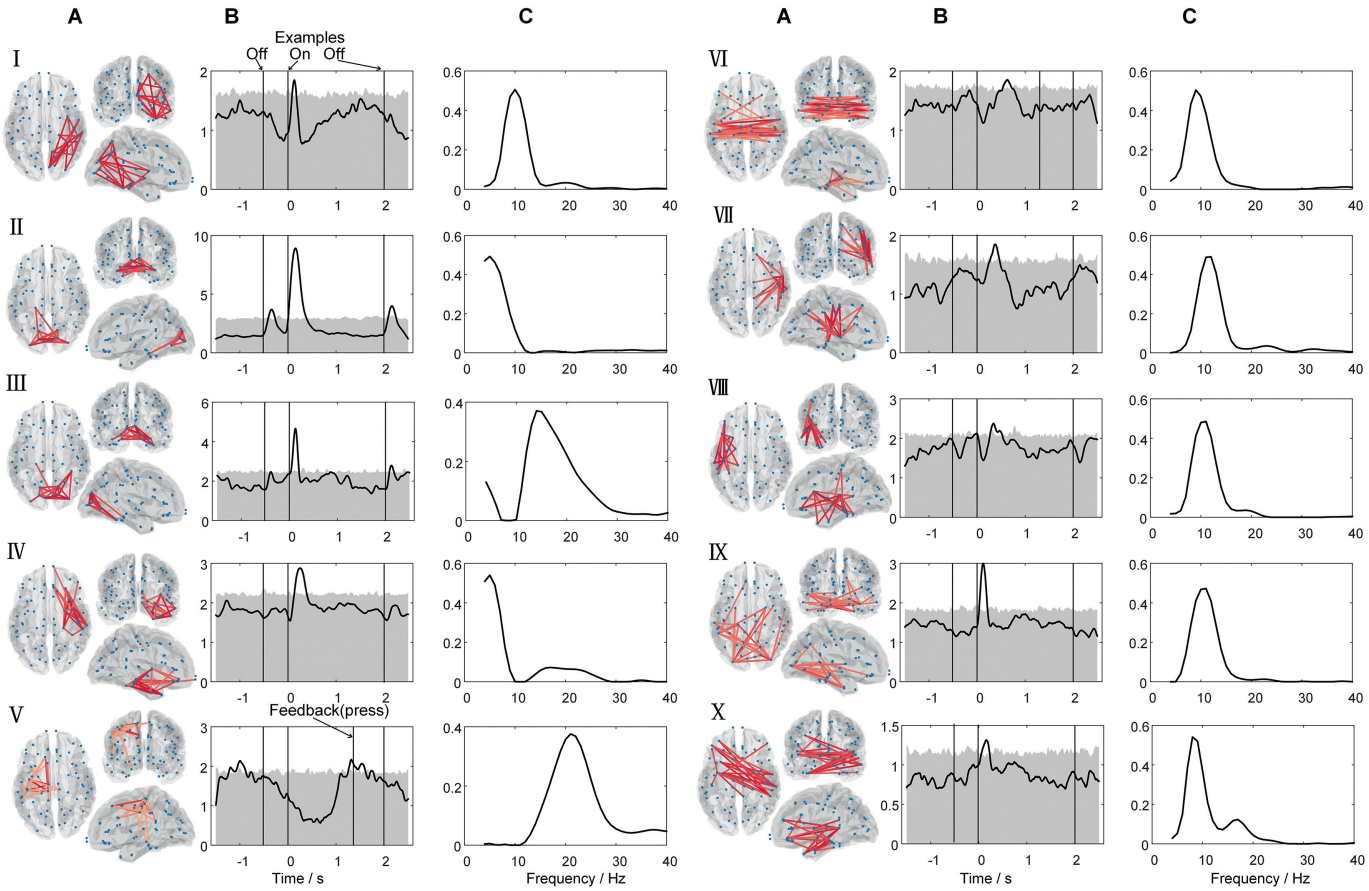

Fig. 5. Results of 2-back working memory task. A) 3D network visualization. B) Average temporal course (black line) and null distribution based on randomized onset times (shaded areas). C) Spectral mode of the network patterns. Row I: right lateralized connections between visual and temporal areas with a spectral mode spanning alpha band. Rows II and III: primary visual networks with theta and high-alpha dominant spectrum. IV: connections between right frontal areas and temporal areas related to theta band. V: Beta-specific motor network. VI: a bilateral temporal connectivity network with dominated alpha rhythm. VII: alpha-dependent right lateralized temporo-parietal network. VIII: language-related network. IX: visual to parietal with alpha-dominant spectrum. X: connections between left frontal regions and right temporal regions.

4. Discussion

The present study introduced a tensor-based framework for deriving large-scale phase-coupled network dynamics with distinct spectral features. This pipeline allows characterization of transient reconfiguration of electrophysiological brain networks at the timescale of milliseconds when applied to MEG data. Previous methods typically required pre-specification of a frequency band and/or a time window around the stimuli onset before the connectivity calculation. Then, network dynamics were examined using matrix decomposition techniques, such as ICA and PCA, in a single frequency band. Compared with ICA-based approaches, the TCA-based framework is completely data-driven and enables the characterization of the temporal, spectral, and spatial features of the electrophysiological network connectivity all at once. Tensor decomposition can provide dimension reduction for big data and extract three interacted, low-dimensional patterns representing the high dimensional time-frequency coupling data. Here, we calculated time-frequency domain phase-coupled functional connectivity quantified by wPLI and applied TCA to extract three interacted, low-dimensional descriptions, including a connectivity factor reflecting spatial network pattern, a temporal factor reflecting rapidly temporal evolution of the functional networks, and a spectral factor reflecting frequency modes of networks. By doing so, we identified the temporal dynamics of phase-coupled networks with specific spectral modes, in a completely data-driven way. This enabled us to identify where, when, and in which frequency band significant modulations in connectivity occur. We validated our proposed framework in a simulation (see Appendix) and a simple movement task compared with the permutation test procedure without TCA (see Supplementary material). Furthermore, we demonstrated the utility of our pipeline applied to a complex cognitive task and showed that frequency-specific functional networks transiently form and dissolve to allow participants to complete a 2-back working memory task.

Tensor analysis methods have been well investigated from a theoretical perspective (Cichocki et al., 2015; Kolda and Bader, 2009; Sidiropoulos et al., 2017; Zhou et al., 2015), and applied to a variety of neuroimaging data (Cong et al., 2015; Spyrou et al., 2019; Williams et al., 2018; Zhu et al., 2019a,b). Some studies have applied tensor factorization to sensor-level EEG data and fMRI data most typically to examine differences between subjects in extracted multi-features (Cong et al., 2012, 2013; Kanatsoulis et al., 2019), rather than across functional connectivity. Some recent studies have examined the temporal evolution of functional networks based on TCA across adjacency matrix, subjects, and time, but did not investigate the spectral features, and only studied channel-level EEG connectivity rather than source-reconstructed MEG connectivity networks (Spyrou et al., 2019; Tang et al., 2019). Although TCA was also applied to EEG channel level connectivity over time, frequency and subjects to explore the connectivity patterns within the considered electrodes (Pester et al., 2015), and to ongoing EEG data over temporal sliding windows, frequency, and subjects to link musical features to brain networks (Zhu et al., 2019a,b), we here applied TCA to atlas-based source-level MEG data over network connectivity, time and frequency to explore the formation and dissolution of frequency-dependent functional networks during task performance. The introduced MEG-TCA-network pipeline is able to reliably determine spectral-specific functional networks since functional connectivity is calculated for a set of atlas-based ROIs in anatomical space that covers almost the entire brain, aiding the interpretation of MEG functional network studies, as well as the comparison with other modalities (e.g. fMRI). By establishing a novel link between tensor analysis and frequency specific networks, we found that analysis of the extracted factors can directly identify spatial patterns of functional connectivity with distinct spectral modes as well as reveal temporal dynamics on the timescale of milliseconds.

It should be noted that the temporal courses of the functional networks shown in Figs. 4 and 5 indicate a decrease and increase in connectivity. That is, the peaks refer to the time points when two or more brain areas defining a network are most phase-synchronized. Just because regions involved in networks are not synchronized at particular time points does not mean that these regions are not engaged in the task. This is an important point, as many areas involved in networks are likely to be engaged continuously over the working memory task. In addition, our pipeline has an excellent temporal resolution since we calculated the connectivity at each time point. Fig. 4 demonstrates that a beta-dependent network of brain connections involving primary somatosensory and motor cortices, as well as supplementary motor regions, was successfully identified based upon the finger movement task, which is in agreement with the ICA-based study (O'Neill et al., 2017). This sensorimotor network was modulated significantly by the finger movement. In contrast to the motor areas, which engaged in both movements due to contralateral effects, network connectivity is centered on the right primary somatosensory cortex for left-hand movement (Row I of Fig. 4A), and on the left primary somatosensory cortex for right-hand movement (Row III of Fig. 4A). Another difference of the motor connectivity between right- and left-hand movement is the greater variability in time course of the connectivity across subjects during left-hand movements, since the non-dominant hand was used for the majority of participants. Furthermore, a primary visual network with spectral modes across the theta and alpha bands, modulated by visual cues, was also derived by our pipeline in both left- and right-hand movement. The beta and alpha oscillations engaged in the visual networks were observed. Accumulating evidence has shown that information is sampled periodically at low frequencies (theta: 4–7 Hz and alpha: 8–12 Hz). Specifically, the alpha and theta rhythms seem to coexist in the brain and support different functions (Dugué and VanRullen, 2017; Dugué et al., 2017). If alpha has been related to an ongoing, sensory rhythm, theta appears related to attentional exploration of the visual space (Senoussi et al., 2019). This theta-specific primary visual network was not obvious in the ICA-based study (O'Neill et al., 2017), where the data were filtered into beta bands (13–30 Hz) before calculating connectivity. Thus, the ICA-based study failed to derive the visual network during the movement task (O'Neill et al., 2017). We also validated our pipeline by comparing one of the results from the hand movement (see Fig. S1), with the permutation test procedure (Maris and Oostenveld, 2007). These results validate our proposed pipeline by identifying the sensorimotor connectivity with enhanced beta frequency modes, modulated by movements, and a theta-specific visual network modulated significantly by visual cues.

In the working memory task, the formation of networks including visual and sensorimotor regions with distinct spectral modes is consistent with the presentation of visual stimuli and execution of the motor response (O'Neill et al., 2017; Woodward et al., 2013; Yamashita et al., 2015). A modulation in the theta band was also observed. Numerous studies demonstrated that human theta can be engaged in the working-memory task and the synchronized theta oscillations might be coordinated by working-memory task (Raghavachari et al., 2006). Nodes in the occipital lobe typically include the lateral fusiform gyrus which is specialized for perception of faces (Dima et al., 2018; Elbich et al., 2019). Networks of connectivity from the posterior superior temporal sulcus to both the right occipital face area and the right fusiform face area, with specific beta modes, emerged during the presentation of the face examples, which is in line with a recent study (Elbich et al., 2019). Other frequency-specific networks encompass brain regions that are considered to be important for the higher-order cognition needed for successful completion of the working memory task. Enhanced alpha (8–14 Hz) activity in broad brain areas, including the dorsolateral prefrontal cortex (DLPFC), parietal and occipital regions, and superior temporal cortices, is particularly evident in the majority of these networks. Many studies of the neural oscillatory dynamics serving working memory processing have implicated broad alpha rhythm activity in these brain areas as being essential for task performance (Embury et al., 2019; Heinrichs-Graham and Wilson, 2015). Particularly, the right DLPFC is recruited in network IV connection with the right superior temporal sulcus, which is mainly involved in theta frequency activity. Network VI also shows that the

DLPFC is connecting bilaterally with the inferior superior temporal sulcus in alpha frequency domain. It has been shown that the alpha oscillations in the left and right DLPFC, widely known to play a cognitive and attentional control function in working memory (Barbey et al., 2013; O'Neill et al., 2017), synchronize temporally as a function of time during decoding, maintenance, and retrieval phases (Heinrichs-Graham and Wilson, 2015). Network VI incorporates bilateral inferior temporal gyri regions considered important for semantic processing, which has been referred to as a semantic network (O'Neill et al., 2017). This alpha-specific network was also observed in a previous study, in which the connectivity between the DLPFC and ventral visual regions varied with cognitive load in a working memory task (Barbey et al., 2013; O'Neill et al., 2017; Popov et al., 2018). Another cognitive network VIII with spectral mode peaking in 10 Hz was also identified and termed the language network by other researchers (O'Neill et al., 2017). According to previous studies, working memory is more efficient for social information than for nonsocial information (Thornton and Conway, 2013). Participants could use the strategy of chunking or verbal labeling to enhance working memory performance for social information. Indeed, this left-lateralized network is anchored in the angular gyrus with extensions to the inferior frontal gyrus, inferior temporal gyrus, and a number of nodes spanning the inferior to superior precentral gyrus. These regions are consistent with previous accounts of semantic cognition (O'Neill et al., 2017). Overall, the transient frequency-specific networks elicited by 2-back working memory task are plausible given the previous studies on working memory and sensory processes.

The proposed analysis framework can identify the spectral, temporal, and spatial patterns of the electrophysiological networks that are transient form and dissolve during task performance. In doing so, several key points should be considered while interpreting the results generated by our pipeline. It should be noted that there is significant variability in the temporal courses of frequency-specific connectivity across subjects since temporal resolution is on the timescale of milliseconds; this variance is exhibited in the average time courses across subjects. For example, the low-level visual network is highly synchronized across subjects during the presentation of the image example. Thus, the individual temporal change of this visual network was similar and did not jitter in all subjects, which was demonstrated by the fact that the peak of the average time course would be far greater than the null distributions (gray shaded areas) and the duration of the above null distributions would be very short (thin curve; see Fig. 4 II). The time courses of motor network time-locked button presses fluctuated across subjects; thus, the duration of the above null distributions of the time courses would be long, showing the time-locked temporal change jittered across subjects (see Fig. 4 III). Although relatively poor between-subject reproducibility of MEG connectivity measurements has been demonstrated (Colclough et al., 2016; Wens et al., 2014), our framework still allows detection of the quasi-time-locked temporal change in frequency-specific networks using large cohorts during task performance. In addition, we perform tensor factorization on the time-concatenated three-way tensor form, where the underlying spatial connectivity patterns and the frequency mode are common to all subjects while each subject has its own temporal courses. Then the individual time courses were averaged across subjects to identify components modulated by task. This less-relaxed assumption could discard some components possibly involved in the task due to the inter-subject differences. In other words, the task-modulated temporal patterns of some components would be diminished due to inter-subject variability of the task-induced response. For example, in the movement task, some networks involving the somatomotor cortex with alpha dominant spectrum (see. Fig. S5 IV, XI and XII) show modulations of connectivity which seem to be related to the stimulus despite the temporal courses below the threshold. Future work should therefore seek other strategies to not only consider the inter-subject synchronization but also the inter-subject variability. Actually, this assumption for MEG connectivity study has also been introduced in previous studies (O'Neill et al., 2017; Vidaurre et al., 2018). For example, O'Neill et al. applied ICA to the time-concatenated adjacency matrix calculated by the envelope correlation to character temporal dynamics of networks (O'Neill et al., 2017), where all subjects share common spatial connectivity patterns but have different temporal courses. In fact, the connectivity within several well-known distributed networks is stable even though their temporal variability is significant across subjects. However, the temporal courses of connectivity networks may be similar among subjects when performing the same repeated task. An alternative method is to apply tensor decomposition to a fourth-order tensor with time, frequency, connection, and subject modes, to examine the specificity of subjects (Pester et al., 2015). This will be one of our future study directions.

In addition, we here used the wPLI (phase-based method) as a means of quantifying the connectivity. Since phase reflects the timing of population-level activity, it can be conceptualized as a "functional configuration" or a "functional state" (Cohen, 2014). However, the phase-coupling-based methods might be non-sensitive to the induced synchronization (e.g. beta event-related synchronization in post-movement). The envelopes of band limited oscillations metrics have been proved to detect fluctuations of connectivity during the well-known post-movement beta rebound (Seedat et al., 2020; Tewarie et al., 2019a; Vidaurre et al., 2016). Another limitation is that we only considered the low-frequency coupling (1–48Hz). There is enough evidence that the high frequency rhythms are important to understand transient coherent functioning in the brain in other fields as epilepsy or vision (Jensen et al., 2007; J.-P. Lachaux, Axmacher, Mormann, Halgren and Crone, 2012; J.-P. Lachaux et al., 2005). However, we here only considered the width-band signal since we assume no prior knowledge about which frequency bands are dominant. This would result in failing to extract the high-frequency coupling by tensor decomposition since the low-frequency signal were dominate in the working memory task. It would be better to examine the high-frequency coupling by tensor decomposition separately for those researchers who are interested in the high-frequency activity.

Another consideration in the application of tensor decomposition is the selection of the number of components. Choosing the number of components is not a limitation of our algorithm directly, but rather is a challenging and fundamental problem for all tensor-based methodologies. In this study, we performed an empirical study using a range of numbers of components for tensor models and applied the DIFFIT method to determine the optimal number of components. In addition, we also tried other numbers, showing that varying this parameter in our current work made little difference to the overall results. It should also be noted that the components were retained based on the fact that their temporal dynamics were modulated significantly by the task. However, if a network does not show significant modulation with the task, it does not simply mean that this network is not genuinely representative of connectivity. If the current pipeline is applied for a resting-state study, other techniques should be considered to validate the extracted networks.

5. Conclusion

The characterization of electrophysiological brain networks based on the phase synchronization of spatially separate brain regions, which are transient and dynamic on the timescale of milliseconds, in order to support specific cognitive tasks, is one of the important challenges in cognitive neuroscience. In this paper, we propose a TCA-based pipeline to describe temporal, spectral, and spatial signatures of such dynamic brain networks using MEG data. We applied CP decomposition to a third-order tensor formed by time-frequency domain phase-coupled connectivity, to extract three interacted, low-dimensional descriptions of connectivity data, including a connectivity factor reflecting spatial pattern, a temporal factor reflecting rapidly temporal evolution of the functional networks, and a spectral factor reflecting frequency modes of networks. The proposed framework allows us to identify the temporal dynamics of phase-coupled networks in specific spectral modes in a completely data-driven way. We validated our pipeline in a simulation and a simple

motor task, successfully identifying a beta-specific sensorimotor network during finger movement and a theta-specific visual network modulated by visual cues. We also used the proposed pipeline with a relatively complex task (2-back working memory task) showing transient reconfiguration of electrophysiological brain networks on the timescale of milliseconds. These findings demonstrate that the proposed framework seems valuable in the characterization of electrophysiological brain network connectivity.

Data and code availability

The data used in the manuscript are from the human connectome project (HCP; www.humanconnectome.org). The analysis code will be found in the first author' website soon.

Declaration of competing interest

None of the authors have potential conflicts of interest to be disclosed.

CRediT authorship contribution statement

Yongjie Zhu: Conceptualization, Data curation, Formal analysis, Investigation, Methodology, Visualization, Writing - original draft, Writing - review & editing. **Jia Liu:** Data curation, Formal analysis, Methodology, Writing - review & editing. **Chaoxiong Ye:** Writing - review & editing. **Klaus Mathiak:** Methodology, Writing - review & editing. **Piia Astikainen:** Writing - review & editing. **Tapani Ristaniemi:** Supervision, Conceptualization, Writing - review & editing. **Fengyu Cong:** Supervision, Conceptualization, Funding acquisition, Project administration, Resources, Writing - review & editing.

Acknowledgment

This work was supported by the National Natural Science Foundation of China (Grant No. 91748105&81471742), the Fundamental Research Funds for the Central Universities [DUT2019] in Dalian University of Technology in China, and the scholarship from China Scholarship Council (No. 201600090042; No. 201600090044). Y. Zhu was also supported by the Mobility Grant from the University of Jyvaskyla. We would like to thank the anonymous reviewers for constructive suggestions and comments.

Appendix A. Supplementary data

Supplementary data to this article can be found online at https://doi.org/10.1016/j.neuroimage.2020.116924.

Appendix. Validation by simulation

The validation of our proposed pipeline provided in this manuscript focuses on its application to real MEG dataset. However, our pipeline also has been validated by simulation data. The performance of the wPLI as a measure of connectivity in source level has been addressed well in previous publications (Palva et al., 2018), and we will not examine its performance repeatedly here. However, the ability of tensor factorization (CP decomposition in this paper), applied to connectivity in a time-frequency domain, to explore the temporal, spectral and spatial features of functional networks has not been tested. In the current study, we validated the ability of tensor factorization by performing CP decomposition on a third-order tensor formed by a set of simulated brain networks.

Simulation methods

We firstly used the outer product of three predefined factors, temporal, spectral, and connection factors, to generate a simulated adjacency tensor $\mathcal{Q}_{sim}$ as the ground true connectivity networks. A noise (bandwidth:1–48 Hz) tensor $\mathcal{N}_{sim}$ with same dimensions was added to form a synthetic adjacency tensor $\mathcal{P}_{sim}$. It can be represented by

$$\mathcal{P}_{sim} = \mathcal{Q}_{sim} + \mathcal{N}_{sim} = \sum_{j=1}^{J} \boldsymbol{a}^j_{sim} \circ \boldsymbol{b}^j_{sim} \circ \boldsymbol{c}^j_{sim} + \mathcal{N}_{sim}$$

where $\boldsymbol{a}^j_{sim}$, $\boldsymbol{b}^j_{sim}$ and $\boldsymbol{c}^j_{sim}$ represented connectivity factor, spectral factor and temporal factor of the j-th component. Here, three spatially distinct connectivity patterns were constructed based on a previous study (O'Neill et al., 2017). The spatial factors of connectivity, including visual, sensorimotor, and fronto-parietal networks, were separately represented by an adjacency matrix (see Fig. A1). Their temporal and spectral signatures were demonstrated in Fig. A1. The temporal factors were constructed by 4000 ms of Hanning windows. We set the amplitude to unit length 1, and the full width half maximum to 200 ms, and their onsets were set to 150, 300, and 500 ms. The spectral factors were constructed by filtering white noise with bandwidth centered at 5 Hz, 12 Hz, and 20 Hz. The outer product of temporal factors, spectral factors, and connectivity factors (vectorized adjacency matrices) was performed to adjacency tensor $\mathcal{Q}_{sim}$. The noise tensor $\mathcal{N}_{sim}$ was constructed by source reconstructing recorded empty room MEG data (also provided by HCP) onto a simulated brain geometry. The wPLI was calculated based on the methods described in this paper. Noise tensor $\mathcal{N}_{sim}$ effectively represented connectivity networks of interest.

In order to test the ability of tensor analysis to extract interpretable descriptions including spectral, temporal, and spatial connectivity signatures of brain networks under noise, we tested the performance in the presence of different noise-levels and defined a similarity merit to characterize how well a single component with their three factors represented the simulated temporal, spectral, and spatial connectivity of a network. We also tested the impact of selection of the frequency on the separation in simulation. The bandwidth of noise varies from 1 Hz to B ($B \in [30,\ 100\ Hz]$) with fixed SNR = 0 dB.

Temporal similarity: For each component, we calculated the correlation coefficients between its temporal factor and all the true time courses of the three simulated networks. We thought of the maximum correlation coefficient as the best-matching simulated networks. The temporal similarity was defined as the mean of maximum correlation across all the components.

Spectral similarity: Similar to temporal similarity, we calculated the correlation coefficients between the spectral factor of each component and all the true spectrum of the three simulated networks. The max correlation coefficient was considered as the best matching simulated networks. The

spectral similarity was defined as the mean of this maximum correlation across all the components.

Connected similarity: We also calculated the correlation coefficients between connect factor of each component and all the true adjacency matrices of the three simulated networks. The max correlation coefficient was considered as the best-matching simulated networks. The connected similarity was defined as the mean of this maximum correlation across all the components.

Simulation results

Fig. A1 demonstrates the temporal, spectral, connectivity factors of simulated and reconstructed networks. To test the performance of the CP decomposition, we ran this analysis 20 times under different noise levels, between −35 dB and 25 dB in steps of 2 dB, and calculated the mean of temporal, spectral and connected similarity across runs with varying the signal to noise ratio (SNR) of the simulated data. As expected, the figure of similarity was high at high SNR, meaning that our simulated networks are reconstructed successfully (Fig. A2B). However, a sharp transition below a minimum threshold SNR was observed, at which the similarity merits were very low and simulated networks were unrecoverable. As can be seen, a different threshold value can be found for the temporal, spectral, connectivity factors and they were estimated successfully after −5 dB SNR. Fig. A2. C) demonstrated the similarity merits against bandwidth. As can be seen, the widths of band have little effect on the separation.

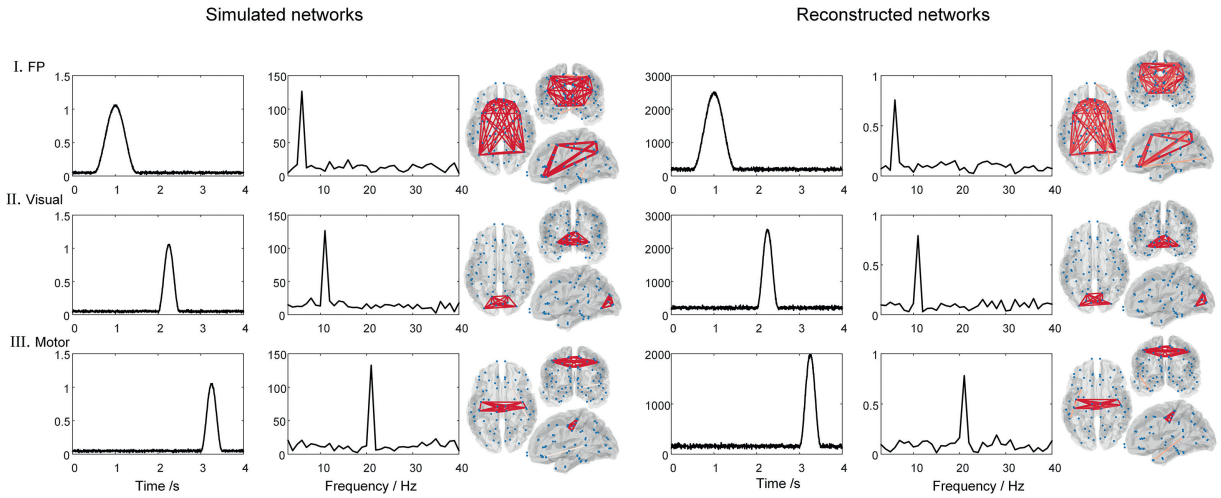

Fig. A1. Simulation results. Left: Simulated networks. Right: Reconstructed networks. Row I: Theta-oscillatory frontoparietal network forming in 1 s after onset. Row II: Alpha-oscillatory visual network forming around 2 s after stimuli onset. Row III: Beta-oscillatory network forming around 3 s after stimuli onset.

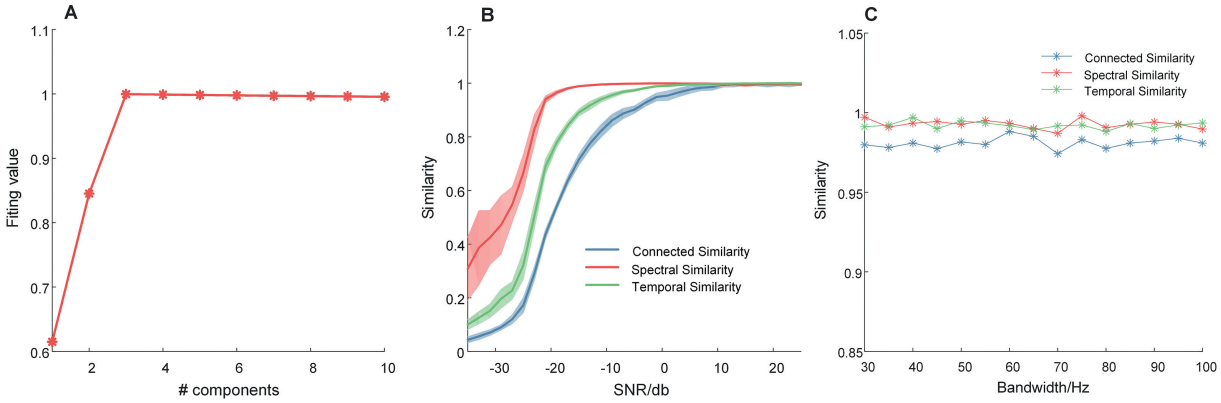

Fig. A2. A) Fit values as number of components. This plot unambiguously reveals J = 3 against the true number of components in the simulated data, in agreement with the ground truth. B) Similarity merits against SNR. As the SNR increases, similarity of three factors becomes higher and higher. After around −5 dB SNR, they can be reconstructed from data with a high accuracy. C) The similarity merits against bandwidth.

References

Al-sharoa, E., Al-khassaweneh, M., Aviyente, S., 2018. Tensor based temporal and multilayer community detection for studying brain dynamics during resting state fMRI. IEEE (Inst. Electr. Electron. Eng.) Trans. Biomed. Eng. 66 (3), 695–709.

Babiloni, F., Cincotti, F., Babiloni, C., Carducci, F., Mattia, D., Astolfi, L., Cheng, J., 2005. Estimation of the cortical functional connectivity with the multimodal integration of high-resolution EEG and fMRI data by directed transfer function. Neuroimage 24 (1), 118–131.

Bader, B.W., Kolda, T.G., 2012. Matlab Tensor Toolbox Version 2.5. Available online, January, 7.

Baker, A.P., Brookes, M.J., Rezek, I.A., Smith, S.M., Behrens, T., Smith, P.J.P., Woolrich, M., 2014. Fast transient networks in spontaneous human brain activity. eLife 3, e01867.

Barbey, A.K., Koenigs, M., Grafman, J., 2013. Dorsolateral prefrontal contributions to human working memory. Cortex 49 (5), 1195–1205. https://doi.org/10.1016/j.cortex.2012.05.022.

Betti, V., Corbetta, M., de Pasquale, F., Wens, V., Della Penna, S., 2018. Topology of functional connectivity and hub dynamics in the beta band as temporal prior for natural vision in the human brain. J. Neurosci. 38 (15), 3858–3871.
Betti, V., Della Penna, S., de Pasquale, F., Mantini, D., Marzetti, L., Romani, G.L., Corbetta, M., 2013. Natural scenes viewing alters the dynamics of functional connectivity in the human brain. Neuron 79 (4), 782–797.
Betzel, R.F., Bassett, D.S., 2017. Multi-scale brain networks. Neuroimage 160, 73–83.
Betzel, R.F., Gu, S., Medaglia, J.D., Pasqualetti, F., Bassett, D.S., 2016. Optimally controlling the human connectome: the role of network topology. Sci. Rep. 6, 30770.
Bola, M., Sabel, B.A., 2015. Dynamic reorganization of brain functional networks during cognition. Neuroimage 114, 398–413.
Brookes, M.J., Liddle, E.B., Hale, J.R., Woolrich, M.W., Luckhoo, H., Liddle, P.F., Morris, P.G., 2012a. Task induced modulation of neural oscillations in electrophysiological brain networks. Neuroimage 63 (4), 1918–1930.
Brookes, M.J., O'Neill, G.C., Hall, E.L., Woolrich, M.W., Baker, A., Corner, S.P., Barnes, G.R., 2014. Measuring temporal, spectral and spatial changes in electrophysiological brain network connectivity. Neuroimage 91, 282–299.
Brookes, M.J., Woolrich, M.W., Barnes, G.R., 2012b. Measuring functional connectivity in MEG: a multivariate approach insensitive to linear source leakage. Neuroimage 63 (2), 910–920.
Buzsáki, G., Draguhn, A., 2004. Neuronal oscillations in cortical networks. Science 304 (5679), 1926–1929.
Cichocki, A., Mandic, D., De Lathauwer, L., Zhou, G., Zhao, Q., Caiafa, C., Phan, H.A., 2015. Tensor decompositions for signal processing applications: from two-way to multiway component analysis. IEEE Signal Process. Mag. 32 (2), 145–163.
Cohen, M.X., 2014. Analyzing Neural Time Series Data: Theory and Practice. MIT press.
Colclough, G.L., Woolrich, M.W., Tewarie, P., Brookes, M.J., Quinn, A.J., Smith, S.M., 2016. How reliable are MEG resting-state connectivity metrics? Neuroimage 138, 284–293.
Cong, F., Lin, Q.-H., Kuang, L.-D., Gong, X.-F., Astikainen, P., Ristaniemi, T., 2015. Tensor decomposition of EEG signals: a brief review. J. Neurosci. Methods 248, 59–69.
Cong, F., Phan, A.H., Astikainen, P., Zhao, Q., Wu, Q., Hietanen, J.K., Cichocki, A., 2013. Multi-domain feature extraction for small event-related potentials through nonnegative multi-way array decomposition from low dense array EEG. Int. J. Neural Syst. 23 (02), 1350006.
Cong, F., Phan, A.H., Zhao, Q., Huttunen-Scott, T., Kaartinen, J., Ristaniemi, T., Cichocki, A., 2012. Benefits of multi-domain feature of mismatch negativity extracted by non-negative tensor factorization from EEG collected by low-density array. Int. J. Neural Syst. 22 (06), 1250025.
de Pasquale, F., Della Penna, S., Snyder, A.Z., Marzetti, L., Pizzella, V., Romani, G.L., Corbetta, M., 2012. A cortical core for dynamic integration of functional networks in the resting human brain. Neuron 74 (4), 753–764.
de Pasquale, F., Della Penna, S., Sporns, O., Romani, G., Corbetta, M., 2016. A dynamic core network and global efficiency in the resting human brain. Cerebr. Cortex 26 (10), 4015–4033.
Desikan, R.S., Ségonne, F., Fischl, B., Quinn, B.T., Dickerson, B.C., Blacker, D., Albert, M.S., 2006. An automated labeling system for subdividing the human cerebral cortex on MRI scans into gyral based regions of interest. Neuroimage 31 (3), 968–980.
Dima, D.C., Perry, G., Messaritaki, E., Zhang, J., Singh, K.D., 2018. Spatiotemporal dynamics in human visual cortex rapidly encode the emotional content of faces. Hum. Brain Mapp. 39 (10), 3993–4006. https://doi.org/10.1002/hbm.24226.
Dugué, L., VanRullen, R., 2017. Transcranial magnetic stimulation reveals intrinsic perceptual and attentional rhythms. Front. Neurosci. 11, 154.
Dugué, L., Xue, A.M., Carrasco, M., 2017. Distinct perceptual rhythms for feature and conjunction searches. J. Vis. 17 (3), 22-22.
Elbich, D.B., Molenaar, P.C., Scherf, K.S., 2019. Evaluating the organizational structure and specificity of network topology within the face processing system. Hum. Brain Mapp. 40 (9), 2581–2595.
Embury, C.M., Wiesman, A.I., Proskovec, A.L., Mills, M.S., Heinrichs-Graham, E., Wang, Y.P., Wilson, T.W., 2019. Neural dynamics of verbal working memory processing in children and adolescents. NeuroImage 185, 191–197.
Engel, A.K., Gerloff, C., Hilgetag, C.C., Nolte, G., 2013. Intrinsic coupling modes: multiscale interactions in ongoing brain activity. Neuron 80 (4), 867–886.
Fries, P., 2005. A mechanism for cognitive dynamics: neuronal communication through neuronal coherence. Trends Cognit. Sci. 9 (10), 474–480.
Fries, P., 2015. Rhythms for cognition: communication through coherence. Neuron 88 (1), 220–235.
Heinrichs-Graham, E., Wilson, T.W., 2015. Spatiotemporal oscillatory dynamics during the encoding and maintenance phases of a visual working memory task. Cortex 69, 121–130. https://doi.org/10.1016/j.cortex.2015.04.022.
Hillebrand, A., Barnes, G.R., Bosboom, J.L., Berendse, H.W., Stam, C.J., 2012. Frequency-dependent functional connectivity within resting-state networks: an atlas-based MEG beamformer solution. Neuroimage 59 (4), 3909–3921.
Hipp, J.F., Hawellek, D.J., Corbetta, M., Siegel, M., Engel, A.K., 2012. Large-scale cortical correlation structure of spontaneous oscillatory activity. Nat. Neurosci. 15 (6), 884.
Hunyadi, B., Dupont, P., Van Paesschen, W., Van Huffel, S., 2017. Tensor decompositions and data fusion in epileptic electroencephalography and functional magnetic resonance imaging data. Wiley Interdiscipl. Rev.: Data Min. Knowl. Discov. 7 (1), e1197.
Jensen, O., Kaiser, J., Lachaux, J.-P., 2007. Human gamma-frequency oscillations associated with attention and memory. Trends Neurosci. 30 (7), 317–324.
Kanatsoulis, C.I., Sidiropoulos, N.D., Akçakaya, M., Fu, X., 2019. Regular sampling of tensor signals: theory and application to fMRI. In: Paper Presented at the ICASSP 2019-2019 IEEE International Conference on Acoustics, Speech and Signal Processing (ICASSP).
Khambhati, A.N., Kahn, A.E., Costantini, J., Ezzyat, Y., Solomon, E.A., Gross, R.E., Seger, S., 2019. Functional control of electrophysiological network architecture using direct neurostimulation in humans. Netw. Neurosci. 3 (3), 848–877.
Kolda, T.G., Bader, B.W., 2009. Tensor decompositions and applications. SIAM Rev. 51 (3), 455–500.
Kopell, N.J., Gritton, H.J., Whittington, M.A., Kramer, M.A., 2014. Beyond the connectome: the dynome. Neuron 83 (6), 1319–1328.
Lachaux, J.-P., Axmacher, N., Mormann, F., Halgren, E., Crone, N.E., 2012. High-frequency neural activity and human cognition: past, present and possible future of intracranial EEG research. Prog. Neurobiol. 98 (3), 279–301.
Lachaux, J.P., George, N., Tallon-Baudry, C., Martinerie, J., Hugueville, L., Minotti, L., Renault, B., 2005. The many faces of the gamma band response to complex visual stimuli. Neuroimage 25 (2), 491–501.
Lachaux, J.P., Rodriguez, E., Martinerie, J., Varela, F.J., 1999. Measuring phase synchrony in brain signals. Hum. Brain Mapp. 8 (4), 194–208.
Larson-Prior, L.J., Oostenveld, R., Della Penna, S., Michalareas, G., Prior, F., Babajani-Feremi, A., Stout, J., 2013. Adding dynamics to the Human Connectome Project with MEG. Neuroimage 80, 190–201.
Lin, F.H., Belliveau, J.W., Dale, A.M., Hämäläinen, M.S., 2006. Distributed current estimates using cortical orientation constraints. Hum. Brain Mapp. 27 (1), 1–13.
Liu, Y., Moser, J., Aviyente, S., 2014. Network community structure detection for directional neural networks inferred from multichannel multisubject EEG data. IEEE (Inst. Electr. Electron. Eng.) Trans. Biomed. Eng. 61 (7), 1919–1930.
Mackevicius, E.L., Bahle, A.H., Williams, A.H., Gu, S., Denisenko, N.I., Goldman, M.S., Fee, M.S., 2019. Unsupervised discovery of temporal sequences in high-dimensional datasets, with applications to neuroscience. eLife 8, e38471.
Mahyari, A.G., Aviyente, S., 2014. Identification of dynamic functional brain network states through tensor decomposition. In: Paper Presented at the 2014 IEEE International Conference on Acoustics, Speech and Signal Processing (ICASSP).
Mahyari, A.G., Zoltowski, D.M., Bernat, E.M., Aviyente, S., 2016. A tensor decomposition-based approach for detecting dynamic network states from EEG. IEEE (Inst. Electr. Electron. Eng.) Trans. Biomed. Eng. 64 (1), 225–237.
Maris, E., Oostenveld, R., 2007. Nonparametric statistical testing of EEG-and MEG-data. J. Neurosci. Methods 164 (1), 177–190.
Mørup, M., Hansen, L.K., 2009. Automatic relevance determination for multi-way models. J. Chemometr.: J. Chemometr. Soc. 23 (7-8), 352–363.
Mørup, M., Hansen, L.K., Herrmann, C.S., Parnas, J., Arnfred, S.M., 2006. Parallel factor analysis as an exploratory tool for wavelet transformed event-related EEG. Neuroimage 29 (3), 938–947.
O'Neill, G.C., Tewarie, P., Vidaurre, D., Liuzzi, L., Woolrich, M.W., Brookes, M.J., 2018. Dynamics of large-scale electrophysiological networks: a technical review. Neuroimage 180, 559–576.
O'Neill, G.C., Barratt, E.L., Hunt, B.A., Tewarie, P.K., Brookes, M.J., 2015. Measuring electrophysiological connectivity by power envelope correlation: a technical review on MEG methods. Phys. Med. Biol. 60 (21), R271.
O'Neill, G.C., Tewarie, P.K., Colclough, G.L., Gascoyne, L.E., Hunt, B.A., Morris, P.G., Brookes, M.J., 2017. Measurement of dynamic task related functional networks using MEG. NeuroImage 146, 667–678.
Oldfield, R.C., 1971. The assessment and analysis of handedness: the Edinburgh inventory. Neuropsychologia 9 (1), 97–113.
Ozdemir, A., Bernat, E.M., Aviyente, S., 2017. Recursive tensor subspace tracking for dynamic brain network analysis. IEEE Trans. Signal Inf. Process. Netw. 3 (4), 669–682.
Palva, J.M., Wang, S.H., Palva, S., Zhigalov, A., Monto, S., Brookes, M.J., Jerbi, K., 2018. Ghost interactions in MEG/EEG source space: a note of caution on inter-areal coupling measures. Neuroimage 173, 632–643.
Pester, B., Ligges, C., Leistritz, L., Witte, H., Schiecke, K., 2015. Advanced insights into functional brain connectivity by combining tensor decomposition and partial directed coherence. PloS One 10 (6).
Popov, T., Jensen, O., Schoffelen, J.M., 2018. Dorsal and ventral cortices are coupled by cross-frequency interactions during working memory. Neuroimage 178, 277–286. https://doi.org/10.1016/j.neuroimage.2018.05.054.
Quinn, A.J., Vidaurre, D., Abeysuriya, R., Becker, R., Nobre, A.C., Woolrich, M.W., 2018. Task-evoked dynamic network analysis through hidden markov modeling. Front. Neurosci. 12, 603.
Raghavachari, S., Lisman, J.E., Tully, M., Madsen, J.R., Bromfield, E., Kahana, M.J., 2006. Theta oscillations in human cortex during a working-memory task: evidence for local generators. J. Neurophysiol. 95 (3), 1630–1638.
Salinas, E., Sejnowski, T.J., 2001. Correlated neuronal activity and the flow of neural information. Nat. Rev. Neurosci. 2 (8), 539.
Samdin, S.B., Ting, C.-M., Ombao, H., Salleh, S.-H., 2016. A unified estimation framework for state-related changes in effective brain connectivity. IEEE (Inst. Electr. Electron. Eng.) Trans. Biomed. Eng. 64 (4), 844–858.
Schölvinck, M.L., Leopold, D.A., Brookes, M.J., Khader, P.H., 2013. The contribution of electrophysiology to functional connectivity mapping. Neuroimage 80, 297–306.
Seedat, Z.A., Quinn, A., Vidaurre, D., Liuzzi, L., Gascoyne, L.E., Hunt, B.A., Woolrich, M.W., 2020. The role of transient spectral 'bursts' in functional connectivity: A magnetoencephalography study. NeuroImage, 116537.
Senoussi, M., Moreland, J.C., Busch, N.A., Dugué, L., 2019. Attention explores space periodically at the theta frequency. J. Vis. 19 (5), 22-22.
Sidiropoulos, N.D., De Lathauwer, L., Fu, X., Huang, K., Papalexakis, E.E., Faloutsos, C., 2017. Tensor decomposition for signal processing and machine learning. IEEE Trans. Signal Process. 65 (13), 3551–3582.
Siegel, M., Donner, T.H., Engel, A.K., 2012. Spectral fingerprints of large-scale neuronal interactions. Nat. Rev. Neurosci. 13 (2), 121.

Spyrou, L., Parra, M., Escudero, J., 2019. Complex tensor factorization with PARAFAC2 for the estimation of brain connectivity from the EEG. IEEE Trans. Neural Syst. Rehabil. Eng. 27 (1), 1–12.
Tang, M., Lu, Y., Yang, L., 2019. Temporal-spatial patterns in dynamic functional brain network for self-paced hand movement. IEEE Trans. Neural Syst. Rehabil. Eng. 27 (4), 643–651.
Tewarie, P., Hunt, B.A., O'Neill, G.C., Byrne, A., Aquino, K., Bauer, M., Brookes, M.J., 2019a. Relationships between neuronal oscillatory amplitude and dynamic functional connectivity. Cerebr. Cortex 29 (6), 2668–2681.
Tewarie, P., Liuzzi, L., O'Neill, G.C., Quinn, A.J., Griffa, A., Woolrich, M.W., Brookes, M.J., 2019b. Tracking dynamic brain networks using high temporal resolution MEG measures of functional connectivity. Neuroimage 200, 38–50.
Thornton, M.A., Conway, A.R., 2013. Working memory for social information: chunking or domain-specific buffer? Neuroimage 70, 233–239.
Timmerman, M.E., Kiers, H.A., 2000. Three-mode principal components analysis: choosing the numbers of components and sensitivity to local optima. Br. J. Math. Stat. Psychol. 53 (1), 1–16.
Varela, F., Lachaux, J.-P., Rodriguez, E., Martinerie, J., 2001. The brainweb: phase synchronization and large-scale integration. Nat. Rev. Neurosci. 2 (4), 229.
Vervliet, N., Debals, O., De Lathauwer, L., 2016. Tensorlab 3.0—numerical optimization strategies for large-scale constrained and coupled matrix/tensor factorization. In: Paper Presented at the 2016 50th Asilomar Conference on Signals, Systems and Computers.
Vidaurre, D., Hunt, L.T., Quinn, A.J., Hunt, B.A., Brookes, M.J., Nobre, A.C., Woolrich, M.W., 2018. Spontaneous cortical activity transiently organises into frequency specific phase-coupling networks. Nat. Commun. 9 (1), 2987.
Vidaurre, D., Quinn, A.J., Baker, A.P., Dupret, D., Tejero-Cantero, A., Woolrich, M.W., 2016. Spectrally resolved fast transient brain states in electrophysiological data. Neuroimage 126, 81–95.
Vidaurre, D., Smith, S.M., Woolrich, M.W., 2017. Brain network dynamics are hierarchically organized in time. Proc. Natl. Acad. Sci. Unit. States Am. 114 (48), 12827–12832.
Vinck, M., Oostenveld, R., Van Wingerden, M., Battaglia, F., Pennartz, C.M., 2011. An improved index of phase-synchronization for electrophysiological data in the presence of volume-conduction, noise and sample-size bias. Neuroimage 55 (4), 1548–1565.
Wang, D., Zhu, Y., Ristaniemi, T., Cong, F., 2018. Extracting multi-mode ERP features using fifth-order nonnegative tensor decomposition. J. Neurosci. Methods 308, 240–247.
Wens, V., Bourguignon, M., Goldman, S., Marty, B., De Beeck, M.O., Clumeck, C., De Tiege, X., 2014. Inter-and intra-subject variability of neuromagnetic resting state networks. Brain topogr. 27 (5), 620–634.
Williams, A.H., Kim, T.H., Wang, F., Vyas, S., Ryu, S.I., Shenoy, K.V., Ganguli, S., 2018. Unsupervised discovery of demixed, low-dimensional neural dynamics across multiple timescales through tensor component analysis. Neuron 98 (6), 1099–1115.
Winkler, A.M., Ridgway, G.R., Webster, M.A., Smith, S.M., Nichols, T.E., 2014. Permutation inference for the general linear model. Neuroimage 92, 381–397.
Woodward, T.S., Feredoes, E., Metzak, P.D., Takane, Y., Manoach, D.S., 2013. Epoch-specific functional networks involved in working memory. Neuroimage 65, 529–539.
Yamashita, M., Kawato, M., Imamizu, H., 2015. Predicting learning plateau of working memory from whole-brain intrinsic network connectivity patterns. Sci. Rep. 5, 7622.
Zhou, G., Cichocki, A., 2012. Canonical polyadic decomposition based on a single mode blind source separation. IEEE Signal Process. Lett. 19 (8), 523–526.
Zhou, G., Cichocki, A., Zhao, Q., Xie, S., 2015. Efficient nonnegative tucker decompositions: algorithms and uniqueness. IEEE Trans. Image Process. 24 (12), 4990–5003.
Zhou, G., Zhao, Q., Zhang, Y., Adalı, T., Xie, S., Cichocki, A., 2016. Linked component analysis from matrices to high-order tensors: applications to biomedical data. Proc. IEEE 104 (2), 310–331.
Zhu, Y., Li, X., Ristaniemi, T., Cong, F., 2019a. Measuring the task induced oscillatory brain activity using tensor decomposition. In: Paper Presented at the ICASSP 2019-2019 IEEE International Conference on Acoustics, Speech and Signal Processing (ICASSP). IEEE, pp. 8593–8597.
Zhu, Y., Liu, J., Mathiak, K., Ristaniemi, T., Cong, F., 2019b. Deriving electrophysiological brain network connectivity via tensor component analysis during freely listening to music. IEEE Trans. Neural Syst. Rehabil. Eng. 28 (2), 409–418.

V

DERIVING ELECTROPHYSIOLOGICAL BRAIN NETWORK CONNECTIVITY VIA TENSOR COMPONENT ANALYSIS DURING FREELY LISTENING TO MUSIC

by

Yongjie Zhu, Jia Liu, Klaus Mathiak, Tapani Ristaniemi & Fengyu Cong 2019

IEEE Transactions on Neural Systems and Rehabilitation Engineering, 28(2), 409-418

DOI: https://doi.org/10.1109/TNSRE.2019.2953971

Deriving Electrophysiological Brain Network Connectivity via Tensor Component Analysis During Freely Listening to Music

Yongjie Zhu, *Student Member, IEEE*, Jia Liu, *Student Member, IEEE*, Klaus Mathiak, Tapani Ristaniemi, *Senior Member, IEEE*, and Fengyu Cong, *Senior Member, IEEE*

***Abstract*— Recent studies show that the dynamics of electrophysiological functional connectivity is attracting more and more interest since it is considered as a better representation of functional brain networks than static network analysis. It is believed that the dynamic electrophysiological brain networks with specific frequency modes, transiently form and dissolve to support ongoing cognitive function during continuous task performance. Here, we propose a novel method based on tensor component analysis (TCA), to characterize the spatial, temporal, and spectral signatures of dynamic electrophysiological brain networks in electroencephalography (EEG) data recorded during free music-listening. A three-way tensor containing time-frequency phase-coupling between pairs of parcellated brain regions is constructed. Nonnegative CANDECOMP/PARAFAC (CP) decomposition is then applied to extract three interconnected, low-dimensional descriptions of data including temporal, spectral, and spatial connection factors. Musical features are also extracted from stimuli using acoustic feature extraction. Correlation analysis is then conducted between temporal courses of musical features and TCA components to examine the modulation of brain patterns. We derive several brain networks with distinct spectral modes (described by TCA components) significantly modulated by musical features, including higher-order cognitive, sensorimotor, and auditory networks. The results demonstrate that brain networks during music listening in EEG are well characterized by TCA components, with spatial patterns of oscillatory phase-synchronization in specific spectral modes. The proposed method provides evidence for the time-frequency dynamics of brain networks during free music listening through TCA, which allows us to better understand the reorganization of electrophysiological networks.**

***Index Terms*— Tensor decomposition, frequency-specific brain connectivity, freely listening to music, oscillatory coherence, electroencephalography (EEG).**

Manuscript received August 29, 2019; revised November 5, 2019; accepted November 13, 2019. Date of publication December 18, 2019; date of current version February 12, 2020. This work was supported in part by the National Natural Science Foundation of China under Grant 91748105 and Grant 81471742, in part by the Fundamental Research Funds for the Central Universities under Grant DUT2019, in part by the Dalian University of Technology in China, and in part by the Scholarship from China Scholarship Council under Grant 201600090042 and Grant 201600090044. The work of Y. Zhu was supported by the Mobility Grant from the University of Jyväskylä. *(Corresponding author: Fengyu Cong.)*

Y. Zhu is with the School of Biomedical Engineering, Faculty of Electronic Information and Electrical Engineering, Dalian University of Technology, Dalian 116024, China, with the Faculty of Information Technology, University of Jyväskylä, 40014 Jyväskylä, Finland, and also with the Department of Psychiatry, Psychotherapy and Psychosomatics, Medical Faculty, RWTH Aachen University, 52074 Aachen, Germany.

J. Liu and F. Cong are with the School of Biomedical Engineering, Faculty of Electronic Information and Electrical Engineering, Dalian University of Technology, Dalian 116024, China, and also with the Faculty of Information Technology, University of Jyväskylä, 40014 Jyväskylä, Finland (e-mail: cong@dlut.edu.cn).

K. Mathiak is with the Department of Psychiatry, Psychotherapy and Psychosomatics, Medical Faculty, RWTH Aachen University, 52074 Aachen, Germany.

T. Ristaniemi is with the Faculty of Information Technology, University of Jyväskylä, 40014 Jyväskylä, Finland.

Digital Object Identifier 10.1109/TNSRE.2019.2953971

I. Introduction

THE electrophysiological network, characterized by neuronal synchronization between spatially separate brain regions, plays an important role in the human cognition [1], [2]. Such neuronal-synchronized networks are transient and dynamic, established on the specific frequency modes in order to support ongoing cognitive operations [3]–[7]. The characterization of the functional networks during resting state, referred to as resting-state brain networks (RSNs), has been widely studied during past few decades [8]–[10]. Recently, growing interest has been directed to probing the reorganization of brain functional networks during naturalistic stimuli [11]–[13] and a strong relationship between the functional networks during resting state and continuous task performance has been demonstrated [14], [15]. For example, Alavash and colleagues found that functional networks in challenging listening situations showed higher segregation of temporal auditory, ventral attention, and frontal control regions, compared to resting state [13]. Alluri et al. explored the neural correlates of music features processing as it occurs in a realistic or naturalistic environment [16], [17]. However, those functional connectivity studies have been based on functional magnetic resonance imaging (fMRI), which is indirect assessments of brain activity. Actually, little is known about how oscillatory basis is involved in the brain network activity during music listening. In this paper, we develop a tensor-based method which allows us to characterize the spatial, temporal, and spectral signatures of electrophysiological brain network connectivity using electroencephalography (EEG) recorded during freely listening to music.

Tensor component analysis (TCA), as a well-established tool for signal processing and machine learning [18]–[20],

has shown to be powerful for neuroimaging data processing and analysis in cognitive neuroscience [21]–[26]. A tensor is a multi-dimensional representation of data or a multi-way array. Each dimension in the tensor is called a way or mode. For a matrix, a two-way array, matrix decomposition (e.g., independent component analysis, ICA) can be used for data processing. Analogously, for a tensor, tensor decomposition (or TCA) is able to be applied as well. TCA can reveal the true underlying structure of multi-way data and explore the interactions among multiple modes. For instance, TCA-based methods have been successfully applied to EEG data which is in general represented in time, frequency, and space [23]. In fMRI studies, the tensor modes could correspond to voxels, time, and patients [27]. In neurophysiological studies, the different modes could span neurons, time, and trials [28]. TCA can unsupervised uncover the main features of the neuroimaging data and extract low-dimensional descriptions of the big data. Several TCA-based modes have been used for decomposition and extraction of multi-way representation of data. The CANDECOMP/PARAFAC (CP) [29] is one of the fundamental models for tensor decomposition, which is a generalization of singular value decomposition (SVD) to higher-order tensor. TCA with CP model decomposes the multi-dimensional data into sum of rank-1 tensors of lower dimensions. Therefore, it can be applied to extract multi-interconnected and low-dimensional descriptions of original data. For example, performing TCA to the time-frequency transformed multi-channel EEG tensor, three interacted low-dimensional descriptions of data are extracted, including temporal factor representing temporal evolution of the oscillatory source, spectral factor representing oscillatory frequency, and the spatial factor representing location of the oscillatory source [30]. It should be noted that time-frequency representation of EEG data is usually nonnegative and CP decomposition with nonnegative constraints is adopted. Previous TCA-based studies of brain connectivity mainly focused on the aim of detection of change points [31]–[34] and spatial-temporal properties of the network community [35]–[37]. The spectral mode of brain networks was not considered especially for the fMRI neuroimaging data. Thus, these studies failed to examine the underling spectral mode of oscillatory networks. However, dynamics of large-scale networks during task performance have been shown to fluctuate across different frequency bands [6], [38]. For example, using magnetoencephalography (MEG), self-peace motor task studies demonstrated that the motor networks measured by the correlation of band-limited power is dominant in beta band [38], [39]. Further, few studies have attempted to explore spectral patterns of the brain functional connectivity during continuous task performance.

In this paper, we examined the spatio-temporal-spectral modes of covariation among separate regions in the listening brain. We recorded the EEG data during freely listening to music. Source-level data was obtained by source localization based on minimum-norm estimate. We then computed the time-frequency domain connectivity between all pairs of separate brain regions predefined though cortical parcellation, based on a sliding window technique. We used the weighted phase lag index (wPLI) as a metric to quantify the brain connectivity since it is insensitive to signal leakage and similar bias effects [40], [41]. We were able to obtain an adjacency matrix for each time window and frequency point. We reshaped the upper triangular parts of adjacency matrix into a vector. We then constructed a three-way tensor containing time, frequency, and connectivity modes for each subject. We performed CP decomposition on the temporal-concatenated adjacency tensor for multi-subjects. It should be noted that it is distinct from our previous study [5], where CP decomposition was applied to time-frequency representations of source-level EEG data. In the present study, we extracted low-dimensional, spatio-temporal-spectral modes of covariation including connectivity factor reflecting network community, temporal factors reflecting temporal evolution of functional networks and the spectral factors reflecting spectral features of networks. Time series of five long-term acoustic feature were extracted from the audio stimuli by music information retrieval techniques used in previous studies [17], [42]. Finally, we analyzed the correlation between temporal courses and the musical feature time series to identify frequency-specific brain networks modulated by musical features.

II. Material and Methods

A. Data Description

We used EEG data of 14 right-hand adults aged 20 to 46 years old. None of them reported hearing loss or history of neurological disease. No participants had musical expertise. This study was approved by the local ethics committee. During the experiment, participants were presented with a music played through audio headphones. This music was a 512 s long musical clips of modern tango, which had suitable duration for the experimental setting due to its high range of fluctuation in several musical features [17]. EEG data were recorded at a sampling rate of 2048 Hz with BioSemi electrode caps of 64-channels while participants were freely listening to musical clip.

Here, we examined five acoustic features including tonal and rhythmic features. They were extracted by applying a frame-by-frame analysis technique [17], [42]. The length of each frame was set as 3 seconds and the overlap between adjacent frames was set as 2 seconds. Thus, one temporal course with 510 samples was created for each musical feature with a sampling rate of 1 Hz. The five acoustic features consist of two tonal musical feature, Mode and Key Clarity, and three rhythmic features, including Fluctuation Centroid, Fluctuation Entropy and Pulse Clarity. Mode denotes the strength of major or minor mode. Key Clarity represents the measure of the tonal clarity. Fluctuation Centroid is defined as the geometric mean of the fluctuation spectrum, indicating the global repartition of rhythm periodicities within the range of 0–10Hz [17]. Fluctuation entropy is the Shannon entropy of the fluctuation spectrum, representing the global repartition of rhythm periodicities. Pulse Clarity naturally estimates the clarity of the pulse.

B. Preprocessing and Source Reconstruction

We re-referenced EEG data using common average electrodes. We visually inspected for rejecting artifacts and bad

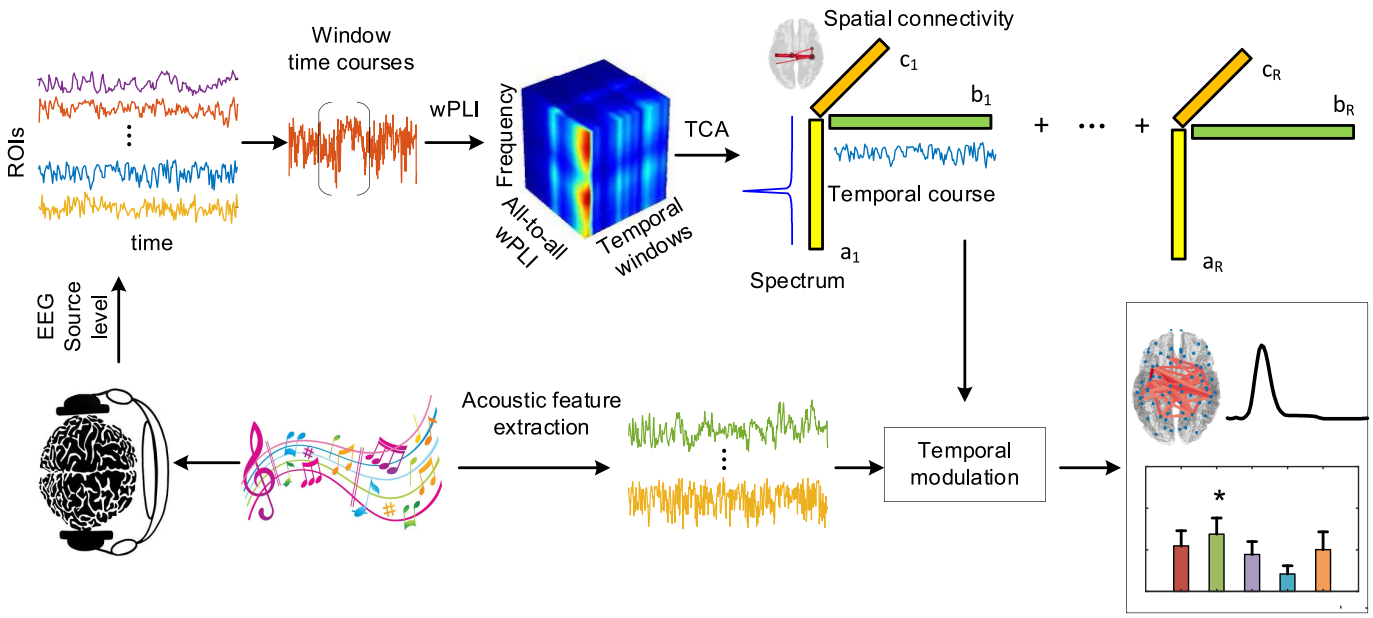

Fig. 1. Analysis pipeline. EEG data were recorded during freely listening to music. Source-reconstructed data were divided into 68 ROIs based on anatomical brain regions. Each windowed signal was transformed with a Morlet wavelet and wPLI was calculated between all pairs of ROIs. For each time window and frequency-point, an adjacent matrix was thus obtained. Then a three-way tensor was formed including spectral mode, temporal mode, and spatial connectivity mode (vectorized using upper triangular parts of an adjacent matrix). Nonnegative CP decomposition was applied to the temporally concatenated tensor across subjects. On the other hand, musical features were extracted using acoustic feature extraction. The temporal courses of decomposed components and musical feature time series were analyzed to examine the modulated brain networks.

channels were interpolated with mean value of their spherical adjacent channels. A 50 Hz notch filter was applied to remove powerline interference. High-pass and low-pass filters with 2 Hz and 35 Hz cutoff were then used since our previous investigation of the frequency range uncovered that no useful information was observed in higher frequencies [12], [42]. The data were finally down-sampled to 256 Hz. Independent component analysis (ICA) was performed on individual EEG data to remove EOG (e.g. eye blinks) [43]. A schematic of the subsequent data processing is demonstrated in Fig. 1. Following data preprocessing, the forward model and inverse model were computed using a MATLAB toolbox Brainstorm [44]. The symmetric boundary element method (BEM) was used to calculate the forward model with a default MNI MRI template (Colin 27). To solve the inverse model, weighted minimum-norm estimate (wMNE) [45] was applied, which is well-suited for estimation for brain connectivity since it takes the volume conduction into consideration and reduces single leakage [3]. The source orientations were constrained to be normal to the brain cortical surface when calculating the inverse problem. Then, the cortical surface was parcellated into 68 anatomical regions based on the Desikan-Killiany Atlas (DKA) [46]. In order to obtain a representative time series for every region, the center of mass of each region was defined as seed voxel and used as a single representative location. Thus, for each subject, a source-level data matrix $\mathbf{P}$ was created with dimension $n_n \times n_s$, where $n_n = 68$ represents the number of anatomical regions and n_s represents the number of samples.

C. Dynamic Functional Connectivity Estimation

We attempt to examine the time-frequency dynamics of brain functional connectivity. This means that we require estimating connectivity between all pairs of DKA regions, as a function of time and frequency using a sliding-window technique [47], [48]. Firstly, source space data matrix $\mathbf{P}$ was segmented by overlapping time window. A single window data is denoted as $\boldsymbol{P}_w$ with dimensions $n_n \times f\tau$. Here, w represents window number, τ denotes the window length in seconds and f is sampling frequency. Hamming-window with $\tau = 3s$ and 2 s overlap of adjacent windows were set, resulting in a sampling rate of 1 Hz in temporal dimension. This sampling rate was in line with musical feature time series.

To calculate phase-coupling between all pairs of regions in frequency domain, spectral densities should be estimated. We applied continuous wavelet transform with Morlet wavelets to the segmented data $\boldsymbol{P}_w$. The Morlet wavelet contained 3 cycles at the lowest frequency (2 Hz) and the number of cycles was increasing up to 12 cycles at the highest frequency (35 Hz). This resulted in 42 linearly spaced frequency points. A four-way tensor was thus obtained with dimensions $n_n \times n_m \times n_f \times n_w$, where $n_w = 512$ denotes the number of windows, $n_f = 42$ is the number of frequency point and $n_m = f\tau$ is the number of samples in a single window.

Weighted phase lag index (wPLI) is defined as the sign of the phase difference between two signals weighted by the magnitude of the imaginary component of the cross-spectrum [41]. It is computed as

$$wPLI_{(f,w)} = \frac{\left|\sum_{t=1}^{f\tau} im\left(S_1^w(f,t)\, S_2^{w*}(f,t)\right)\right|}{\sum_{t=1}^{f\tau}\left|im\left(S_1^w(f,t)\, S_2^{w*}(f,t)\right)\right|}, \quad (1)$$

where $S_1^w(f,t)$ and $S_2^w(f,t)$ are wavelet-decomposed time-frequency representations from DKA region 1 and region 2 respectively, and segmentation w. $*$ means the complex

conjugate, $im(\quad)$ represents the imaginary part of a complex value, $|\quad|$ is an absolute value operation. Note that wPLI here descripts the degree of phase synchronization between regions in a period of time ($\tau = 3\ s$). After calculation of wPLI, for each subject, a three-way tensor containing connections $\boldsymbol{Q}$ was generated with dimensions $n_c \times n_w \times n_f$, where $n_c = 2278$ is the number of pairs of regions $(68*(68-1)/2)$. Finally, these three-way tensors $\boldsymbol{Q}$ were temporally concatenated across subjects, resulting in a group-level tensor $\boldsymbol{\mathcal{X}}$ with dimensions $n_c \times n_w n_p \times n_f$, where n_p is the number of subjects.

D. Learning Underlying Brain Networks via Tensor Decomposition

CP model, as a fundamental model for TCA, decomposes a tensor into multiple components through a high-order singular value decomposition. It has found many applications in several fields, especially for signal processing and machine learning [18], [19]. Given a three-way tensor $\boldsymbol{\mathcal{X}} \in \mathbb{R}_+^{n_c \times n_t \times n_f}$ from constructed tensor containing connectivity, a rank-R nonnegative CP mode factorizes $\boldsymbol{\mathcal{X}}$ into R components, each of which contains a rank-1 tensor produced by the outer-product of 3 column vectors. It is generally solved through the following minimization problem with Frobenius norm of the error:

$$\min_{A,B,C} \frac{1}{2} \left\| \boldsymbol{\mathcal{X}} - \sum_{r=1}^{R} \mathbf{A}_r \otimes \mathbf{B}_r \otimes \mathbf{C}_r \right\|_F^2, \tag{2}$$

where $\boldsymbol{A} = [\boldsymbol{a}_1, \boldsymbol{a}_2, \cdots, \boldsymbol{a}_R]$, $\boldsymbol{B} = [\boldsymbol{b}_1, \boldsymbol{b}_2, \cdots, \boldsymbol{b}_R]$, and $\boldsymbol{C} = [\boldsymbol{c}_1, \boldsymbol{c}_2, \cdots, \boldsymbol{c}_R]$ are called loading matrices or factor matrices. Here, those loading matrices represent connectivity factor matrix, spectral factor matrix, and temporal factor matrix respectively. $\|\quad\|_F$ represents Frobenius norm. $\otimes$ means Kruskal operator. The estimated loading matrices with Kruskal operator form can be written as the sum of R rank-1 tensors with outer-product of column vectors form:

$$\sum_{r=1}^{R} \boldsymbol{A}_r \otimes \boldsymbol{B}_r \otimes \boldsymbol{C}_r = \sum_{r=1}^{R} \boldsymbol{a}_r \circ \boldsymbol{b}_r \circ \boldsymbol{c}_r, \tag{3}$$

where, $\boldsymbol{a}_r, \boldsymbol{b}_r$, and $\boldsymbol{c}_r$ character the spatio-temporal-spectral property of underling brain pattern. $\boldsymbol{a}_r$ can be considered as spatial topology of brain network pattern and $\boldsymbol{b}_r$ can be thought of as spectral mode of brain network pattern across oscillatory frequency. These spatial topology factors and spectral factors form structure that is common across time, which can be termed as frequency-specific brain network connectivity. The last set of factors $\boldsymbol{c}_r$ represent temporal factors of the underling brain pattern, which describes the temporal dynamic of such frequency-specific brain network connectivity. Since values of wPLI are nonnegative, we add a nonnegative constraint to Eq. (2), $\boldsymbol{a}_r \geq 0, \boldsymbol{b}_r \geq 0, \boldsymbol{c}_r \geq 0$.

There are many optimization algorithms for CP decomposition with nonnegative constraint, such as multiplicative updating (MU) method, alternating least squares (ALS) and hierarchical alternating least squares (HALS) [49]. Here, we apply ALS due to its good performance and fast speed on convergence. The ALS algorithm applies a gradient descent method to solve the minimization problem in Eq (2) iteratively. At each iteration, one factor matrix is updated while other two matrices are fixed. For brief illustration, consider estimating spatial topology matrix $\boldsymbol{A}$, fixing spectral factor matrix $\boldsymbol{B}$, and temporal matrix $\boldsymbol{C}$, which resulting in the following update rule:

$$\boldsymbol{A} \leftarrow \arg\min_{A} \frac{1}{2} \left\| \boldsymbol{\mathcal{X}} - \sum_{r=1}^{R} \boldsymbol{a}_r \circ \boldsymbol{b}_r \circ \boldsymbol{c}_r \right\|_F^2. \tag{4}$$

It can be estimated as a linear least-squares problem and has a closed-form solution. The solution of CP model using ALS algorithm is available in many open source toolboxes [50], [51].

E. Selection of Component Number

All TCA-based method for learning hidden data structures require determining the number of components either manually or via criteria such as DIFFIT method [52] and CORCONDIA method [53]. Indeed, DIFFIT and CORCONDIA measure the change of the data fitting (i.e. explained variance of the original data) and the core tensor of the decomposition among a number of models, respectively. It should be noted that the number of components R can be chose with a larger number than the minimization of each model size, which is not restricted by the size in each mode since the rank of tensor can be even larger than the max of each model size [29]. Here for simplicity, we use DIFFIT method to choose the number of components. DIFFIT, the difference in data fitting, is computed based on model reconstruction error and the explained variance of data [52], [54]. Let component number $R \in [1, \mathcal{R}]$, where $\mathcal{R}$ is the empirically maximal number of latent components. The data fit can be obtained as

$$Fit\,(R) = 1 - \frac{\left\| \boldsymbol{\mathcal{X}} - \sum_{r=1}^{R} \boldsymbol{a}_j \circ \boldsymbol{b}_j \circ \boldsymbol{c}_j \right\|_F}{\|\boldsymbol{\mathcal{X}}\|_F}. \tag{5}$$

Unlike PCA, the estimation of TCA may have local minima (suboptimal solution), and not guarantee that optimization routines will converge to the global optimal solution. Thus, we run ALS optimization procedure at each component number R 20 times from random initial conditions. We then average data fits across many runs, resulting in averaged data fit $\overline{Fit}(J)$. The change fit of two adjacent data fit is

$$DIF\,(R) = \overline{Fit}(R) - \overline{Fit}\,(R-1)\,. \tag{6}$$

Next, the ratio of the adjacent difference fits is defined as

$$DIFFIT\,(R) = \frac{DIF\,(R)}{DIF\,(R+1)}. \tag{7}$$

Generally, the candidate model $\tilde{R}$ with largest *DIFFIT* value is thought of as the appropriate model order of TCA for original tensor.

F. Modulation of Temporal Evolution by Musical Features

How does music modulate frequency-specific brain networks during real-world? We address this question for each

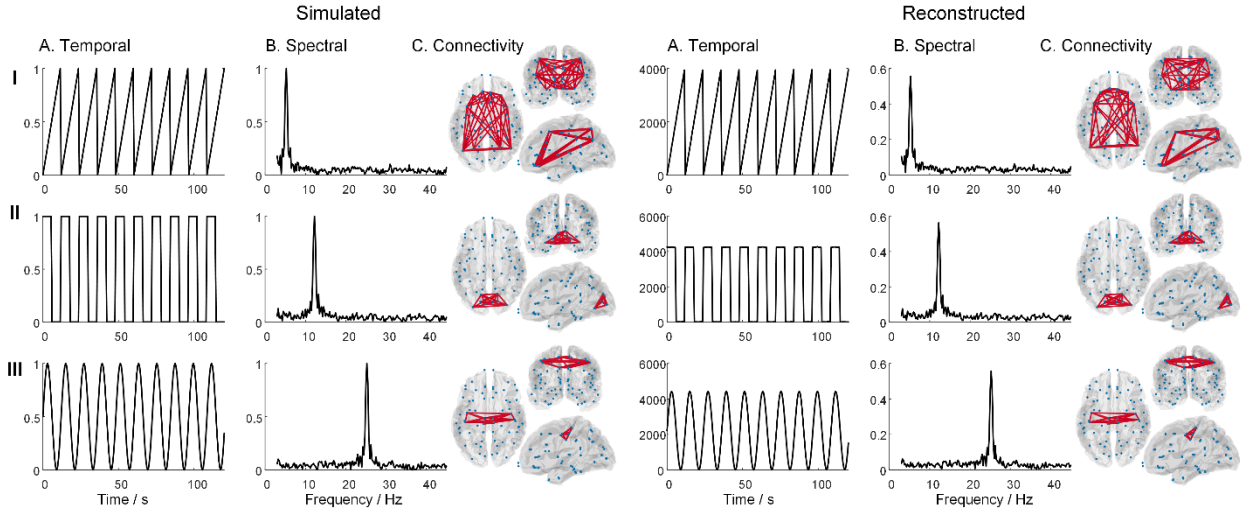

Fig. 2. Results for simulation. Left: the temporal, spectral, and spatial connectivity modes of three synthetic brain network patterns. Right: corresponding spectral and spatial connectivity modes of reconstructed brain patterns.

musical feature, temporal courses of brain networks (component) and subject. We aim to undertake a correlation analysis between temporal profile and musical time series, through evaluating the statistical significance of correlation based on a surrogate permutation procedure [55]. We obtained $\tilde{R}$ TCA components with three factors, charactering the temporal evolution, spectral mode, and spatial topology of brain networks. The temporal factor matrix $\boldsymbol{C}$ (with dimensions $n_w n_p \times \tilde{R}$) was firstly reshaped into a three-way tensor $\mathcal{C}$ (with dimensions $n_w \times n_p \times \tilde{R}$), which includes individual temporal course for each component. For each component and each subject, we computed the correlation coefficient between each musical feature time series and temporal course as the modulation score. We then determined which component was significantly modulated by testing whether its modulation score was significantly different from the scores of surrogate data. The surrogate data were generated by a phase-randomization procedure [56], which rotated the intrinsic phase and preserved the properties of the temporal course in the spectral domain. We repeated the phase-randomization procedure 5000 times for each component. We calculated the correlation coefficient between musical feature time series and phase-randomized temporal courses to obtain a distribution of surrogate modulation scores. The 95th percentile ($p_{correct} = 0.05$) of surrogate modulation scores was selected as the threshold (control modulation scores for comparation) for each subject. Finally, for each component, we performed two-tailed t-tests for modulation score of each musical feature to determine which component (brain network pattern) was modulated significantly differently (at $p_{correct} = 0.05$ level) from the defined thresholds.

III. Results

A. Simulation Results

We firstly validated the proposed method using simulation data, which proved instructive to examine the performance of the methodology. The performance of wPLI, as a measure to examine functional connectivity in source space, has been validated well in previous study [40]. Thus, we here will not examine the performance of wPLI repeatedly. We only tested the ability of TCA, applied to time-frequency connectivity data, to character the temporal, spectral, and spatial changes in electrophysiological brain network over time scales of minutes.

We constructed an adjacency tensor $\mathcal{S}_{sim}$ using outer product of temporal, spectral, and spatial topology factors of predefined true sources. The synthetic adjacency tensor was generated by $\mathcal{M}_{sim} = \mathcal{S}_{sim} + \mathcal{N}_{sim} = \sum_{r=1}^{R} \boldsymbol{a}^r_{sim} \circ \boldsymbol{b}^r_{sim} \circ \boldsymbol{c}^r_{sim} + \mathcal{N}_{sim}$, where $\mathcal{N}_{sim}$ is a noise tensor with dimensions same as $\mathcal{S}_{sim}$. Three distinct brain network patterns were predefined based on a previous work ($R = 3$), which consists of visual, sensorimotor, and fronto-parietal networks with distinct spectral modes [39]. Their temporal, spectral, and spatial topology profiles were shown in Fig. 2. Temporal factor matrix was constructed with triangle, square, and sine waves and spectral factor was composed of peaks at 5 Hz, 12 Hz and 25 Hz. We here demonstrated the results under the signal to noise ratio (SNR) of 10dB. As can be seen, the three underling true brain patterns with distinct temporal-spectral-spatial modes were successfully extracted using TCA.

B. Results From Music-Listening EEG Data

Figs. 3 and 4 demonstrate the identified brain network patterns (TCA components) during music listening: their spectral and spatial topology (connectivity) profiles, as well as their modulation by five musical features. The modulation score was averaged across subjects. Here, 25 components were extracted by CP decomposition according to DIFFIT method (See APPENDIX), and we presented 9 components that shown significant musical feature modulation. We observed two bilateral frontal functional networks, referred to as anterior higher-order cognitive brain networks in accordance with previous literature, but with distinct spectral modes (Rows I and II of Fig. 3). One of them is dominated by low-frequency oscillations

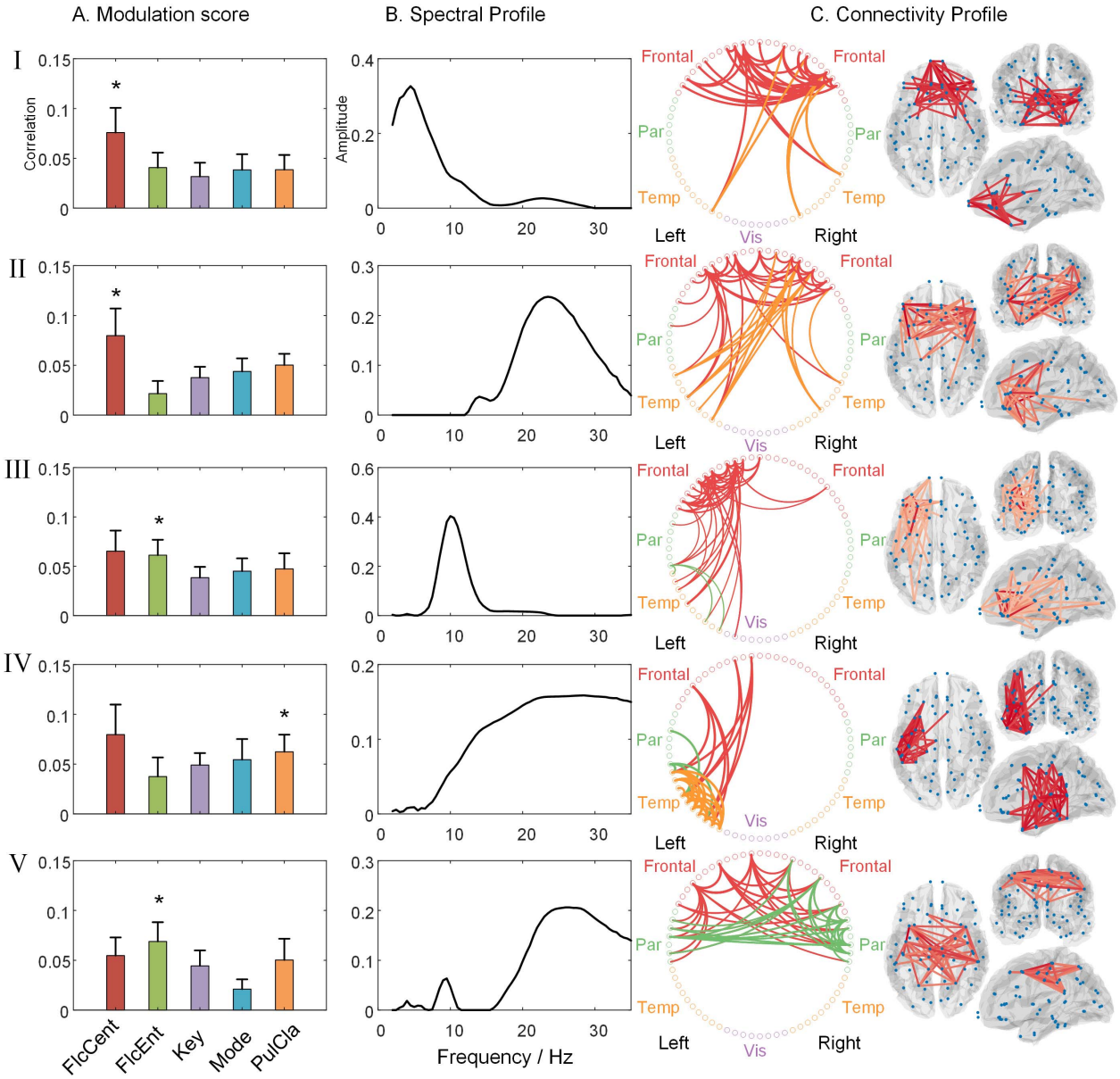

Fig. 3. Results for music-listening data. A. The modulation scores for each musical feature are computed from temporal course and averaged across subjects. Error bars represent standard errors of mean. An asterisk indicates that the component is modulated significantly differently from surrogate data. B. The spectral profiles are obtained from the spectral factor matrix. C. The circular phase-coupling plots and the 3D visualization of the connectivity profiles. Each node/dot represents one brain region. I. Anterior higher-order cognitive network with dominant delta/theta frequencies. II. Beta-specific higher-order cognitive network. III &IV. Language-related network with distinct spectral modes. V. Beta-specific motor network.

(Delta and Theta rhythms, 3-8 Hz) and another is centered at Beta rhythm (20-30 Hz). The regions involved by the two anterior higher-order cognitive networks are part of the default mode network (DMN), which here contains temporal poles, the ventromedial prefrontal cortex and posterior cingulate cortex. They are individually modulated by Fluctuation Centroid. Row III of Fig. 3 shows a 10 Hz unilateral functional networks, which mainly involves Broca's arears and temporal poles that are often associated with semantic integration. This brain pattern is significantly modulated by Fluctuation Entropy. Row IV of Fig. 3 shows a strong connectivity between temporal lobe and the frontal regions with a Beta-specific spectrum, which is significantly modulated by Pulse Clarity. We also found a Beta-specific sensorimotor component (Row V of Fig. 3), which involves regions including motor areas and is modulated by Fluctuation Entropy.

Fig. 4 demonstrates several brain connectivity networks mainly associated with auditory regions. The neural oscillations involved are dominated by Beta rhythm. Row I of Fig. 4 shows a bilateral temporal connectivity networks but no connections between left and right. The Beta rhythm was involved in this connectivity and it was modulated by Pulse Clarity. Rows II and III show strong connections between left temporal regions and right temporal regions with high-Beta

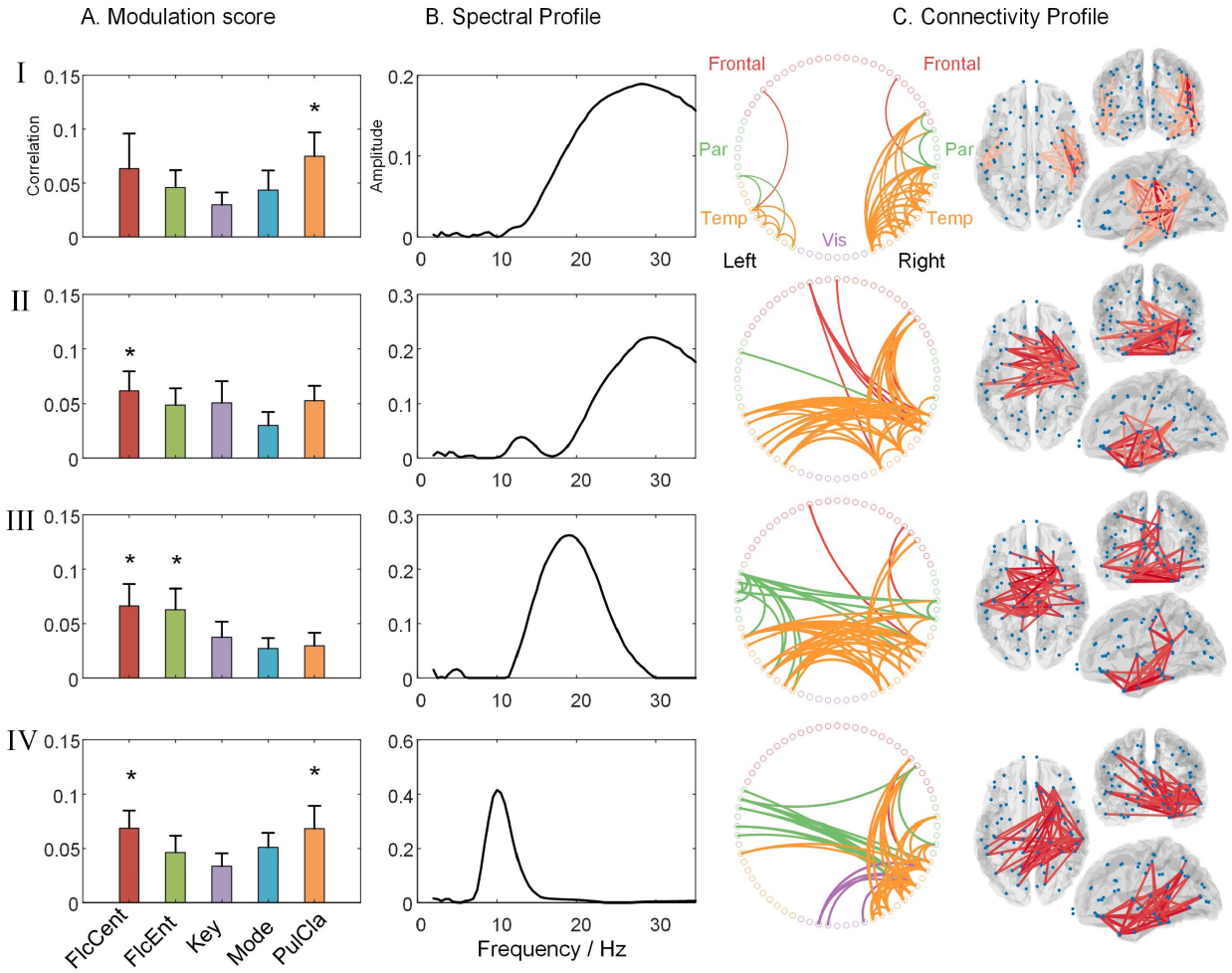

Fig. 4. Auditory-involved networks. I. Left and right temporal connectivity networks with dominant coherence in Beta range. II &III. Left to right temporal arears connections. IV. Alpha-specific right temporal network.

and low-Beta spectral modes. The temporal course of brain pattern in Row II is modulated by Fluctuation Centroid, as well as in Row III is modulated by both Fluctuation Centroid and Fluctuation Entropy. Row IV demonstrates connections between right temporal regions and left parietal regions. Its neural oscillations are dominated by Alpha rhythm (Peaks at 10 Hz) and its temporal course is significantly correlated with Fluctuation Centroid and Pulse Clarity.

IV. Discussion

In this paper, we introduced a TCA-based approach applied to EEG data, which allows us to characterize the time-frequency dynamics of electrophysiology networks during naturalistic music stimuli. We constructed a three-way tensor containing temporal evolution of frequency-specific functional connectivity in source space and used CP decomposition to extract the low-dimensional descriptions of brain networks. Using the proposed method, we extracted large-scale brain networks during freely listening to music, which was described by TCA components. Such TCA component, we refer to as a brain pattern, was pictured with a distinct spatially and spectrally defined pattern of network activity across the set of predefined-atlas regions spanning the whole brain. These patterns of frequency-specific phase-coupling were observed to be temporally modulated by musical feature time series and corresponded to plausible functional systems, including auditory, motor, and higher-order cognitive networks. As far as the authors are aware, this is the first complete formulation of an TCA-based approach for the analysis of electrophysiology network dynamics using ongoing EEG in source space during naturalistic and continuous music listening.

The two higher-order cognitive brain pattern (or networks) involved a subdivision of the DMN regions. These subdivisions had distinguishing features in different frequency bands, with one exhibiting high coherence in the Delta/Theta range (3–8 Hz) (Row I of Fig. 3) and the other showing a high coherence in the Beta range (20-30 Hz) (Row II of Fig. 3). The involved regions were composed of temporal poles, the ventromedial prefrontal cortex, and posterior cingulate cortex. Temporal poles are well believed to be related to semantic integration [6], [57] and the ventromedial prefrontal cortex is typically specialized for emotion regulation [58], which shows strong connection with the posterior cingulate cortex, a key region of the DMN [59]. Thus, the forming of these connectivity patterns is plausible to understand semantics expressed by music and induce related emotion during music

listening. For the neural oscillations, previous studies reported that cortical rhythm activity in the Beta range is related to behavioral performance during music listening and associated with predicting the upcoming note events [12], [60], which confirms our results that the frontal high-order networks with a high coherence in the Beta range emerged during music listening. In addition, the Delta-specific high-order cognitive network (Row I of Fig. 3) was also consistent with the previous studies, which showed that oscillations in the Delta played an important role in predicting the occurrence of auditory targets [61]. Rows III and IV of Fig. 3 demonstrated another two cognitive networks termed 'language network', one of which was specific to Fluctuation Entropy with a high coherence in Alpha band and another of which was modulated significantly by Pulse Clarity with a high coherence in Beta band. Previous studies revealed that brain functional networks engaged in music processing has strict similarities with that for language processing [62], [63]. Thus, the nodes of the language network including Broca's arears and the superior temporal sulcus, may be implicated during continuously listening to music. Recent spectral analysis techniques also demonstrated frequency-specific neural activity during processing language, where semantic and syntactic unification involves the alpha and beta bands by stronger recruitment of regions relevant for unification as indicated by the event-related desynchronization [64]. This study thus supports our findings that language network with strong coupling in alpha and beta bands emerged. For the motor networks (row V of fig. 4), it is believed that perception and execution of actions are strongly coupled in the brain as a result of learning a sensorimotor task, which facilitates not only predicting the action of others but also interacting with them [16]. During music listening, a tight coupling emerges between the perception and production of sequential information in hierarchical organization [16], [65]. Brain regions associated with motor networks may be involved due to the imitation and synchronization during musical activities (e.g. ensemble playing or singing). These networks involved in auditory areas (Fig. 4) showed beta-specific modes, which play an important function in music perception in agreement with previous studies [12], [17], [60].

TCA and other tensor analysis methods have been extensively examined from a theoretical perspective [29] and have been found quite many applications for the multi-way neuroimaging data in cognitive research [22], [28], [66]. The majority of studies have applied tensor decomposition to EEG and fMRI data, most typically to examine differences over subjects or time-frequency presentations of signals [23], [30], [67]. However, we do not find many applications regarding the characterization of temporal and spectral evolution of coupling between brain regions. Such coupling, generally termed functional connectivity, has been demonstrated temporal non-stationarity, spatial inhomogeneities, and spectral structure [38], [68]. It is natural to take into account the measure of time-frequency coupling between all pairs of regions based on wavelet transform, yielding a big data in tensor form with three modes corresponding to temporal course, spectrum, and spatial connectivity topology. TCA or tensor

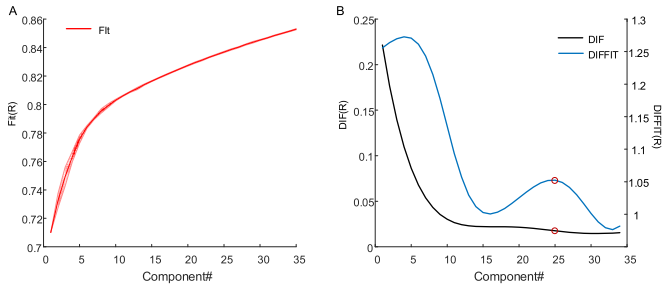

Fig. 5. The Fit, DIF, and DIFFIT curves in function of component R.

decomposition, as a simple extension of PCA, enables to process such high-dimensional data and extract low-dimensional components describing the interactions among modes. One of the key parameters for all TCA-based methods is the determination of component number to be modeled, which is less well prescribed and not a limitation of the proposed approach directly. In this paper, we used DIFFIT method to select the number of components. Note that DIFFIT provides a reference and instruction and is not able to accurately estimate the underlying true number of tensor components. We thus tried to vary this parameter (e.g., $R = from 20\ to 30$) in the current study and also observed the same networks significantly modulated by musical features as $R = 25$.

In addition to parameter selection, another common consideration is signal leakage through ill-posed inverse problem causing spurious correlations between signals. Here, we used wMNE algorithm, which is considered as an optimal source localization method for functional connectivity analysis [3]. Additionally, wPLI was applied to measure the phase coupling in time-frequency domain since it is insensitive to signal leakage and similar bias effects [4]. Yet, it should be noted that those techniques can only reduce the signal leakage problem, not overcome it completely.

Another issue is that we have only used one piece of naturalistic music stimuli to try to formulate an approach for analysis of functional connectivity dynamics during real-world. This work can be thought of as an exploratory study of neural basis of brain network during naturalistic task performance. Future work should adopt more musical clips and examine the repeatability of results. It is also possible to study the differences in brain network connectivity between resting state and music-listening.

V. Conclusion

In this paper, we introduced a data-driven approach to characterize the spatial, temporal, and spectral signatures of electrophysiological brain networks at source level across subjects during music listening. Previous studies have shown that brain connectivity is temporally non-stationary, dependent on frequency of oscillations and exhibit a degree of spatial inhomogeneity. The majority of methods for brain connectivity failed to examine the interactions among spatial, temporal, and spectral modes. Here, we apply TCA to the adjacent tensor constructed by time-frequency phase-coupling between pairs of brain regions. By doing so, we extract brain networks characterized by low-dimensional components with three factors. The temporal courses, representing the time evolution of

frequency-specific brain connectivity, are analyzed by correlation with time series of musical features extracted from music stimuli. We firstly validate the proposed method in simulation. Then we use it to the real EEG data recorded during free music listening. The identified brain networks with distinct spectral mode were in line with those previously published in the fMRI and EEG studies. The proposed method seems valuable for characterization of temporal and spectral evolution of coupling between brain regions during freely listening to music or other naturalistic stimuli.

Appendix

We run ALS optimization procedure at each component number R 20 times from random initial conditions. We then average data fits across many runs, resulting in averaged data fit (Fig. 5.A). Subsequently, the DIF, and DIFFIT were computed, as shown in Fig. 5.B. The DIT curve was smoothed by polynomial curve fitting since it usually fails to provide useful information due to fluctuations on DIF [30]. The two local maximums on DIFFIT curve at $R = 5$ and $R = 25$ indicate two positions on DIF curve that have fast dropping rate. Due to the low Fit value at the range $R < 15$, we selected the local maximum $R = 25$ as the appropriate model order.

The data used in the current study are available from the corresponding author on reasonable request and code to reproduce the simulation presented in this paper is available at *https://github.com/yongjiezhu/CPforBrainConnectivity.*

Acknowledgment

Y. Zhu thanks the Brain Imaging Facility of the Interdisciplinary Center for Clinical Research at RWTH Aachen University for providing the excellent working environment to write this article.

References

[1] K. J. Friston, "Functional and effective connectivity in neuroimaging: A synthesis," *Human Brain Mapping*, vol. 2, nos. 1–2, pp. 56–78, 1994.

[2] E. S. Finn *et al.*, "Functional connectome fingerprinting: Identifying individuals using patterns of brain connectivity," *Nature Neurosci.*, vol. 18, no. 11, p. 1664, 2015.

[3] M. Bola and B. A. Sabel, "Dynamic reorganization of brain functional networks during cognition," *Neuroimage*, vol. 114, pp. 398–413, Jul. 2015.

[4] A. Hillebrand, G. R. Barnes, J. L. Bosboom, H. W. Berendse, and C. J. Stam, "Frequency-dependent functional connectivity within resting-state networks: An atlas-based MEG beamformer solution," *Neuroimage*, vol. 59, no. 4, pp. 3909–3921, 2012.

[5] Y. Zhu, X. Li, T. Ristaniemi, and F. Cong, "Measuring the task induced oscillatory brain activity using tensor decomposition," in *Proc. IEEE Int. Conf. Acoust., Speech Signal Process. (ICASSP)*, May 2019, pp. 8593–8597.

[6] D. Vidaurre *et al.*, "Spontaneous cortical activity transiently organises into frequency specific phase-coupling networks," *Nature Commun.*, vol. 9, no. 1, p. 2987, 2018.

[7] C. Schmidt, D. Piper, B. Pester, A. Mierau, and H. Witte, "Tracking the reorganization of module structure in time-varying weighted brain functional connectivity networks," *Int. J. Neural Syst.*, vol. 28, no. 4, 2018, Art. no. 1750051.

[8] J. S. Damoiseaux *et al.*, "Consistent resting-state networks across healthy subjects," *Proc. Nat. Acad. Sci. USA*, vol. 103, no. 37, pp. 13848–13853, 2006.

[9] D. Mantini, M. G. Perrucci, C. Del Gratta, G. L. Romani, and M. Corbetta, "Electrophysiological signatures of resting state networks in the human brain," *Proc. Nat. Acad. Sci. USA*, vol. 104, no. 32, pp. 13170–13175, Aug. 2007.

[10] M. J. Brookes *et al.*, "Investigating the electrophysiological basis of resting state networks using magnetoencephalography," *Proc. Nat. Acad. Sci. USA*, vol. 108, no. 40, pp. 16783–16788, 2011.

[11] E. Simony *et al.*, "Dynamic reconfiguration of the default mode network during narrative comprehension," *Nature Commun.*, vol. 7, Jul. 2016, Art. no. 12141, doi: 10.1038/ncomms12141.

[12] Y. Zhu *et al.*, "Exploring frequency-dependent brain networks from ongoing EEG using spatial ICA during music listening," *bioRxiv*, Jan. 2019, Art. no. 509802.

[13] M. Alavash, S. Tune, and J. Obleser, "Modular reconfiguration of an auditory control brain network supports adaptive listening behavior," *Proc. Nat. Acad. Sci. USA*, vol. 116, no. 2, pp. 660–669, 2019.

[14] M. Demirtaş *et al.*, "Distinct modes of functional connectivity induced by movie-watching," *NeuroImage*, vol. 184, pp. 335–348, Jan. 2019.

[15] M. W. Cole, T. Ito, D. S. Bassett, and D. H. Schultz, "Activity flow over resting-state networks shapes cognitive task activations," *Nature Neurosci.*, vol. 19, no. 12, p. 1718, 2016.

[16] V. Alluri, P. Toiviainen, I. Burunat, M. Kliuchko, P. Vuust, and E. Brattico, "Connectivity patterns during music listening: Evidence for action-based processing in musicians," *Hum. Brain Mapping*, vol. 38, no. 6, pp. 2955–2970, 2017.

[17] V. Alluri, P. Toiviainen, I. P. Jääskeläinen, E. Glerean, M. Sams, and E. Brattico, "Large-scale brain networks emerge from dynamic processing of musical timbre, key and rhythm," *NeuroImage*, vol. 59, no. 4, pp. 3677–3689, 2012.

[18] N. D. Sidiropoulos, L. De Lathauwer, X. Fu, K. Huang, E. E. Papalexakis, and C. Faloutsos, "Tensor decomposition for signal processing and machine learning," *IEEE Trans. Signal Process.*, vol. 65, no. 13, pp. 3551–3582, Jul. 2017.

[19] A. Cichocki *et al.*, "Tensor decompositions for signal processing applications: From two-way to multiway component analysis," *IEEE Signal Process. Mag.*, vol. 32, no. 2, pp. 145–163, Mar. 2015.

[20] G. Zhou, A. Cichocki, Q. Zhao, and S. Xie, "Nonnegative matrix and tensor factorizations: An algorithmic perspective," *IEEE Signal Process. Mag.*, vol. 31, no. 3, pp. 54–65, May 2014.

[21] F. Cong *et al.*, "Benefits of multi-domain feature of mismatch negativity extracted by non-negative tensor factorization from EEG collected by low-density array," *Int. J. Neural Syst.*, vol. 22, no. 6, 2012, Art. no. 1250025.

[22] F. Cong *et al.*, "Multi-domain feature extraction for small event-related potentials through nonnegative multi-way array decomposition from low dense array EEG," *Int. J. Neural Syst.*, vol. 23, no. 2, 2013, Art. no. 1350006.

[23] F. Cong, Q.-H. Lin, L.-D. Kuang, X.-F. Gong, P. Astikainen, and T. Ristaniemi, "Tensor decomposition of EEG signals: A brief review," *J. Neurosci. Methods*, vol. 248, pp. 59–69, Jun. 2015.

[24] G. Zhou *et al.*, "Linked component analysis from matrices to high-order tensors: Applications to biomedical data," *Proc. IEEE*, vol. 104, no. 2, pp. 310–331, Feb. 2016.

[25] H. Lee, Y.-D. Kim, A. Cichocki, and S. Choi, "Nonnegative tensor factorization for continuous EEG classification," *Int. J. Neural Syst.*, vol. 17, no. 4, pp. 305–317, 2007.

[26] Y. Zhang, Q. Zhao, G. Zhou, J. Jin, X. Wang, and A. Cichocki, "Removal of EEG artifacts for BCI applications using fully Bayesian tensor completion," in *Proc. IEEE Int. Conf. Acoust., Speech Signal Process. (ICASSP)*, Mar. 2016, pp. 819–823.

[27] B. Hunyadi, P. Dupont, W. Van Paesschen, and S. Van Huffel, "Tensor decompositions and data fusion in epileptic electroencephalography and functional magnetic resonance imaging data," *Wiley Interdiscipl. Rev., Data Mining Knowl. Discovery*, vol. 7, no. 1, 2017, Art. no. e1197.

[28] A. H. Williams *et al.*, "Unsupervised discovery of demixed, low-dimensional neural dynamics across multiple timescales through tensor component analysis," *Neuron*, vol. 98, no. 6, pp. 1099–1115, 2018.

[29] T. G. Kolda and B. W. Bader, "Tensor decompositions and applications," *SIAM Rev.*, vol. 51, no. 3, pp. 455–500, 2009.

[30] D. Wang, Y. Zhu, T. Ristaniemi, and F. Cong, "Extracting multi-mode ERP features using fifth-order nonnegative tensor decomposition," *J. Neurosci. Methods*, vol. 308, pp. 240–247, Oct. 2018.

[31] A. G. Mahyari and S. Aviyente, "Identification of dynamic functional brain network states through tensor decomposition," in *Proc. IEEE Int. Conf. Acoust., Speech Signal Process. (ICASSP)*, May 2014, pp. 2099–2103.

[32] A. G. Mahyari, D. M. Zoltowski, E. M. Bernat, and S. Aviyente, "A tensor decomposition-based approach for detecting dynamic network states from EEG," *IEEE Trans. Biomed. Eng.*, vol. 64, no. 1, pp. 225–237, Jan. 2017.

[33] Y. Liu, J. Moser, and S. Aviyente, "Network community structure detection for directional neural networks inferred from multichannel multisubject EEG data," *IEEE Trans. Biomed. Eng.*, vol. 61, no. 7, pp. 1919–1930, Jul. 2014.

[34] S. B. Samdin, C.-M. Ting, H. Ombao, and S.-H. Salleh, "A unified estimation framework for state-related changes in effective brain connectivity," *IEEE Trans. Biomed. Eng.*, vol. 64, no. 4, pp. 844–858, Apr. 2017.

[35] A. Ozdemir, E. M. Bernat, and S. Aviyente, "Recursive tensor subspace tracking for dynamic brain network analysis," *IEEE Trans. Signal Inf. Process. Over Netw.*, vol. 3, no. 4, pp. 669–682, Dec. 2017.

[36] E. Al-sharoa, M. Al-khassaweneh, and S. Aviyente, "Tensor based temporal and multilayer community detection for studying brain dynamics during resting state fMRI," *IEEE Trans. Biomed. Eng.*, vol. 66, no. 3, pp. 695–709, Mar. 2019.

[37] M. Tang, Y. Lu, and L. Yang, "Temporal–spatial patterns in dynamic functional brain network for self-paced hand movement," *IEEE Trans. Neural Syst. Rehabil. Eng.*, vol. 27, no. 4, pp. 643–651, Apr. 2019.

[38] M. J. Brookes *et al.*, "Measuring temporal, spectral and spatial changes in electrophysiological brain network connectivity," *NeuroImage*, vol. 91, pp. 282–299, May 2014.

[39] G. C. O'Neill *et al.*, "Measurement of dynamic task related functional networks using MEG," *NeuroImage*, vol. 146, pp. 667–678, Feb. 2017.

[40] J. M. Palva *et al.*, "Ghost interactions in MEG/EEG source space: A note of caution on inter-areal coupling measures," *NeuroImage*, vol. 173, pp. 632–643, Jun. 2018.

[41] M. Vinck, R. Oostenveld, M. Van Wingerden, F. Battaglia, and C. M. A. Pennartz, "An improved index of phase-synchronization for electrophysiological data in the presence of volume-conduction, noise and sample-size bias," *NeuroImage*, vol. 55, no. 4, pp. 1548–1565, Apr. 2011.

[42] F. Cong *et al.*, "Linking brain responses to naturalistic music through analysis of ongoing EEG and stimulus features," *IEEE Trans. Multimedia*, vol. 15, no. 5, pp. 1060–1069, Aug. 2013.

[43] F. Cong, I. Kalyakin, T. Huttunen-Scott, H. Li, H. Lyytinen, and T. Ristaniemi, "Single-trial based independent component analysis on mismatch negativity in children," *Int. J. Neural Syst.*, vol. 20, no. 4, pp. 279–292, 2010.

[44] F. Tadel, S. Baillet, J. C. Mosher, D. Pantazis, and R. M. Leahy, "Brainstorm: A user-friendly application for MEG/EEG analysis," *Comput. Intell. Neurosci.*, vol. 2011, p. 8, Jan. 2011.

[45] F.-H. Lin, J. W. Belliveau, A. M. Dale, and M. S. Hämäläinen, "Distributed current estimates using cortical orientation constraints," *Hum. Brain Mapping*, vol. 27, no. 1, pp. 1–13, 2006.

[46] R. S. Desikan *et al.*, "An automated labeling system for subdividing the human cerebral cortex on MRI scans into gyral based regions of interest," *NeuroImage*, vol. 31, no. 3, pp. 968–980, Jul. 2006.

[47] B. Cai *et al.*, "Capturing dynamic connectivity from resting state fMRI using time-varying graphical lasso," *IEEE Trans. Biomed. Eng.*, vol. 66, no. 7, pp. 1852–1862, Jul. 2019.

[48] E. A. Allen, E. Damaraju, S. M. Plis, E. B. Erhardt, T. Eichele, and V. D. Calhoun, "Tracking whole-brain connectivity dynamics in the resting state," *Cerebral Cortex*, vol. 24, no. 3, pp. 663–676, 2014.

[49] A. Cichocki, R. Zdunek, A. H. Phan, and S.-I. Amari, *Nonnegative Matrix and Tensor Factorizations: Applications to Exploratory Multi-Way Data Analysis and Blind Source Separation*. Hoboken, NJ, USA: Wiley, 2009.

[50] B. W. Bader *et al. MATLAB Tensor Toolbox, Version [VERSION]*. Accessed: Jan. 7, 2012. [Online]. Available: https://www.tensortoolbox.org

[51] N. Vervliet, O. Debals, and L. De Lathauwer, "Tensorlab 3.0—Numerical optimization strategies for large-scale constrained and coupled matrix/tensor factorization," in *Proc. 50th Asilomar Conf. Signals, Syst. Comput.*, Nov. 2016, pp. 1733–1738.

[52] M. E. Timmerman and H. A. Kiers, "Three-mode principal components analysis: Choosing the numbers of components and sensitivity to local optima," *Brit. J. Math. Stat. Psychol.*, vol. 53, no. 1, pp. 1–16, 2000.

[53] R. Bro and H. A. L. Kiers, "A new efficient method for determining the number of components in PARAFAC models," *J. Chemometrics*, vol. 17, no. 5, pp. 274–286, 2003.

[54] M. Mørup and L. K. Hansen, "Automatic relevance determination for multi-way models," *J. Chemometrics, A J. Chemometrics Soc.*, vol. 23, nos. 7–8, pp. 352–363, 2009.

[55] D. Kim, K. Kay, G. L. Shulman, and M. Corbetta, "A new modular brain organization of the BOLD signal during natural vision," *Cerebral Cortex*, vol. 28, no. 9, pp. 3065–3081, 2017.

[56] D. Prichard and J. Theiler, "Generating surrogate data for time series with several simultaneously measured variables," *Phys. Rev. Lett.*, vol. 73, no. 7, p. 951, 1994.

[57] K. Tsapkini, C. E. Frangakis, and A. E. Hillis, "The function of the left anterior temporal pole: Evidence from acute stroke and infarct volume," *Brain*, vol. 134, no. 10, pp. 3094–3105, 2011.

[58] L. K. Fellows and M. J. Farah, "The role of ventromedial prefrontal cortex in decision making: Judgment under uncertainty or judgment per se," *Cerebral Cortex*, vol. 17, no. 11, pp. 2669–2674, 2007.

[59] M. E. Raichle, A. M. MacLeod, A. Z. Snyder, W. J. Powers, D. A. Gusnard, and G. L. Shulman, "A default mode of brain function," *Proc. Nat. Acad. Sci. USA*, vol. 98, no. 2, pp. 676–682, 2001.

[60] K. B. Doelling and D. Poeppel, "Cortical entrainment to music and its modulation by expertise," *Proc. Nat. Acad. Sci. USA*, vol. 112, no. 45, pp. E6233–E6242, 2015.

[61] L. H. Arnal, K. B. Doelling, and D. Poeppel, "Delta-beta coupled oscillations underlie temporal prediction accuracy," *Cerebral Cortex*, vol. 25, no. 9, pp. 3077–3085, 2014.

[62] L. Fadiga, L. Craighero, and A. D'Ausilio, "Broca's area in language, action, and music," *Ann. New York Acad. Sci.*, vol. 1169, no. 1, pp. 448–458, 2009.

[63] S. Koelsch, E. Kasper, D. Sammler, K. Schulze, T. Gunter, and A. D. Friederici, "Music, language and meaning: Brain signatures of semantic processing," *Nature Neurosci.*, vol. 7, no. 3, p. 302, 2004.

[64] N. H. L. Lam, J.-M. Schoffelen, J. Uddén, A. Hultén, and P. Hagoort, "Neural activity during sentence processing as reflected in theta, alpha, beta, and gamma oscillations," *NeuroImage*, vol. 142, pp. 43–54, Nov. 2016.

[65] I. Molnar-Szakacs and K. Overy, "Music and mirror neurons: From motion to'e'motion," *Social Cognit. Affect. Neurosci.*, vol. 1, no. 3, pp. 235–241, 2006.

[66] E. L. Mackevicius *et al.*, "Unsupervised discovery of temporal sequences in high-dimensional datasets, with applications to neuroscience," *eLife*, vol. 8, Feb. 2019, Art. no. e38471.

[67] C. I. Kanatsoulis, N. D. Sidiropoulos, M. Akçakaya, and X. Fu, "Regular sampling of tensor signals: Theory and application to FMRI," in *Proc. IEEE Int. Conf. Acoust., Speech Signal Process. (ICASSP)*, May 2019, pp. 2932–2936.

[68] F. Li *et al.*, "The dynamic brain networks of motor imagery: Time-varying causality analysis of scalp EEG," *Int. J. Neural Syst.*, vol. 29, no. 1, 2018, Art. no. 1850016.